RELIABILITY ANALYSIS OF DEGRADING UNCERTAIN STRUCTURES

WITH APPLICATIONS TO FATIGUE AND FRACTURE UNDER RANDOM LOADING

By André Teófilo Beck, M. Eng.

A thesis submitted to the School of Engineering
for the Degree of Doctor of Philosophy

The University of Newcastle, Australia
June 2003.

I hereby certify that the work embodied in this thesis is the result of original research and has not been submitted for a higher degree to any other University or Institution.

André Teófilo Beck

ACKNOWLEDGEMENTS

To my supervisor, Rob Melchers, for his guidance, support, encouragement and friendship.

To my family, for the love and support from overseas.

To my Brazilian family in Newcastle, for the friendship and for the innumerous south-Brazilian specialty barbecues and parties: David and Jussara, Maggie and Natan, Ken and Aurea, Daniel and Raquel, Bred and Lidi, Victor and Louisse, various Renatos, various Daniels, Flavia, Bruno and Negão.

To mi Colombiana querida, Catalina.

To Andrew and Gary, for your friendship and the dives...
To Elena, Ryall, Tomm and Michael for the stupendous bike rides...

To the friendly professors, staff and fellow students from the Department of Civil, Surveying and Environmental Engineering.

To my room-mates Kinsley, Stephen and, very specially, Bill Gray, for the welcomed interruptions that kept my brain from frying at some instances.

To the rocks, beaches, surf, mountains, lakes, deserts, bush, possums, kanguroos, kookaburras and aboriginals of Australia, for reminding me constantly that I was still alive.

Finally, but not least important, to the Brazilian Council for Development of Post Graduate Education (CAPES), for the financial support of this candidature. This "thanks" is extended to the Brazilian tax payer and to the vote of trust the nation placed on me.

RELIABILITY ANALYSIS OF DEGRADING UNCERTAIN STRUCTURES WITH APPLICATIONS TO FATIGUE AND FRACTURE UNDER RANDOM LOADING

By André Teófilo Beck, M. Eng.

A thesis submitted to the School of Engineering
for the Degree of Doctor of Philosophy

The University of Newcastle, Australia
June 2003.

ABSTRACT

In the thesis, the reliability analysis of structural components and structural details subject to random loading and random resistance degradation is addressed. The study concerns evaluation of the probability of failure due to an overload of a component or structural detail, in consideration of random (environmental) loads and their combination, uncertain resistance parameters, statistical and phenomenological uncertainty and random resistance degradation mechanisms. Special attention is devoted to resistance degradation, as it introduces an additional level of difficulty in the solution of time variant reliability problems.

The importance of this study arrives from the ageing of existing infrastructure in a world wide scale and from the lack of standards and codes for the ongoing safety management of general structures past their original design lives. In this context, probabilistic-based risk assessment and reliability analysis provide a framework for the safety management of ageing structures in consideration of inherent load and resistance uncertainty, current state of the structure, further resistance degradation, periodic inspections, in the absence of past experience and on an individual basis. In particular, the critical problem of resistance degradation due to fatigue is addressed.

The formal solution of time variant reliability problems involves integration of local crossing rates over a conditional failure domain boundary, over time and over random resistance variables. This solution becomes very difficult in the presence of resistance degradation, as crossing rates become time dependent, and the innermost integration over the failure domain boundary has to be repeated over time. Significant simplification is achieved when the order of integrations is changed, and crossing rates are first integrated over the random failure domain boundary and then over time. In the so-called ensemble crossing rate or Ensemble Up-crossing Rate (EUR) approximation, the arrival rate of the first crossing over a random barrier is approximated by the ensemble average of crossings. This approximation conflicts with the Poisson assumption of independence implied in the first passage failure model, making results unreliable and highly conservative.

Despite significant simplification of the solution, little was known to date about the quality of the EUR approximation. In this thesis, a simulation procedure to obtain Poissonian estimates of the arrival rate of the first up-crossing over a random barrier is introduced. The procedure is used to predict the error of the EUR approximation. An error parameter is identified and error functions are constructed. Error estimates are used to correct original EUR failure probability results and to compare the EUR with other common simplifications of time variant reliability problems. It is found that EUR errors can be quite large even when failure probabilities are small, a result that goes against previous ideas.

A *barrier failure dominance* concept is introduced, to characterize those problems where an up-crossing or overload failure is more likely to be caused by a small outcome of the resistance than by a large outcome of the load process. It is shown that large EUR errors are associated with barrier failure dominance, and that solutions which simplify the load part of the problem are more likely to be appropriate in this case. It is suggested that the notion of barrier failure dominance be used to identify the proper (simplified) solution method for a given problem. In this context, the EUR approximation is compared with Turkstra's load combination rule and with the point-crossing formula.

It is noted that in many practical structural engineering applications involving environmental loads like wind, waves or earthquakes, load process uncertainty is larger than resistance uncertainty. In these applications, barrier failure dominance in unlikely and EUR errors can be expected to be small.

The reliability problem of fatigue and fracture under random loading is addressed in the thesis. A solution to the problem, based on the EUR approximation, is constructed. The problem is formulated by combining stochastic models of crack propagation with the first passage failure model. The solution involves evaluation of the evolution in time of crack size and resistance distributions, and provides a fresh random process-based approach to the problem. It also simplifies the optimization and planning of non-destructive periodic inspection strategies, which play a major role in the ongoing safety management of fatigue affected structures.

It is shown how sensitivity coefficients of a simplified preliminary First Order Reliability solution can be used to characterize barrier failure dominance. In the fatigue and fracture reliability problem, barrier failure dominance can be caused by large variances of resistance or crack growth parameters. Barrier failure dominance caused by resistance parameters leads to problems where overload failure is an issue and where the simplified preliminary solution is likely to be accurate enough. Barrier failure dominance caused by crack growth parameters leads to highly non-linear problems, where critical crack growth dominates failure probabilities. Finally, in the absence of barrier failure dominance, overload failure is again the issue and the EUR approximation becomes not just appropriate but also accurate.

The random process-based EUR solution of time-variant reliability problems developed and the concept of barrier failure dominance introduced in the thesis have broad applications in problems involving general forms of resistance degradation as well as in problems of random vibration of uncertain structures.

ANÁLISE DE CONFIABILIDADE ESTRUTURAL SOB DEGRADAÇÃO ALEATÓRIA DE RESISTÊNCIA - COM APLICAÇÕES A FADIGA E FRATURA SOB CARREGAMENTOS ESTOCÁSTICOS

Tese submetida em 13 de junho de 2003 à Escola de Engenharia da Universidade de Newcastle, Austrália, como requisito para obtenção do grau de Doutor (Ph. D.)

RESUMO

Esta tese aborda o cálculo de confiabilidade de componentes e detalhes estruturais sujeitos a carregamentos estocásticos e a degradação da resistência ao longo do tempo. Neste típico problema de confiabilidade estrutural dependente do tempo, a falha da estrutura ou componente fica caracterizada na primeira sobrecarga. O problema de confiabilidade consiste em prever a probabilidade de uma falha por sobrecarga, considerando incertezas nos carregamentos e nas suas possíveis combinações, nos parâmetros da resistência, incertezas estatísticas e fenomenológicas, bem como nos mecanismos aleatórios de degradação da resistência. Em especial, a tese aborda o problema de degradação da resistência de estruturas, que introduz sérias dificuldades no cálculo de confiabilidade.

A importância de se considerar degradação de resistência na análise de confiabilidade estrutural está no envelhecimento crescente da infraestrutura instalada, a nível mundial, e na inexistência de normas técnicas genéricas para a análise de segurança e para a extensão da vida útil de estruturas existentes. A análise probabilística de risco e, como parte dela, a análise de confiabilidade estrutural, permite uma análise quantitativa da segurança de estruturas existentes, considerando incertezas em carregamentos e resistência, condição atual da estrutura, inspeções periódicas não-destrutivas, progressiva redução da resistência, na falta de experiência anterior e em uma base individual para cada estrutura. Como exemplo de aplicação, o problema de fadiga e fratura sob carregamentos estocásticos é estudado na tese.

A solução usual de problemas de confiabilidade estrutural dependente do tempo envolve integrais sobre a fronteira do domínio de falha, sobre o tempo e sobre os parâmetros aleatórios de resistência. Sob redução da resistência, a solução usual se torna muito difícil, porque a taxa de falhas se torna dependente do tempo. Nesta tese, uma solução alternativa é estudada. Esta solução, chamada de "*Ensemble Up-crossing Rate approximation*" e abreviada como EUR, consiste em aproximar a taxa de chegada da primeira passagem por uma barreira aleatória pela taxa de passagens média sobre o envelope. Apesar de simplificar muito a solução do problema, esta aproximação dá origem a um erro admitidamente grande, mas que ainda não havia sido estudado em detalhe.

Uma metodologia é introduzida e utilizada para estimar o erro da aproximação EUR. Esta metodologia, baseada em simulação de Monte Carlo, consiste em uma série de experimentos numéricos realizados em computador. Através dela, parâmetros de erro são identificados e funções de erro são construídas. O estudo mostra que o erro da aproximação EUR pode ser grande mesmo em problemas onde as probabilidades de falha são pequenas, um resultado que se contrapõe a suposições anteriores. As estimativas de erro são utilizadas para corrigir resultados da solução EUR original e para comparar esta aproximação com outras soluções simplificadas do problema de confiabilidade estrutural dependente do tempo.

O presente estudo introduz o conceito de *falha dominada pela barreira*. Este conceito é utilizado para descrever problemas de confiabilidade onde a probabilidade de ocorrência de uma falha por sobrecarga é dominada pela realização da barreira e não pela realização do carregamento. Em outras palavras, a probabilidade de que uma pequena realização da resistência da estrutura cause uma falha por sobrecarga é maior do que a probabilidade de que a mesma falha seja causada por uma infeliz combinação de extremos de carregamento.

O estudo mostra ainda que problemas com falha dominada pela barreira geram os maiores erros quando utilizada a aproximação EUR. Assim, os maiores erros da solução EUR podem ser associados com *falha dominada pela barreira*. Nesta mesma situação de falha dominada pela barreira, outras soluções aproximadas, envolvendo simplificações na parte dos carregamentos, são mais apropriadas. Como resultado, propõe-se que o conceito de falha dominada pela barreira seja utilizado como orientação para estabelecer que tipo de solução (aproximada) é adequada para que tipo de problema. Neste contexto e a título de exemplo, a aproximação EUR é comparada com os métodos conhecidos como "*Turkstra's Load Combination Rule*" e "*Point-Crossing Formula*".

Em problemas práticos de análise estrutural, incertezas referentes a carregamentos ambientais como ondas, vento e terremotos, são tipicamente maiores do que incertezas em parâmetros de resistência. Neste tipo de problema, a *falha dominada pela barreira* dificilmente fica caracterizada. Assim, a despeito da grande possibilidade de erro da solução EUR, esta aproximação ainda tem uma importante gama de aplicação.

A tese aborda a análise de confiabilidade a fadiga e fratura de componentes e detalhes estruturais sujeitos a carregamentos estocásticos. Uma solução para este problema, baseada na aproximação EUR, é construída combinando-se modelos estocásticos de propagação de trincas com o modelo de falha à primeira sobrecarga. Esta solução envolve um cálculo da evolução no tempo das funções de distribuição de probabilidade das variáveis (aleatórias) tamanho da trinca e resistência da estrutura, numa abordagem baseada em processos estocásticos. Esta solução é muito apropriada em problemas envolvendo otimização e planejamento de estratégias de inspeções periódicas, as quais são fundamentais no problema de extensão de vida útil de estruturas.

O estudo mostra como os coeficientes de sensibilidade de uma solução preliminar baseada no método de aproximação de primeira ordem (FORM) podem ser utilizados para identificar ou caracterizar falha dominada pela barreira. O estudo mostra que, no problema de fadiga e fratura, falha dominada pela barreira pode ser causada por parâmetros de resistência ou por parâmetros da propagação de trincas. Quando causada por parâmetros de resistência, leva a problemas onde a probabilidade de falha devido a uma sobrecarga pode ser significativa, e para os quais a solução preliminar simplificada pode ser suficiente. Quando incertezas referentes aos parâmetros de propagação de trincas dominam o problema, a falha passa a ser não somente dominada mas determinada pela barreira. Neste caso, a falha ocorre devido ao crescimento crítico da trinca (também conhecida como falha por acúmulo de dano) e não devido a uma sobrecarga. Finalmente, quando a probabilidade de falha não é dominada pela barreira, o modo de falha por sobrecarga volta a ser crítico, e a aproximação EUR torna-se não só adequada como prescisa.

A solução do problema de sobrecarga sob carregamentos aleatórios elaborada nesta tese, que modela a degradação da resistência como um processo estocástico e que está baseada na aproximação EUR, tem ampla aplicação a problemas envolvendo outras formas de redução da resistência, como corrosão, desgaste, fluência, etc, bem como em problemas de vibrações aleatórias em estruturas.

ANÁLISE DE CONFIABILIDADE ESTRUTURAL SOB DEGRADAÇÃO ALEATÓRIA DE RESISTÊNCIA - COM APLICAÇÕES A FADIGA E FRATURA SOB CARREGAMENTOS ESTOCÁSTICOS

Tese submetida em 13 de junho de 2003 à Escola de Engenharia da Universidade de Newcastle, Austrália, como requisito para obtenção do grau de Doutor (Ph. D.)

Orientador:

Prof. Robert E. Melchers, University of Newcastle.

Banca de examinação:

Prof. M. J. Baker, University of Aberdeen, Scotland

Prof. Dr-Ing. R. Rackwitz, Technische Universitaet, Germany

Prof. B. Ellingwood, Georgia Institute of Technology, USA

Esta tese foi examinada conforme os critérios da Universidade de Newcastle para o programa de Doutorado baseado em pesquisa, apresentado na biblioteca de diretrizes da universidade:
(http://www.newcastle.edu.au/policy/academic/doctoral/doctors.htm) e considerada aprovada para a outogação do título de Doutor (PhD.).

Contents

List of Figures

List of Tables

0.1 List of Abbreviations

ANAL	Analytical - refers to distribution-model based solutions
BB	Broad band
BFD	Barrier failure dominance
CDF	Cumulative density function
C.O.V.	Coefficient of variation
CONV	Convolution Integration
EPFM	Elasto-plastic Fracture Mechanics
EUR	Ensemble Up-crossing Rate
FE	Finite Element (analysis)
FORM	First Order Reliability Method
FPI	Fast Probability Integration
HLRF	Hassofer-Lind-Rackwitz-Fiessler optimization algorithm
KS	Kolmogorov-Smirnoff goodness-of-fit test
LEFM	Linear Elastic Fracture Mechanics
LOGN	Log-normal crack propagation rate model
MCS	Monte Carlo Simulation
MKV	Diffusive Markov crack propagation model
NB	Narrow band
NUMER	Numerical - refers to fully numerical solutions
PDF	Probability density function
POD	Probability of detection (of an inspection method)
PS	Pulse-sequence (load process)
PSD	Power Spectrum Density
RP	Random Process
RV	Random Variable
R6	R6 failure assessment diagram
SIF	Stress Intensity Factor
SM	Second-order second moment approximation
SORM	Second Order Reliability Method
TI	Time-integrated (extreme value) analysis
TH	Time-history
TPD	Transition Probability Density
TTCI	Time to crack initiation

0.2 List of Symbols

Random Variables - Random Processes:

R	(Resistance) Random Variable
r	particular outcome of R
μ_R	Mean of R
σ_R	Standard Deviation of R
σ_R^2	Variance of R
$f_R(r)$	Marginal probability density function of variable R
$F_R(r)$	Marginal cumulative distribution of variable R
$\mathbf{R}$	Vector of (resistance) Random Variables
$\mathbf{r}$	Particular outcome of $\mathbf{R}$ (vector)
$\mu_{\mathbf{R}}$	Vector of means
$\sigma_{\mathbf{R}}$	Vector of standard deviations
$\sigma_{\mathbf{R}}^2$	Vector of variances
$f_{\mathbf{R}}(\mathbf{r})$	Joint probability density function of $\mathbf{R}$
$F_{\mathbf{R}}(\mathbf{r})$	Joint cumulative distribution of $\mathbf{R}$
$\mathbf{cov}$	covariance matrix
$S(t)$	(Load) Random Process
$R_{SS}(t)$	Correlation function of process $S(t)$
λ_S	Correlation length of process $S(t)$
α	irregularity factor
$G(w)$	Power Spectrum Density function

Distributions:

$\phi(x)$	probability density of standard normal distribution
$\Phi(x)$	cumulative distribution of standard normal distribution
$N(\mu, \sigma)$	Normal distribution with moments μ and σ
$LN(\mu, \sigma)$	Log-normal distribution
$iLN(\mu, \sigma)$	Inverted log-normal distribution
$RL(p)$	Raleigh distribution with parameter p

$E[.]$	Expected value operator
$P[.]$	Probability of the event in brackets

FORM analysis:

$\mathbb{T}(\mathbf{z})$	Transformation to reduced space
$\mathbf{u} = \mathbb{T}(\mathbf{z})$	Standard normal variable in reduced space
$\mathbf{u}^*$	Design Point in reduced space
u_{n+1}	additional variable in FPI solution
β	Reliability Index
$\boldsymbol{\alpha}^2$	sensitivity coefficients
n_{conv}	number of iterations for convergence
n_{rv}	number of random variables of the problem
n_{si}	number of simulations

Time variant reliability:

$\upsilon_S^+(r,t)$	Rate at which load process $S(t)$ crosses barrier level r from below (up-crossing rate)
$\upsilon^+(r,t)$	Corrected up-crossing rate
$\upsilon_A^+(r,t)$	Up-crossing rate of amplitude (envelope) process
$\upsilon_D^+(g,t)$	Failure domain out-crossing rate
$\upsilon_I^+(r,t)$	Conditional up-crossing rate for which the assumption of independence is adequate
$\eta^+(r,t)$	Hypothetical function for which Poisson assumption is exact

$P_f(t)$	Failure probability
$P_S(t)$	Probability of survival
P_{f_0}	Initial failure probability ($t=0$)
$P_f(t\|r)$	Conditional failure probability

μ	Mean of normalized random barrier
σ	Standard Deviation of normalized random barrier
$\upsilon_{ED}^+(\mu,\sigma,t)$	Ensemble up-crossing rate
$\upsilon_{EI}^+(\mu,\sigma,t)$	Conditional ensemble up-crossing rate for which the assumption of independence is exact or.... ...Poissonian arrival rate of first crossing over random barrier.
$E_p(\mu,\sigma,t)$	EUR error parameter
$E_D(\mu,\sigma,t)$	Dependency EUR error
$\overline{E}_D(\mu,\sigma,t)$	Approximated EUR error
$\upsilon_{EC}^+(\mu,\sigma,t)$	Corrected ensemble up-crossing rate
$\overline{E}_D^{TVa}(\mu,\sigma,t)$	Averaged error estimate for time-variant barriers
$\overline{E}_D^{TVr}(\mu,\sigma,t)$	Reduced error estimate for time-variant barriers

Crack Propagation:

$A(t)$	Crack size random process
A_0	Initial crack size
A_{crit}	Critical crack size
A_{th}	Threshold crack size
c	Crack propagation rate (deterministic)
$X(t)$	Unitary crack propagation rate random process
K_{IC}	Critical stress intensity factor
S_y	Yielding stress
ΔS	Stress ranges
m	Crack propagation exponent
ΔK	Stress intensity factor
$Y(a)$	Geometry function
$Q(.)$	Generic crack propagation function
$m(A,t)$	Drift coefficient
$\sigma(A,t)$	Diffusion coefficient
T	Design life or reference time
$T_\mu(a)$	Mean time to grow function
$TTTG(a_0,a)$	Total time to grow function

0.3 Motivation

The technological development experienced in most countries in the post second world war years has been accompanied by a massive build-up of civil infrastructure. This infrastructure includes large fleets of commercial airliners, military aircraft, ships, oil tankers, offshore platforms, pipeline systems, railways, road and railway bridges, re-entry spacecraft, mining equipment, nuclear and conventional power generators, transmission towers, dams, buildings and so many others. This huge amount of structural systems is in the process of ageing, and an increasing number of these structures is facing retirement of service. Perception that the investment in existing facilities and their replacement costs are extremely high are driving governments, regulating agencies, companies, engineers and decision makers alike to face a very concerning question:

"How can the life of ageing infrastructure be safely extended?"

In addition to the life extension problem, it is recognized that in many cases the level of loading of existing structures has exceeded expected design loads, due to increasing demands placed on these structures. Hence, there are potential serviceability and safety concerns about existing structures (Melchers, 2001).

There are significant differences between the design of an yet-to-be-built structure and the assessment of the same structure after many years in service. Whereas design codes tend to be conservative, excess of conservativeness in the assessment of existing structures may predict imminent failure and lead to unnecessary inspections, repairs or condemnation, at very high costs. Probabilistic-based risk assessment can be used to guide the development of codes for the on-going safety management of ageing infrastructure.

Probabilistic-based risk assessment provides a framework to manage the operation of existing structures in consideration of inherent uncertainty, in the absence of past experience, and on an individual basis. Moreover, it provides defensible estimates of the safety of individuals and of the safety and performance of structural systems in accordance to specified minimum safety levels. In probabilistic-based risk assessment, or more specifically in structural reliability analysis, account can be given to the uncertain initial state of a structure, to random or varying structural parameters, to the action and combination of random environmental loads, to operational uncertainty and to further resistance degradation of ageing structures.

The general problem of time-variant structural reliability analysis under resistance degradation has not received as much attention from the structural engineering community as

might be desired. In the chapters that follow, it will be shown that the handling of significant resistance degradation under random loading through existing time-variant reliability techniques poses severe difficulties. These difficulties concern the excessive number of numerical out-crossing rate calculations that are required when limit state functions are not given in closed form, load processes are non-stationary, resistance parameters are uncertain and when there is significant resistance degradation. This thesis addresses and makes some contributions towards time-variant reliability analysis of degrading uncertain structures.

Fatigue and fracture are one of the most important forms of structural degradation, accounting directly or indirectly for 10 to 40% of the US GDP (Fuchs and Stephens, 1977). Fatigue and fracture are the single most common "predictable" cause of failure of engineering structures. It is a particularly important failure mode of metal structures subject to random environmental loading. In the study of fatigue and crack propagation many early researches adopted a deterministic point of view, despite the inherent scatter observed in fatigue experiments and in the field. Today, fatigue and crack propagation are widely accepted to be random phenomena, and adopting a probabilistic standpoint helps understanding of the problem.

In this thesis, contributions are made towards probabilistic-based risk assessment procedures for structures subject to fatigue and fracture under random loading. More specifically, stochastic models of crack propagation are combined with time variant reliability models, providing a framework for risk assessment which accounts for critical crack growth and overload failure modes, and also allows the consideration of non-destructive inspections and repairs.

0.4 Outline

This thesis is divided in two complementary parts. The first half of the thesis is dedicated to time-variant reliability analysis under general forms of resistance degradation, and addresses the ensemble up-crossing rate approximation. In the second half, this approximation is applied to the problem of fatigue and fracture reliability analysis under random loading. The literature review sections are divided accordingly. Literature Review Part I (chapter 1) addresses general time-variant reliability analysis. Literature Review Part II (chapter 7) addresses random fatigue and crack propagation. It is considered that this disposition enhances the clarity of the exposition. At the end of each chapter, a *Concluding Remarks* section summarizes the most important results of that chapter and introduces the topics to be addressed in the following chapter. Figures are grouped consecutively at the end of each chapter.

Part I

TIME VARIANT RELIABILITY ANALYSIS OF DEGRADING UNCERTAIN STRUCTURES

Chapter 1

LITERATURE REVIEW PART I

1.1 Introduction

In the context of structural reliability analysis, time variant reliability analysis involves evaluating the probability that a vector random load process $\mathbf{S}(t)$ exceeds the uncertain or random resistance $\mathbf{R}(t)$ of a structure or structural component at any time during the structure's life:

$$P_f(T) = P\left[\min_{0\leq t\leq T} g(\mathbf{R}, \mathbf{S}, t) \leq 0\right] \tag{1.1}$$

where $g(\mathbf{r}, \mathbf{s}, t) = 0$ defines the failure surface which divides the failure $\{\mathbf{r}, \mathbf{s}|g(\mathbf{r}, \mathbf{s}, t) < 0\}$ and survival $\{\mathbf{r}, \mathbf{s}|g(\mathbf{r}, \mathbf{s}, t) > 0\}$ domains. The problem is depicted in figure 1-1 for a scalar load and resistance.

In this chapter the solution of time variant reliability problems is reviewed, through successive levels of simplification or generalization. First, the first passage failure model for a deterministic or "known" resistance and for a scalar load process is reviewed. This solution is then generalized to include (multi-dimensional) resistance uncertainty or variability. Finally, the generalization of results to multi-dimensional vector load processes is reviewed. The review is focused on those methods which are relevant to the following developments and raises the issues that are addressed in the thesis.

1.2 First passage failure model

A fundamental problem of time variant reliability analysis is the evaluation of the probability that a random load process exceeds the resistance of a structure at any time during its (design) life (figure 1-2). In the first passage model, failure is characterized at the first time such overload occurs. The probability of survival of the structure up to a time $t = T$ is thus

given by the probability that the load process $S(t)$ starts in the safe domain at $t = 0$ and does not exceed resistance level r during this time interval (Melchers, 1999):

$$P_S(r,T) = P[N_S^+(r,T) = 0 | S(0) < r] \cdot P[S(0) < r] \tag{1.2}$$

where $N_S^+(r,t)$ is the number of up-crossings of barrier level r by process $S(t)$ and $P[S(0) < r] = P_{S_0}(r)$ is the probability that the process $S(t)$ starts in the safe domain at $t = 0$, i.e., the initial probability of survival.

The term $P[S(0) < r]$ is the complement of the initial failure probability ($P[S(0) < r] = 1 - P_{f_0}(r)$), which can be solved through well researched time invariant reliability techniques, such as the First and Second Order Reliability Methods (FORM and SORM). The major difficulty in evaluating $P_S(r,T)$ is evaluation of term $P[N_S^+(r,T) = 0 | (S(0) < r)]$. A common assumption (and a first approximation) is to consider the number of up-crossings of barrier level r to follow a Poisson counting process. With this assumption, the time interval between successive up-crossings becomes independent, and the number of up-crossings follows a Poisson distribution (Cramer and Leadbetter, 1967):

$$P[N_S^+(r,T) = 0 | S(0) < r] \approx P[N_S^+(r,T) = 0] = \frac{[\upsilon_S^+(r)T]^0}{0!} \exp[-\upsilon_S^+(r)T] = \exp[-\upsilon_S^+(r)T] \tag{1.3}$$

where $\upsilon_S^+(r)$ is the rate at which load process $S(t)$ exceeds barrier level r, also called the up-crossing rate. With the so-called Poisson approximation, equation (1.2) becomes:

$$P_S(r,T) = \exp[-\upsilon_S^+(r)T] \cdot P_{S_0}(r) \tag{1.4}$$

The failure probability up to time T is the complement of equation (1.4):

$$P_f(r,T) = 1 - P_S(r,T) = P_{f_0}(r) + (1 - P_{f_0}(r)) \cdot (1 - \exp(-\upsilon_S^+(r)T)) \tag{1.5}$$

When barrier level r is not constant ($r = r(t)$) or when the load process $S(t)$ is smoothly non-stationary, the up-crossing rate becomes a function of time and term $\upsilon_S^+(r)T$ in the formulation above is replaced by $\int_0^T \upsilon_S^+(r,t)dt$:

$$P_f(r,T) = P_{f_0}(r) + (1 - P_{f_0}(r)) \cdot (1 - \exp(-\int_0^T \upsilon_S^+(r,t)dt)) \tag{1.6}$$

Hence, evaluation of failure probabilities becomes a problem of evaluating up-crossing

rates. For a stationary scalar Gaussian process and a time-invariant barrier, for example, one has:

$$\upsilon_S^+(r) = \upsilon_0 \exp\left(-\frac{1}{2}\left(\frac{r-\mu_S}{\sigma_S}\right)^2\right) \tag{1.7}$$

where $\upsilon_0 = \frac{w_0}{2\pi}$ is the mean crossing rate, $w_0 = \sqrt{\frac{\lambda_2}{\lambda_0}} = \frac{\sigma_{\dot{S}}}{\sigma_S}$ and the λ_i are spectral moments.

1.3 Conditional up-crossing rates

The Poisson approximation is said to be asymptotically exact as the barrier level goes to infinity (Cramer and Leadbetter, 1967). It is usually appropriate for high barrier levels (high reliability structures), since barrier up-crossings are rare, but it becomes less appropriate as the barrier level decreases. The Poisson assumption is not adequate for very narrowband processes, as the up-crossings tend to occur in clumps. These limitations can be overcome by adapting expressions like (1.7), so as to make the Poisson assumption of independence more appropriate, using techniques such as these described by Ditlevsen (1986) and Vanmarcke (1975). A proper interpretation of Poissonian up-crossing rates can be obtained from a closer examination of equation (1.4). Assume that there exists a function $\eta_s^+(r,t)$ for which equation (1.4) is exact, rather than just an approximation:

$$P_S(r,t) = P_S(r,0) \cdot \exp\left[-\int_0^t \eta_s^+(r,s)ds\right] \tag{1.8}$$

Taking the derivative of (1.8) with respect to time, one obtains (Lutes and Sarkani, 1997):

$$\frac{\partial}{\partial t}P_S(r,t) = P_S(r,t) \cdot \eta_s^+(r,t) \tag{1.9}$$

from which $\eta_s^+(r,t)$ is obtained as:

$$\begin{aligned}
\eta_s^+(r,t) &= \frac{1}{P_S(r,t)}\frac{\partial}{\partial t}P_S(r,t) \\
&= \frac{1}{P_S(r,t)}\lim_{\Delta t\to 0}\left(\frac{P_S(r,t)-P_S(r,t+\Delta t)}{\Delta t}\right) \\
&= \lim_{\Delta t\to 0}\left(\frac{1}{\Delta t}\frac{P_f(r,t+\Delta t)-P_f(r,t)}{1-P_f(r,t)}\right)
\end{aligned} \tag{1.10}$$

From equation (1.10) one can describe $\eta_s^+(r,t)$ as:

$$\eta_s^+(r,t) = \lim_{\Delta t\to 0} P[\text{occurrence of one up-crossing in } (t,t+\Delta t) \text{ given that:} \tag{1.11}$$

(1) $S(0) < r$ and

(2) no up-crossings occur before t]

...or the limit, as Δt goes to zero, of the probability of occurrence of one up-crossing in the interval $(t, t + \Delta t)$ given that the load process starts in the safe domain and has no up-crossings prior to t.

From equation (**??**) it can be seen that the usual Poisson assumption, which makes:

$$\eta_s^+(r,t) = \upsilon_s^+(r) \tag{1.12}$$

is only a (first) approximation, which completely neglects the initial condition and the conditioning to no prior up-crossings. The original Poisson approximation can therefore be improved by making $\upsilon_s^+(r)$ reflect these conditions.

The first of these improvement accounts, in an approximate way, for the initial condition $S(0) < r$. The time between successive up-crossings is composed of two segments, T_a and T_b, which are the times spent above and below level r, respectively (figure 1-3). In the usual Poisson approximation, the time between successive up-crossings $(T_a + T_b)$ is assumed independent, hence exponentially distributed, and the average time between successive up-crossings becomes (Ditlevsen, 1986):

$$E[T_a + T_b] = \frac{1}{\upsilon_S^+(r)} \tag{1.13}$$

since $\upsilon_S^+(r)$ can be seen as the arrival rate of up-crossings. The long-run fraction of time that process $S(t)$ spends below level r is:

$$\frac{E[T_b]}{E[T_a + T_b]} = \int_{-\infty}^{r} f_S(s)ds = F_S(r) \tag{1.14}$$

where the expected value is over the ensemble and asymptotic over time for $t \to \infty$. Combining equations (1.13) and (1.14) one obtains:

$$E[T_b] = \frac{F_S(r)}{\upsilon_S^+(r)} \tag{1.15}$$

When the barrier level r is low and it is known that $S(0) < r$, the time until the first up-crossing is expected to be significantly smaller than the time between successive up-crossings $(T_a + T_b)$. Since the time until the first up-crossing is also a time spent below level r, it is better to approximate it by T_b rather than by $(T_a + T_b)$. It is difficult to derive an exact expression for T_b, however. To assume time intervals T_b to be independent and exponentially

distributed conflicts with placing the same assumption on $T_a + T_b$, but it can be done as an approximation. With this approximation, the arrival rate becomes:

$$\eta_s^+(r,t) = \frac{1}{E[T_b]} = \frac{\upsilon_S^+(r)}{F_S(r)} \tag{1.16}$$

This is an improvement of equation (1.12) which takes into account the initial condition. The approximation of equation (1.16) actually improves $\upsilon_s^+(r)$ for low barrier levels, but has little effect for $r \to \infty$ as $F_S(r) \to 1$.

For narrow-banded processes, the up-crossings tend to occur in clumps as, due to the slow varying amplitude of the process, one up-crossing of level r at a time t_1 is very likely to be followed by another up-crossing one period later (figure 1-4) . The original Poisson assumption becomes excessively conservative. However, each clump of up-crossings of level r by process $S(t)$ represents a single up-crossing of level r by the envelope or amplitude process $A(t)$. In this case, equation (1.12) becomes (Vanmarcke, 1975):

$$\eta_s^+(r,t) = \upsilon_A^+(r) \tag{1.17}$$

The envelope up-crossing rate, using Cramer and Leadbetter's (1966) definition of amplitude, is: $\upsilon_A^+(r) = qr\sqrt{2\pi}\upsilon_S^+(r)$, where $q = \sqrt{1 - \lambda_1^2/\lambda_0\lambda_2}$ is a bandwidth parameter and λ_i are the spectral moments. Equation (1.17) can be up-dated to take into account the initial condition. Following previous assumptions, one obtains:

$$\eta_s^+(r,t) = \frac{\upsilon_A^+(r)}{F_A(r)} \tag{1.18}$$

Equation (1.18) is appropriate for very narrow-band processes and low barrier levels. For broad-banded processes and high barrier levels, however, up-crossings by the amplitude process are not necessarily followed by up-crossing by $S(t)$ itself, and the number of amplitude crossings becomes larger than the actual number of $S(t)$ crossings. However, since equation (1.12) is appropriate for broad-band processes and high barrier levels, it is possible to make an interpolation between these two results. By estimating the fraction of qualified amplitude crossings (i.e., amplitude up-crossings that are indeed followed by at least one up-crossings by $S(t)$), Vanmarcke (1975) derived an approximation for the mean clump size (i.e., the average number of $S(t)$ up-crossings per clump) for a Gaussian load process:

$$E[N_{S_{pc}}^+(r)] = \frac{1}{1 - \exp(-qr\sqrt{2\pi})} \tag{1.19}$$

For narrow band processes and low barrier levels, product qr is small and $E[N^+_{S_{pc}}] \approx \frac{\upsilon^+_S(r)}{\upsilon^+_A(r)} = \frac{1}{qr\sqrt{2\pi}}$. For broad band processes and increasing barrier levels product $qr \to \infty$ and $E[N^+_{S_{pc}}] \to 1$. If the qualified amplitude crossings are assumed to follow a Poisson counting process, the arrival rate of qualified amplitude crossings or arrival rate of clumps of $S(t)$ crossings becomes:

$$\eta^+_s(r,t) = \upsilon^+_S(r)\frac{1}{E[N^+_{S_{pc}}(r)]} = \upsilon^+_S(r)(1-\exp(-qr\sqrt{2\pi})) \tag{1.20}$$

Including the initial condition, equation (1.20) becomes:

$$\eta^+_s(r,t) = \upsilon^+_S(r)\frac{(1-\exp(-qr\sqrt{2\pi}))}{F_S(r)} \tag{1.21}$$

Equation (1.21) takes into account clumps of up-crossings of narrow-band processes. However, even clumps of $S(t)$ up-crossings (or amplitude crossings) do occur in clumps. The clumping of clumps of up-crossings can be taken into account, in an approximate way, by replacing parameter q by q^b in equation (1.21), with parameter $b \approx 1.2$ being obtained from MC simulation results (Vanmarcke, 1975):

$$\eta^+_s(r,t) = \upsilon^+_S(r)\frac{(1-\exp(-q^{1.2}r\sqrt{2\pi}))}{F_S(r)} \tag{1.22}$$

Equation (1.22), herein referred to as Vanmarcke's up-crossing rate approximation, is valid for continuous Gaussian processes of any bandwidth and has no limitations regarding barrier level. It can also be written in terms of up-crossing rates as:

$$\eta^+_s(r,t) = \upsilon^+_S(r)\frac{1-\exp[\frac{\upsilon^+_A(r)}{\upsilon^+_S(r)}]}{1-\frac{\upsilon^+_S(r)}{\upsilon^+_S(0)}} \tag{1.23}$$

1.4 Random resistance and/or system parameters

Solution to the First Passage failure model just reviewed involved a deterministic barrier level (resistance). In typical structural engineering problems, resistance is random. Hence, a random barrier level has to be included in the First Passage failure model.

1.4.1 Resistance versus system parameters

In time variant structural reliability analysis, the role of random resistance parameters and the role of random system parameters is, for computational purposes, the same. Since the focus of this thesis is on structural degradation problems, "resistance" and "system" parameters

will be simply referred to as "resistance" parameters. In contrast, in problems of random vibration the focus is generally on random system parameters.

In typical structural analysis problems, loads are characteristically random processes of time, whereas resistance or system parameters can be modelled as random variables or, in some instances, as slow varying random processes of time. The distinction between "load" and "resistance" parameters, however, goes beyond the effect of these variables on the structure. It is often the case that random processes are modelled as "loads", whereas random variables are modeled as "resistance" or "system" parameters. Hence, random resistance parameters include all random parameters of the problem which are not modelled as "loads". This can include material properties, geometry variables, statistical estimates, model uncertainty, as well as uncertain parameters of the random load processes.

1.4.2 Random resistance degradation models

The resistance of real structures is typically random or uncertain, and this uncertainty can play a significant role in the failure of a structure. Structures experience resistance degradation over time, which can affect their on-going safety. The First Passage failure model just reviewed considered a deterministic (known) barrier level $r(t)$. In order to obtain a more realistic failure model, random resistance has to be incorporated in the solution. The way in which this is done can depend on how random resistance is described or modelled. Hence, a distinction is made here between parametrically defined random process resistance models and general random process resistance models.

In parametrically defined random process resistance models, resistance uncertainty or randomness is described by a vector of initial condition random variables $\mathbf{R}_0$ and a deterministic degradation function $\deg(t)$:

$$R(t) = \deg(t) \cdot f(\mathbf{R}_0) \tag{1.24}$$

For such models, a distinct resistance degradation time-history $r(t)$ is obtained for every outcome $\mathbf{R}_0 = \mathbf{r}_0$ of the models random variables (as illustrated in figure 1-5). The mechanical resistance degradation solution $\deg(t)$ is deterministic, and hence a multitude of deterministic algorithms and codes (e.g., finite element analysis) can be used directly in the reliability evaluation. Because the uncertainty in the resistance is completely described by a vector of random variables, these models can also be called "random variable" resistance degradation models. Such models are used, for example, in random vibration analysis, to describe system

parameter uncertainty (Igusa and Kiureghian, 1988; Cherng and Wen, 1994). Clearly, for problems with no resistance degradation, one has $\deg(t) = 1$.

In more general problems, where resistance can be affected by random factors occurring during the structure's life, resistance is more properly modelled as a slow varying random process of time. Such resistance variation can be described by a Transition Probability Density function $f_R(r,t)$, or TPD in short. Evaluation of the TPD involves solution of a stochastic resistance degradation model. A typical example of random process resistance degradation is crack propagation under random loading, when the crack propagation rate is modeled as a random process of time (Beck and Melchers, 2002). This includes a multitude of Diffusive Markov crack propagation models (Ortiz, 1984; Madsen et al., 1986; Yang et al., 1987; Itagaki et al., 1992; Sobczyk and Spencer, 1992 and others). The problem is addressed in detail in the second part of this thesis. Another example of random process resistance degradation is fatigue induced stiffness degradation (Sobczyk and Trebicky, 2000).

In some cases, it may be possible to describe general random process resistance degradation models by some approximate expression with the form of equation (1.24). If this is the case, deterministic solution methods can be used to solve the mechanical part of the problem. However, such approximation is not always possible and, in many instances, it is not desirable. As will be shown in the sequel, the reliability analysis based on random process models can eventually be simpler and easier than using an equivalent parametric random process model. The opposite is more likely, i.e., one can always use the deterministic resistance degradation function of random variable degradation models to project the percentiles of the initial resistance distribution, hence deriving a TPD description for the random variable resistance degradation model.

1.4.3 Random variable resistance and Fast Probability Integration

For random variable or parametrically defined random process resistance degradation problems, or in problems with no resistance degradation at all, a distinct barrier $r(t)$ is obtained for every outcome $\mathbf{R} = \mathbf{r}$ of the resistance random variables (as illustrated in figure 1-5). A conditional First Passage failure probability (equation 1.6) is obtained for each outcome $\mathbf{r}$:

$$P_f(T \mid \mathbf{r}) = P_{f_0}(\mathbf{r}) + (1 - P_{f_0}(\mathbf{r})) \cdot (1 - \exp(-\int_0^T \upsilon^+(\mathbf{r}, s)ds)) \tag{1.25}$$

The overall or unconditional failure probability is then obtained by integrating the conditional failure probability over the resistance distribution:

$$P_f(T) = \int_{\mathbf{R}} P_f(T \mid \mathbf{r}) f_{\mathbf{R}}(\mathbf{r}) d\mathbf{r} \tag{1.26}$$

This integration can, in principle, be performed by simulation. Of course, each integration point of (1.26) represents a complete time-variant reliability analysis for a fixed barrier level. It will be seen in the sequel that, for multi-dimensional problems, and when the dimension of $\mathbf{R}$ is large, direct integration becomes prohibitive.

The failure probability in equation (1.26) can be approximated by FORM or SORM, using Wen and Chen's (1987) Fast Probability Integration technique. This technique introduces an auxiliary variable $u_{n+1} = \Phi^{-1}[P_f(T \mid \mathbf{r})]$, and solves for the augmented limit state function:

$$g^+(\mathbf{u}^+) = u_{n+1} - \Phi^{-1}\left[P_f(T \mid \mathbb{T}^{-1}(\mathbf{u}))\right] \tag{1.27}$$

where $\mathbf{u} = \mathbb{T}(\mathbf{r})$ is the transformation to the standard normal space, $\Phi[]$ is the Gaussian cumulative distribution function and $\mathbf{u}^+$ is the vector $\mathbf{u}^+ = \{u_{n+1}, u_n, u_{n-1}, ..., u_1\}^T$. A Fast Probability Integration solution by FORM using the HLRF algorithm is presented in appendix (section 1.8.1).

The Fast Probability Integration formulation is equivalent to finding a design point in $\mathbf{R}$ where the time-dependent performance function $h(\mathbf{r}, S, t)$ attains its minimum (Madsen, 1986):

$$P_f(T \mid \mathbf{r}) = P\left[\min_{0 \le t \le T} h(\mathbf{r}, S, t) \le 0\right] \tag{1.28}$$

where the auxiliary variable is $R_{n+1} = \min_{0 \le t \le T} h(\mathbf{r}, S, t)$.

Computation of the failure probability through equation (1.27) requires $(n_{rv} + 1) * n_{conv}$ computations of the deterministic resistance degradation function, where n_{rv} is the number of resistance random variables and n_{conv} is the number of iterations for convergence of the algorithm associated with solution of (1.27). This solution is restricted to a particular evaluation time, and has to be completely repeated if the failure probability is to be evaluated over the lifetime of the structure. The total computation time may hence become prohibitive, even when using FORM, if resistance degradation is computed numerically (e.g., finite element analysis). Some convergence problems may also be encountered due to the very small conditional failure probabilities (Rackwitz, 1993; Marley and Moan, 1994).

It is seen that random resistance parameters add a significant level of difficulty to the analysis. In the formal solution to the problem, crossing rates are integrated over time, and conditional failure probabilities are integrated over random resistance parameters. Significant simplification is achieved when this order of integration is changed, as follows.

1.4.4 Random resistance and the ensemble up-crossing rate approximation

Solution of the First Passage failure model with a random barrier can be significantly simplified by changing the order of integration over time and over random resistance parameters. In the so-called "ensemble" up-crossing rate approach (Wen and Chen, 1989), the up-crossing rate for a deterministic barrier level r is integrated over the resistance distribution:

$$\upsilon^{+}_{ED}(t) = \int_{R} \upsilon^{+}(r,t) f_R(r,t) dr \tag{1.29}$$

If crossings of the random barrier can now be assumed independent, integration over time is straightforward and one obtains:

$$P_f(t) = P_{f_0}(R) + (1 - P_{f_0}(R)) \cdot (1 - \exp(-\int_0^t \upsilon^{+}_{ED}(s) ds)) \tag{1.30}$$

The Ensemble Up-crossing Rate approximation (EUR in short) consists of approximating the arrival rate of up-crossings over the random barrier by the ensemble average of up-crossings (Pearce and Wen, 1984). Following Wen and Chen (1989), the solution is an approximation since:

> "The resistance variables remain the same rather than change independently from one load application to the next, as would be expected in a Poisson failure process. Neglecting this dependence through the resistance generally leads to an overestimation of the failure probability."

Hence, averaging over the resistance makes the ensemble up-crossing rates dependent, and to stress this fact, the subscript $_{ED}$ - for Ensemble and Dependent - is used in equation (1.29). The direct implication of this dependency is that the Poisson assumption of independent up-crossings (implied in expression 1.30) has to be reviewed. To the author's knowledge, no systematic consideration has been given to this problem. The issue is addressed in detail in chapter (3).

Based on the current level of understanding of the problem, it is assumed that (Pearce and Wen, 1984; Wen and Chen, 1989; Schall et al., 1991):

1. EUR errors are proportional to failure probabilities;
2. the EUR approximation is appropriate for very small failure probabilities but excessively conservative otherwise;
3. the approximation is appropriate for even higher barrier levels and even lower failure probabilities as compared with deterministic barrier problems;

A closer look at the problem, however, suggests that the EUR approximation would be:

1. appropriate for small variances of the random barrier or, more specifically, a function of the relative magnitude between the variance of the resistance and the variance of the load process (σ_R^2/σ_S^2);

2. affected by the appropriateness of the assumption of independence in the original (deterministic) up-crossing rates $\upsilon_S^+(r)$;

3. more appropriate for partially correlated random process barriers than for fully correlated (parametric) barriers.

4. better in the case of time-variant than of time-invariant random barriers, as a variation in the barrier should reduce the dependency error;

Statement 1 is based on the fact that, for zero variance of the random barrier, the EUR solution should be the same as the First Passage solution for a deterministic barrier. This and other expectations are examined in detail in chapters 3 and 5.

Advantages of the EUR approximation, in comparison to other solutions, will be made evident in the sequel.

Equation (1.29) is a formal representation of the EUR approximation for scalar problems. It is very appropriate for problems involving general random process resistance degradation, as it is based explicitly on an integration over the resistance distributions ($f_R(r,t)$). The solution, however, is easily generalized for multi-dimensional problems involving random process or parametric resistance degradation. For multi-dimensional problems, the integration in (1.29) is not necessarily done explicitly. Broadly speaking, ensemble up-crossing rates are obtained whenever a random safe domain boundary is considered in the out-crossing rate integration (section 1.6 in the sequel).

1.4.5 Random barrier probability bounds

As was noted earlier in this literature review, the main difficulty in evaluating failure probabilities in time variant reliability problems is evaluation of the term $E[N_S^+(r,T)]$, i.e. the expected number of up-crossings in a given time interval. It was shown how, for a deterministic barrier, this quantity can be approximated from the up-crossing rate by means of the Poisson assumption of independence. For random barriers, the problem acquires an new dimension. Re-writing equation (1.6) explicitly in terms of random resistance R:

$$P_f(R,T) = P_{f_0}(R) + (1 - P_{f_0}(R)) \cdot (1 - \exp(-E[N_S^+(R,T)])) \tag{1.31}$$

Solution of (1.31) for random barriers generally involves some conservative estimation of $E[N_S^+(R,T)]$. An upper bound for the failure probability can always be obtained as:

$$\begin{aligned} P_f(T) &\lesssim (1-\exp(-E[N_S^+(R,T)])) \\ &\lesssim E[N_S^+(R,T)] \end{aligned} \tag{1.32}$$

Equation (1.32) is always an upper bound to the failure probability, regardless of how conservative the estimate of $E[N_S^+(R,T)]$ is. However, the near equality only holds when $P_{f_0}(R) \approx 0$, when $(1-\exp(-E[N_S^+(R,T)]))$ is very small and when the estimate $E[N_S^+(R,T)]$ is not too conservative. Hence, the problem is still to obtain an appropriate estimate for $E[N_S^+(R,T)]$.

Schall et al. (1991) provide some important insight into how this is done in problems involving a non-ergodic random (variable) resistance vector $\mathbf{R}$ and a sequence of stationary ergodic sea states, characterized by the sequence $\mathbf{Q} = \{Q_1, Q_2, ...Q_n\}^T$. The authors present the following results:

$$\begin{aligned} P_f(T) &\simeq 1 - E_{\mathbf{R}}[\exp(-E_{\mathbf{Q}}[N_S^+(\mathbf{R},\mathbf{Q},T)])] \\ &\lesssim 1 - \exp(-E_{\mathbf{R}}[E_{\mathbf{Q}}[N_S^+(\mathbf{R},\mathbf{Q},T)]]) \qquad (1.33) \\ &\gtrsim 1 - E_{\mathbf{R}}[E_{\mathbf{Q}}[\exp(-N_S^+(\mathbf{R},\mathbf{Q},T))]] \qquad (1.34) \end{aligned}$$

where $E[.]$ is the expectation over the indicated variables. The upper and lower bounds are referred to as the "inside" and the "outside" integration scheme, respectively, whereas the first line represents the appropriate integration order for the problem considered by the authors.

It can be seen that the Fast Probability Integration solution represents the (appropriate) outer integration scheme for $\mathbf{R}$-type random barriers. The ensemble up-crossing rate approximation, on the other hand, represents an "inside" integration (or upper bound to P_f), with the additional approximation that the expectation over $\mathbf{R}$ is taken inside the integral over time:

$$E_{\mathbf{R}}[N_S^+(\mathbf{R},T)] < \int_0^T E_{\mathbf{R}}[\upsilon^+(\mathbf{R},t)]dt \tag{1.35}$$

and hence the bound in (1.33) becomes even wider.

Although the outside integration is the appropriate scheme for $\mathbf{R}$-type random barriers, there are situations where significant simplification is achieved by means of the EUR approximation. One important and very general example is multi-dimensional problems involving

resistance degradation, as will be seen in the sequel.

Another interesting situation is that where the random barrier is a slow-varying random process of time. Such situation arises when the correlation length of the random barrier is greater than the correlation length of the load process, but smaller than ∞. In other words, the barrier is a slow-varying random process of time, as compared with the load process. This situation is in-between the fully correlated barrier (**R**-type) and that of an uncorrelated barrier. The solution for an uncorrelated barrier could perhaps be approximated by the solution for "**Q**" variables in the formulation above, and one could expect the EUR approximation to be more appropriate (at least in comparison to random variable barriers). This situation is explored in chapter 6.

1.5 Simplified solutions for stationary problems

1.5.1 The time-integrated approach

When the time-variant reliability problem involves a single (scalar) load process, the load process is stationary and the barrier level is constant ($\mathbf{r}(t) = \mathbf{r}$), integration over time (equation 1.6) can be transferred to the load process, converting the problem into a time-invariant one. If the load process starts in the safe domain and has no up-crossings of barrier level r in time interval ($0 \leq t \leq T$), then the maximum value of the load process in that time interval is also less than r. Since $S(t)$ is a random process, its maximum value in time interval $(0, T)$ is the random variable $S_T(s)$, described by an extreme value distribution $f_{S_T}(s)$ (section 1.8.2). The failure probability is then given by the probability that the extreme value $S_T(s)$ be larger than the resistance:

$$P_f(T) = P[S_T(s) \geq f(\mathbf{R})]$$

where $f(.)$ is a functional relationship that relates resistance variables with a scalar resistance measure, in terms of loads (the collapse load, for example). The limit state function for this problem becomes:

$$g(\mathbf{R}, S_T) = f(\mathbf{R}) - S_T(s) = 0 \tag{1.36}$$

and the failure probability is given by the multi-dimensional integration over the joint probability distribution of $\mathbf{R}$ and $S_T(s)$:

$$P_f(T) = \int_{g(\mathbf{r},s)\leq 0} f_{\mathbf{R},S_T}(\mathbf{z})d\mathbf{z} \tag{1.37}$$

Equation (1.37) can be solved through time-invariant reliability techniques such as FORM and SORM.

The time integrated approach is completely equivalent to the up-crossing solution (equation 1.6) for a scalar and stationary load and time-invariant resistance. When more than one load process is involved, a load-combination problem exists.

1.5.2 Turkstra's load-combination rule

The load combination problem is a special case of the out-crossing problem which arises when the probability distribution of the combined effect of two or more stochastic loads is sought (Melchers, 1999). A complete review of the load combination problem is out of the scope of this literature review. Instead, attention is focused on a deterministic load combination rule by Turkstra (1970), which leads to a very simple time-invariant approximation to the stochastic load combination problem. This rule addresses the maximum value of a load process formed by a linear sum of n component processes:

$$X(t) = X_1(t) + X_2(t) + \ ... \ + X_n(t) \tag{1.38}$$

It can be derived from a consideration of a combination of Borges processes (Turkstra and Madsen, 1980) or from the "point-crossing" formula (Larrabee and Cornell, 1979). Loosely, it states that the maximum of $X(t)$ can be approximated from combinations of the maximum of one component load $X_i(t)$ added to the "arbitrary point-in-time" value $\widetilde{X}_j(t)$ of the remaining loads:

$$\max X \approx \max_{i=1}^{n} \left(\max X_i + \sum_{j=1, j\neq i}^{n} \widetilde{X}_j \right) \tag{1.39}$$

A time-invariant reliability problem can be formulated based on the rule. In this formulation, the extreme value probability distribution of one of the component load processes is considered in combination with the "arbitrary point-in-time" distribution of the remaining loads. A total of n time-invariant reliability problems are obtained, as the extreme value of each of the load components has to be considered at a time. The overall probability of failure is the largest P_f among the n combinations. The limit state functions for the n time-invariant

reliability problems are:

$$g_i(\mathbf{R}, \mathbf{X}) = f(\mathbf{R}) - X_{T_i} - \sum_{j=1, j\neq i}^{n} \widetilde{X}_j = 0 \tag{1.40}$$

where X_{T_i} is the extreme value of load process i in time interval $(0, T)$ and $\widetilde{X}_j$ is the "arbitrary point-in-time" distribution of load process j.

Since expression (1.39) is unconservative, the actual failure probability is larger than the largest P_f among the n combinations. Hence, the solution is potentially inaccurate, although suitable for code calibration due to its simplicity. Of course, a conservative upper bound to the P_f can always be obtained if one assumes the extreme values of all load components to coincide:

$$g_{ub}(\mathbf{R}, \mathbf{X}) = f(\mathbf{R}) - \sum_{i=1}^{n} X_{T_i} = 0 \tag{1.41}$$

1.6 General solutions for multi-dimensional problems

The First Passage failure probability model reviewed earlier can be generalized to non-stationary problems involving more than one load process. In the context of Structural Reliability, these problems are referred to as multi-dimensional or multi-variate problems, in contrast to scalar problems involving a single load process. The up-crossing rate concept is generalized to that of an out-crossing rate, i.e., the rate at which the random vector load process crosses out of a safety domain.

Multi-variate solutions for out-crossing rates are generally based on a generalization of a classic result by Rice (1954), which gives the up-crossing rate for a scalar load process and a given barrier level r as:

$$\begin{aligned} \upsilon_S^+(r) &= \int_{S(\mathbf{t})=r} E[\dot{S}|\ S(t) = s]^+\ f_S(s) ds \\ &= \int_0^\infty x\ f_{S\dot{S}}(r, x) dx \end{aligned} \tag{1.42}$$

where $E[.]^+$ is the expectation over positive values and $f_{S\dot{S}}(s, \dot{s})$ is the joint probability distribution of $S(t)$ and its time-derivative $\dot{S}(t)$.

For the multi-dimensional problem, Rice's result is generalized as (Belyaev, 1968):

$$\begin{aligned} \upsilon_D^+(\mathbf{s}) &= \int_{g(\mathbf{s})=0} E[\dot{\mathbf{S}}|\ \mathbf{S}(t)=\mathbf{s}]^+\ f_{\mathbf{S}}(s)ds \\ &= \int_{g(\mathbf{s})=0}\int_0^\infty x\ f_{\mathbf{S}\dot{\mathbf{S}}}(s,x)\,dx\,ds \end{aligned} \tag{1.43}$$

where $\mathbf{S}(t)$ is a vector load process, $D_f = \{\mathbf{s}|g(\mathbf{s}) \leq 0\}$ is the failure domain, $g(\mathbf{s}) = 0$ is the failure domain boundary (also called failure surface) and $E[\dot{\mathbf{S}}|\ \mathbf{S}(t)=\mathbf{s}]^+\ f_{\mathbf{S}}(s)$ is the local (out)-crossing rate. Evaluation of the mean out-crossing rate through equation (1.43) is not a straightforward task. Some closed form results exist for stationary Gaussian load processes and for geometrically simple failure surfaces (several references in Hagen and Tvedt, 1991; Melchers, 1999). The solution becomes increasingly involved when (not necessarily in this order):

1. the failure surface or limit state function is not given in closed form but is numerical (eg. finite element model);
2. the failure surface is uncertain (i.e., when it is a function of resistance/system random variables);
3. the failure surface is time dependent (problem of resistance degradation);
4. the load processes are not stationary;
5. the load processes are non-Gaussian.

When the failure surface is time dependent and/or when the load processes are not stationary, out-crossing rates in eq. (1.43) become time dependent. Hence, integration of local out-crossing rates over the failure surface has to be repeated over time. When the failure surface is uncertain, out-crossing rates in eq. (1.43) become conditional crossing rates, conditional to a particular outcome $\mathbf{R} = \mathbf{r}$ of the resistance random variables. Generalizing (1.43) for a time-variant resistance one obtains:

$$\upsilon_D^+(\mathbf{r},t) = \int_{g(\mathbf{r},\mathbf{t})=\mathbf{0}} E[(\dot{\mathbf{S}}-\dot{g}(\mathbf{r},\mathbf{t}))|\ \mathbf{S}(t)=\mathbf{s}]^+\ f_{\mathbf{S}}(s)ds \tag{1.44}$$

The unconditional failure probability is obtained by taking the expectation over the resistance random variables, just as in the scalar case. Putting it all together and neglecting P_{f_0}, solution

of a typical problem becomes:

$$P_f(T) \simeq \int_{\mathbf{R}} \left\{ 1 - \exp\left[- \int_0^T \left(\int_{g(\mathbf{r},\mathbf{t})=\mathbf{0}} \left\{ \int_0^\infty x \; f_{\mathbf{S}\dot{\mathbf{S}}}(s,x) dx \right\} ds \right) dt \right] \right\} f_{\mathbf{R}}(\mathbf{r}) d\mathbf{r} \qquad (1.45)$$

This solution can be described as a nested integration of (1) local out-crossing rates over (2) conditional failure surfaces, over (3) time and over (4) resistance random variables. The difficult nested integration in (1.45) was written explicitly to stress the point that solution becomes very involved. If the failure surface is numerical or if it cannot be approximated by any of the simple geometrical forms for which closed form solutions are available, solution of equations (1.44 and 1.45) has to be performed numerically. Some of these solutions are reviewed in the sequel.

1.6.1 Nested FORM/SORM

When the components of the random load vector are stationary and ergodic Gaussian processes, computation of out-crossing rates through equation (1.43) can be simplified by approximating the failure surface by a linear or quadratic surface at a FORM-type linearization point (Madsen and Tvedt, 1990). This allows the mean out–crossing rate to be approximated analytically. For the linear approximation, for example, one obtains:

$$\upsilon_D^+(\beta) \approx \frac{1}{2\pi} \frac{\sigma_{\dot{V}}}{\sigma_V} \exp\left(-\frac{1}{2} \frac{\beta^2}{\sigma_V^2} \right) \qquad (1.46)$$

where $\beta = \alpha^T \cdot \mathbf{u}_s^*$ is the reliability index, $V(t) = \alpha^T \cdot \mathbf{U_S}(t)$ is the load process in direction α^T, $\mathbf{u}_s = \mathbb{T}(\mathbf{s})$ is a transformation to the standard Gaussian space, $\mathbf{U_S}(t)$ is the standard Gaussian load vector, α^T are direction cosines at point $\mathbf{u}_s^*$ and, finally, $\mathbf{u}_s^*$ is the solution to the optimization problem:

$$\begin{aligned} \text{minimize:} \quad & |\mathbf{u}_s| \\ \text{subject to:} \quad & g(\mathbf{u}_s) = 0 \end{aligned} \qquad (1.47)$$

The Fast Probability Integration technique can be employed to take the expectation over the resistance random variables. This converts the two outer integrations in equation (1.45) in an augmented FORM problem:

$$\begin{aligned} \text{minimize:} \quad & |(\mathbf{u}_r, u_{n+1})| \\ \text{subject to:} \quad & g(\mathbf{u}_r, u_{n+1}) = 0 \end{aligned} \tag{1.48}$$

where $\mathbf{u}_r = \mathbb{T}(\mathbf{r})$ is the standard Gaussian resistance vector and $u_{n+1} = \Phi^{-1}\left[P_f(T \mid \mathbb{T}^{-1}(\mathbf{u}_r))\right]$ is an auxiliary variable.

Hence, a nested application of FORM (or SORM) is obtained. Such a nested solution can be quite involved numerically and is suitable only for small variabilities in $\mathbf{R}$ (Rackwitz, 1994). For non-stationary loads or time-variant limit state functions, the inner FORM integration has to be repeated over time, the numerical effort implied in the nested FORM solution may become prohibitive and results may become unreliable.

1.6.2 Directional simulation

A distinct numerical solution to the problem stated in equation (1.45) is obtained by directional simulation (Melchers, 1992). In this solution, a scalar problem is obtained for each simulated direction α. The scalar problem is solved analytically or by radial sampling. The failure probability is obtained by averaging scalar solutions over the simulated directions α:

$$P_f(T) = \int_A f_A(\alpha) \left[\int_R P_f(v|\alpha) \cdot f_{V|A}(v|\alpha) dv \right] d\alpha \tag{1.49}$$

with $V = R/A + cte$ being a radial variable. This solution involves evaluation of the resistance distribution in each simulated direction α, $f_{V|A}(v|\alpha)$ and the directional probability of failure:

$$P_f(v|\alpha) = P_{f_0}(v|\alpha) + \left(1 - \exp\left[-\int_0^T v_D^+(v|\alpha) dt\right]\right) \tag{1.50}$$

where:

$$v_D^+(v|\alpha) = E[\dot{S}(t) \cdot \mathbf{n}(r|\alpha)]^+ \; f_S(r) \tag{1.51}$$

This solution is significantly simplified when the expectation over $\mathbf{R}$ is taken over the mean out-crossing rate:

$$v_D^+(\alpha) = \int_0^\infty E[\dot{S}(t) \cdot \mathbf{n}(r|\alpha)]^+ f_S(r) \;\; f_{V|A}(r|\alpha) dr \tag{1.52}$$

since the unconditional out-crossing rate is then obtained directly by an integration over α:

$$\upsilon_D^+(\mathbf{s}) = \int_A f_A(\alpha)\, \upsilon_D^+(\alpha) d\alpha \tag{1.53}$$

It is noted that equation (1.52) represents the EUR approximation applied in the directional simulation solution of multi-variate problems.

1.6.3 Parallel system sensitivity analysis

A general and practical solution of the out-crossing problem was presented by Hagen and Tvedt (1991), based on unpublished results by Madsen (Danish Academy of Sciences). An out-crossing of a general differentiable vector process $\mathbf{S}(t)$ corresponds to a zero down-crossing of the scalar process $g(\mathbf{S}(t))$, which can be calculated as (note similarity with equation 1.10):

$$\upsilon_D^+(\mathbf{r}, t) = \lim_{\Delta t \to 0} \frac{1}{\Delta t} P[g(\mathbf{r}, \mathbf{S}, t) > 0 \cap g(\mathbf{r}, \mathbf{S}, t + \Delta t) < 0] \tag{1.54}$$

which can also be written as:

$$\upsilon_D^+(\mathbf{r}, t) = \frac{d}{d\theta}\, P[\dot{g}(\mathbf{r}, \mathbf{S}, t) < 0 \cap g(\mathbf{r}, \mathbf{S}, t) + \theta \dot{g}(\mathbf{r}, \mathbf{S}, t) < 0]\Big|_{\theta=0} \tag{1.55}$$

where $P_\theta[\cdot]$ is the probability of an associated parallel system and $\frac{d}{d\theta}\, P[\cdot]|_{\theta=0}$ is a sensitivity measure of this problem. Equation (1.55) can be evaluated using time-invariant reliability methods such as FORM or SORM, with the only requirement being that the algorithm for computation of sensitivity factors be capable of identifying sensitivity due to rotation of the limit state function.

The solution is very general and practical, and can be applied for Gaussian and non-Gaussian, stationary and non-stationary load processes, and for time-variant limit state functions. When the problem is stationary, only one evaluation of (1.55) is necessary, whereas for non-stationary problems this evaluation has to be repeated over time. The solution in equation (1.55) is conditional on a particular outcome $\mathbf{r}$ of the resistance random variables, and that has been made explicit in the formulation.

In the parallel system sensitivity solution, it is particularly simple to average the (conditional) out-crossing rates over $\mathbf{R}$, as it suffices to include the random resistance variables in the parallel system sensitivity analysis:

$$\upsilon_D^+(t) = \frac{d}{d\theta}\, P[\dot{g}(\mathbf{R}, \mathbf{S}, t) < 0 \cap g(\mathbf{R}, \mathbf{S}, t) + \theta \dot{g}(\mathbf{R}, \mathbf{S}, t) < 0]\Big|_{\theta=0} \tag{1.56}$$

Computation of (1.56) represents little extra effort in comparison to (1.55), due to the increased dimensionality of the problem. The whole solution, however, is still very simple. It takes a couple of time-invariant sensitivity analysis over variables $\mathbf{R}$ and $\mathbf{S}$ (for a time-variant barrier) and a numerical integration over time. It is important to note that implied in equation (1.56) is, of course and again, the EUR approximation.

1.7 Discussion

In this literature review, it was seen that the solution of general time-variant reliability problems involves evaluation of the rate at which a vector load processes crosses out of a random or uncertain and possibly time-variant safe domain.

The formal solution to this problem involves an integration of local out-crossing rates over the boundary of a (conditional) safe domain, an integration of (conditional) out-crossing rates over time and an integration of (conditional) failure probabilities over random resistance parameters. The innermost integration is numerical unless for stationary Gaussian load processes and geometrically simple failure surfaces. For more general problems, the integration over the safe domain boundary can be approximated by FORM or evaluated by directional simulation. Integration over time is straightforward, as long as out-crossings can be considered to follow a Poisson process. Integration over random resistance parameters is numerical in most cases. For stationary Gaussian load processes, the integrations over safe domain boundary, time and resistance parameters can be approximated by a nested FORM solution. For more general problems, directional simulation is required. These solutions are not straightforward, especially when the safe domain boundary is given numerically, e.g., as the solution to a finite element model. When resistance degradation is taken into account, the (formal) solution becomes close to intractable, because out-crossing rates become time-dependent and (the inner) integration over the safe domain boundary has to be repeated over time.

In the formal solution, out-crossing rates are integrated over time and the resulting (conditional) failure probabilities are then integrated over random resistance parameters. The problem can be significantly simplified by changing the order of integration. In the ensemble out-crossing rate approximation, the out-crossing rate for a (conditional) safe domain boundary is first averaged over resistance parameters and then integrated over time. Alternatively, the ensemble out-crossing rate is obtained directly, by considering a random safe domain boundary in the out-crossing rate evaluation. Integration over the resistance makes the assumption of independent out-crossings less appropriate. As a result, first passage failure

probabilities may become excessively conservative for problems with other than extremely low failure probabilities.

The ensemble up-crossing rate approximation has the potential for simplifying the solution of time variant reliability problems under resistance degradation. Hagen and Tvedt (1991) suggested a parallel system sensitivity solution to evaluate out-crossing rates for problems involving general random processes but deterministic safety domains. A natural extension of this solution is to include random resistance parameters in the parallel system sensitivity analysis (Sudret et al., 2002). For resistance degradation problems, it then suffices to repeat the parallel system sensitivity analysis in time. Each parallel system sensitivity analysis, in this case, avoids one nested FORM analysis or one complete directional simulation analysis, at a huge saving of computation time.

It was emphasized that a parallel system sensitivity analysis for out-crossing rates, including random resistance parameters, results in an ensemble out-crossing rate. Hence, in order for this solution to be validated, the ensemble out-crossing rate approximation needs to be addressed. If ensemble out-crossings can be assumed to follow a Poisson process, than integration over time is straightforward and the parallel system sensitivity solution with random resistance parameters holds.

Unfortunately, little is known about the quality of the EUR approximation, about its limits of application or, more fundamentally, whether the Poisson assumption holds. Limited analysis of the approximation are made by Pearce and Wen (1984) and by Wen and Chen (1989). The approximation is suggested for slow-varying random process barriers by Schall et al. (1991) and by Rackwitz (1993). It is also employed in conjunction with directional simulation by Melchers (1992) and in the parallel system sensitivity solution by Sudret et al. (2002). None of these references addresses the issue of whether or when ensemble up-crossing rates can still be assumed to follow a Poisson process.

In the first half of this thesis, the EUR approximation is addressed. A Monte Carlo simulation procedure for obtaining conditional up-crossing rate statistics is introduced in chapter 2. The procedure is used in chapter 3 to predict the error of the EUR approximation, for both Gaussian and non-Gaussian barriers. In chapter 4, EUR error expressions are used to derive corrections to the original EUR approximation. In chapter 5 the order of magnitude of the EUR error is studied, the method is compared to other simplified solutions of time-variant reliability problems, and limits of application of these approximations are established. The influence of the correlation length of slow-varying random process barriers in the EUR error is studied in chapter 6. In the second part of the thesis, a solution for fatigue and fracture

reliability analysis under random loading, based on the EUR approximation, is constructed.

1.8 Appendix

1.8.1 Fast Probability Integration using the HLRF algorithm

The failure probability in equation (1.26) can be approximated by FORM or SORM, using Wen and Chen's (1987) Fast Probability Integration technique. This technique introduces an auxiliary variable $u_{n+1} = \Phi^{-1}\left[P_f(T \mid \mathbf{r})\right]$, and solves for the augmented limit state function:

$$g^+(\mathbf{u}^+) = u_{n+1} - \Phi^{-1}\left[P_f(T \mid \mathbb{T}^{-1}(\mathbf{u}))\right] \tag{1.57}$$

where $\mathbf{u} = \mathbb{T}(\mathbf{r})$ is the transformation to the standard normal space, $\Phi[\cdot]$ is the Gaussian cumulative distribution function and $\mathbf{u}^+$ is the vector $\mathbf{u}^+ = \{u_{n+1}, u_n, u_{n-1}, ..., u_1\}^T$. With this approximation, the integral in equation (1.26) becomes:

$$P_f(T) = \int_{g^+(\mathbf{u}^+)\leq 0} f_{\mathbf{u}^+}(\mathbf{u}^+)du \tag{1.58}$$

The FORM approximation linearizes the integration domain of equation (1.58) at the design point $\mathbf{u}^{+*}$, which is the solution to the optimization problem:

$$\begin{aligned} \text{minimize:} \quad & d = \sqrt{(\mathbf{u}^+)^T \cdot \mathbf{u}^+} \\ \text{subject to:} \quad & g^+(\mathbf{u}^+) = 0 \end{aligned} \tag{1.59}$$

The design point can be found using the HLRF algorithm, (Hassofer and Lind, 1974; Rackwitz and Fiessler, 1978), which gives the sequence:

$$\mathbf{u}^+_{k+1} = \frac{\nabla g^+(\mathbf{u}^+_k)^T \cdot \mathbf{u}^+_k - g^+(\mathbf{u}^+_k)}{\nabla g^+(\mathbf{u}^+_k)^T \cdot \nabla g^+(\mathbf{u}^+_k)} \nabla g^+(\mathbf{u}^+_k) \tag{1.60}$$

where $\nabla g^+(\mathbf{u}^+_k)$ is the gradient of the augmented limit state function at iteration point k. The first term of the gradient is $\frac{\partial g^+(\mathbf{u}^+_k)}{\partial \mathbf{u}^+_k} = 1$, and the remaining terms are obtained from the gradient of the "original" limit state function:

$$\nabla g^+(\mathbf{u}^+_k) = \{1, \frac{\nabla g(\mathbf{u}_k)}{\phi(P_f(T \mid \mathbb{T}^{-1}(\mathbf{u}_k)))}\} \tag{1.61}$$

where $\phi()$ is the Gaussian probability density function and $g(\mathbf{u}_k) = P_f(T \mid \mathbb{T}^{-1}(\mathbf{u}_k))$ or $g(\mathbf{r}_k) = P_f(T \mid \mathbf{r}_k)$ is the "original" limit state function (equation 1.25). The gradient $\nabla g(\mathbf{u}_k)$ can be evaluated numerically by central differences.

1.8.2 Extreme value distribution

The extreme value of n independent observations of a random variable S is itself a random variable, and its PDF is given by:

$$F_{S_n}(s) = (F_s(s))^n \tag{1.62}$$

The PDF of a single peak (single extreme) of a Gaussian random process is given by Huston and Skopinski (1953), as presented in Madsen et al., 1987:

$$f_e(s) = \sqrt{1-\alpha^2}\phi\left(\frac{s}{\sqrt{1-\alpha^2}}\right) + \alpha \cdot s \cdot \exp(-\frac{s^2}{2})\Phi\left(\frac{\alpha \cdot s}{\sqrt{1-\alpha^2}}\right) \tag{1.63}$$

It is completely defined by irregularity factor α, the limiting forms being a Rayleigh distribution for $\alpha = 1$ (only positive peaks) and a normal distribution for $\alpha = 0$ (equal number of positive and negative peaks), as depicted in figure 1-7.

The number of peaks of a random process in time interval $(0, T)$ is given by:

$$n_{peaks} = \frac{1}{\alpha}\frac{w_0 T}{2\pi}$$

where w_0 is the zero crossing frequency and α is the irregularity factor. The extreme value of the Gaussian random process is obtained by integrating equation (1.63) and substituting in equation (1.62):

$$F_{S_T}(s) = (\int_0^s f_e(z)dz)^{n_{peaks}} \tag{1.64}$$

Solution of equation (1.64), using some asymptotic results that assume n_{peaks} to be large, leads to the double exponential extreme value distribution:

$$F_{S_T}(s) \simeq \exp\left[-n\exp\left(-\frac{1}{2}(\frac{s-\mu_s}{\sigma_s})\right)^2\right]$$

where $n = \frac{w_0 T}{2\pi} = \alpha \cdot n_{peaks}$. Figure 1-8 shows the behavior of this asymptotic extreme value distribution for increasing n.

1.9 Figures

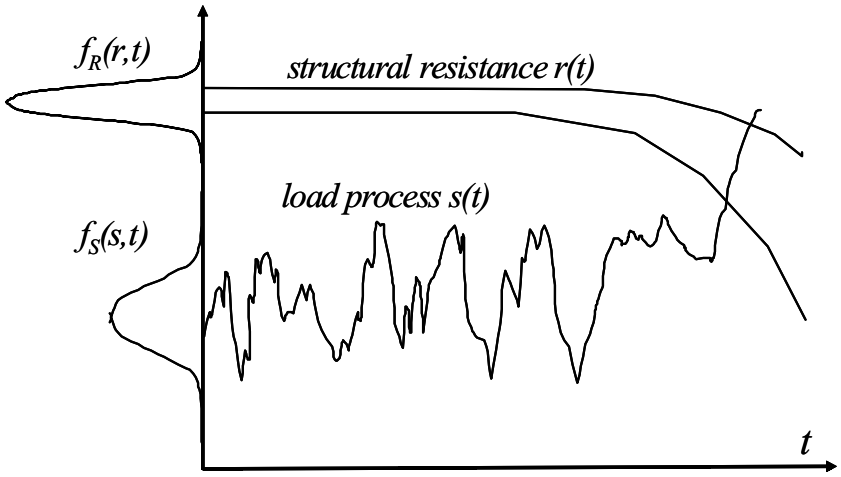

Figure 1-1: Typical scalar time-variant reliability problem.

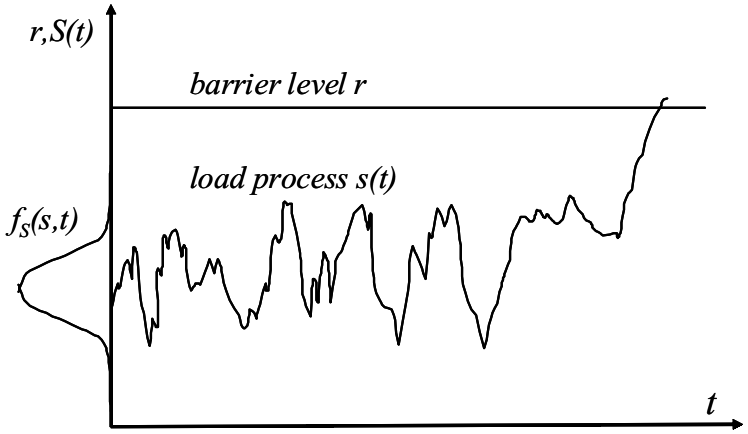

Figure 1-2: First Passage Failure model for fixed barrier level $R(t) = r$.

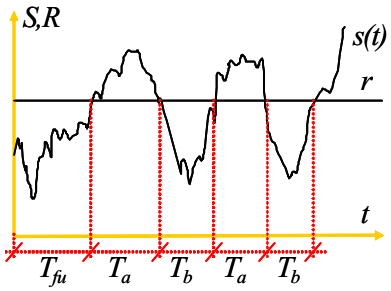

Figure 1-3: Composition of time between sucessive up-crossing, low barrier level.

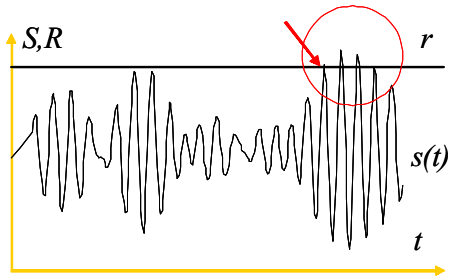

Figure 1-4: Clumping of up-crossings characteristic of narrow-band processes.

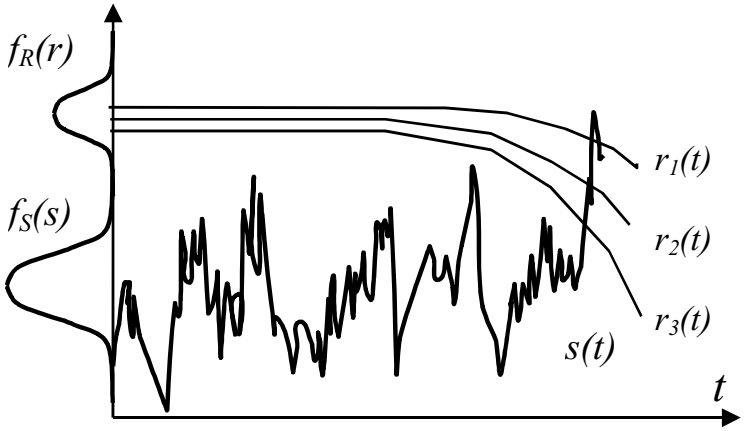

Figure 1-5: Parametric resistance degradation and Fast Probability Integration solution.

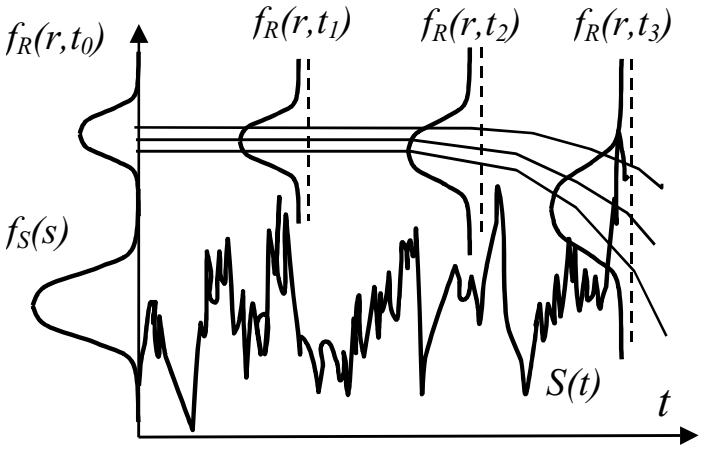

Figure 1-6: Resistance TPD and ensemble up-crossing rate approximation.

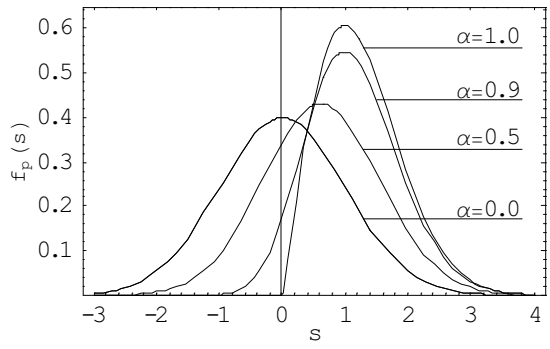

Figure 1-7: PDF of single peak of Gaussian process.

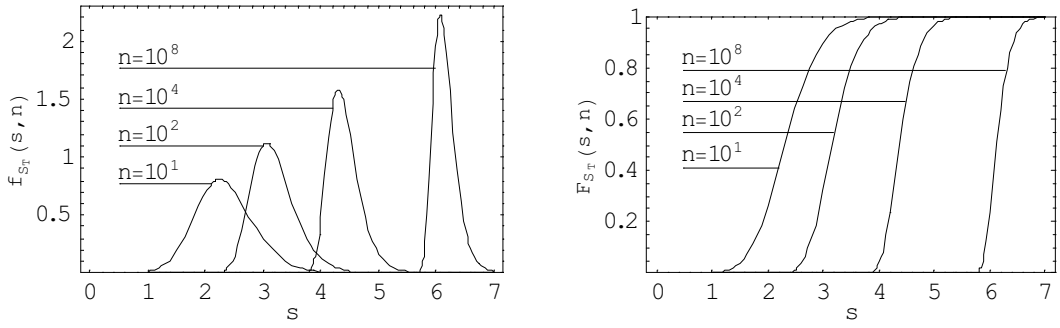

Figure 1-8: Extreme value distribution of Gaussian process as function of number of cycles.

Chapter 2

A SIMULATION PROCEDURE FOR OBTAINING CONDITIONAL UP-CROSSING STATISTICS

2.1 Introduction

In this chapter, a simulation procedure to obtain conditional up-crossing statistics is introduced. The procedure is first applied to deterministic barriers, in order to 1) check the experimental procedure and 2) compare conditional up-crossing rate statistics with closed form up-crossing rate expressions. The analysis of deterministic barrier crossings through the proposed procedure does not provide any immediately useful results, but it is presented here for completeness. In the following chapter, the procedure is applied to random barrier problems, where more important results are obtained.

2.2 Conditional up-crossings

The Poisson assumption in the First Passage failure model introduces the non-intuitive idea that the time between successive up-crossings be independent. As independence is a statistical concept, it does not apply to any particular observed up-crossing event. Hence, the concept of independence is not very helpful in analyzing up-crossing events. The First Passage failure probability equation (1.6), however, can be used to obtain a more intuitive and helpful interpretation, i.e., that of conditional up-crossings. Following Lutes and Sarkani

(1997), assume that there exists an "independent" crossing rate function $\upsilon_I^+(r,s)$ for which the Poisson assumption is exact. Derivation of expression (1.6) with respect to time and a solution for $\upsilon_I^+(r,s)$ yields (see section 1.3):

$$\upsilon_I^+(r,s) = \lim_{\Delta t \to 0} \left(\frac{1}{\Delta t} \frac{P_f(r,t+\Delta t) - P_f(r,t)}{1 - P_f(r,t)} \right) \tag{2.1}$$

Equation (2.1) is given the following interpretation:

$$\upsilon_I^+(r,s) = \lim_{\Delta t \to 0} P[\text{occurrence of one up-crossing in } (t, t+\Delta t) \text{ given that:} \tag{2.2}$$

$$(1)\ S(0) < r \text{ and}$$

$$(2) \text{ no up-crossings occur before } t]$$

It is seen that the "independent" crossing rate in equation (2.2) is formally a "conditional" crossing rate. Hence, the terms "independent" and "conditional" are synonymous in the context of this discussion. The subscript $_I$ is maintained, however, as indicating "the crossing rate for which the assumption of independence is exact". In contrast, "dependent" or "unconditional" crossings rates are the ones for which the assumption of independence is not approximate or inexact.

Vanmarcke's (1975) improved up-crossing rate expression (equation 1.23) is an analytical approximation to equation (2.2), which is better than the first approximation $\upsilon_I^+(r,s) = \upsilon_S^+(r,s)$. The inclusion-exclusion series of Rice (1954) is also an approximation to equation (2.2), but without the initial condition (Ditlevsen, 1986). There are closed form solutions (to equation 2.2) for highly idealized pulse processes (Veneziano et al., 1979). However, to the authors knowledge, there are no general exact closed form solutions to expression (2.2). In this section, a simulation procedure is introduced to obtain a numerical estimate of the exact conditional up-crossing rates.

2.3 Simulation procedure

Consider an experiment where, in multiple observations of the load process through a "window" between t and $t+\Delta t$ (as illustrated in figure 2-1), the number of times n_1 that the process starts in the safe domain and up-crosses barrier level r for the first time between t and $t+\Delta t$ is computed. After n repetitions of the experiment, it is clear that $\upsilon_I^+(r,s)$ could be directly estimated as $\upsilon_I^+(r,s) \simeq \frac{n_1}{n}$. Obtaining such statistics, however, would be virtually impossible, due to the huge number of samples that would be required to obtain a sufficient

number of up-crossings between t and $t+\Delta t$. Moreover, Δt is supposed to be very small and the observations would have to be repeated for all Δt intervals in $(0,T)$.

A less demanding and more practical procedure is to obtain statistics of the first barrier crossings up to a given time t and somehow average this number over the whole time interval $(0,t)$. Consider an experiment where the number of first up-crossings (n_1) up to time t and the number n_0 of failure starts are recorded. In each realization of the experiment, only three results are possible, defining three events as follows:

1. $E_0 \equiv$ barrier crossing at $t=0$ (or $S(0)<r$, computed as n_0);
2. $E_1 \equiv$ barrier up-crossing in interval $(0,t]$ (computed as n_1);
3. $E_2 \equiv$ no barrier up-crossings at all (computed as n_2).

The events E_0, E_1 and E_2 form a set of mutually exclusive and exhaustive events. Now the conditional **first** barrier up-crossings are assumed to follow a non-stationary Poisson counting process, with a time-variant arrival rate $\upsilon_I^+(r,t)$, and one obtains:

$$\begin{aligned} P[N_s^+=0|S(0)<r] &= \frac{[-\int_0^t \upsilon_I^+(r,s)ds]^0}{0!}\exp[-\int_0^t \upsilon_I^+(r,s)ds] \\ &= \exp[-\int_0^t \upsilon_I^+(r,s)ds] \end{aligned} \tag{2.3}$$

where N_s^+ is the number of first up-crossings in the interval $(0,t]$ (either 0 or 1). Statistics of $P[N_s^+=0|S(0)<r]$ can be obtained from the proposed experiment, since:

$$\begin{aligned} P[N_s^+=0|S(0)<r] &= P[E_2|\overline{E}_0] \\ &= \frac{P[\overline{E}_0|E_2]\cdot P[E_2]}{P[\overline{E}_0]} \end{aligned} \tag{2.4}$$

Since the events are mutually exclusive, $P[\overline{E}_0|E_2]=1$ and because they are exhaustive, $P[E_2]=1-P[E_0]-P[E_1]$. Hence:

$$\begin{aligned} P[N_s^+=0|S(0)<r] &= \frac{1-P[E_0]-P[E_1]}{1-P[E_0]} \\ &\simeq \frac{1-\frac{n_0+n_1}{n}}{1-\frac{n_0}{n}} \end{aligned} \tag{2.5}$$

In expression (2.5), of course, n_1 is the number of first up-crossings observed, up to time t, in n realizations of the experiment. Hence, combining expressions (2.3) and (2.5), the

conditional first up-crossing arrival rate can be estimated from the Monte Carlo experiment:

$$\int_0^t \upsilon_I^+(r,s)ds \simeq -\ln\left(\frac{1-\frac{n_0+n_1}{n}}{1-\frac{n_0}{n}}\right) \tag{2.6}$$

The right-hand side of expression (2.6) is obtained experimentally, and $\upsilon_I^+(r,t)$ is calculated via finite differences. For deterministic barriers, $\upsilon_I^+(r,t)$ can as well be approximated by its time-average (as will be seen in section 2.6), avoiding the instability of a numerical derivation. Hence:

$$\upsilon_I^+(r,t) \simeq -\frac{1}{t}\ln\left(\frac{1-\frac{n_0+n_1}{n}}{1-\frac{n_0}{n}}\right) \tag{2.7}$$

The arrival rate $\upsilon_I^+(r,t)$ is still a function of time as assumed. It is noted that expression (2.7) is the inverse of the First Passage failure probability equation (1.6):

$$\upsilon_I^+(r,t) \simeq -\frac{1}{t}\ln\left(\frac{1-P_f(r,t)}{1-P_{f_0}(r)}\right) \tag{2.8}$$

The conditional up-crossing rate in equation (2.7) is actually the ensemble average (over n repetitions of the experiment) of the arrival rate of the first up-crossings. By the definition in equation (1.10), the interval Δt is supposed to be very small. This interval can be increased (to t) because only the first up-crossing is being computed.

Although it seems to represent little or no improvement over a direct Monte Carlo simulation for $P_f(r,t)$, the proposed procedure is a useful way of verifying approximate closed form up-crossing rate expressions. Use of the simulation procedure can also be justified if it can generate information about $\upsilon_I^+(r,t)$ that can be generalized and extended to broader situations. The proposed procedure provides interesting results when used to analyze ensemble up-crossing rates of random barriers (chapter 3).

2.4 From conditional crossing rates to the arrival rate of the first crossing

In the experimental procedure just introduced the sampling time was increased from a narrow Δt to the whole time t, on the grounds that only the first up-crossing is computed. In this section, an alternative justification of equation (2.6) is given.

It is clear, from the definition of the first passage problem, that one is interested in the first crossing of the barrier. The solution for the first passage failure model is only built

over up-crossing rates because they are easier to evaluate, for a general random process. The required extension to conditional crossing rates then becomes evident.

Imagine one experiment where one computes t_1, the time for the first up-crossing. In n realizations of the experiment, the expected value of the time for the first up-crossing would be:

$$\overline{t}_{1^{st}} = \frac{1}{n}\sum_{i=1}^{n}(t_1)_i \tag{2.9}$$

The arrival rate of the first crossing would be:

$$\lambda_{1^{st}} = \frac{1}{\overline{t}_{1^{st}}} = \frac{n}{\sum_{i=1}^{n}(t_1)_i} \tag{2.10}$$

There are a couple of problems with this experiment as well. One is that the samples would have to run indefinitely, until the first crossing were observed. For high barriers, this would introduce problems regarding truncation of some samples. Moreover, the arrival rate would have to be derived from the first passage time, which would become impossible if the arrival rate were time-variant.

Now consider again the experiment introduced in the last section, where one computes the number of first crossings up to a given time t. Clearly, for some samples in this experiment the first crossing would be to the right of t, i.e., after t, but this does not matter. The issue is to count the number n_1 of first crossings before t, as well as the number n_0 of first crossings at time zero.

If one assumes the first crossings to follow a Poisson process with a time-variant arrival rate, the time until the first crossing becomes exponentially distributed and one has:

$$P[T_1(r) < t] = F_{T_1}(r,t) = 1 - \exp[-\int_0^t \upsilon_1^+(r,s)ds] \tag{2.11}$$

This cumulative probability can be approximated from the proposed experiment as $\frac{n_0+n_1}{n}$. Hence:

$$1 - \exp[-\int_0^t \upsilon_1^+(r,s)ds] \simeq \frac{n_0+n_1}{n} \tag{2.12}$$

or:

$$\int_0^t \upsilon_1^+(r,s)ds \simeq -\ln\left(\frac{1-\frac{n_0+n_1}{n}}{1-\frac{n_0}{n}}\right) \tag{2.13}$$

which is again equation (2.6). It is noted that the Poisson assumption used to derive equation

(2.13) guarantees that the arrival rates $\upsilon_1^+(r,t)$ provide exact failure probabilities when used in the (Poisson-assumed) First Passage failure model.

2.5 Simulation of random load processes

The simulation procedure described in the previous sections is based on simulation of samples of load process and barrier. In the studies that follow, two continuous standard Gaussian load processes $S(t)$ are considered. In this section, these processes and their simulation are described.

One of the processes considered is characteristically narrow-banded (NB), with a uniform power spectrum density (PSD) limited between $w_1 = 2\pi - 1$ and $w_2 = 2\pi + 1$, and bandwidth parameter $\alpha = 0.98$. The other process is a First-order Markov process, characteristically broad-banded (BB), with an exponential correlation function and $\alpha = 0.40$ (Soong and Grigoriu, 1993):

$$R_{SS}(t_2 - t_1) = \sigma_S^2 \exp(-\frac{t_2 - t_1}{\lambda}) \tag{2.14}$$

The correlation length for this process is $\lambda = 1.0$ and the PSD function is:

$$G(w) = \frac{2\sigma_S^2 \lambda}{\pi(w^2 + \lambda^2)},\ 0 < w \tag{2.15}$$

The PSD function of the broad-band process is truncated at $w_2 = 10$, and the frequency content is adjusted to:

$$\begin{aligned} G_t(w) &= \frac{\sigma_S^2}{\int_0^{w_2} G(w)dw} \frac{2\sigma_S^2 \lambda}{\pi(w^2 + \lambda^2)},\ 0 < w < w_2 \\ &= 0 \qquad\qquad\qquad\qquad\qquad\qquad\quad ,\ w_2 < w \end{aligned} \tag{2.16}$$

The truncated PSD function is used in Monte Carlo simulation and evaluation of spectral moments:

$$\lambda_i = \int_0^{w_2} w^i G_t(w)dw \tag{2.17}$$

The correlation and PSD functions of these processes are illustrated in figure 2-2. The processes are such that one cycle or load peak is nearly equivalent to one time unit: $\frac{n_{cycles}}{T} = \frac{1}{\alpha}\frac{W_0}{2\pi} = \frac{1}{\alpha}\frac{1}{2\pi}\sqrt{\frac{\lambda_2}{\lambda_0}} \approx 1$. In this case, one cycle represents one second, one hour or one year.

A straightforward procedure for generating samples of a random process $S(t)$ is based on a discrete spectral representation of the process (Shinozouka and Yan, 1972; Grigoriu, 2000).

The PSD of the process is discretized in a finite number m of frequency components:

$$\int_{w_1}^{w_2} G_t(w)dw \approx \sum_{k=1}^{m} G_t(w_k)\Delta w_k \tag{2.18}$$

where $\Delta w_k = \frac{w_2 - w_1}{m}$ and w_k is the median of the k^{th} frequency interval. Samples of the discretized process are obtained from:

$$S_m(t) = \sum_{k=1}^{m} G_t(w_k)\Delta w_k \left(V_k \cos(w_k\, t) + W_k \sin(w_k\, t)\right) \tag{2.19}$$

where V_k and W_k are independent Gaussian variables with zero mean and unit variances. A pair of independent Gaussian variables V_k,W_k can be obtained from two independent variables u_1 and u_2, uniformly distributed between 0 and 1, through (Soong and Grigoriu, 1993):

$$\begin{aligned} V_1 &= \sqrt{-2\log u_1}\cos(2\pi\, u_2) \\ W_1 &= \sqrt{-2\log u_1}\sin(2\pi\, u_2) \end{aligned} \tag{2.20}$$

Due to the finite number of frequency components considered, the samples generated using the algorithm above are periodic. The period of the samples is:

$$T_p = \frac{2\pi\, m}{w_2} \tag{2.21}$$

Numerical results show that a better reproduction of the load process is obtained when a whole periodic sample is simulated. Simulation of samples larger than T_p does not make sense. Hence, the choice of m and of the truncating frequency w_2 define the appropriate sampling time for the simulation. If w_2 is too large, a very large number of frequency components m has to be used to obtain a reasonable sampling time T_p.

$S_m(t)$ in equation (2.19) is a sum of discrete frequency components with random amplitudes. Generation of one sample of $S_m(t)$ requires the simulation of $2m$ random variables (the amplitudes). One of the critical issues of the simulation is the number of frequency components m to be considered. Clearly, the more frequency components are used, the better $G_m(w)$ approximates $G_t(w)$, and the better $S_m(t)$ approximates $S(t)$. The (periodic) sampling time is also directly proportional to the number of frequency components considered.

Evaluation of each point of the time-history $S_m(t)$ involves a sum with m components. Evaluation of a discrete number of points from equation (2.19) is the most time-consuming part of the simulation. Hence, the number of points of the discrete time-history n and the number of frequency components m cannot be too large. There is also a requirement that

$n \geq 2m$.

Figure 2-3 shows how well parameters of the standard Gaussian NB and BB processes are reproduced and how large are the extreme values simulated, in one sample of each process, as a function of the number of frequency components m. In the results shown in figure 2-3, the number of points of each time-history was fixed to $n = 2m$, the sampling time T is a complete cycle $T = T_p$ and the same seed is used for all samples.

2.6 Application to deterministic barriers

In this section, the simulation procedure just introduced is used to study crossings of Gaussian load processes through deterministic barriers. The purpose of this study is to verify the simulation algorithm and validate the simulation procedure to obtain conditional crossing rates.

In figures 2-4 and 2-5 conditional crossing rates $\upsilon_I^+(r,t)$ obtained from equation (2.7) are compared with the original crossing rate $\upsilon_s^+(r)$ and with Vanmarcke's corrected crossing rate expression, as a function of barrier level r. Figure 2-4 shows the logarithm of the crossing rates, and figure 2-5 shows the ratio between other crossing rates and $\upsilon_s^+(r)$, for the narrow-band and broad-band load processes. In deriving these results it was noticed that using the rule $n = 2m$ leads to an under-estimation of the crossing rates, especially for the NB load process. Figures 2-4 and 2-5 were obtained using $m = 10^3$ frequency components and $n = 5m = 5 \cdot 10^3$ time points, with (periodic) sampling times of $T = T_p = 431$ and 324 cycles, for the NB and BB processes, respectively. 10^5 time-histories of each load process were simulated. Ensemble and time statistics computed during the simulation show that parameters of the random processes (μ and σ) are accurately reproduced. This, together with up-crossing rate results just presented, shows that the simulation algorithm is working satisfactorily.

The effect of the initial condition ($S(0) < r$) for low barrier levels can be observed by comparing the crossing rates in time. Figure 2-6 shows that for a couple of cycles after $t = 0$ the closed form up-crossing rate expressions, in particular Vanmarcke's expression, overpredict the conditional crossing rate. This behavior is in accordance with observations by Lutes and Sarkani (1997, page 195), who attribute it to the fact that up-crossing rate $\upsilon_s^+(r)$ (expression 1.12) completely neglects and that Vanmarcke's expression (equation 1.23) does not represent the initial condition exactly. This result, confirming observations by Lutes and Sarkani (1997), shows that the simulation procedure to obtain conditional crossing rates works accordingly.

For completeness, failure probabilities computed from distinct up-crossing rate expressions are compared with MC simulation results in figure 2-7, for barrier levels $r = 3$ and $r = 5$. Failure probabilities computed from the estimated conditional up-crossing rates through:

$$P_f(r,t) = P_{f_0}(r) + (1 - P_{f_0}(r)) \cdot (1 - \exp[-\upsilon_I^+(r,t) \cdot t]) \tag{2.22}$$

are also shown in figure 2-7, in a black continuous line and virtually indistinguishable from MC simulation results. This result indicates that:

1. the assumption that conditional up-crossing rates (equation 2.6) follow a time-variant Poisson counting process is highly appropriate;

2. the time-variant arrival rate of conditional up-crossings $\upsilon_I^+(r,t)$ can be approximated by its time-average ($\int_0^t \upsilon_I^+(r,s)ds \simeq \upsilon_I^+(r,t) \cdot t$).

Results presented in this section for crossings of deterministic barriers are not immediately useful. However, very interesting results are obtained when the simulation procedure is applied to problems involving random barriers, as will be seen in the next chapter.

2.7 Figures

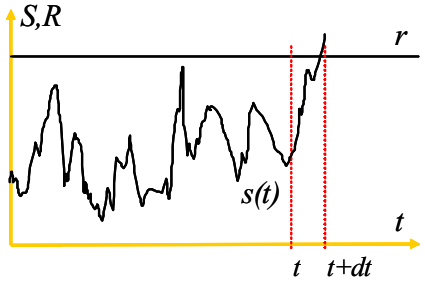

Figure 2-1: Obtaining conditional up-crossing statistics.

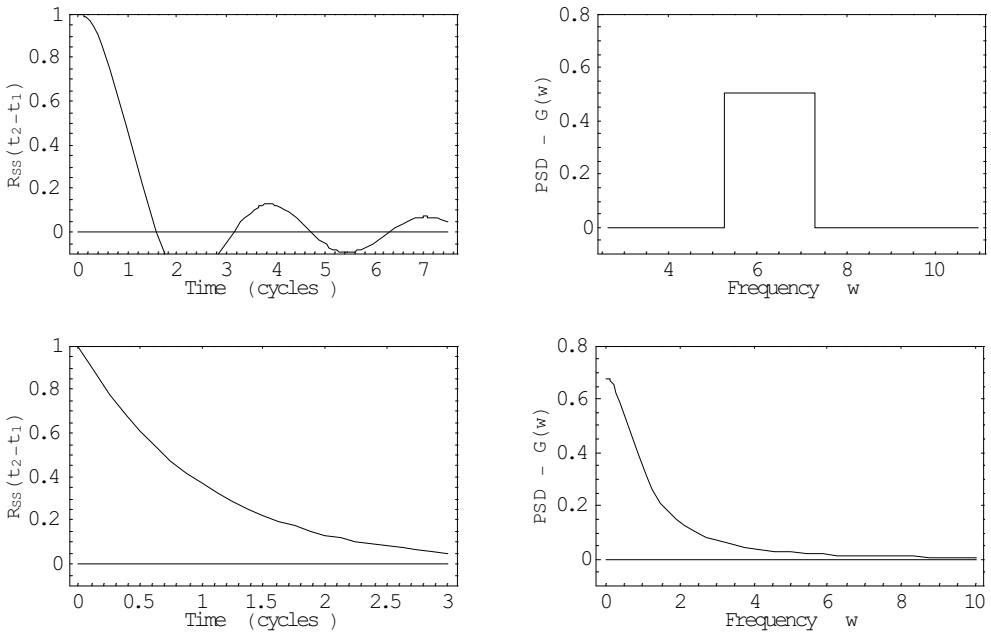

Figure 2-2: Correlation function (left) and PSD (right) of NB (top) and BB (bottom) load processes.

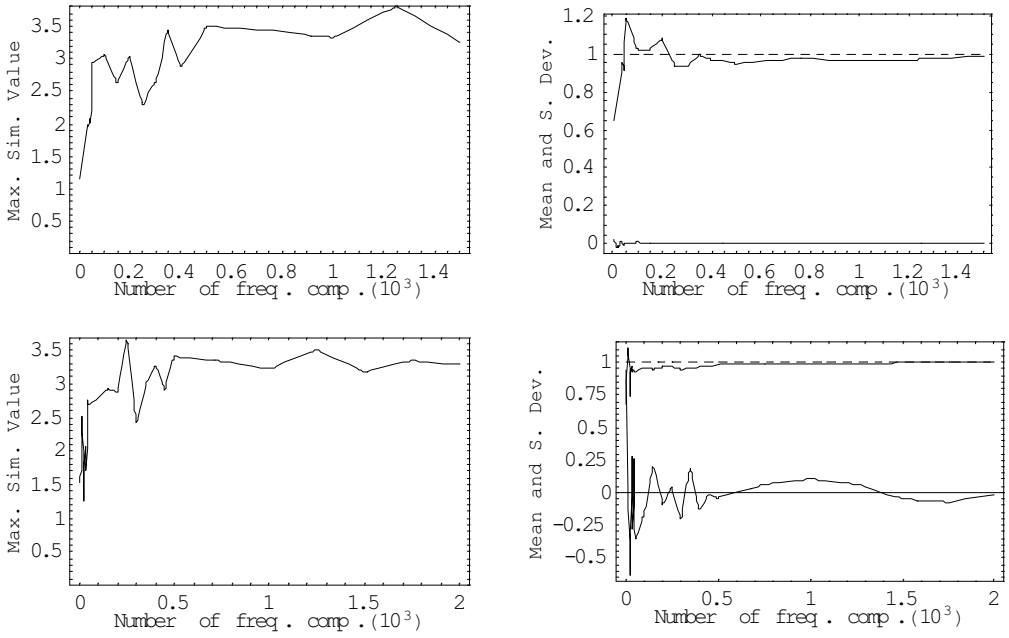

Figure 2-3: Effect of number of frequency components m in extreme value (left) and parameters (right) of simulated load process time-history, NB (top) and BB (bottom).

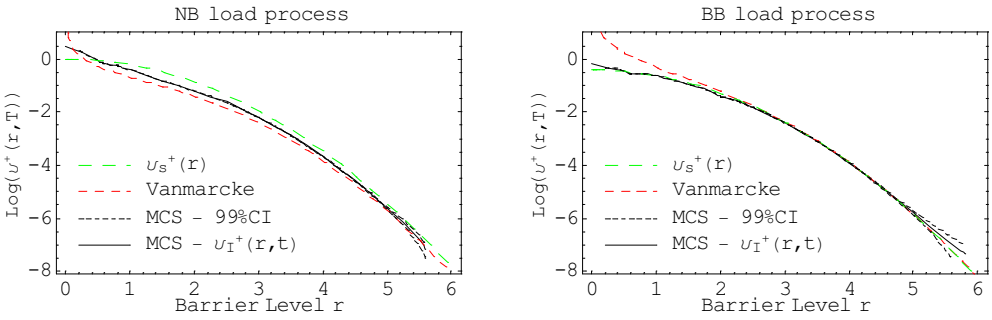

Figure 2-4: Comparison of up-crossing rates at $t = T/2$.

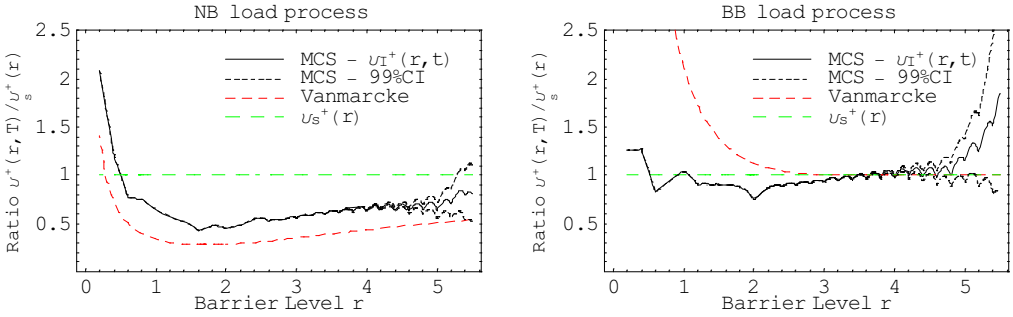

Figure 2-5: Ratio $\frac{v^+(r,t)}{v_S^+(r,t)}$ for different up-crossing rate expressions.

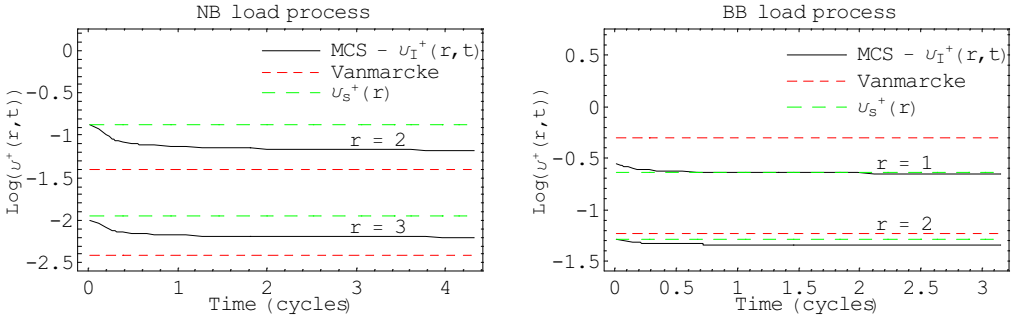

Figure 2-6: Comparison of up-crossing rates in time.

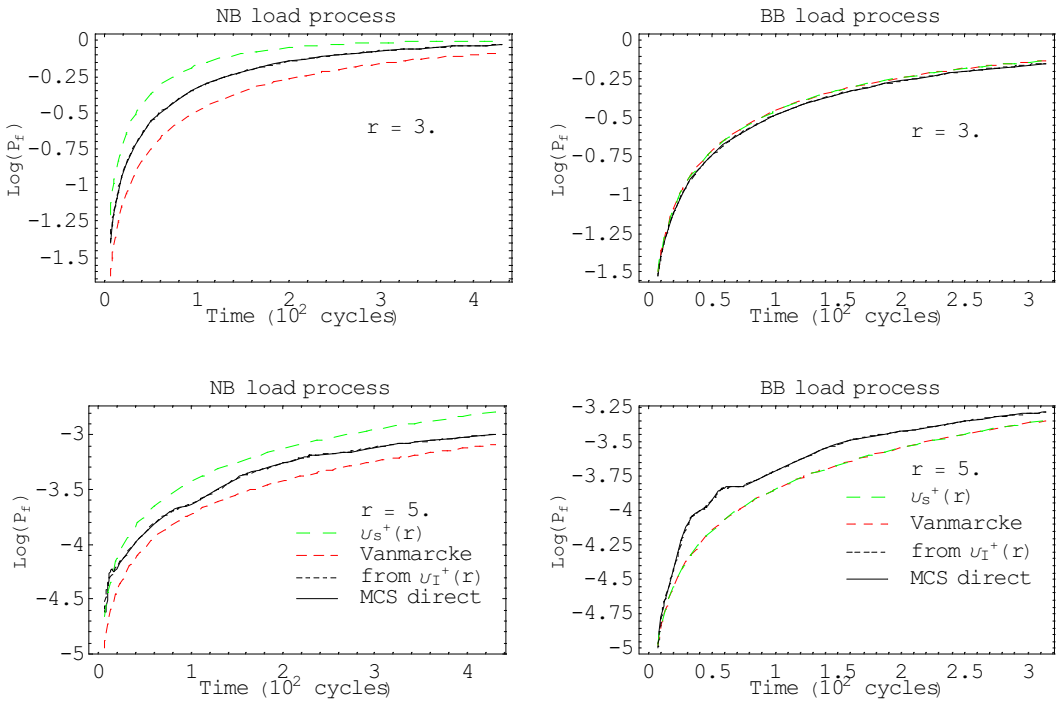

Figure 2-7: Failure probability results for constant barrier levels.

Chapter 3

ESTIMATION OF THE ENSEMBLE UP-CROSSING RATE ERROR

3.1 Introduction

The simulation procedure introduced in the last chapter is used here to estimate the error of the EUR approximation. First, the conditional up-crossing rate concept is extended for the random barrier case. The simulation procedure is then used to compare dependent ensemble crossing rates with equivalent independent ensemble crossing rates. The error involved in the EUR approximation is predicted, and an error parameter is identified. Results are obtained for Gaussian load processes and for Gaussian and non-Gaussian barriers. Results derived in this chapter are extensively used in chapters 4, 5, 6 and 11.

3.2 Preliminary considerations

In the ensemble up-crossing rate solution, the rate at which a random load process up-crosses a deterministic barrier level is integrated over the resistance distribution:

$$\upsilon^{+}_{ED}(R,t) = \int_{R} \upsilon^{+}(r,t) f_R(r,t) dr \tag{3.1}$$

Following Pearce and Wen (1983), the inaccuracy implied in this solution is the approximation of the arrival rate of the first crossing through the random barrier by the ensemble average of up-crossings. Integration over the resistance makes ensemble up-crossing rates "dependent" through the resistance, as noted by Wen and Chen (1989). The direct impli-

cation of this dependency is that the Poisson assumption of independent up-crossings in the First Passage failure model has to be re-considered. This was emphasized in equation (3.1) with adoption of subscript $_{ED}$ (E for ensemble and D for dependent).

The conditional up-crossing rate interpretation given in section 1.3 can be extended to random barriers by including the additional condition that the barrier changes independently for each load application, in view of Wen and Chen's (1989) comment quoted in section 1.4.4. Hence, if there exists an equivalent "independent" ensemble up-crossing rate $\upsilon^+_{EI}(R,t)$ for which the Poisson assumption is more appropriate (or perhaps even exact), following the same developments that led to equation (2.2) one obtains:

$$\upsilon^+_{EI}(R,t) = \lim_{\Delta t \to 0} P[\text{occurrence of one up-crossing in } (t, t+\Delta t) \text{ given that:} \tag{3.2}$$

(1) $S(0) < R$;
(2) no up-crossings occur before t and
(3) barrier changes independently for each load application]

Vanmarcke's (1975) result and the inclusion-exclusion series of Rice (1954) are analytical approximations to equation (2.2), for deterministic barriers. To the authors knowledge, there are no such approximations for the random barrier case (equation 3.2). Equation (3.2) cannot be given an analytical form, but statistics of $\upsilon^+_{EI}(R,t)$ can be obtained from the numerical experiment introduced in the previous chapter. The experiment is carried out in the same manner as for the deterministic barrier, but a new (independent) resistance outcome is simulated for each sampled load process time-history.

The "independent" ensemble up-crossings are assumed to follow a non-stationary Poisson counting process, with a time-variant arrival rate $\upsilon^+_{EI}(R,t)$. From equation (2.6), one obtains:

$$\begin{aligned} \int_0^t \upsilon^+_{EI}(R,s)ds &= -\ln\left(\frac{1-\frac{n_0+n_1}{n}}{1-\frac{n_0}{n}}\right) \\ &= -\ln\left(\frac{P_f(R,t)-1}{P_{f_0}(R)-1}\right) \end{aligned} \tag{3.3}$$

The right-hand side of expression (3.3) is obtained from the Monte Carlo experiment, and the up-crossing rate is obtained by a finite difference derivation. Expression (3.3) reflects the conditions stated in equation (3.2), whereas the original ensemble up-crossing rate approximation (equation 3.1) completely neglects them. Hence, the Poisson assumption of

independence is more likely to be appropriate for $\upsilon^+_{EI}(R,t)$ than for $\upsilon^+_{ED}(R,t)$.

3.3 Error measure

The whole idea in this chapter is to obtain an estimate of the EUR error by comparing $\upsilon^+_{EI}(R,t)$ with $\upsilon^+_{ED}(R,t)$. Clearly, there are many possible error measures that can be used in this comparison. A particular error measure choice should be appropriate for the problem in hand. An error in ensemble up-crossing rates is reflected in an error in failure probabilities, which can be very small for practical problems. In practical terms, small failure probabilities are compared in terms of the power-of-ten exponent that gives the number of zeros before the first significant digit, e.g.: $P_f(t) = 10^{-5}$. A difference between -5 and -4 in the failure probability exponent can be the difference between an acceptable and an unaceptable structural design, for example. Hence, an appropriate error measure for small failure probabilities and for small crossing rates is one that gives the error in terms of orders of magnitude. An order-of-magnitude error is obtained by taking the logarithm of the ratio between the two up-crossing rates:

$$E_D(\mu,\sigma,t) = \log_{10}\left(\frac{\upsilon^+_{ED}(\mu,\sigma,t)}{\upsilon^+_{EI}(\mu,\sigma,t)}\right) \tag{3.4}$$

where $E_D(\mu,\sigma,t)$ is the EUR order-of-magnitude dependency error or simply EUR error. With this error measure, the difference between $\upsilon^+_{ED}(R,t) = 10^{-4}$ and $\upsilon^+_{EI}(R,t) = 10^{-5}$ crossings per cycle is one order of magnitude.

3.4 Up-crossing rate expression for ensemble integration

The EUR error measured trough equation (3.4) refers to an ensemble crossing rate $\upsilon^+_{ED}(\mu,\sigma,t)$, obtained from the integration in equation (3.1), which by its turn depends on a particular expression of the (deterministic) barrier crossing rate $\upsilon^+(r,t)$. Hence, an appropriate barrier crossing rate $\upsilon^+(r,t)$ has to be used in this analysis. Error expressions derived in the sequel will be, to some extent, dependent on this expression.

Vanmarcke's corrected up-crossing rate expression (equation 1.23, section 1.3) is appropriate for Gaussian processes of any bandwidth or barrier level. However, this expression tends to infinity when the barrier level approaches the mean of the load process. This is appropriate for deterministic barriers, since failure is certain and the first passage failure probability goes instantly to one. For random barriers, however, low barrier level realizations occur only with a given probability, and up-crossing rates that approach infinity inappropriately affect integration over the resistance (equation 3.1). Hence, it is interesting to make a

new interpolation, between crossings by the load process at very low levels, and Vanmarcke's result for mid-to-high barrier levels. The resulting expression, obtained by the author, is an interpolation between crossings by the load process at very low levels, crossings by the amplitude process at intermediate levels and crossings by the load process, again, at high barrier levels:

$$\upsilon^+(r,t) = \upsilon_S^+(r,t)\left(\frac{\upsilon_S^+(r,t)}{\upsilon_S^+(0,t)} + (1 - \exp[\frac{\upsilon_A^+(r,t)}{\upsilon_S^+(r,t)}])\right) \tag{3.5}$$

Expression (3.5) is used in the next section to derive EUR error expressions based on simulation. In a later section, an extrapolation of simulation results is considered. Because extrapolation results refer to very high barrier levels, an alternative expression is used to obtain $\upsilon_{ED}^+(\mu,\sigma,t)$ directly, avoiding the numerical integration in equation 3.1. The expression used in the error extrapolation is due to Owen (1980), and is valid for Gaussian load processes and high Gaussian barriers, where the initial condition and the conditioning to no prior up-crossings in the original crossing rate expression $\upsilon_S^+(r)$ can be neglected:

$$\begin{aligned}
\upsilon_{ED}^+(\mu_R,\sigma_R) &= \int_R \upsilon_S^+(r) f_R(r) dr \\
&= \int_R \frac{W_0}{2\pi} \exp\left[-\frac{1}{2}\left(\frac{r-\mu_S}{\sigma_S}\right)^2\right] \frac{1}{\sqrt{2\pi}\sigma_R} \exp\left[-\frac{1}{2}\left(\frac{r-\mu_R}{\sigma_R}\right)^2\right] dr \\
&= \frac{W_0}{2\pi} \frac{\sigma_S}{\sqrt{\sigma_S^2+\sigma_R^2}} \exp\left[-\frac{1}{2}\left(\frac{\mu_R-\mu_S}{\sqrt{\sigma_S^2+\sigma_R^2}}\right)^2\right]
\end{aligned} \tag{3.6}$$

where W_0 is the zero-crossing frequency of the load process, and indexes $_S$ and $_R$ refer to load and resistance parameters, respectively.

3.5 Simulation results for Gaussian random barriers

In this section, the simulation procedure introduced in chapter 2 is applied to Gaussian random barriers. An array of 442 time-invariant Gaussian barriers is obtained by varying the means from $\mu_R = 2$ to $\mu_R = 10$, with increments of 0.5, and by varying the standard deviations from $\sigma_R = 0.0$ to $\sigma_R = 2.5$, with increments of 0.1 (all in load process standard deviation units). The same standard Gaussian narrow-banded (NB) and broad-banded (BB) load processes described in section 2.5 are considered. A total of $m = 10^3$ frequency components are used in the discretization, resulting in (periodic) sampling times of $T = 863$ and $T = 628$ cycles for the NB and BB processes, respectively. The barrier parameter range is chosen

so as to result in reasonable failure probabilities, for 10^5 samples of each load process[1]. A new sample of each barrier is simulated for each realization of the load processes. The total computation time for one set of results is around 48 hours in an 800 MHz Pentium PC.

First, the random barriers are reduced by making $\mu = \frac{\mu_R - \mu_S}{\sigma_S}$ and $\sigma = \frac{\sigma_R}{\sigma_S}$, where indexes $_R$ and $_S$ are used for resistance and load parameters, respectively. Since the load processes considered are standard Gaussian ($S = N(0,1)$), barrier parameters don't change, hence $R = N(\mu_R, \sigma_R) = N(\mu, \sigma)$. However, in order to extend the results presented in this section to non-standard Gaussian load processes, load process and barrier parameters have to be reduced as indicated.

Figure 3-1 shows the up-crossing rates $\upsilon^+_{EI}(\mu, \sigma, t)$ and $\upsilon^+_{ED}(\mu, \sigma, t)$ for both narrow-band and broad-band load processes, as functions of time. Since the random barriers are time-invariant, $\upsilon^+_{ED}(\mu, \sigma, t)$ does not vary in time; $\upsilon^+_{EI}(\mu, \sigma, t)$, however, shows a strong asymptotic behavior over time. The time length over which $\upsilon^+_{EI}(\mu, \sigma, t)$ varies is much longer than the length of variation observed for the deterministic barriers (figure 2-6). It is very important to note the significant difference between the asymptotic limit of $\upsilon^+_{EI}(\mu, \sigma, t)$ and the stationary value $\upsilon^+_{ED}(\mu, \sigma, t)$, which already indicates that the ensemble up-crossing rate approximation is largely conservative.

Figure 3-2 shows the *order of magnitude* EUR error (equation 3.4) for selected random barriers and the NB and BB load processes. It is confirmed in this figure that the EUR error is very large. An error of 3 orders of magnitude, for example, means that an ensemble up-crossing rate calculated as being around 10^{-1} could in fact be as low as 10^{-4} crossings/cycle. Equivalent errors (2 to 3 orders of magnitude) are also obtained in failure probabilities. The magnitude of the EUR error is discussed further in chapter 5.

Figure 3-3, column 1, shows contours of the error for the maximum sampling time $t = T$ ($T = 863$ and $T = 628$ cycles for NB and BB processes, respectively), as a function of the random barrier parameters μ and σ. It can be seen that the error decreases with $\mu = \frac{\mu_R - \mu_S}{\sigma_S}$ and increases with $\sigma = \frac{\sigma_R}{\sigma_S}$. The error contours are reasonably described (figure 3-3, column 2) by the function:

$$E_P(\mu, \sigma) = \sqrt{\frac{\sigma^2 + 1}{\mu}} \tag{3.7}$$

which is called the EUR order-of-magnitude error parameter or simply error parameter. The

[1] The number of crossings and the variance of simulation results varies significantly within the sampled barrier domain. However, with the parameters considered, the sampling error is very small in the barrier parameter domain where the EUR error is non-zero.

numeral 1 in the error parameter expression is believed to be the standard deviation of the (standard) load process. The complete description of the error contours, for the maximum sampling time $t = T$ (figure 3-3, column 2 and figure 3-4), is obtained by the function:

$$\overline{E}_D(\mu, \sigma, T) = p_s \cdot \text{erf}\left[\frac{p_r}{\sqrt{2}}\left(\sqrt{\frac{\sigma^2+1}{\mu}} - p_l\right)\right] \tag{3.8}$$

where the p's are calibration parameters and $\text{erf}(x)$ is the error function, which is related to the Gaussian cumulative distribution function: $\text{erf}(x) = 2\Phi(\sqrt{2}x) - 1$. Range and location parameters are found to be $p_r = 3.0$ and $p_l = 0.5$, for both the narrow-band (NB) and broad-band (BB) load processes. Moreover, these parameters appear to be independent of time, except for small intervals after $t = 0$. Scale parameter p_s describes the amplitude of the error as a function of time. The value of error parameters, especially p_s, is dependant on the particular level up-crossing rate expression $\upsilon^+(r,t)$ used in the computation of $\upsilon^+_{ED}(\mu, \sigma, t)$ (equation 3.1). Error parameters derived here refer to the "corrected" analytical ensemble-integration up-crossing rate expression (equation 3.5).

With the observation that scale parameter p_s is the only parameter that varies significantly in time, description of the error is greatly simplified. The approximated error expression becomes:

$$\overline{E}_D(\mu, \sigma, t) \approx \; p_s(t)\,\text{erf}\left[\frac{3.0}{\sqrt{2}}\left(\sqrt{\frac{\sigma^2+1}{\mu}} - 0.5\right)\right] \tag{3.9}$$

where function $p_s(t)$ is obtained by an interpolation between a couple of values $p_s(t_k)$ evaluated at discrete times t_k, as shown in Table 3.1. A reasonable interpolation of $p_s(t)$ is obtained using a function $t^{0.3}$:

$$p_s(t) \approx a^* \; t^{0.3} + b^* \tag{3.10}$$

where coefficients $\{a^*, b^*\}$ are obtained as the solution to the minimum-square problem:

$$\{a^*, b^*\} = \min \frac{1}{2}[p_s(t_k) - (a \; t_k^{0.3} + b)]^2, \qquad t_k \in \{t_1, t_2, ..., t_n\} \tag{3.11}$$

For the broad-banded load process and small ($t < 100$ cycles) time, however, as well as for the narrow-banded load process and not so small ($t < 300$ cycles) time, the location parameter $p_l = 0.5$ does not fit the numerical data, perhaps because for such small time the assumption of independence of the "independent" ensemble up-crossing rates is still inadequate. Re-evaluation of this parameter yields $p_l = 0.55$ for the NB process at $t = 47$ cycles and p_l

Table 3.1: Points of interpolation of scale parameter.

NB process		BB process	
t_k	$p_s(t_k)$	t_k	$p_s(t_k)$
0	0.00	0	0.00
047	2.00	049	1.45
314	2.80	149	1.95
543	3.10	277	2.25
863	3.30	628	2.65

$= 0.60$ for the BB process at $t = 49$ cycles. Equation (3.9) is adjusted accordingly for these parameters and times. The interpolated error function and numerical results are compared in figure 3-5 for selected random barriers.

Although equation (3.8) fits the simulated numerical data quite well (figures 3-3 and 3-4), it presents two inconsistencies or limitations. The first, and most obvious, is that it yields negative errors for $\sqrt{(\sigma^2+1)/\mu} < 0.5$, a consequence of using the error function $\mathrm{erf}(x) = 2\Phi(\sqrt{2}x) - 1$ to describe the error in the gradient direction. Hence, equations (3.8 and 3.9) have to be limited to the positive range:

$$\begin{aligned} \overline{E}_D(\mu,\sigma,t) &= p_s(t)\cdot \mathrm{erf}\left[\frac{3.0}{\sqrt{2}}\left(\sqrt{\frac{\sigma^2+1}{\mu}}-0.5\right)\right], \qquad \text{for} \quad \sqrt{\frac{\sigma^2+1}{\mu}} > 0.5 \\ &= 0 \qquad\qquad\qquad\qquad\qquad\qquad\qquad\qquad\qquad\qquad \text{otherwise.} \end{aligned} \tag{3.12}$$

The second inconsistency is the fact that the error is not zero when the standard deviation of the random barrier is nil, as should be expected. For $\sigma = 0$ and $\mu > 4$, however, the error in the former error expression turns out negative, and hence the limit in equation (3.12) applies. Barriers with $\mu < 4$ have little practical interest, hence the limit above virtually eliminates this inconsistency as well.

Inserting the quantities $\mu = \frac{\mu_R - \mu_S}{\sigma_S}$ and $\sigma = \frac{\sigma_R}{\sigma_S}$ in equation (3.7), an expression for the EUR error parameter for general Gaussian processes $S = N(\mu_S, \sigma_S)$ and general Gaussian barriers $R = N(\mu_R, \sigma_R)$ is obtained:

$$E_P(R,S) = \sqrt{\frac{1}{\sigma_S}\frac{(\sigma_S^2+\sigma_R^2)}{(\mu_R-\mu_S)}} \tag{3.13}$$

3.6 Comparison with failure probabilities

Interesting results are obtained when the EUR error is compared with corresponding failure probabilities. This is done in figure 3-6, where EUR errors and failure probabilities are plotted as a function of the error parameter $\sqrt{(\sigma^2+1)/\mu}$. This figure is obtained by lumping together the data in figure 3-3, with each point $(\mu, \sigma, E_D(\mu, \sigma, T))$ generating one point $(\sqrt{(\sigma^2+1)/\mu}, E_D(\mu, \sigma, T))$. The figure shows the numerical EUR error (dark dots), the negative logarithm of the "exact" (MC simulation) failure probability ($-\log_{10}(P_{f_{MC}}(T))$ - gray dots) and the analytical error expression (eq. 3.8 - continuous line). It can be seen in this figure that, as failure probabilities increase, the EUR error increases. However, EUR errors are not directly proportional to failure probabilities. The small scatter of EUR error points reveals that $\sqrt{(\sigma^2+1)/\mu}$ is indeed an appropriate error parameter. The same cannot be said about failure probabilities. The high scatter of $P_f(T)$ points seen in the figure shows that failure probability is not appropriate parameter of the order-of-magnitude EUR error.

Figure 3-6 shows that the largest EUR errors, for large values of the error parameter, correspond to very large failure probabilities and are out of the range of practical interest. However, the figure also shows that, for intermediate values of the error parameter, the EUR error can be large while failure probabilities are small. As an example, drawn from the figure, an error of two orders of magnitude is possible with $P_f(T) = 10^{-3}$. Hence, it is the intermediate range of the error parameter (say, $0.5 < \sqrt{(\sigma^2+1)/\mu} < 1.2$) which is critical for practical purposes.

The notion that EUR errors can be large is not new (Pearce and Wen, 1984; Schall et al., 1991 and Wen and Chen, 1989). However, these results show that the general assumption that EUR errors are proportional to failure probabilities (Pearce and Wen, 1984; Schall et al., 1991 and Wen and Chen, 1989) can be misleading, since order-of-magnitude EUR errors can be large even when failure probabilities are small. The issue is addresses further in chapter 5.

It should be noted that, although MC simulation failure probabilities plotted in figure 3-6 do not converge to one, the corresponding EUR approximated failure probabilities do. For example, using the largest MC simulation failure probability and NB error drawn from the figure, the EUR failure probability is:

$$
\begin{aligned}
P_{f_{EUR}}(T) &= 1-(1-P_{f_{MC}}(T))^{10^{E_D(T)}} \\
&\approx 1-(1-10^{-0.5})^{10^{2.7}} \\
&\approx 1.
\end{aligned}
$$

Hence, the EUR error is only bounded (from above) because failure probabilities are limited to one. This realization reveals that the upper bound of the error, as per expression (3.8), is not an absolute upper bound, and that the derived error parameters are also not absolute. The issue is addressed further in next section.

3.7 Extrapolation of the EUR error expression

In this section, the analytical EUR error expression derived via simulation is extended to wider barrier parameters ($\mu > 11$ and $\sigma > 2.5$). An extrapolated set of 272 random barriers is considered, with means ranging from 10 to 40, with increments of 2, and standard deviations ranging from 0.5 to 8.5, with increments of 0.5. Because the failure probability for most of these barriers is very small, the simulation procedure cannot be used to obtain conditional up-crossing rate statistics. Alternatively, conditional up-crossing rates are obtained from a reference solution based on an extreme value interference problem, as described next.

Extreme value distributions $f_{S_T}(s)$ of the Gaussian load processes are obtained as described in section 1.8.2, for the same sampling times $T = 863$ and $T = 628$ cycles (NB and BB processes, respectively). A "reference" or "exact" failure probability is obtained as the solution to the one-dimensional convolution integral:

$$
P_{f_{EX}}(T) = \int_{-\infty}^{+\infty} f_{S_T}(s)\, F_R(s) ds \tag{3.14}
$$

This result is assumed close enough to the exact failure probability because the problem is scalar, the barriers are time-invariant, the load process is ergodic and the number of cycles T is large enough for the asymptotic extreme value distribution to be valid. Conditional ensemble up-crossing rates are evaluated through equation (3.3), with "exact" failure probabilities (right hand term) calculated from the extreme-value interference solution rather than through Monte Carlo simulation. Crossing rates are obtained by finite difference derivation. Putting it in words, this solution stands for obtaining up-crossing rates from a sensitivity analysis of extreme value distributions. A finite difference parameter $\Delta x = 10$ cycles is used for this

sensitivity analysis. Dependent ensemble up-crossing rates are obtained from the closed form expression (equation 3.6) and the dependency error is measured following equation (3.4).

Results for the extrapolated data set are presented in figures 3-7 and 3-8. It can be seen in figure 3-7 that, as for the simulated data set, the EUR error is bounded (from above) because failure probabilities are limited to one. Error expression (3.5) is shown in figure 3-7 as a doted line. A perfect match between the two sets of results should not be expected, because the error illustrated in figures 3-6 and 3-7 refer to two distinct crossing rate expressions (equations 3.5 and 3.6). Clearly, for the extrapolated data set error parameters have to be reviewed:

$$\overline{E}_D(\mu, \sigma, T) = p_s(T) \cdot \text{erf}\left[\frac{p_r}{\sqrt{2}}\left(\sqrt{\frac{\sigma^2+1}{\mu}} - p_l\right)\right] \tag{3.15}$$

Expression (3.15) does not fit the extrapolated data points very tightly over the whole error parameter range. Since the final part of the curve (where failure probabilities converge to one) is of limited practical interest, curve fitting is restricted to the smaller error parameter range. In this way, equation (3.15) is made to follow numerical results in the region where EUR errors are large and failure probabilities are small. Error parameters for the extrapolated data set, leading to the curves shown in figure 3-7 (continuos lines) are $p_l = 0.43$, $p_r = 2.0$ and $p_s(T) = 3.4$ for the NB process and $p_l = 0.43$, $p_r = 1.7$ and $p_s(T) = 2.55$ for the BB load process. Figure 3-8 shows contour lines of the numerical EUR error and of equation (3.15), for the extrapolated data, as a function of random barrier parameters.

The error fitting exercise for both simulated and extrapolated data sets shows that range and scale parameters (p_r and $p_s(T)$) are interdependent. Hence, the derived error expressions and error parameters are valid for the respective parameter range only. Error expression (3.15), with parameters indicated above, is valid for the range of barrier parameters of the extrapolated data set ($10.0 \leq \mu \leq 40.0$, $0.5 \leq \sigma \leq 8.5$) and, strictly speaking, for $P_f(T) < 1.0$. Barriers of practical problems can be expected to be well within this range. For barriers below this range, error expression for the simulated data set can be used. For barriers out of this range ($\mu > 40.0$, $\sigma > 8.5$), an upper bound of the error is obtained by making a linear extrapolation of the curves in figure 3-7:

$$\overline{E}_D(\mu, \sigma, T) < 5\left(\sqrt{\frac{\sigma^2+1}{\mu}} - 0.5\right) \tag{3.16}$$

Despite the differences related to crossing rate expressions considered in each case, the general agreement of the two sets of results, in terms of overall behavior, demonstrates con-

sistency between the two procedures (simulation and extreme-value analysis) used to obtain conditional ensemble up-crossing rate statistics.

3.8 Upper-bound solutions

Findings presented in the last two sections make appropriate a word of caution about the use of upper-bound solutions to failure probabilities. It is known that an upper-bound to $P_f(T)$ can be obtained as (Ditlevsen and Madsen, 1996):

$$P_f(T) \leq P_{f_0} + E[N^+(0,T)] \tag{3.17}$$

$$\leq P_{f_0} + \int_0^T \upsilon^+(t)dt \tag{3.18}$$

The advantage of this upper-bound solution is that it does not require the assumption of (conditional) Poissonian up-crossings. Hence, in the random barrier problem, it allows one to replace $\upsilon^+(t)$ by the ensemble up-crossing rate $\upsilon^+_{ED}(t)$ (Sudret et al., 2002). No error here, because the upper bound is still an upper bound. Results presented earlier in this chapter, obtained from a simulation procedure where the Poisson assumption is observed, have shown that the error in the EUR approximation can be very large. Hence, if the same approximation is used in the upper-bound solution, the P_f bound in equation (3.17) will be very far from the true P_f when the EUR error is large. Generalizing, EUR error results obtained earlier in this chapter can be extended to the upper-bound solution:

> "For the random barrier problem, the closeness of the upper-bound solution to the real P_f will be proportional to error parameter $\sqrt{(\sigma^2+1)/\mu}$, and not necessarily proportional to failure probabilities as generally assumed."

3.9 Non-gaussian random barriers

In this section, the EUR error estimation is extended to problems involving non-Gaussian barriers. Three non-Gaussian data sets are considered. One data set is formed by truncated Gaussian barriers, with same moments as the Gaussian data set of section 3.5 ($\mu_R = 2$ to $\mu_R = 10$ and $\sigma_R = 0.0$ to $\sigma_R = 2.5$). The second data set is formed by log-normal random barriers, also with same barrier moments. For these two data sets, the same narrow-band and broad-band standard Gaussian load processes are considered again. A third data set is formed by Gaussian barriers (3.5), but with a standard Gaussian pulse sequence process (sampling time of $T = 3000$ cycles).

In order to understand the effect of non-gaussianity in the EUR error, it is appropriate to analyze the ensemble up-crossing rate equation a little further:

$$\upsilon^{+}_{ED}(R) = \int_{R} \upsilon^{+}(r) f_R(r) dr \tag{3.19}$$

The kernel of equation (3.19) is the product of a (generally) exponentially decreasing function of r, $\upsilon^{+}(r)$, by the resistance distribution, $f_R(r)$. Under normal circumstances, this product can be expected to have a maximum between μ_S and μ_R. This maximum, and hence the ensemble up-crossing rate, is severely affected by the way the resistances lower tail spreads towards the load process. The EUR error, as will be shown in results that follow, is also affected by this lower tail. As an example, figure 3-9 shows up-crossing rate $\upsilon^{+}(r)$ for a Gaussian load process and three "second moment equivalent" random barriers. The moments of the three barriers are $(\mu, \sigma) = (6, 1)$, but their distributions are distinct. One barrier is Gaussian, one is log-normal (limited by $r > 0$) and the third is an inverted log-normal distribution (limited by $r < 12$). Also shown in the figure (right) is the kernel of equation (3.19), or the product $\upsilon^{+}(r) f_R(r)$. It can be seen that, despite the similarity of the barriers, the area under the curves (and, consequently, the ensemble up-crossing rate) varies significantly. Unfortunately, for such problems point-wise equivalent normal transformations such as the "Principle of Normal Tail approximation" (Ditlevsen, 1981) are not useful, since the ensemble up-crossing rate is affected by the whole lower tail of the resistance. This result, together with the fact that non-Gaussian barriers cannot be uniquely described by μ and σ, show that a straightforward generalization of results derived for Gaussian barriers is not possible. A different approach is required.

In order to identify the appropriate error parameter for the non-Gaussian barriers, the data points of the non-Gaussian data sets have to be lumped together as was done for the Gaussian barriers in figure 3-6. Starting with the Gaussian data set as an example, each point $(\mu, \sigma, E_D(\mu, \sigma, T))$ is "mapped" into one point $(\sqrt{(\sigma^2 + 1)/\mu}, E_D(\mu, \sigma, T))$, as seen in figure 3-10 (center). For comparison with the EUR error parameter, the Gaussian data set is also lumped in terms of ensemble up-crossing rates $\upsilon^{+}_{ED}(\mu, \sigma)$ (figure 3-10, left) and in terms of the C.O.V. $(\frac{\sigma}{\mu})$ of the random barrier (figure 3-10, right). As seen in section 3.6, the scatter of each lumped data set shows how good each (tentative) error parameter is. Hence, it is confirmed that, for Gaussian barriers, $\sqrt{(\sigma^2 + 1)/\mu}$ is a much better error parameter than ensemble up-crossing rates (or failure probabilities) and then the C.O.V. of the random barrier.

The procedure is repeated for the non-Gaussian data sets, which are lumped in terms of

$\upsilon^{+}_{ED}(\mu,\sigma)$, $\sqrt{(\sigma^2+1)/\mu}$ and $\frac{\sigma}{\mu}$. Results are shown in figure 3-11 for the log-normal barriers and for the pulse-sequence load process with Gaussian barriers, and in figure 3-12 for the truncated Gaussian barriers. The scatter of the lumped non-Gaussian data sets is significantly reduced with the Gaussian EUR error parameter, but even better parameters can be identified. These parameters are $\sqrt{(\sigma+1)/\mu}$ for the log-normal barriers and $\sqrt{(\sigma^2/2+1)/\mu}$ for the pulse-sequence load process, as shown in figure 3-11.

For comparison, all data sets are also plotted using the coefficient of variation (σ/μ) of the random barrier as error parameter (third column in the figures). It can be clearly seen that the C.O.V. is not as good an error parameter as $\sqrt{(\sigma^2+1)/\mu}$, although it is much better than the ensemble up-crossing rate. For all barriers considered, the EUR error can be reasonably approximated, as a function of the respective error parameter "x", by the error function:

$$E_D(x,T) \approx c_1 \,\mathrm{erf}\left[\frac{a_1}{\sqrt{2}}(x-b_1)\right] \tag{3.20}$$

where error coefficients (a_1, b_1, c_1) are obtained by curve fitting. Similar error expressions as a function of the C.O.V. can also be obtained:

$$E_D(\frac{\sigma}{\mu},T) \approx c_2 \,\mathrm{erf}\left[\frac{a_2}{\sqrt{2}}\left(\frac{\sigma}{\mu}-b_2\right)\right] \tag{3.21}$$

Error coefficients (a_1, b_1, c_1) and (a_2, b_2, c_2) are given in Table 3.2 for the Gaussian and non-gaussian barriers considered in this section. For completeness, μ versus σ contours of the EUR error and analytical error functions (eq. 3.20) are shown in figure 3-13 for the log-normal random barriers and for the pulse-sequence load process. Figure 3-14 shows the error fitting in the cross-sections indicated in figure 3-13.

Expressions (3.20 and 3.21) only provide EUR error estimates at the simulated time $t = T$, which are close to the asymptotic limit of these errors. A complete description of the error's time variation, as for the Gaussian barriers, would require similar expressions and parameters to be obtained for another 3 or 4 time points, and interpolation to be used between these expressions.

The log-normal and truncated normal barriers considered in this section can be uniquely described by only two parameters (μ and σ). Derivation of similar results for other non-Gaussian barriers is not so simple, and probably has to be made conditional to additional parameters of the barrier.

Table 3.2: Coefficients of EUR error functions for Gaussian and non-Gaussian barriers.

Load	Barrier	a_1	b_1	c_1	a_2	b_2	c_2	error parameter x
NB	Gaussian	3.00	0.50	3.30	6.00	0.12	2.70	$\sqrt{\frac{\sigma^2+1}{\mu}}$
NB	Truncated Gaussian	2.50	0.48	3.00	4.00	0.10	3.00	$\sqrt{\frac{\sigma^2+1}{\mu}}$
BB	Gaussian	3.00	0.50	2.65	6.00	0.12	2.35	$\sqrt{\frac{\sigma^2+1}{\mu}}$
BB	Truncated Gaussian	2.70	0.50	2.60	5.00	0.10	2.50	$\sqrt{\frac{\sigma^2+1}{\mu}}$
BB	Log-normal	3.14	0.60	2.90	2.60	0.18	2.90	$\sqrt{\frac{\sigma+1}{\mu}}$
PS	Gaussian	4.50	0.38	3.35	6.00	0.08	3.35	$\sqrt{\frac{\sigma^2/2+1}{\mu}}$

3.10 Concluding remarks

In this chapter, a Monte Carlo simulation-based methodology to evaluate the error of the EUR approximation was introduced. The methodology was applied to scalar problems involving Gaussian load processes and Gaussian and non-Gaussian barriers. Suitable error parameters were identified and error functions were constructed.

The analytical error expressions derived can be used to limit the use of the EUR approximation, in terms of random barrier parameters, or to correct EUR failure probability results (chapter 4). Error expressions and other results presented in this chapter are used to compare the EUR approximation with other common simplifications of time-variant reliability problems in chapter 5. Results are extended to (slow-varying) random process barriers in chapter 6, and are applied to fatigue and fracture reliability analysis in chapter 11.

Derived error expressions are valid only for the particular random load processes and barriers considered in this study, but the numerical methodology is, in principle, applicable to other random processes and barriers as well. The methodology is quite general in the sense that MC simulation results based on simple analytical time-invariant barriers can be used to obtain error expressions to be used in practical problems with expensive, numerically computed, random barriers. Importantly, the EUR error estimate is obtained from small simulated samples of the load processes, but can be readily extended for much longer time intervals at no extra cost. Difficulties involved in the error prediction for non-Gaussian barriers and processes were identified in this chapter, namely, random barriers that cannot be uniquely described just by the mean and standard deviation.

It was shown that the EUR approximation error, when measured in terms of orders of magnitude, is not necessarily proportional to failure probabilities, as generally believed. A proper error parameter was identified, and it was shown that EUR errors can indeed be large even when failure probabilities are small.

The study of the ensemble up-crossing rate approximation presented herein is believed to be a new development, and is believed to provide new insights into characteristics of the EUR approximation. The importance of this contribution can be judged from the generality of the EUR approximation in terms of time-variant reliability analysis of uncertain structures, and from a number of possible applications.

3.11 Figures

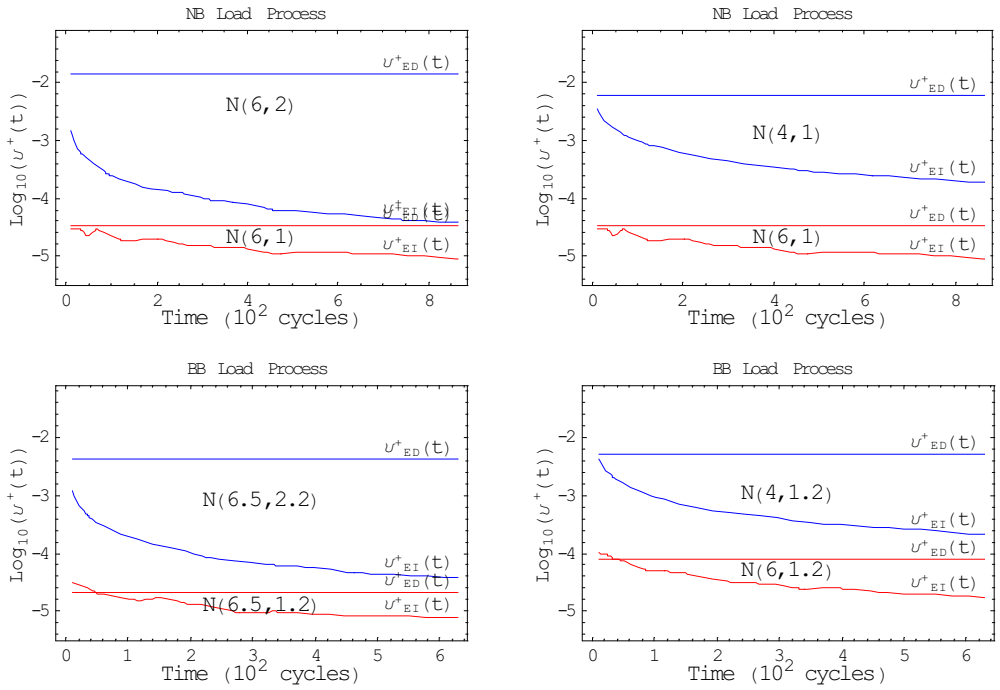

Figure 3-1: Ensemble up-crossing rates $\upsilon_{EI}^{+}(\mu,\sigma,t)$ and $\upsilon_{ED}^{+}(\mu,\sigma,t)$ for selected random barriers $N(\mu,\sigma)$.

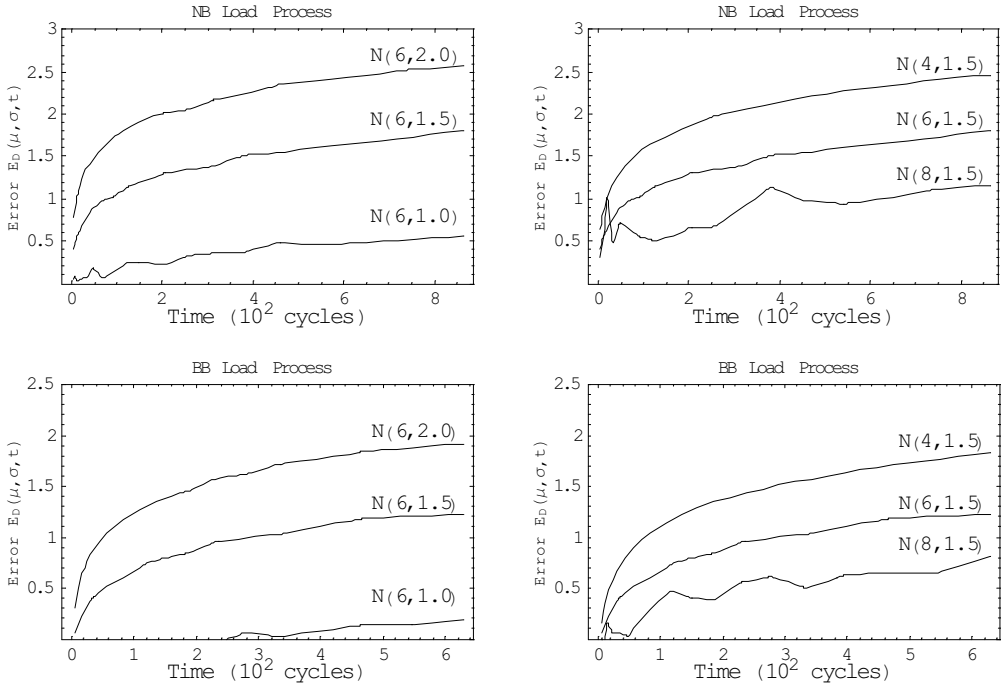

Figure 3-2: Variation of the EUR error in time for selected random barriers $N(\mu,\sigma)$.

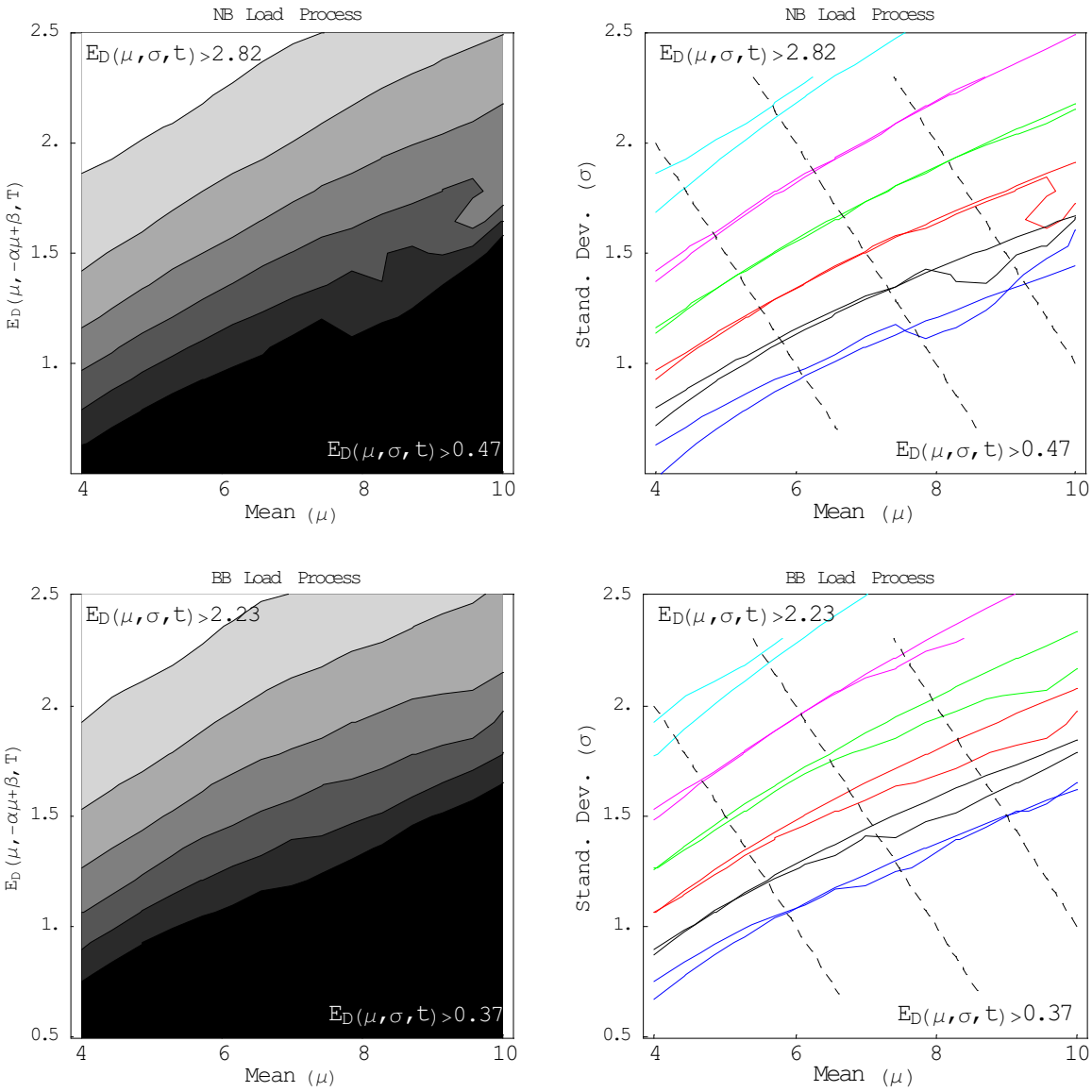

Figure 3-3: Dependency errors $E_D(\mu, \sigma, T)$ and $\overline{E}_D(\mu, \sigma, T)$ as function of barrier parameters μ and σ.

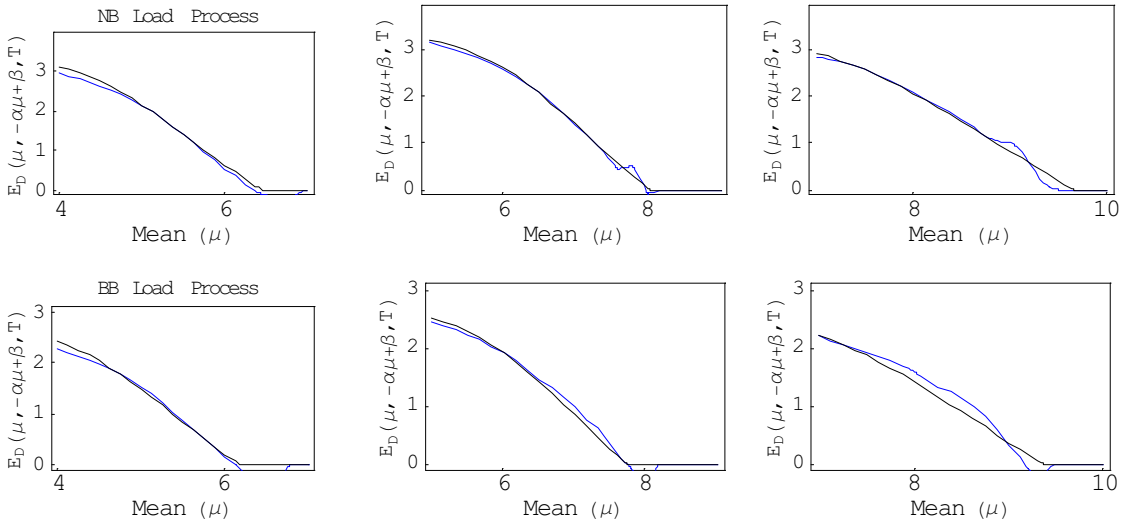

Figure 3-4: Dependency errors $E_D(\mu, \sigma, T)$ and $\overline{E}_D(\mu, \sigma, T)$ in diagonal direction, as indicated in figure 3-3, column 2.

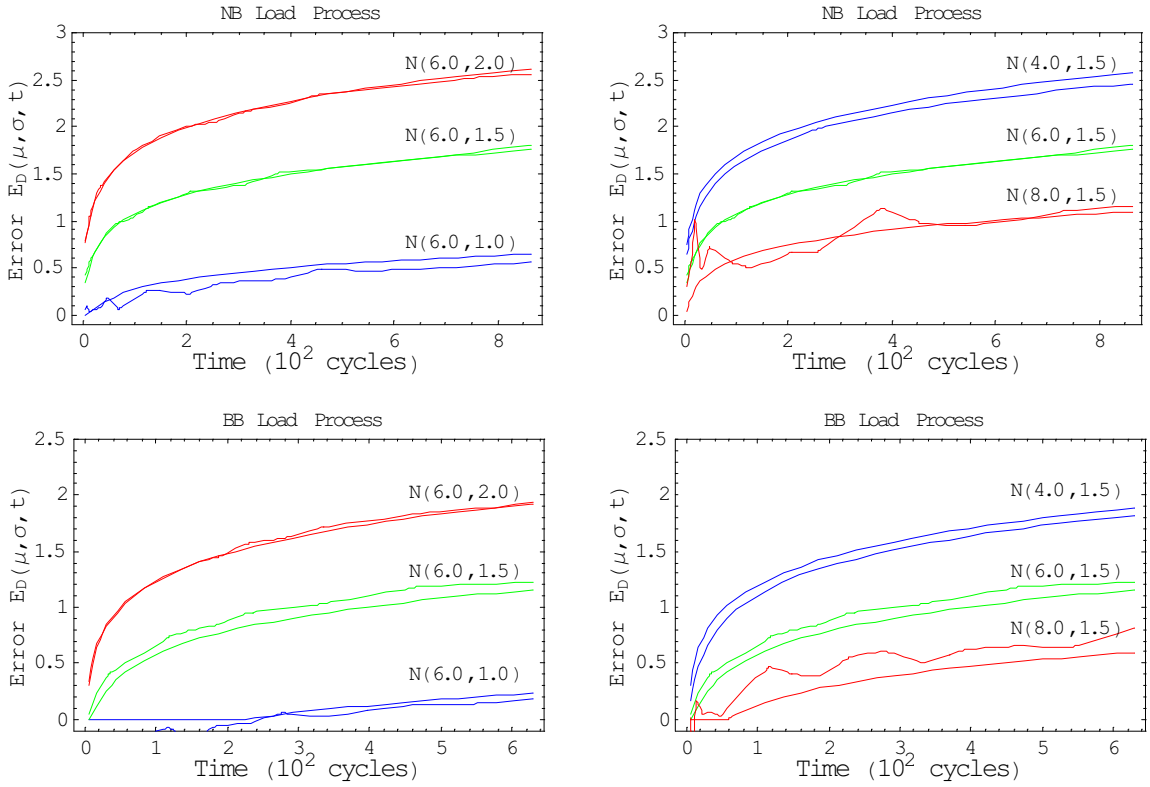

Figure 3-5: Time variation of the estimated and numerical errors for selected random barriers.

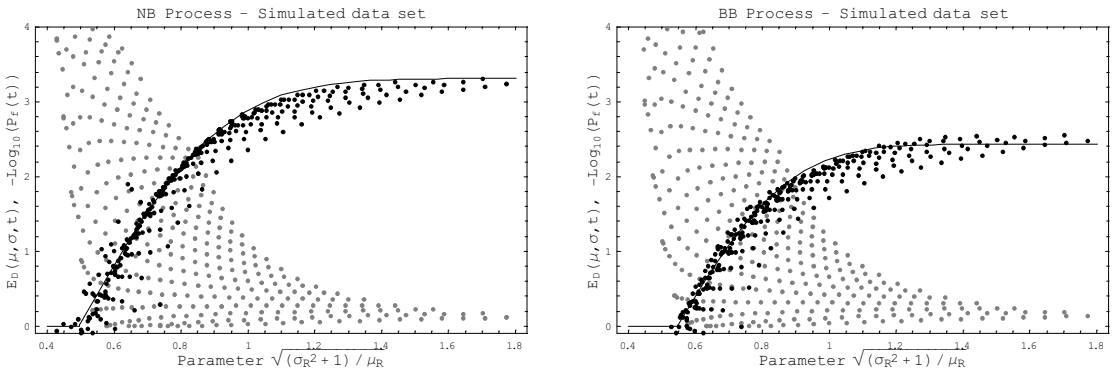

Figure 3-6: EUR error and failure probabilities as a function of error parameter, simulated data sets.

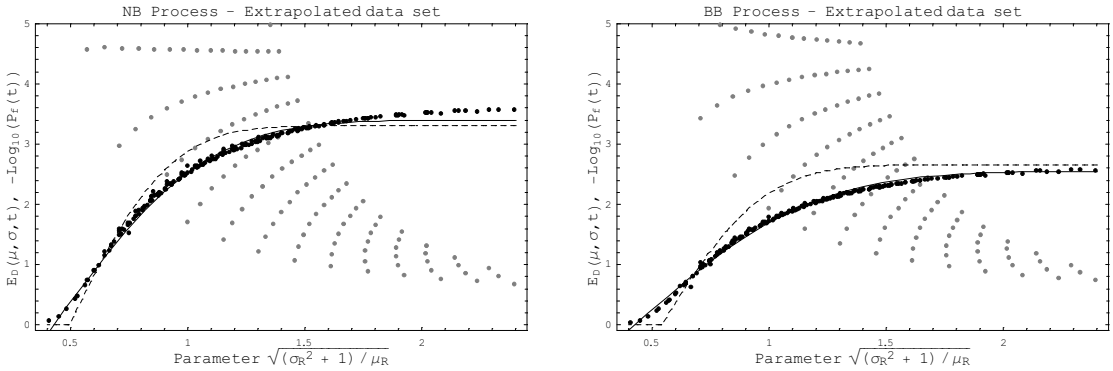

Figure 3-7: EUR error and failure probabilities as a function of error parameter, extrapolated data sets.

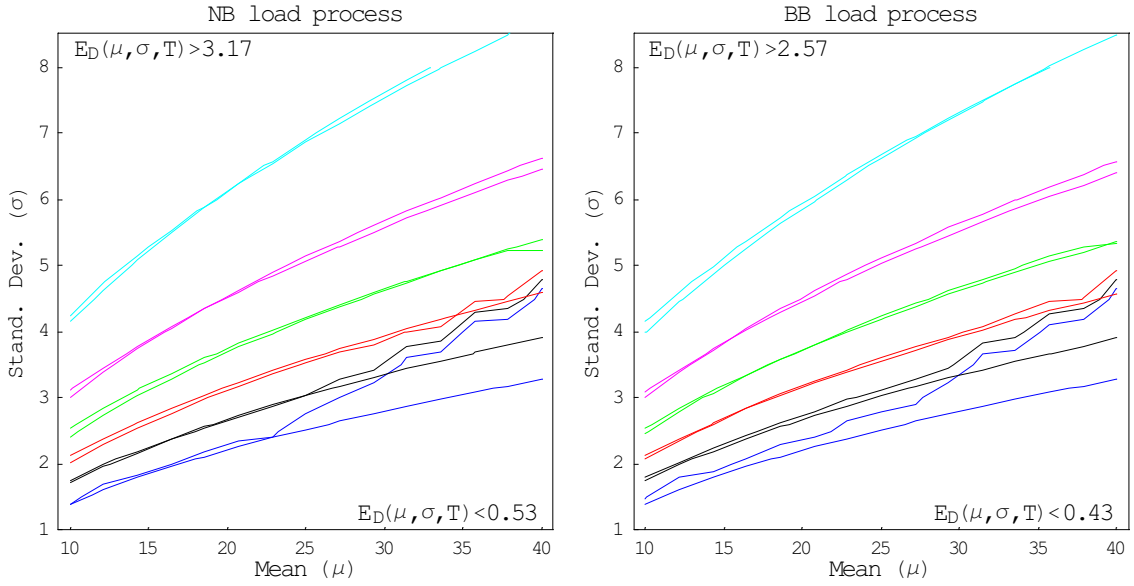

Figure 3-8: Numerical and estimated error contours as function of barrier parameters μ and σ, extrapolated data sets.

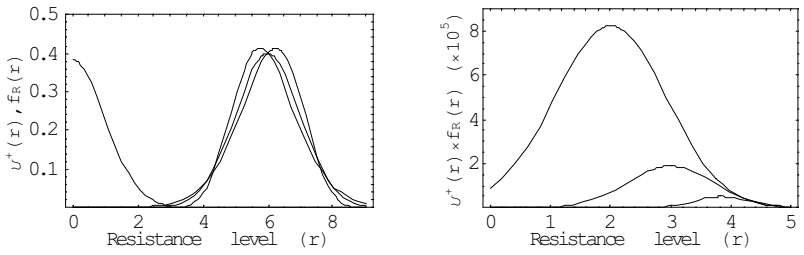

Figure 3-9: Analysis of the kernel of equation (3.19).

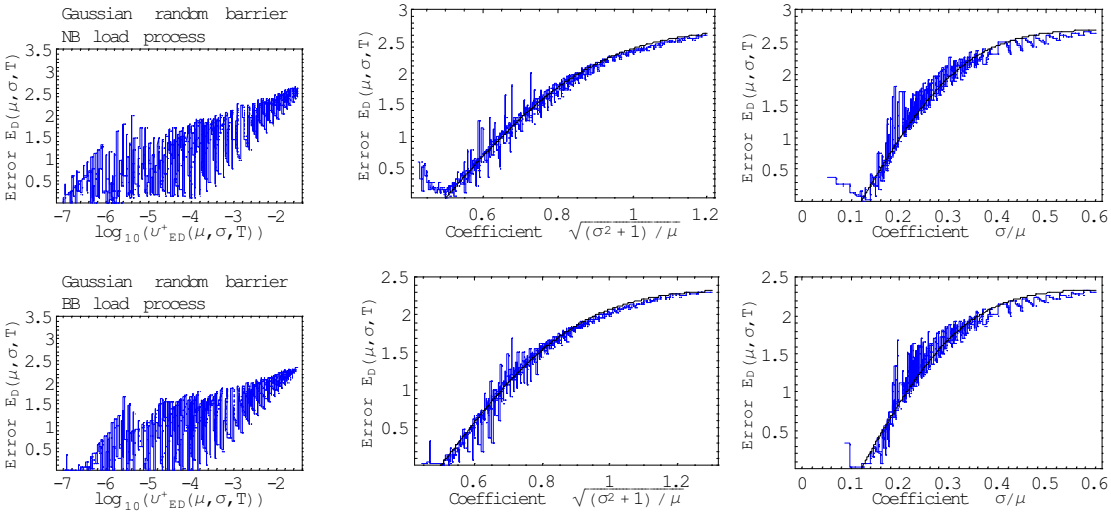

Figure 3-10: Lumped data sets as function of $v^+_{ED}(\mu,\sigma)$ (left), $\sqrt{(\sigma^2+1)/\mu}$ (center) and $\frac{\sigma}{\mu}$ (right), Gaussian random barriers.

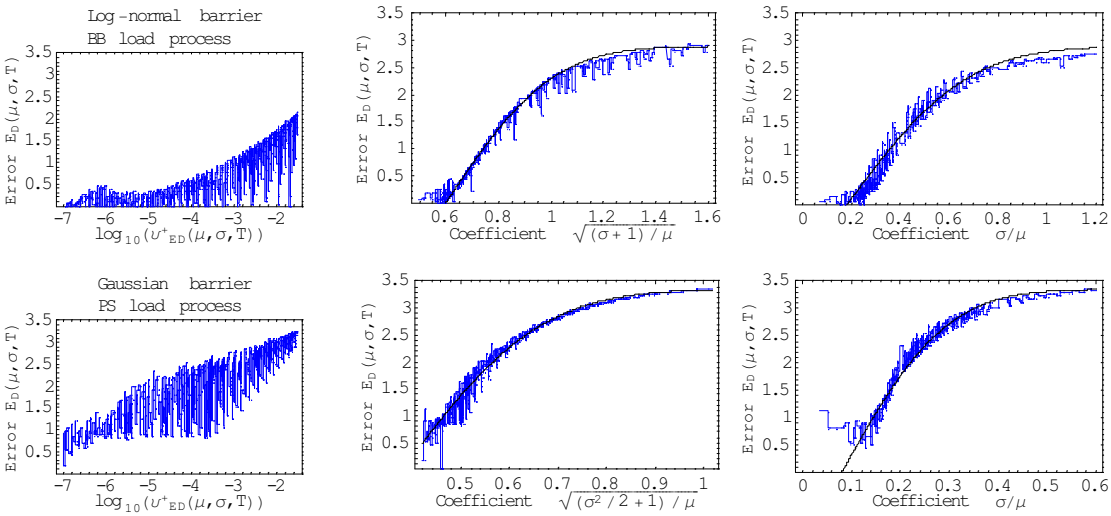

Figure 3-11: Lumped data sets as function of $v^+_{ED}(\mu,\sigma)$ (left), $\sqrt{(\sigma^2+1)/\mu}$ (center) and $\frac{\sigma}{\mu}$ (right), log-normal barriers (top) and pulse-sequence load process (bottom).

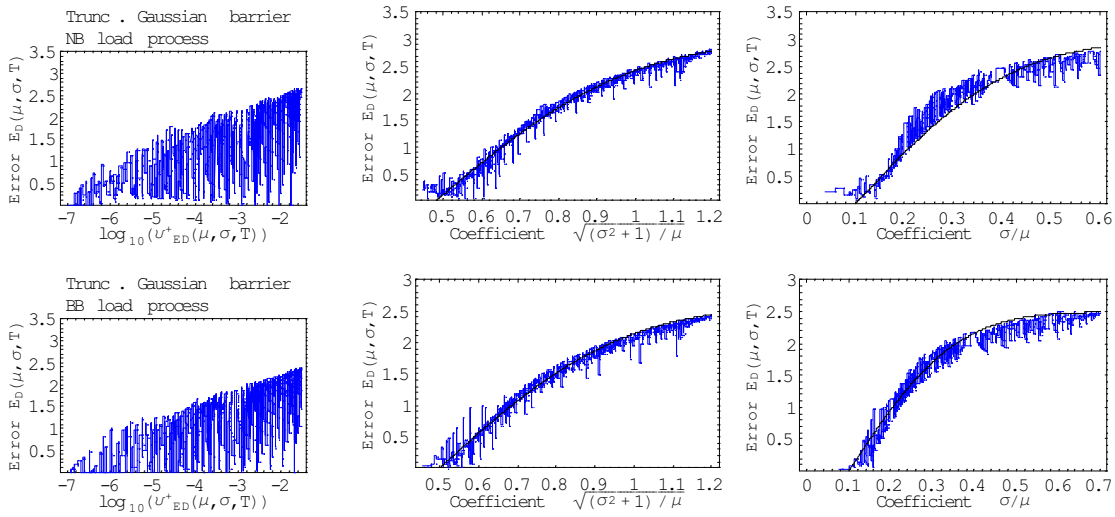

Figure 3-12: Lumped data sets as function of $v^{+}_{ED}(\mu,\sigma)$ (left), $\sqrt{(\sigma^2+1)/\mu}$ (center) and $\frac{\sigma}{\mu}$ (right), truncated Gaussian random barriers.

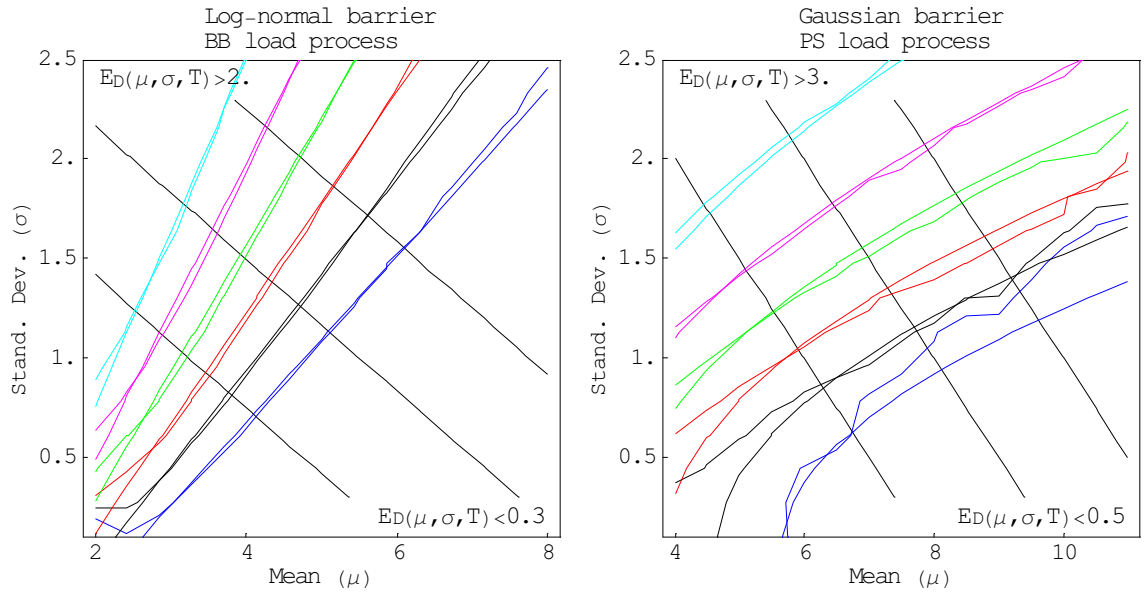

Figure 3-13: Error contours for log-normal barriers and pulse-sequence load process as function of barrier parameters.

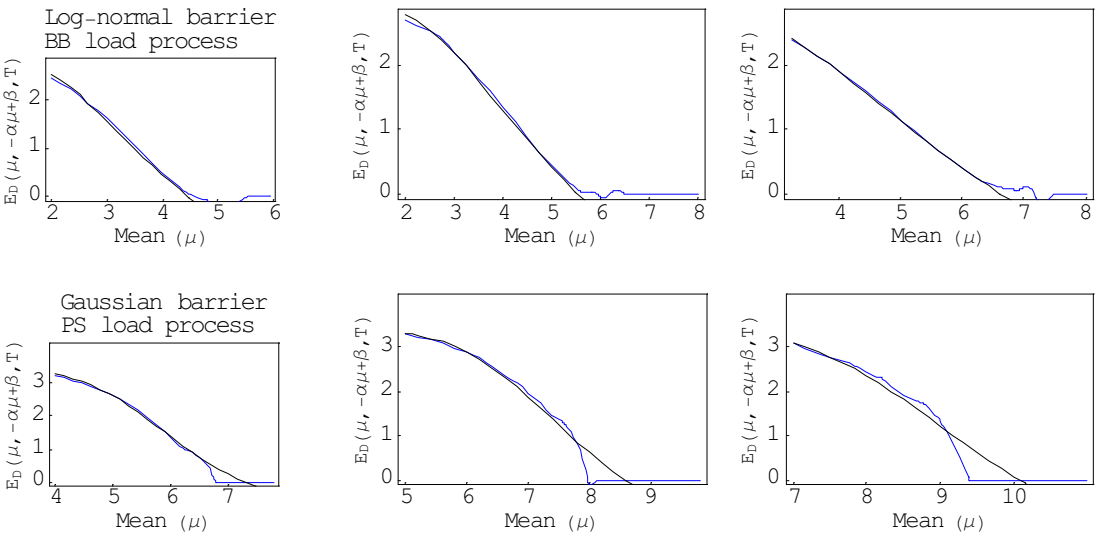

Figure 3-14: Error in transversal directions indicated in figure 3-13.

Chapter 4

CORRECTION OF EUR FAILURE PROBABILITIES

4.1 Introduction

In this chapter, the error expressions derived in chapter 3 are used to obtain a correction of the original ensemble up-crossing rate approximation. The correction is applied first to time-invariant random barriers, and then extended to time-variant parametrically defined random barriers. Results show that the error in the original EUR approximation is substantially reduced.

Correction of EUR failure probability results from a given error expression is a more demanding problem than a simple limitation of the EUR approximation, as the error estimation needs to be more accurate. Also, in order to establish limits of application for the EUR approximation, it is important that error estimates be conservative (i.e., the actual error be smaller than the predicted error). In order to derive corrections to P_f estimates, however, the error prediction needs to be unconservative, so that resulting (corrected) failure probabilities are still conservative.

4.2 Correction of crossing rates from error estimates

Once the EUR error is predicted, error estimates can be used to correct original EUR failure probability results. For time-invariant random barriers, such correction is straightforward, as a corrected up-crossing rate estimate can be obtained directly from equation (3.4):

$$\upsilon_E^{+TI}(\mu,\sigma,t) = \upsilon_{ED}^{+}(\mu,\sigma,t) \cdot 10^{-\overline{E}_D(\mu,\sigma,t)} \tag{4.1}$$

where $\upsilon_E^{+TI}(\mu, \sigma, t)$ is the up-dated or corrected ensemble up-crossing rate estimate for time-invariant random barriers. Formally, the quantity $\upsilon_E^{+TI}(\mu, \sigma, t)$ is the time-variant arrival rate of first up-crossings over the random barrier. Hence, corrected failure probabilities at any time t are evaluated as:

$$P_f(\mu, \sigma, t) = P_{f_0}(\mu, \sigma) + (1 - P_{f_0}(\mu, \sigma)) \cdot (1 - \exp[-\int_0^t \upsilon_E^{+TI}(\mu, \sigma, s)ds]) \qquad (4.2)$$

where $P_{f_0}(\mu, \sigma)$ is the initial failure probability for the random barrier. Given the asymptotic character of the ensemble up-crossing rate error, expression (4.2) can be readily extrapolated beyond the sampling time T used in the Monte Carlo simulation, at no additional computational cost.

4.3 Application to time-invariant random variable barriers

The EUR correction developed above is first applied for time-invariant random variable barriers. Figure 4-2 shows results for the narrow-band (NB) and the broad-band (BB) processes, with time $t = T$. Figure 4-3 shows similar results with time extrapolated to $t = 5T$. In the figures, the original EUR solutions (no correction), the corrected EUR solutions and the "exact" MC simulation solutions are compared for a selection of time-invariant random barriers, following the legend shown in figure 4-1. In figures 4-2 to 4-14, column A) is a representation of the random barrier, column B) compares the error in failure probabilities and column C) shows failure probability results.

It can be seen in figures 4-2 and 4-14 that the EUR error is correctly predicted, and "exact" MC failure probability results can be reproduced. For the time-invariant random barrier case, this is no surprise, as the EUR error is predicted from failure probability results, and then used to correct failure probability results. The situation becomes more complicated, however, for time-variant barriers, as will be seen next.

4.4 Application to time-variant parametrically defined random process barriers

The experimental procedure introduced in chapter 2 and used in chapter 3 to predict the EUR error does not provide quantitative information about how barrier variations affect the EUR error. However, insight obtained from the time-invariant barrier study and numerical experimentation can be used to obtain empirical, approximate estimates of the EUR error

for time-variant barriers.

Results presented in chapter 3 show that the EUR error grows asymptotically in time and increases when the error parameter (eq. 3.7) increases[1]. Barrier variations occur over a period of time, hence asymptotic error increase in time and error increase due to barrier parameter variations cannot be isolated. More importantly, error increase due to parameter variation can also be expected to be reflected asymptotically in time. The impossibility of separating the asymptotic time effects from barrier variation effect makes the error estimation for time-variant barriers more difficult. An empirical approximation can still be derived, however. First, the case of small barrier variations occurring at large times is considered. This situation is simpler because error variation is mainly due to barrier parameter variation. The more general situation of large and small barrier variations at small times is then considered.

4.4.1 Error averaging for small barrier variations

Due to the asymptotic nature of the EUR error, barrier variations can be expected to have a slow and long-lasting effect on the EUR error. Hence, the EUR error at time t can be expected to be affected by barrier variations occurring at all times before t. Moreover, one can assume barrier variation occurring closer to t to have a larger effect on the EUR error than barrier variations occurring much earlier. Given these observations, a simple weighted integral is proposed to average the EUR error at a given time t:

$$\overline{E}_D^{TVa}(\mu, \sigma, t) = \int_0^1 w(z) \cdot \overline{E}_D(\mu, \sigma, t - \lambda z) dz \tag{4.3}$$

where $\overline{E}_D^{TVa}(\mu, \sigma, t)$ is the averaged time-variant barrier error estimate, $w(z) = 2(1-3z^2+2z^3)$ is the weighting function (an Hermite polynomial) and λ gives the length of the integration interval in time. The integration interval is initially set to $\lambda = t$. The weight function was chosen arbitrarily, on the basis that $w(1) = 0$ and $w(0) = 2$, the derivatives at both limits is zero and the integral from $z = 0$ to $z = 1$ results in an unit area.

Because the integral over $w(z)$ results in an unit area, equation (4.3) yields the time-invariant error estimate $\overline{E}_D(\mu, \sigma, t)$ when this error is constant. This means that equation (4.3) is strictly valid only when the barrier does not change and for very large times (as the time-invariant error $\overline{E}_D(\mu, \sigma, t)$ increases with time). It will be seen, however, that expression (4.3) still provides reasonable error estimates when barrier variations are small. The averaging error correction also does not distinguish between error increase due to parameter variation

[1] Because this thesis is focused on resistance degradation problems, only increases of the EUR error and of the error parameter are considered.

and asymptotic error increase in time. This difficulty can be partially removed by limiting the integration interval for large times, hence removing asymptotic error increase (for time-invariant barriers) at small times. This is done by making: $\lambda = \min(t, \lambda_{max})$, where λ_{max} is set to 2500 cycles. Hence, the error is averaged over the last t cycles, if $t < 2500$ cycles, or over 2500 cycles if $t > 2500$ cycles. Numerical results are not terribly sensitive to the choice of λ_{max} , with $\lambda_{max} = 2300$ cycles or $\lambda_{max} = 2700$ cycles being equally possible.

Equation (4.3) was tested for a range of time-variant random barriers, with prescribed parameter variations. These barriers were formed by combining 1) linear and 2) cubic variations of 1) the mean only; 2) the standard deviation only; 3) both mean and standard deviation variations, with same exponent and 4) both mean and standard deviation variations, with distinct exponents. Different barrier parameter variations were considered, leading to large and small barrier variations. Barrier variations were also extended over longer time intervals. The case of delayed barrier variations has also been considered, with some barriers being time-invariant up to $t = T/2$, and varying in time after that.

Results are presented in figures 4-4 to 4-6. Figure 4-4 shows results for small barrier variations occurring over an extended time interval ($t = 5T$), with $\lambda_{max} = 2500$ cycles. Column 2 in the figure shows that persistent corrections from the time-invariant error estimate are obtained. The error estimate is unconservative, because at 3000 cycles the asymptotic error increase is still significant, but this leads to a conservative failure probability correction (column 3). Figure 4-5 shows results for the same barriers of figure 4-4 but with variations over a smaller time interval ($t = T$). It can be seen that the error estimate becomes slightly conservative in this case, although still very good overall. A comparison of figures 4-5 and 4-4 reveals that indeed the EUR error approaches the time-invariant estimate as the time interval increases, as could be expected. Hence, for small barrier variations occurring over longer time intervals (say, $t > 5T$) , the time-invariant error estimate can be used directly. The time-invariant error estimate is always a conservative estimate for time-variant barriers.

Unfortunately, when barrier variations are large (Figure 4-6, with $t = 5T$), the averaging error estimate becomes excessively unconservative. A better error estimate for large barrier variations is presented in the next section.

4.4.2 Error reduction for small and large barrier variations over small time intervals

As stated earlier, at small times the EUR error increases with barrier parameter variations and increases asymptotically in time, even if the barrier does not change. These two effects

cannot be isolated, making the error estimation more difficult. However, an empirical multiplication factor can be derived based on insight gained from previous results and numerical experimentation.

It was seen in the previous section that barrier variations cause an attenuation of the dependency error. Hence, the EUR error for a time-variant barrier can be assumed to be a fraction of the error for a time-invariant barrier of same parameters:

$$\overline{E}_D^{TVr}(\mu,\sigma,t) = \overline{E}_D(\mu,\sigma,t) \cdot r_f(\mu,\sigma,t) \tag{4.4}$$

where $r_f(\mu,\sigma,t)$ is an empirical reduction factor. A function that has to be identified. The EUR error parameter is used to quantify barrier variations in terms of variation of barrier parameters $\mu(t)$ and $\sigma(t)$:

$$E_P(t) = \sqrt{\frac{\sigma(t)^2+1}{\mu(t)}} \tag{4.5}$$

Hence, barrier variations are quantified by variations of the (now time-variant) error parameter $E_P(t)$. A barrier variation between t_1 and t_2 is quantified and adimensionalyzed as:

$$\left(1 - \frac{E_P(t_2) - E_P(t_1)}{E_P(t_2)}\right) \tag{4.6}$$

If there is no barrier variation, the quantity above results in one. It does not go to zero, however, because the error parameter is generally not smaller than 0.5 ($E_P(t) > 0.5$).

Due to the asymptotic nature of the EUR error, the error estimate $\overline{E}_D^{TVr}(\mu,\sigma,t)$ at any time t can be expected to be affected by barrier variations occurring at all times before t. Moreover, intuition suggests that barrier variations occurring closer to t have larger impact on $\overline{E}_D^{TVr}(\mu,\sigma,t)$ than barrier variations occurring much earlier. Hence, as for the averaged error estimate, a weighted integral is used to average the effect of barrier variations prior to t:

$$\begin{aligned} \overline{E}_D^{TVr}(\mu,\sigma,t) &= \overline{E}_D(\mu,\sigma,t) \cdot r_f(\mu,\sigma,t) \\ &= \overline{E}_D(\mu,\sigma,t) \cdot \int_0^1 w(z) \cdot \left(1 - \frac{E_P(t) - E_P(t-\lambda z)}{E_P(t)}\right)^{cte} dz \end{aligned} \tag{4.7}$$

Again, the weighting function is chosen arbitrarily. The exponent *cte* and the time-integration interval λ are obtained experimentally. Expression (4.7) yields the time-invariant error estimate $\overline{E}_D(\mu,\sigma,t)$ when there is no barrier variation. It does not have the limitation of equation

(4.3) regarding averaging asymptotic error growth because the averaging is now over barrier parameter variations. Unfortunately, however, the results depend on the exponent cte and the time-integration interval λ.

For not too long time intervals (say, up to $t = 2T$), reasonable results are obtained by setting $cte = 0.33$ and limiting λ to 500 cycles, as seen in figures 4-7 to 4-10, which show results for small and large barrier variations over $t = T$ and $t = 2T$. For $t = 2T$, it can be seen that the error estimate is slightly unconservative for small barrier variations (figure 4-9), and slightly conservative for large barrier variations (figure 4-10). For $t = 5T$ (figures 4-11 and 4-12) the error estimate becomes increasingly unconservative for small barrier variations, and increasingly conservative for large barrier variations. Similar results are obtained for the NB load process (as shown in figures 4-13 and 4-14 for $t = 2T$).

These results are changed by varying exponent cte and the time-integration interval λ. However, as a crude approximation for not too long time intervals, the values $cte = 0.33$ and $\lambda = 500$ cycles can be used. Surprisingly perhaps, given the empiricism of the time-variant error correction, reasonable corrections of EUR failure probabilities are obtained.

4.5 Concluding remarks

In this chapter, EUR error estimates were used to correct original EUR failure probability results, for both time-invariant and time-variant barriers. EUR error correction is, of course, more critical than simple limitation of the EUR approximation, because a more accurate description of the error is required. Despite the empiricism of the time-variant error corrections developed herein, results show that reasonable corrections are possible. More accurate error estimates would require a less empirical approach to the barrier variation problem than has been indicated herein. Nevertheless, it is considered that the empirical results presented here help raise the level of understanding of the problem.

Only random variable and parametrically defined random process barriers have been considered in this chapter. These are fully correlated barriers, for which both the random variable and the random process (transition probability density) solutions can be easily obtained. In chapter 6 results for slow-varying random process barriers are derived.

4.6 Figures

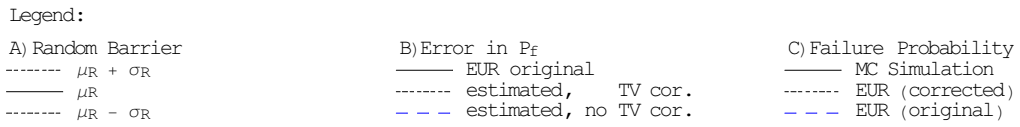

Figure 4-1: Legend for figures 4-2 to 4-14.

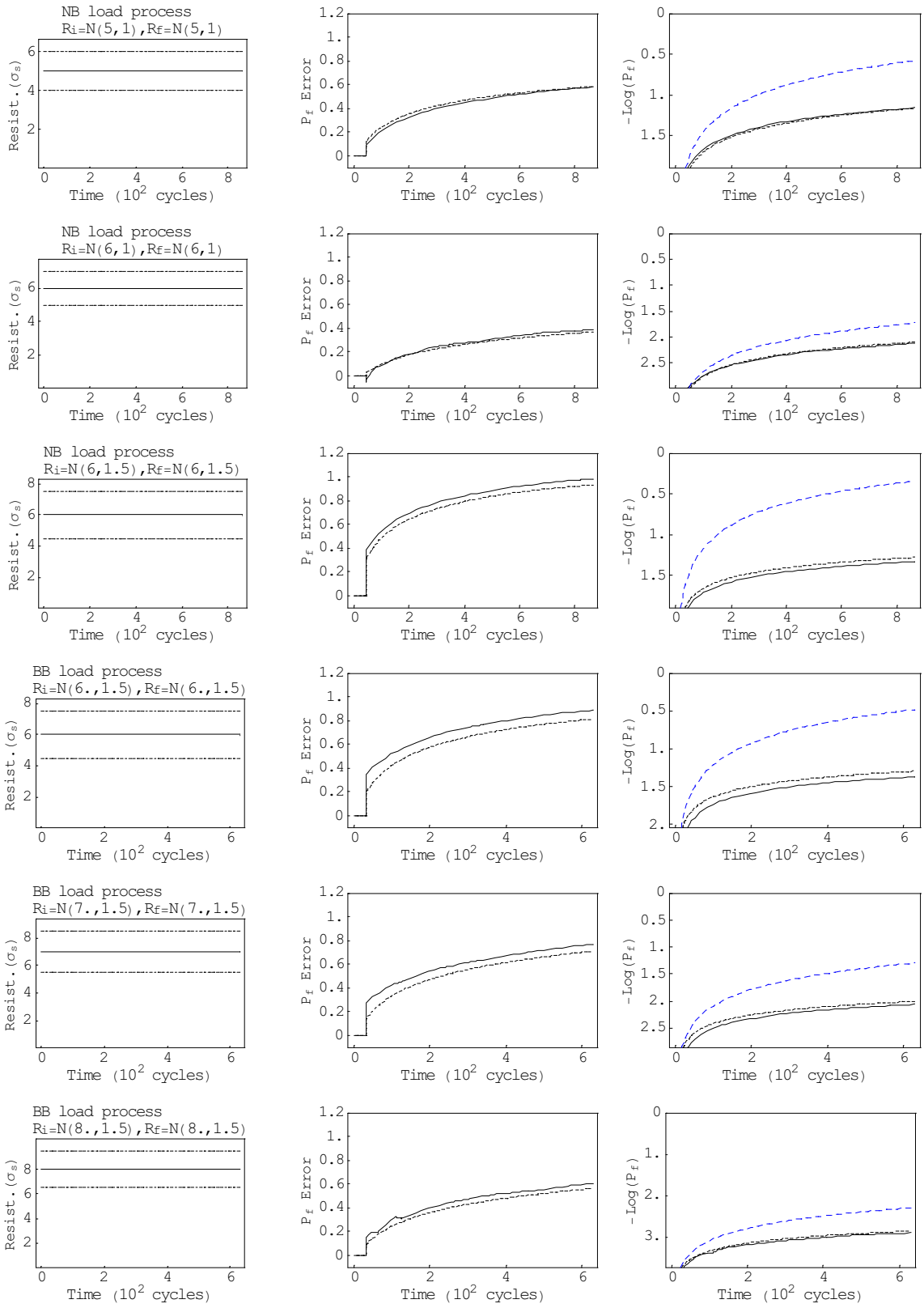

Figure 4-2: Results for time-invariant barriers, NB and BB load processes, $t = T$.

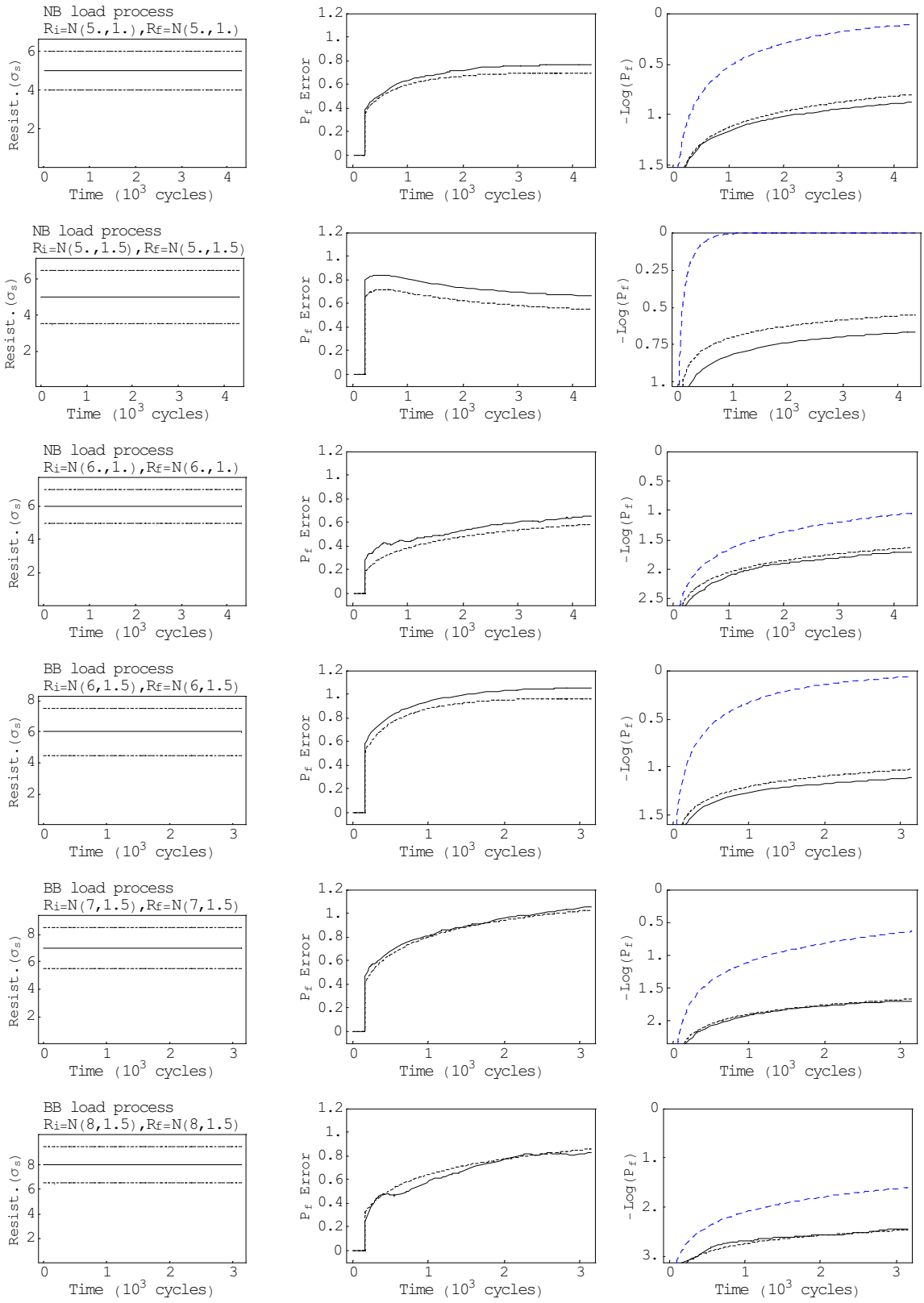

Figure 4-3: Results for time-invariant barriers, NB and BB load processes, $t = 5T$.

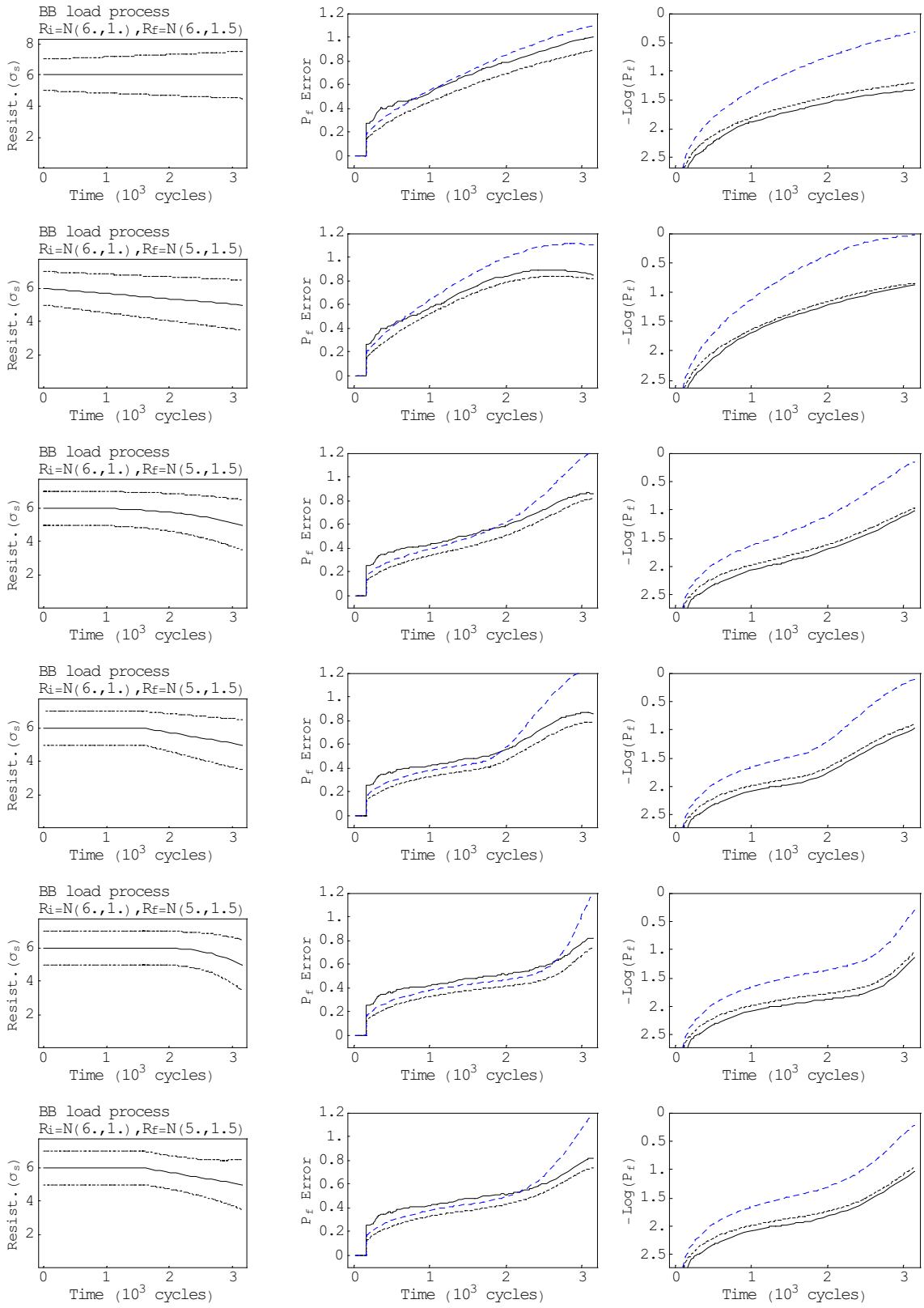

Figure 4-4: Error averaging results for small barrier variations, $t = 5T$.

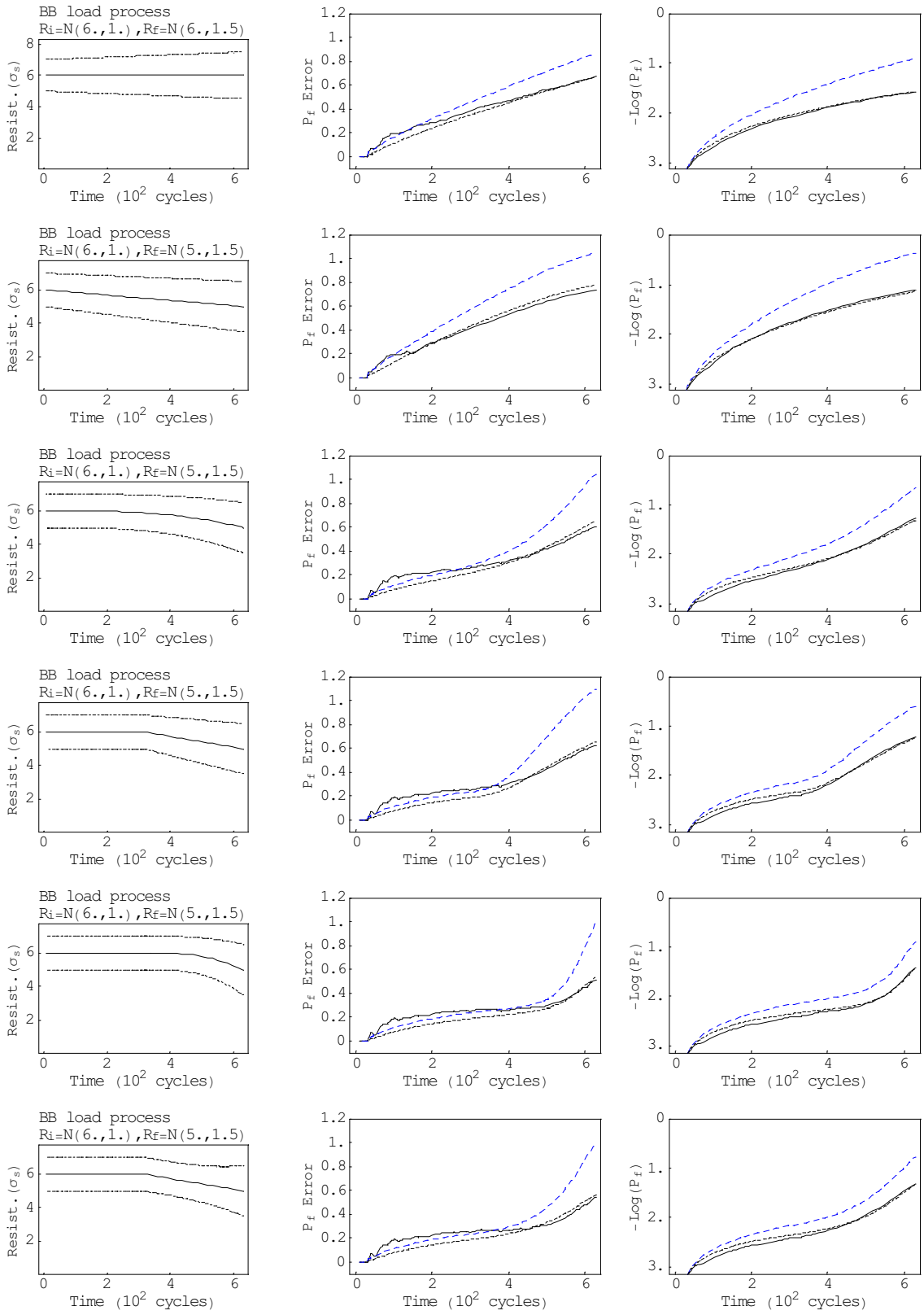

Figure 4-5: Error averaging results for small barrier variations, $t = T$.

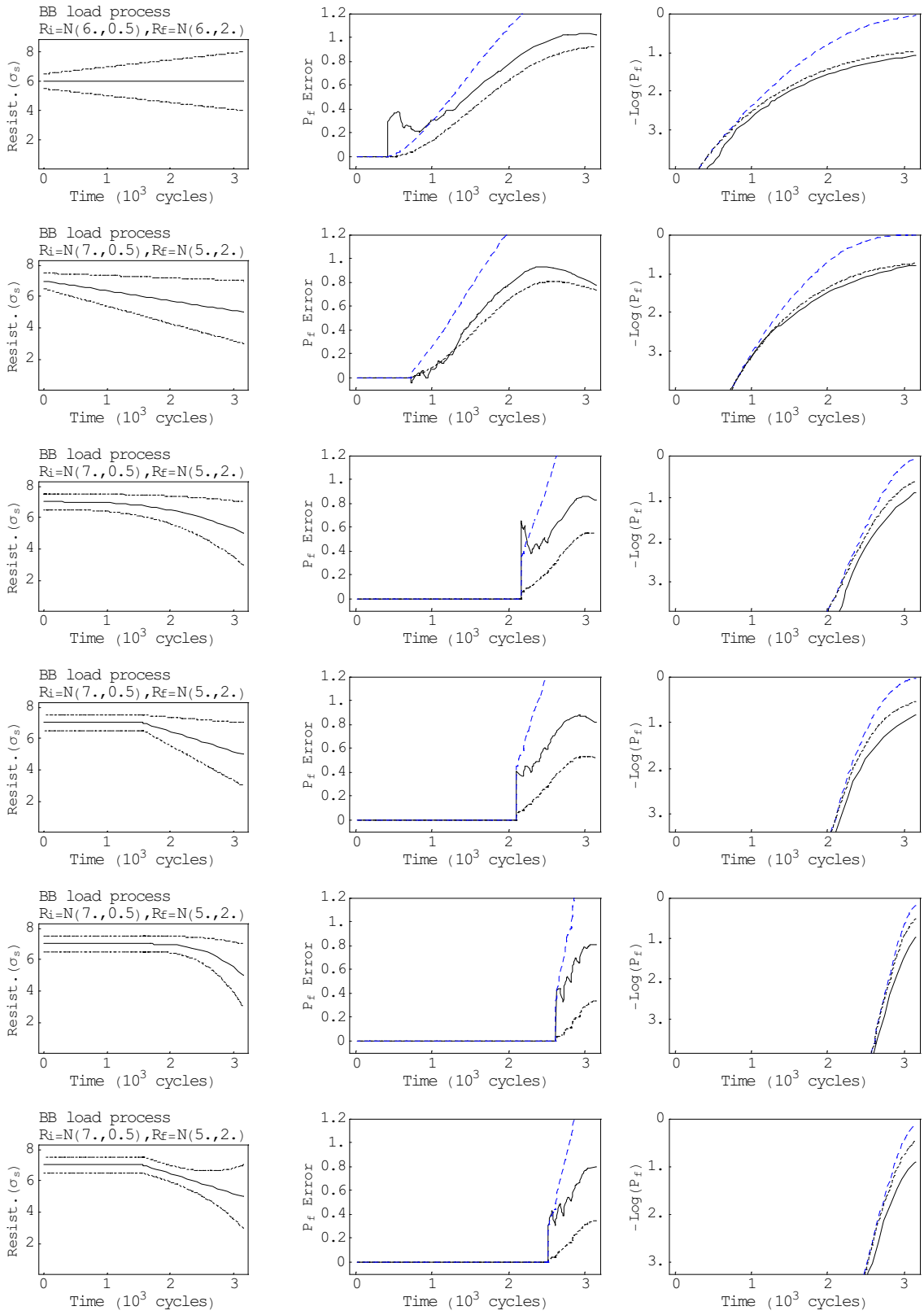

Figure 4-6: Error averaging results for large barrier variations, $t = 5T$.

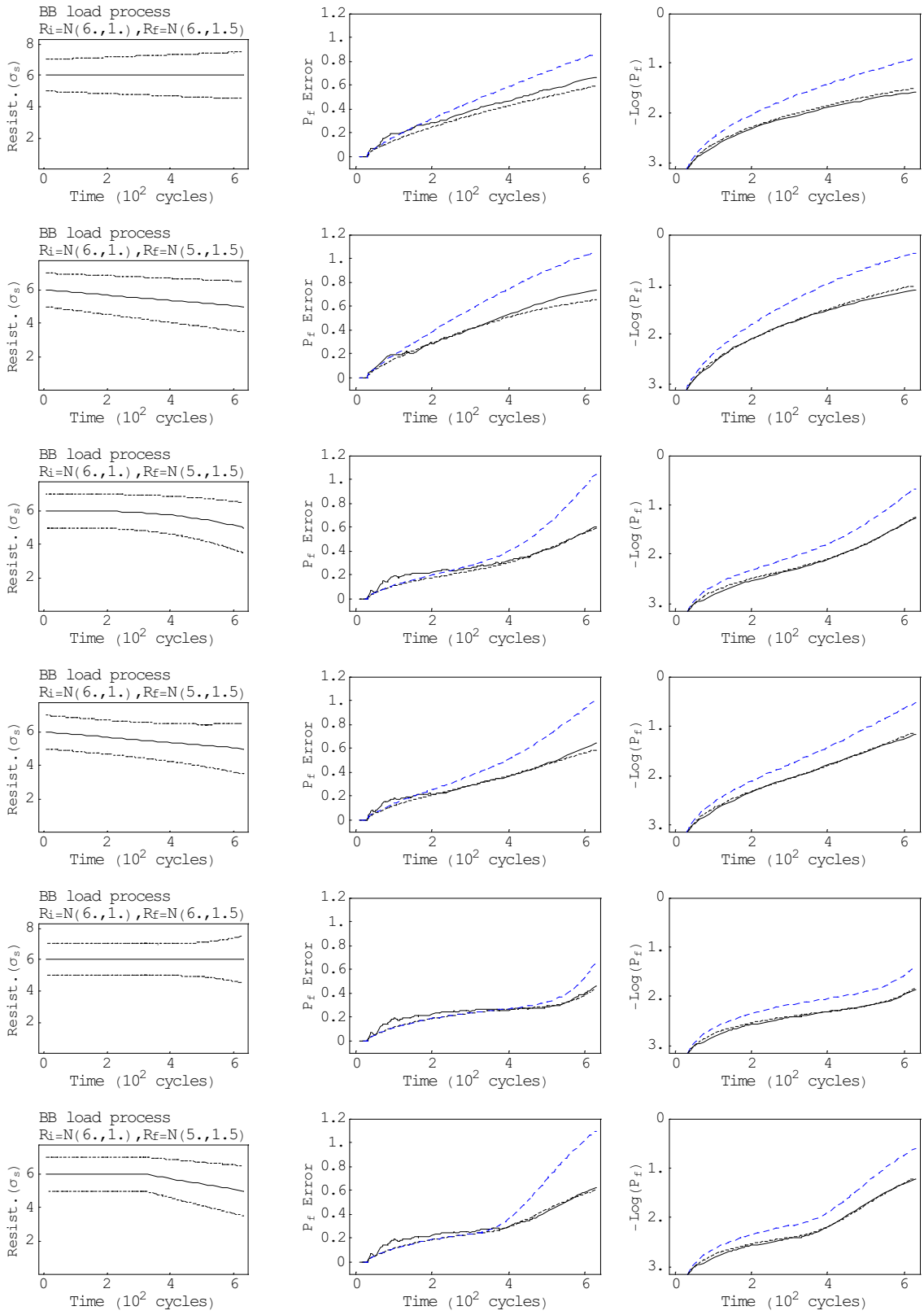

Figure 4-7: Error reduction results, small barrier variations over $t = T$.

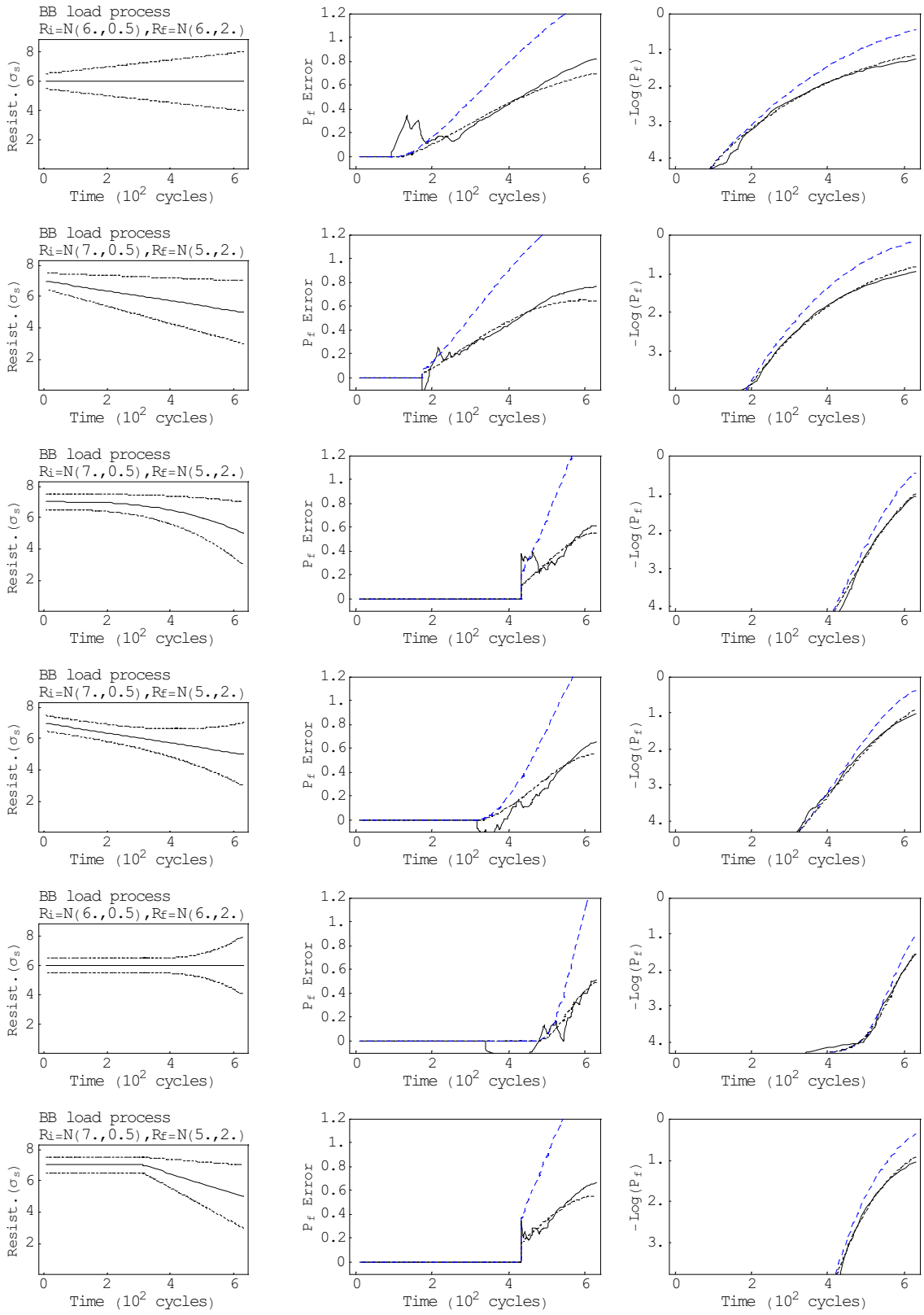

Figure 4-8: Error reduction results, large barrier variations over $t = T$.

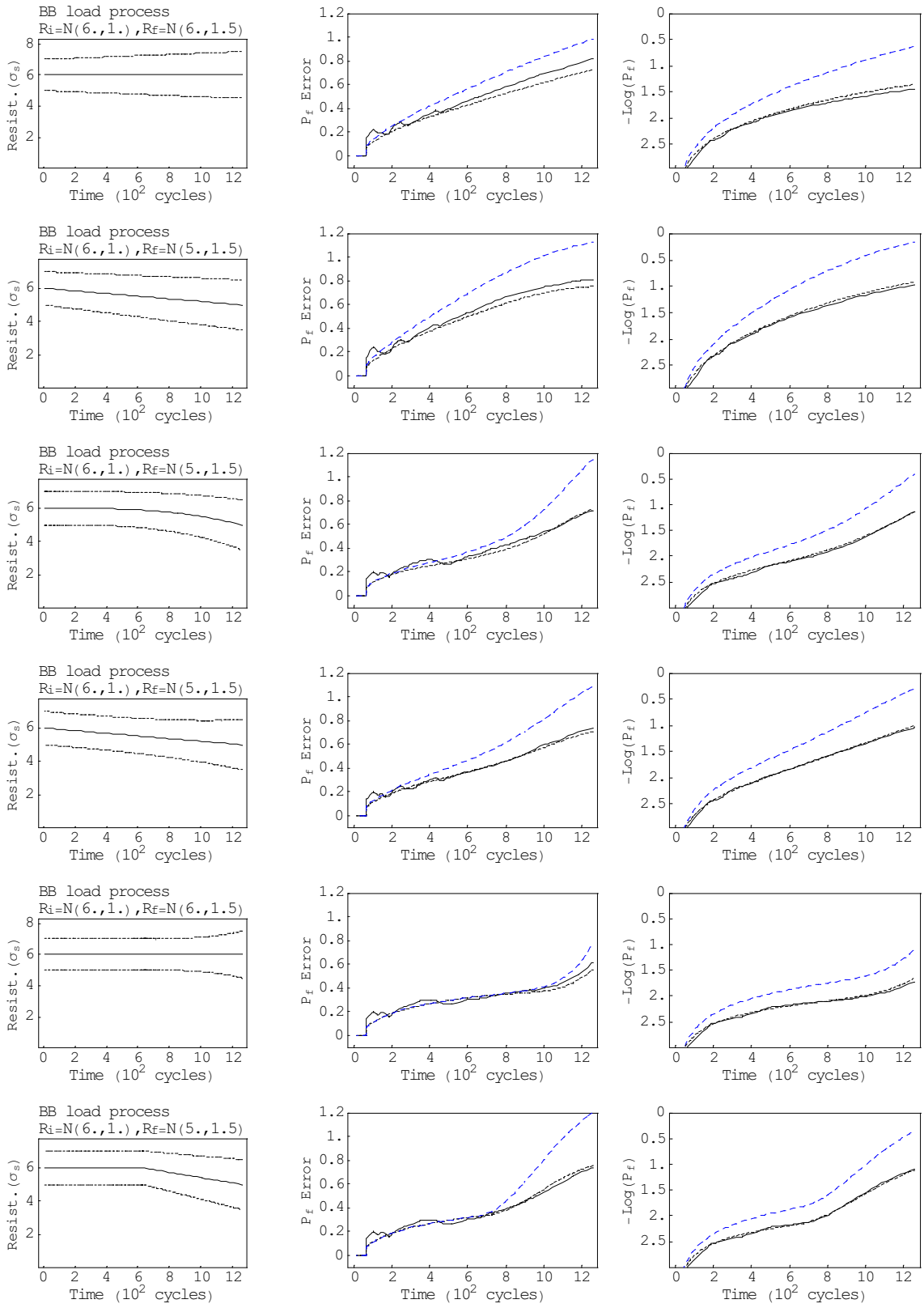

Figure 4-9: Error reduction results, small barrier variations over $t = 2T$.

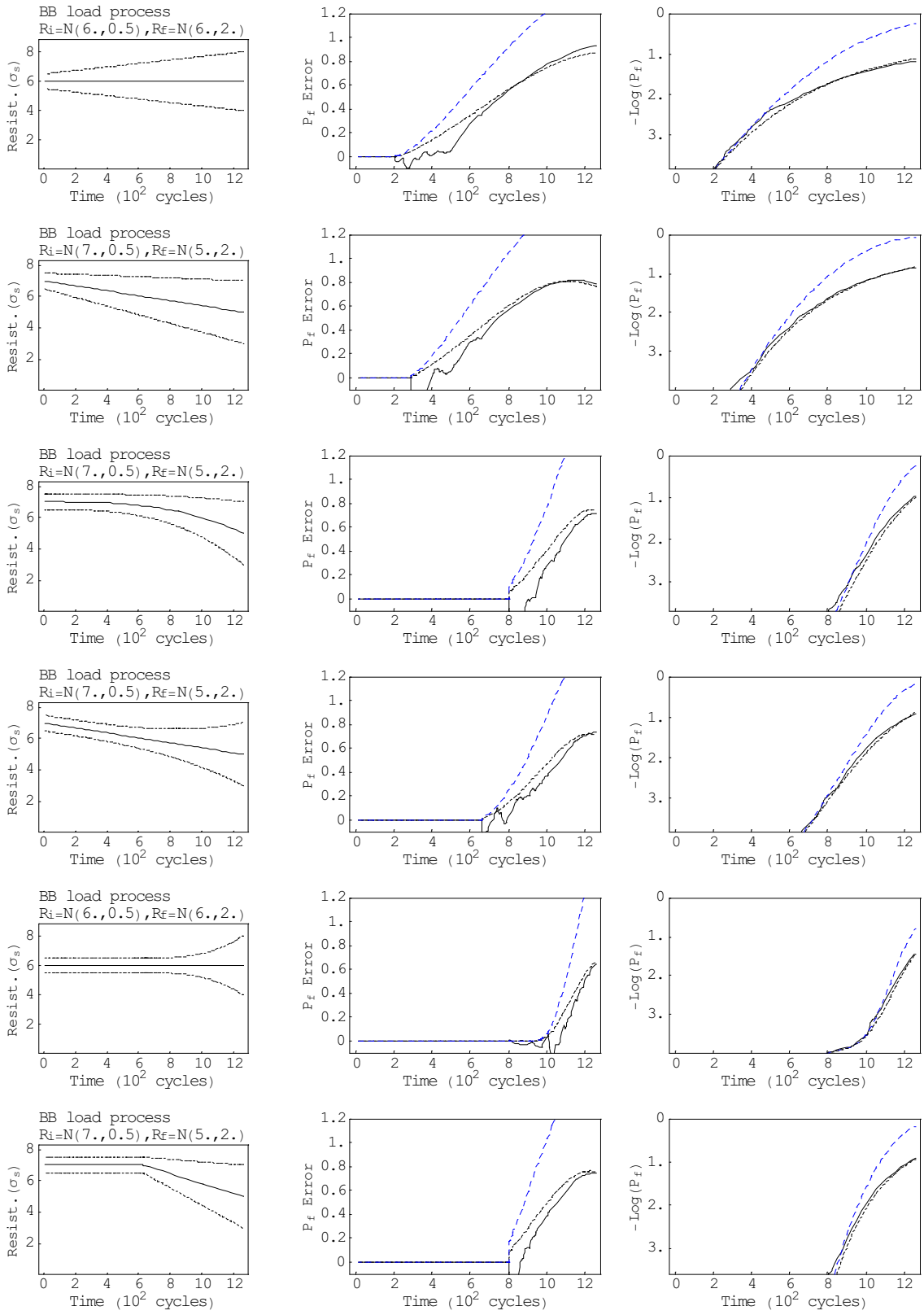

Figure 4-10: Error reduction results, large barrier variations over $t = 2T$.

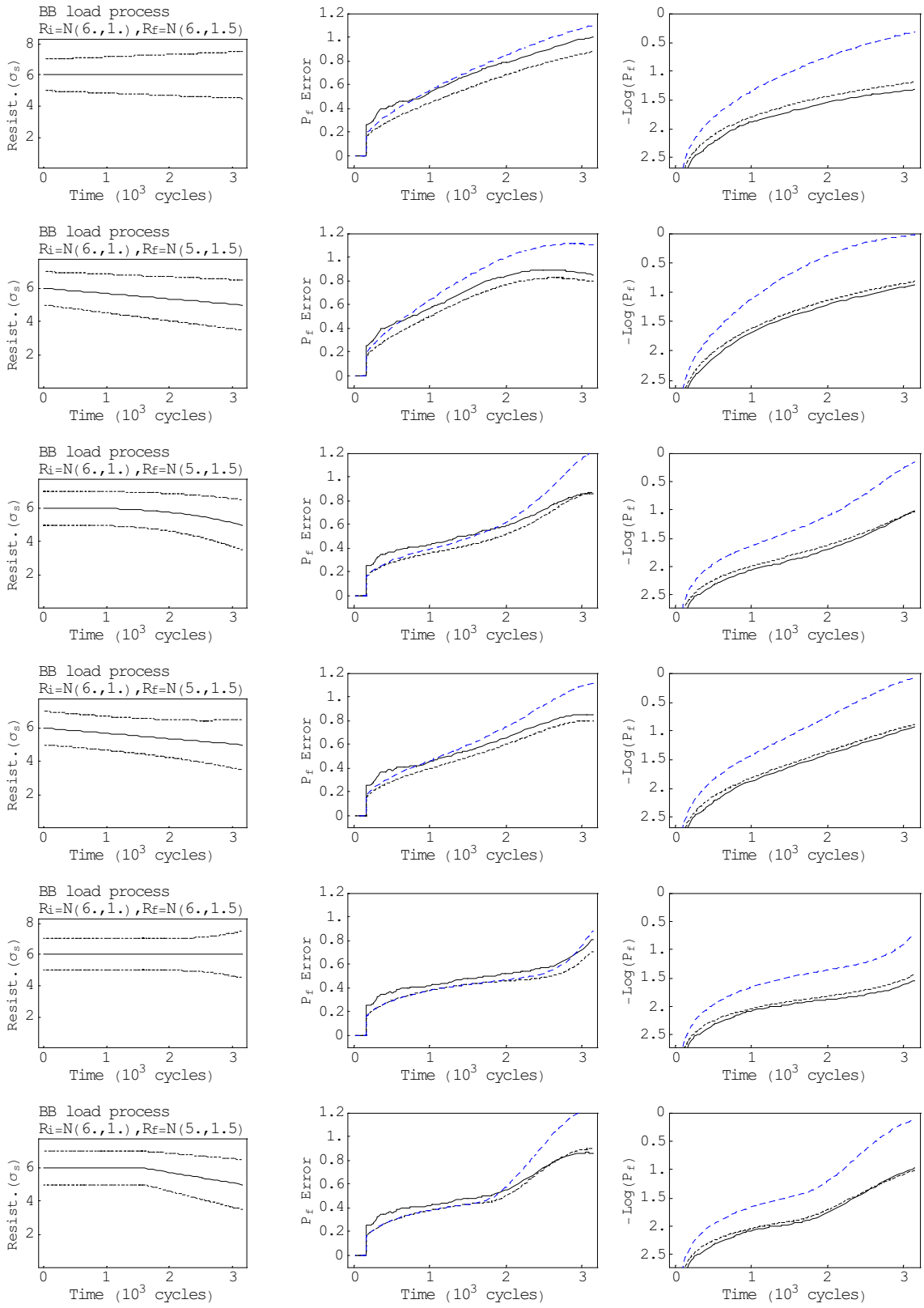

Figure 4-11: Error reduction results, small barrier variations over $t = 5T$.

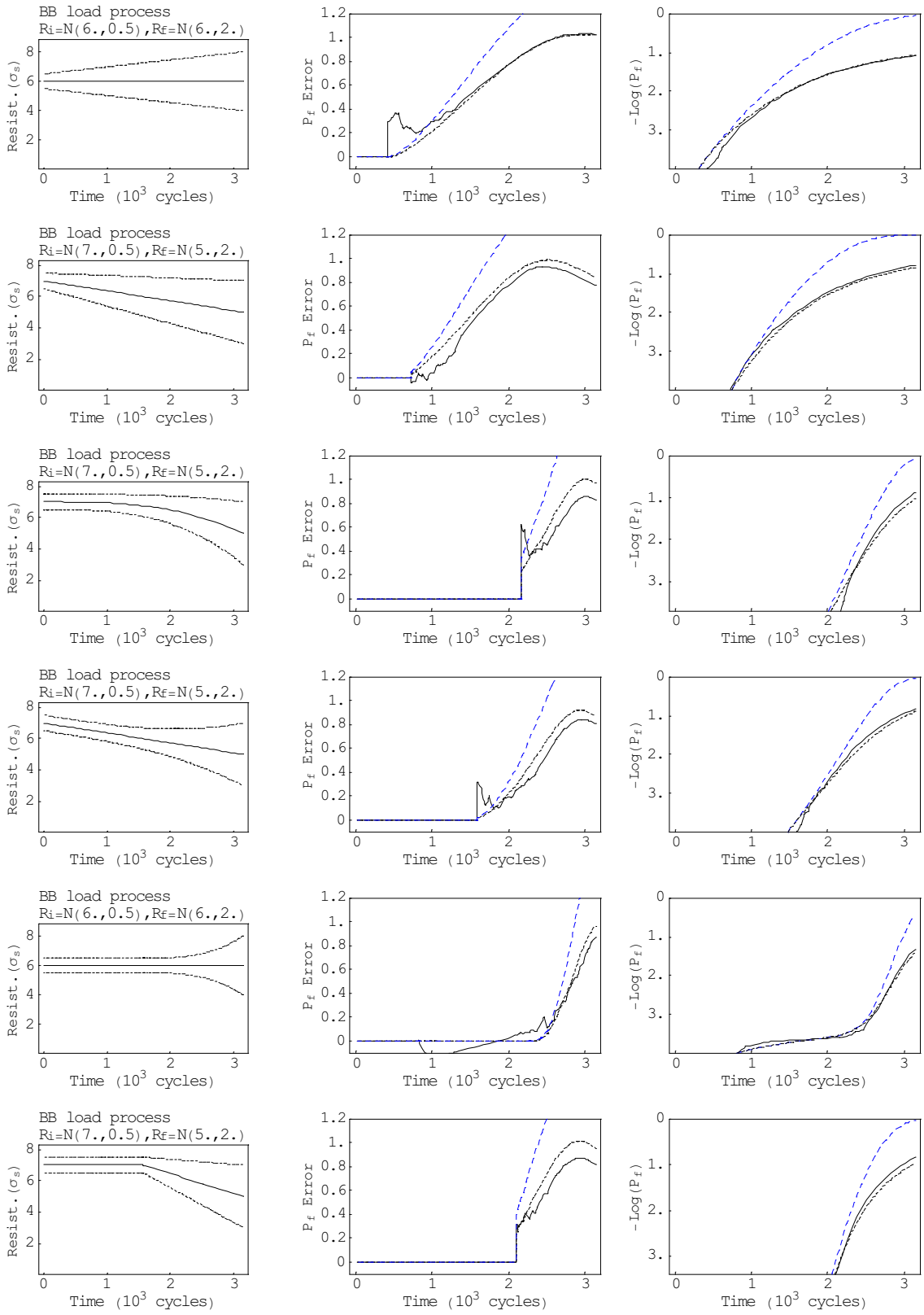

Figure 4-12: Error reduction results, large barrier variations over $t = 5T$.

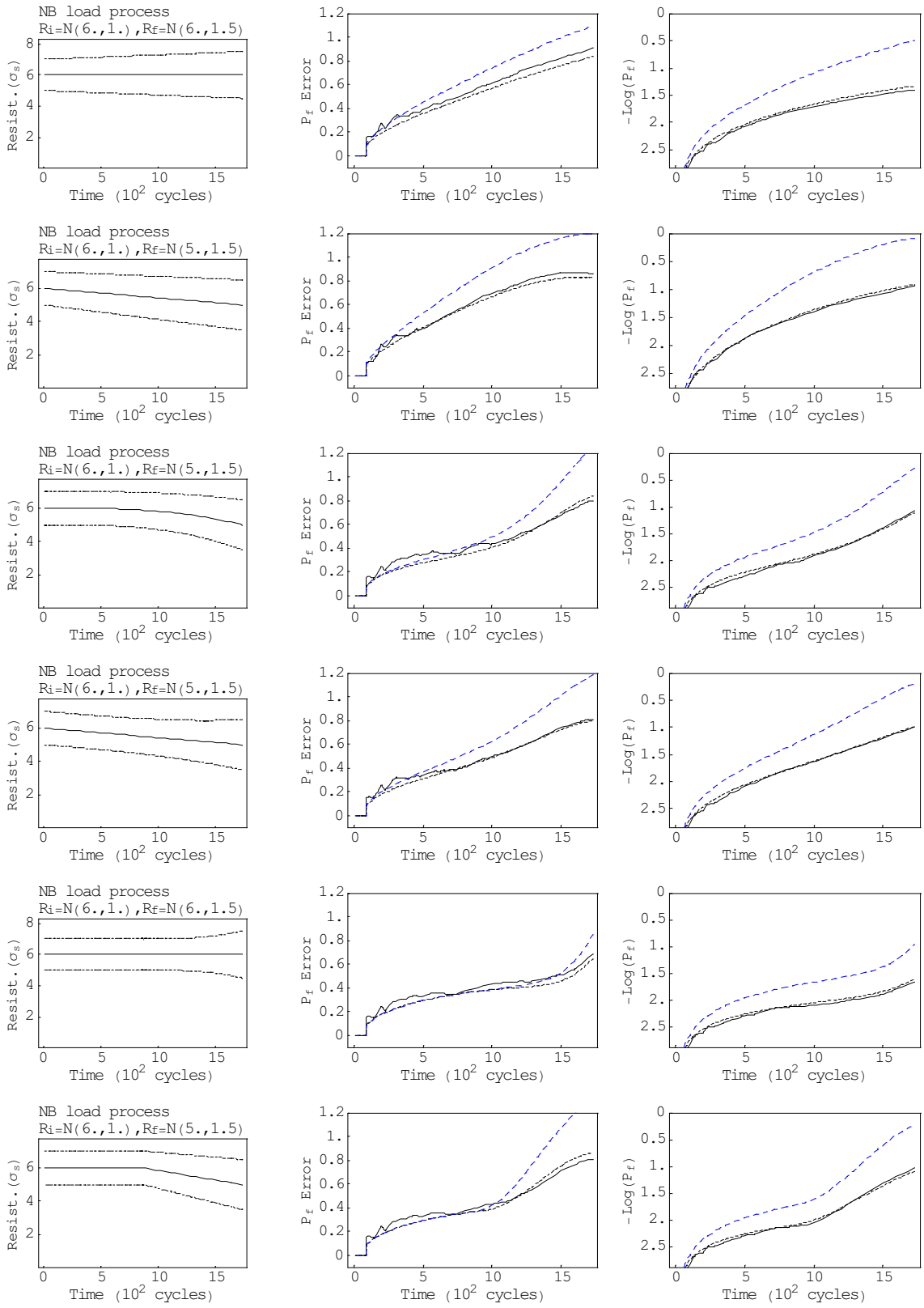

Figure 4-13: Error reduction results, NB load process, small barrier variations over $t = 2T$.

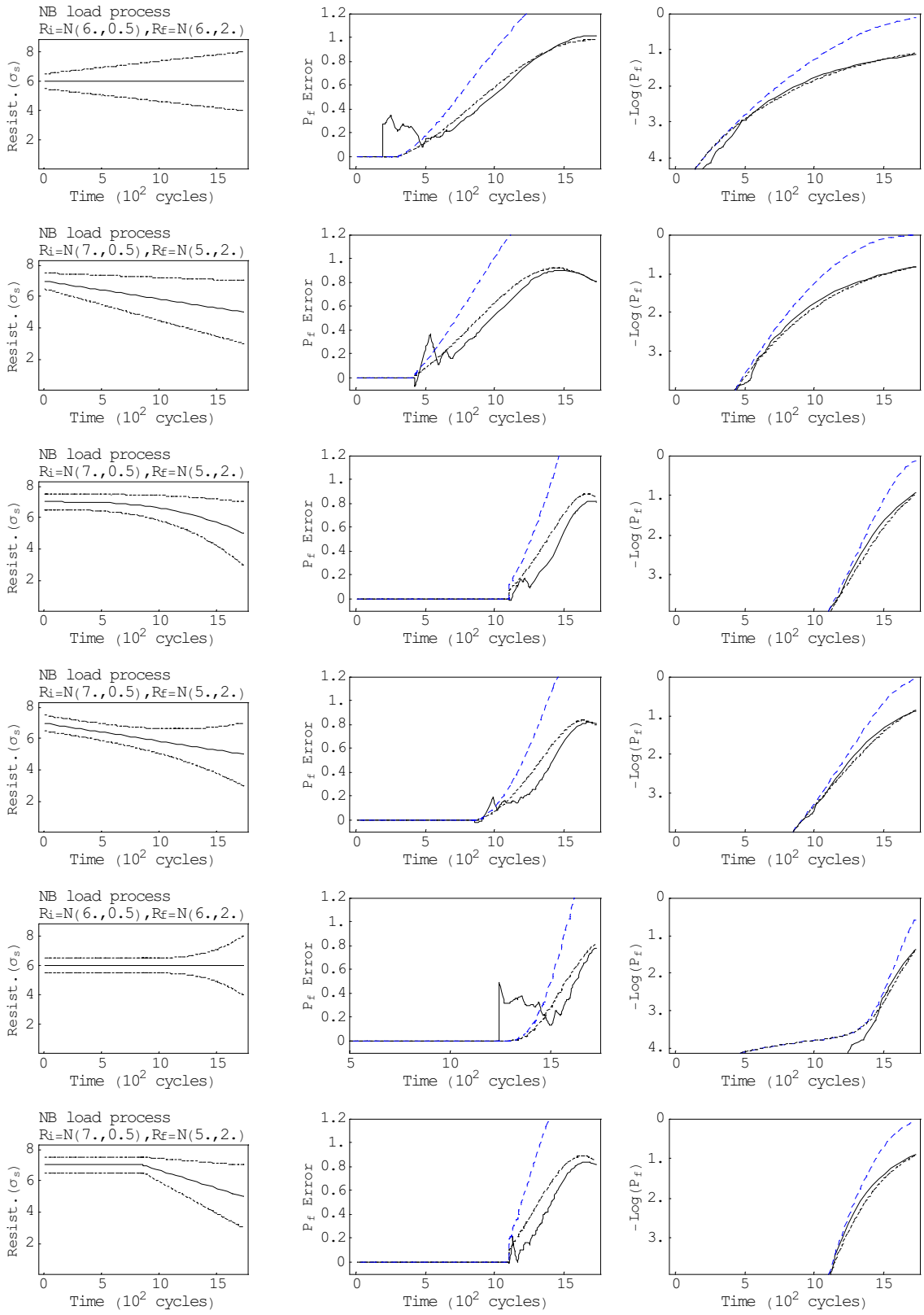

Figure 4-14: Error reduction results, NB load process, large barrier variations over $t = 2T$.

Chapter 5

BARRIER FAILURE DOMINANCE

5.1 Introduction

In this chapter, the order of magnitude of the EUR error is studied a little further. It was already seen in chapter 3 that, contrary to common belief, the EUR error can be large even when failure probabilities are small. In this chapter, it is shown that a combination of large EUR errors and small failure probabilities occurs in problems where the randomness of the resistance dominates the failure probability. A barrier failure dominance concept is introduced to characterize such problems, and it is shown that large EUR errors are associated with barrier failure dominance. It is also shown that some common simplifications of the time-variant reliability problem, other then the EUR approximation, are more likely to be appropriate in the presence of barrier failure dominance. This opposing trend between the EUR and other common approximations is used to establish limits of application for these approximations, in order to minimize the error. The barrier failure dominance concept is first illustrated for scalar problems, and then extended to multi-dimensional problems. In the multi-dimensional extension, the point-crossing formula and Turkstra's load combination rule are considered.

5.2 Discussion on the order of magnitude of the EUR error

Numerical results presented in chapter 3 have shown that EUR errors of 2 or 3 orders of magnitude are commonplace. As stated elsewhere, an error of 3 orders of magnitude means that an (ensemble) up-crossing rate calculated as being 10^{-1} crossings/cycle could, in fact,

be as low as 10^{-4} crossings/cycle. In figures 3-10 to 3-12 the EUR error was plotted against corresponding ensemble up-crossing rate values. The large scatter seen in these figures has shown that $\upsilon^{+}_{ED}(\mu, \sigma, t)$, and hence the failure probability, is not an appropriate parameter of the EUR error. Figures 3-6 and 3-7 confirmed this result, and also showed that the largest EUR errors are associated with large failure probabilities ($P_f(T) \rightarrow 1$). For intermediate values of the error parameter, however, the EUR error can be large even when failure probabilities are small (figures 3-6 and 3-7). As noted earlier, this goes against general belief (Pearce and Wen, 1984 and Wen and Chen, 1989).

The first point is to recognize that an error of one order of magnitude in the up-crossing rate represents an error of one order of magnitude in the failure probability since, for a power exponent $c \leq -2$:

$$\frac{1-\exp[-10^{c} * 10]}{1-\exp[-10^{c} \quad]} = \frac{1-\exp[-10^{c+1}]}{1-\exp[-10^{c} \quad]} \approx \frac{P_f(\,c+1)}{P_f(\,c \quad)} \approx 10 \tag{5.1}$$

The absolute value of the failure probability error, on the other hand, depends on the order of magnitude of the P_f, as well as on the time T spent at a given level:

$$P_f(\,T) \approx 1 - \exp[-\upsilon^{+}_{ED}(\mu, \sigma)\, T] \tag{5.2}$$

Hence, the conclusion is that:

> "For small failure probabilities, the absolute error in $P_f(\,T)$ may be small, but the *order of magnitude* error may be as large as the ensemble up-crossing rate errors found herein."

To illustrate the argument, some additional results for barriers with small failure probabilities are presented in figure 5-1. Barrier parameters are shown in the figure and in Table 5.1. The EUR error is extrapolated from equation (3.9) (and presented in Table 5.1). The actual error (in failure probabilities), however, is obtained by comparing the original EUR solution with an extreme value convolution integration following equation (3.14). Failure probability errors are shown in column A. Column B compares the distinct failure probability results.

Figure 5-1 confirms the statement above, showing that the "order of magnitude" EUR error can indeed be large even for very small failure probabilities. Such result is highly undesirable, since it makes the EUR approximation unreliable. In practical terms, there is no significant difference between failure probabilities of 10^{-15} and 10^{-13}, as for the barrier N(90,11) - the fourth in the figure. However, there is a significant difference between proba-

Table 5.1: Parameters of small Pf random barrier problems.

Barrier	EUR error (eq. 3.9)	Parameter $\sqrt{\frac{\sigma^2+1}{\mu}}$
N(10, 2)	1.16	0.71
N(20, 4)	1.92	0.92
N(40, 6)	2.02	0.96
N(90,11)	2.27	1.16
N(100,15)	2.35	1.50

bilities of 10^{-5} and 10^{-3} (barrier N(20,4) - second in the figure). This could be the difference between an acceptable and an unacceptable structural project.

The conclusion must be that the EUR approximation error can be too large for a range of practical expected failure probabilities. This means that in practice, the approximation may be useful only if one keeps track of barrier parameters and of the EUR error. Nevertheless, the results presented in the next sections show that there is a range of practical structural engineering problems for which the EUR approximation is likely to be good enough.

5.3 Barrier failure dominance concept

Numerical results presented in the previous section confirm that the EUR error can be large even when failure probabilities are small. The barriers considered in these examples have one interesting characteristic in common, namely that for most outcomes of the random barrier, an up-crossing is highly unlikely. Conversely, an up-crossing is highly likely for some limited types of outcomes of the random barrier.

This observation suggests a feature of the out-crossing problem related to random barriers. It leads us to the definition of a *barrier failure dominance* or BFD concept:

> "*Barrier failure dominance* characterizes those problems where an out-crossing or overload failure is more likely to be caused by a very small realization of the barrier (resistance) than by an exceptionally large realization of the load process."

Barrier failure dominance hence characterizes those problems where variance of the barrier dominates failure probabilities.

As will be shown in results that follow, it turns out that large EUR errors can be associated with barrier failure dominance. This is an important result, as barrier failure dominance is not expected to be encountered in real structural engineering applications. This is especially

true for problems involving natural hazards like winds, earthquakes, floods, waves, etc. It follows that, although EUR errors can be quite large, there is a range of practical problems for which the EUR approximation may be good enough. These problems would be those where load process uncertainty is significant compared to resistance uncertainty.

If some problems may be characterized by barrier failure dominance, there will be others where variance of the loads dominates failure probabilities, and where variance of the barrier is of secondary importance. Hence a complementary concept can also be introduced:

> "Under load process failure dominance, failure is more likely to be caused by an unfortunate combination of (exceptionally large) peaks of the load processes than by any specific outcome of the barrier."

Finally, there are likely some problems where no specific dominance can be identified.

More important than these two limiting concepts themselves are the trends that can be expected from such characterisation. As pointed out in the literature review, a complete or strict out-crossing reliability analysis of problems involving time-variant random resistance is far too complicated, and simplifications are often required. Some of these simplifications, such as the time-integrated approach, Turkstra's load combination rule or the point-crossing formula, reduce or simplify the load or the out-crossing part of the problem. For problems of barrier failure dominance, these simplifications are more likely to be appropriate. Since the barrier dominates failure probabilities, load process simplifications become of lesser importance. The ensemble up-crossing rate approximation, on the other hand, simplifies the problem on the barrier side. Hence, this approximation can be expected to be more appropriate in load-process dominated problems. Indeed, it was already shown that the EUR error is small when the C.O.V. of the random barrier is small (figure 3-10).

With this insight, the EUR approximation and other time-variant reliability simplifications can be seen as complementary alternatives to avoid a complete or strict out-crossing rate analysis. When the load process dominates failure probabilities, the EUR approximation is used; when the barrier dominates the P_f, the time-integrated, Turkstra's rule, the point-crossing formula or other similar approximation is adopted. Two important issues are raised in this context:

1. characterization of load or barrier failure dominance and;

2. establishment of limits of application of different approximations when the problem is not characteristically load-dominated nor barrier-dominated.

In the following sections, these issues are addressed and the barrier failure dominance concept is illustrated. In section 5.4, a scalar problem is considered; in sections 5.5 and 5.6, a multi-dimensional problem is analyzed in connection with Turkstra's load combination rule and the point-crossing formula, respectivelly.

5.4 Illustration of *barrier failure dominance* in one dimension

In order to illustrate the concepts introduced in the previous section, the Gaussian data sets of chapter 3 are analyzed again. The idea is to identify and to divide the random barrier domain of these data sets (in terms of μ and σ) in a sub-domain where the EUR error is small and a sub-domain where failure is barrier-dominated. In order to do that, the barrier failure dominance concept has to be quantified. For scalar problems, this can be done in two ways:

1. by comparing the strict extreme-value convolution integration (equation 3.14) with an approximate solution obtained by considering the extreme value of the load process to be deterministic. The chosen criterion is:

$$RB_{\text{dominance}} \equiv \frac{\int_{-\infty}^{+\infty} f_{S_T}(s)\, F_R(s) ds}{F_R(\mu_{ext})} \tag{5.3}$$

   where μ_{ext} is mean of the extreme value distribution in a given time interval. According to this criterion, barrier failure dominance is characterized by $RB_{\text{dominance}} \rightarrow 1$;

2. by analyzing sensitivity coefficients of load and resistance variables in a FORM solution of the problem:

$$g(R, S_T, T) = R - S_T(s) = 0 \tag{5.4}$$

The sensitivity coefficients are evaluated numerically since $S_T(s)$ is not Gaussian. They are obtained as:

$$\frac{\nabla g(u)|_{u^*}}{|\nabla g(u)|_{u^*}|} = \{\alpha_R^2, \alpha_{S_T}^2\} \tag{5.5}$$

where u^* is the design point in the reduced space $\mathbf{u} = \mathbb{T}(\mathbf{r})$. Clearly, for barrier failure dominance problems one would expect $\alpha_R^2 \rightarrow 1$ and $\alpha_{S_T}^2 \rightarrow 0$.

Interesting results are obtained when the barrier failure dominance criterion is compared with the EUR error as a function of the EUR error parameter:

$$E_p(\mu, \sigma) = \sqrt{\frac{\sigma^2 + 1}{\mu}} \tag{5.6}$$

or as a function of the coefficient of variation (σ/μ) of the (reduced) random barrier. Figure 5-2 presents such results for one of the simulated data sets of chapter 3 (BB load process). Here it can be clearly seen that, as the EUR error parameter increases (left in figure), the EUR error (in dark) increases and the barrier failure dominance criterion (in grey) converges to one. The same is true for an increase in the C.O.V. of the random barrier (right in the figure). Sensitivity coefficients follow the same trend (bottom in figure), with the load sensitivity (in grey) converging to zero and the barrier sensitivity (in dark) converging to one as the barriers increasingly dominate failure probabilities.

These results become even more evident when the extrapolated data set is considered (figure 5-3). The EUR error, in this case, is calculated from the extreme value convolution integration. Results are pooled together and plotted as a function of the EUR error parameter (left) and of the C.O.V. of the random barrier (right). The trend is even more evident here, with the EUR error (in dark) increasing and the barrier failure dominance criterion (in grey) converging to one as the EUR error parameter and the C.O.V. increase. As noted in the previous chapter, the small scatter obtained when the EUR error is plotted against the error parameter (left in figure) shows how well this parameter describes the EUR error in comparison to other parameters such as the C.O.V. (right). Surprisingly, perhaps, the RB-dominance criterion is also better described by the EUR error parameter than by the C.O.V.

Results presented in this section show that the EUR error is greater when there is barrier failure dominance, and that it may not be too large in the absence of barrier-dominance. These results also illustrate the opposing trend between the EUR approximation and other approximations either based on, or for which, the barrier failure dominance concept holds. Because the barrier failure dominance criterion considered in this section is only illustrative, establishment of limits of application of the approximated solutions is not attempted. However, this is done for multi-dimensional problems in the next two sections.

5.5 Illustration of BFD in multi-dimensional problem (Turkstra's load combination rule example)

In this section the barrier failure dominance concept is applied to a very simple multi-dimensional problem. The problem consists of a load process formed by the linear sum of three independent standard Gaussian component processes $X_i(t)$, $i = 1, 2, 3$. The limit state function for the problem is:

$$g(\mathbf{X}, \mathbf{R}, t) = f(\mathbf{R}) - X_1(t) - X_2(t) - X_3(t) = 0 \tag{5.7}$$

The barrier failure dominance concept and the EUR approximation are tested and compared, respectively, with the approximation involved in Turkstra's load combination rule. This rule approximates the time-variant problem in equation (5.7) with 3 time-invariant problems on 4 random variables:

$$g(\mathbf{X}, \mathbf{R}, T) = f(\mathbf{R}) - X_{1T} - X_{2M} - X_{3M} = 0 \tag{5.8}$$

where X_{1T} is the extreme value of process X_1 in time interval $(0, T)$ and X_{iM} is the mean-value or point-in-time distribution of process X_i. Clearly, three of such problems would have to be solved if the load components were not identical, since the extreme value of each one of them would have to be considered at a time. Equation (5.8) is solved by FORM and the load sensitivity factor is given by:

$$\alpha_S^2 = \alpha_{X_{1T}}^2 + \alpha_{X_{2M}}^2 + \alpha_{X_{3M}}^2 \tag{5.9}$$

The problem can be converted in a scalar one by working out the parameters of the process $X(t) = X_1(t) + X_2(t) + X_3(t)$. Since the components of the linear sum are Gaussian, $X(t)$ is Gaussian as well, with parameters:

$$\begin{aligned} \mu_X &= \mu_{X_1} + \mu_{X_2} + \mu_{X_3} = 0 \\ \sigma_X^2 &= \sigma_{X_1}^2 + \sigma_{X_2}^2 + \sigma_{X_3}^2 = 3 \end{aligned} \tag{5.10}$$

The exact solution is obtained from the one-dimensional convolution integral involving the extreme value $X_T(x)$ of process $X(t)$:

$$P_{f_{EXACT}}(R, T) = \int_{-\infty}^{+\infty} f_{X_T}(x)\, F_R(x) dx \tag{5.11}$$

For simplicity, the EUR approximation is also evaluated from the scalar problem, with:

$$\upsilon_{ED}^{+}(R) = \int_{0}^{+\infty} \upsilon_{X}^{+}(r) f_R(r) dr \tag{5.12}$$

and:

$$P_{f_{EUR}}(R,T) = P_{f_0}(R) + (1 - P_{f_0}(R)) \cdot (1 - \exp(-\upsilon_{ED}^{+}(R)\, T)) \tag{5.13}$$

The EUR error (in failure probabilities) and the error of Turkstra's load combination rule are both evaluated from the exact interference solution, using the same "order of magnitude" format:

$$E_D(R,T) = Log_{10}(\frac{P_{f_{EUR}}(R,T)}{P_{f_{EXACT}}(R,T)}) \tag{5.14}$$

and:

$$E_{Turkstra}(R,T) = Log_{10}(\frac{P_{f_{EXACT}}(R,T)}{P_{f_{FORM}}(R,T)}) \tag{5.15}$$

where $P_{f_{FORM}}(T)$ is the FORM solution of the problem defined by equation (5.8). In this format the errors can be directly compared, although it should be noted that Turkstra's load combination approximation is unconservative whereas the EUR approximation is conservative.

In the formulation above the dependency on the random barrier and its parameters $R = N(\mu_R, \sigma_R)$ was made explicit. Since the load process $X(t)$ is not standard, equivalent normalized barriers are obtained from:

$$\begin{aligned} \mu &= \frac{\mu_R - \mu_X}{\sigma_X} = \frac{\mu_R}{\sqrt{3}} \\ \sigma &= \frac{\sigma_R}{\sigma_X} = \frac{\sigma_R}{\sqrt{3}} \end{aligned} \tag{5.16}$$

A total of 870 solutions of the problem are obtained by varying the mean of the random barrier from 30 to 60, with increments of one, and the standard deviation from 1 to 15, with increments of 0.5. Results are presented in figure 5-4. The expected trend repeats itself here, with the EUR error (in dark) increasing and the error in Turkstra's approximation (in grey) decreasing as the EUR error parameter and the C.O.V. of the barrier increase. This is very appropriate since one can now establish application limits for these approximations such as to keep the error to a minimum. Disregarding the fact that Turkstra's rule is unconservative, the error is kept below two orders of magnitude if the EUR approximation is used when, as illustrated by the dotted lines in figure 5-4, either:

$$\sqrt{\frac{\sigma^2+1}{\mu}} < 1.10 \quad \text{or} \quad \frac{\sigma}{\mu} < 0.23 \tag{5.17}$$

Otherwise, Turkstra's load combination rule is used. If the unconservative character of Turkstra's approximation is taken into account, one would perhaps increase the limits in (5.17). The limit based on the error parameter should be preferred over the C.O.V. limit since it is more clearly defined. It should also be noted that the error in Turkstra's approximation shows very little scatter when plotted against the EUR error parameter, suggesting that this may not be just an EUR error parameter, but some characteristic parameter of random barrier problems.

There is a clear variation of the load (in grey) and resistance (in dark) sensitivity factors for this problem (figure 5-4, bottom plots). This variation follows the trend observed for the approximation errors: as barrier failure dominance increases (increase in error parameter and C.O.V.), resistance sensitivity factors converge to one. Variation of sensitivity factors can be associated with the limits established in (5.17). Both limits correspond, approximately, to $\alpha_R^2 < 0.95$ and $\alpha_S^2 > 0.05$, although this separation is more evident in terms of the error parameter. Limitation of the approximation's use in terms of sensitivity factors is very appropriate, because it allows extension of the results to problems involving multi-variate resistance without the necessity of deriving a scalar resistance measure to be checked against the limits (5.17). Hence, one could obtain a simplified load combination solution first (by FORM, say) and, if the resistance sensitivity factor turned out less than 0.95, one could be confident of obtaining a better result by means of the EUR approximation.

Turkstra's load combination rule is known to be unconservative, as it neglects events where two or more processes reach "near maximum" simultaneously. Such events are especially significant when there is correlation between the load processes, a case not considered here because the available EUR error estimate is valid for scalar processes only. However, in this section it is shown that the error in Turkstra's load combination rule is also dependent on load process and random barrier parameters. More importantly, it is shown that this error is reduced for increasing barrier failure dominance. This is, to the author's knowledge, a novel result, which is supposed to be valid for more general problems as well (including load process correlation). Moreover, results presented in this section show an opposing trend between the approximation based on Turkstra's load combination rule and the solution based on the EUR approximation, with the first being more appropriate in the presence and the second being more appropriate in the absence of barrier failure dominance. This trend can also be expected to be encountered in more general problems.

5.6 Illustration of BFD in multi-dimensional problem (point-crossing formula example)

In this section, the EUR approximation is compared with approximations involved in the point-crossing formula, for problems involving sums of continuous load processes. The sum of three continuous Gaussian load processes is considered again:

$$X(t) = X_1(t) + X_2(t) + X_3(t) \tag{5.18}$$

Since the component processes are Gaussian, an exact solution can be obtained by deriving the parameters of the resulting process $X(t)$. The exact solution includes calculating the extreme value distribution of process $X(t)$ and solving the one-dimensional convolution integral (equation 5.11). Results shown in this section, however, should be useful, as a general guideline, for problems consisting of sums of non-Gaussian processes.

The point-crossing formula yields the combined up-crossing rate, for the sum of three components processes, as (Larabee and Cornell, 1981):

$$\upsilon_X^+(r) \leq \int_{-\infty}^{\infty} \upsilon_{X_1}^+(r-x)\widehat{f}_{23}(x)dx + \int_{-\infty}^{\infty} \upsilon_{X_2}^+(r-x)\widehat{f}_{13}(x)dx + \int_{-\infty}^{\infty} \upsilon_{X_3}^+(r-x)\widehat{f}_{12}(x)dx \tag{5.19}$$

where

$$\widehat{f}_{ij}(x) = \int_{-\infty}^{\infty} f_{X_i}(x_i) f_{X_j}(x - x_j)dx_i \tag{5.20}$$

is the arbitrary point-in-time distribution of the sum process $X_i(t) + X_j(t)$.

Since the component load processes considered in this section are identical ($N(0,1)$), only one term in equation (5.19) has to be evaluated. Equation (5.19) is exact for some combinations of load processes, for example when two of the processes have discrete distributions. Strictly speaking, (5.19) is exact whenever the processes in the sum satisfy (Larabee and Cornell, 1979):

$$P[\dot{X}_i > 0 \cap \dot{X}_j < 0] = 0 \tag{5.21}$$

i.e., when one process does not cancel out the act of up-crossing by the other process. For a combination of three continuous Gaussian processes, (5.19) can be used as an approximation. By introducing up-crossing rate expressions in equation (5.19) and performing the integrations, and by comparing the resulting expression with the up-crossing rate for the sum

process $X(t)$, the maximum (theoretical) error is found as (Melchers, 1999):

$$\frac{\sigma_{\dot{X}_1} + \sigma_{\dot{X}_2} + \sigma_{\dot{X}_3}}{\sqrt{\sigma^2_{\dot{X}_1} + \sigma^2_{\dot{X}_2} + \sigma^2_{\dot{X}_3}}} \tag{5.22}$$

The maximum error becomes $\sqrt{3}$ when $\sigma_{\dot{X}_1} = \sigma_{\dot{X}_2} = \sigma_{\dot{X}_3}$, as considered in this section.

The array of random barriers considered in the previous section ($\mu = 30$ to 60, $\sigma = 1$ to 15) is considered again. The EUR error is evaluated following equation (5.14). The point-crossing approximation is conservative, hence the error is evaluated as:

$$E_{PC}(R,T) = Log_{10}\left(\frac{P_{f_{PC}}(R,T)}{P_{f_{EXACT}}(R,T)}\right) \tag{5.23}$$

where the point-crossing failure probability, for the random barrier problem, is evaluated as:

$$\begin{aligned} P_{f_{PC}}(R,T) &= \int_R P_{f_{PC}}(r,T) f_R(r) dr \\ &\approx \int_R (1 - \exp[-\upsilon^+_X(r)T]) f_R(r) dr \end{aligned} \tag{5.24}$$

Results are shown in figure 5-5, in terms of the error parameter and the C.O.V. of the random barrier. It can be seen in the figure that the point-crossing error converges to the theoretical maximum ($\log_{10}(\sqrt{3}) = 0.2$) as $\sqrt{(\sigma^2+1)/\mu} \to 0.5$. This error decreases as the error parameter increases, due to the growing contribution of the random barrier to the failure probability (it should be noted that this is the error in failure probabilities, and not in up-crossing rates - the error in up-crossing rates is $\sqrt{3}$ for all values of $\sqrt{(\sigma^2+1)/\mu}$ in this problem). In contrast, the EUR error increases with the error parameter, as expected. Because the point-crossing formula yields a "combined" up-crossing rate for the sum of component load processes, the EUR approximation could actually be combined with the point-crossing solution. It would suffice to integrate the combined up-crossing rate in equation (5.19) over the resistance distribution. Hence, it becomes interesting, in this case, to know the relative magnitude of the errors in the two approximations. Following figure 5-5, the EUR error would be smaller than the point-crossing error when:

$$\sqrt{\frac{\sigma^2+1}{\mu}} < 0.5 \quad \text{or} \quad \frac{\sigma}{\mu} < 0.125 \tag{5.25}$$

Moreover, for a significant part of these intervals, the EUR error can be expected to be negligible, in comparison to the point-crossing error, as the EUR error drops quickly to zero.

5.7 Concluding remarks

The barrier failure dominance concept introduced in this chapter should not be interpreted as a sign that the load combination or the out-crossing problem can be by-passed altogether. The concept was introduced to characterize those problems where variance of the barrier dominates failure probabilities. The idea is used to identify the (random barrier) domain where the EUR approximation error is large, and it is used as a parameter to compare the EUR with other approximations of time-variant reliability problems.

The most important contribution of this chapter is, perhaps, not the barrier failure dominance concept itself, but the observation that large EUR errors are associated with barrier failure dominance. This is a very important result, as barrier failure dominance is not expected to be encountered in practical structural engineering applications. Hence, there is a range of practical problems for which the EUR approximation can be good enough. In addition to that, the realization that the error of other time variant reliability problem simplifications decreases with barrier failure dominance allows one to establish clear application limits for these and other approximations.

The limits obtained for the EUR approximation and for Turkstra's load combination rule represent, of course, particular results for particular problems. A major limitation of these results is that Turkstra's rule does not apply to problems involving resistance degradation. Results obtained for the point-crossing formula are more general, in this sense. Of course, continuous Gaussian processes can be easily combined, and solutions for the out-crossing rate of Gaussian load processes through linear failure domains can be easily derived. However, the general results obtained in this chapter should also apply to non-linear combinations of non-Gaussian processes with non-linear limit state functions.

The ideas developed in this chapter should also be equally applicable to other simplifications of time-variant reliability problems. In particular, the EUR approximation involved in the parallel system sensitivity solution of the out-crossing problem, with resistance random variables included in the solution, can be expected to behave in the same fashion, i.e., the EUR error can be expected to be small for small variances of the resistance random variables.

5.8 Figures

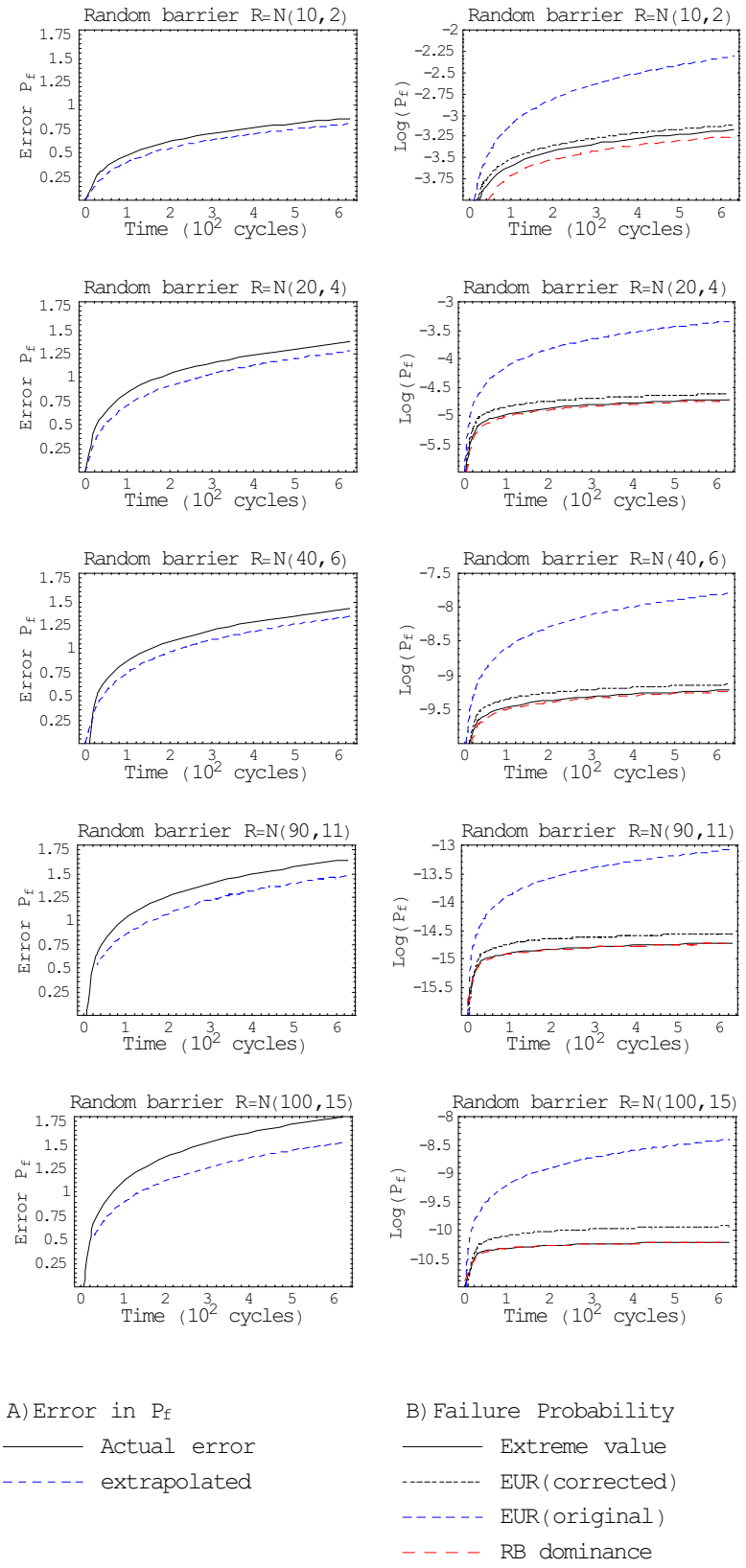

Figure 5-1: Error in $P_f(t)$ for small failure probability random barrier problems.

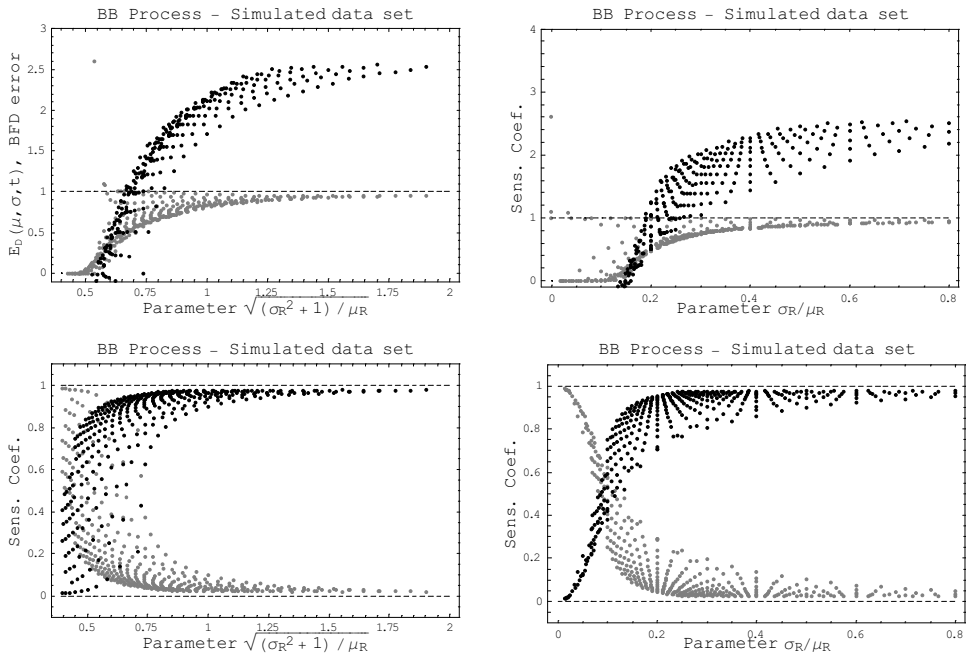

Figure 5-2: Barrier failure dominance criterion (top) and sensitivity coefficients (bottom) for one dimensional problem, simulated data set, as function error parameter (left) and C.O.V. (right).

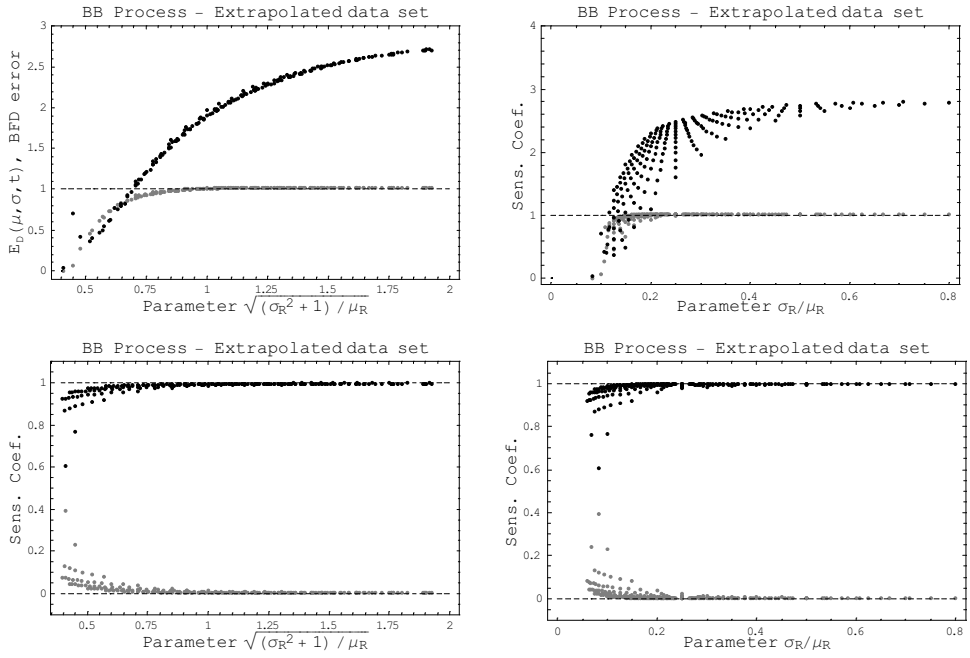

Figure 5-3: Barrier failure dominance criterion (top) and sensitivity coefficients (bottom) for one dimensional problem, extrapolated data set, as function error parameter (left) and C.O.V. (right).

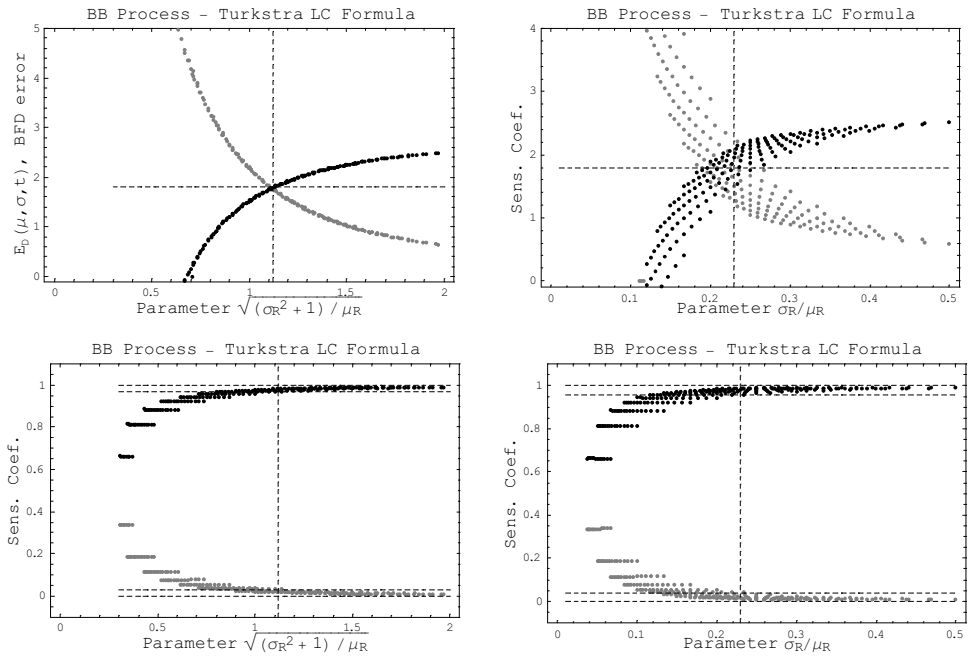

Figure 5-4: Barrier failure dominance for tri-dimensional problem, EUR and Turkstra's approximation errors (top) and sensitivity coefficients (bottom) as function of error parameter (left) and C.O.V. (right).

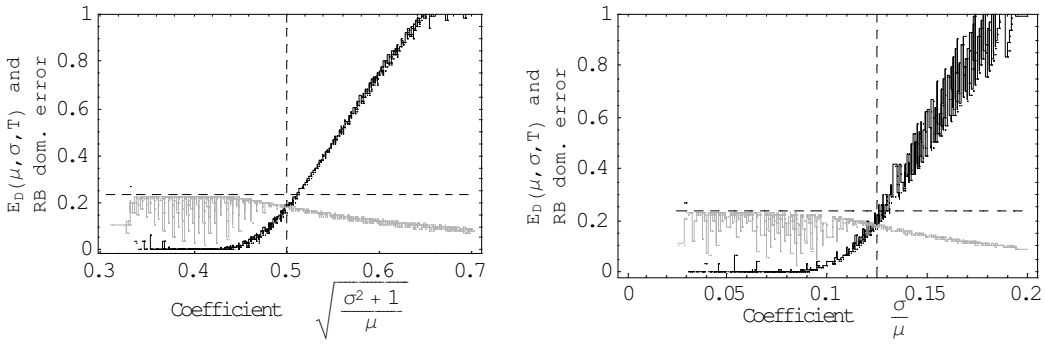

Figure 5-5: Barrier failure dominance for tri-dimensional problem, EUR and point-crossing formula approximation errors as function of error parameter (left) and C.O.V. (right).

Chapter 6

SLOW-VARYING RANDOM PROCESS BARRIERS

6.1 Introduction

In this chapter, the problem of a random load process up-crossing a slow-varying non-ergodic random process barrier is considered. For illustration, a random barrier with exponential correlation function is considered:

$$R_{RR}(t_1, t_2) = R_{RR}(t_2 - t_1) = \sigma^2 \exp\left(-\frac{t_2 - t_1}{\lambda_R}\right) \tag{6.1}$$

where λ_R is the correlation length of the barrier. For the purpose of this discussion, a random variable barrier, or parametrically defined barrier, is a barrier with an infinite correlation length ($\lambda_R = \infty$), or, for practical purposes, with $\lambda_R >> T$. A fast varying random process barrier is one with a correlation length of the same order as the correlation length of the load process ($\lambda_R \approx \lambda_S$). Since ergodicity is assumed for the load process, it can be assumed for the fast varying random barrier as well. Such a fast varying barrier is not practical, and it could be considered as an additional "load" process in the analysis. However, it is seen here as a limiting situation of a random barrier that varies slower than the load process. A slow-varying non-ergodic random process barrier is one with $\lambda_S < \lambda_R < T$.

In this chapter a solution is derived for the case where resistance is not a random variable, nor an ergodic fast varying random process, but a slow-varying random process of time. First, the "inner" and "outer" integration schemes of Schall et al.. (1991) are repeated here:

$$
\begin{aligned}
P_f(T) &\simeq 1 - E_{\mathbf{R}}[\exp(-E_{\mathbf{Q}}[N_S^+(\mathbf{R},\mathbf{Q},T)])] \\
&\lesssim 1 - \exp(-E_{\mathbf{R}}[E_{\mathbf{Q}}[N_S^+(\mathbf{R},\mathbf{Q},T)]]) \qquad (6.2) \\
&\gtrsim 1 - E_{\mathbf{R}}[E_{\mathbf{Q}}[\exp(-N_S^+(\mathbf{R},\mathbf{Q},T))]] \qquad (6.3)
\end{aligned}
$$

It is clear that a random variable barrier with $\lambda_R = \infty$ requires an "outer" integration (eq. 6.3). It is also natural to assume that, for a fast varying random barrier with $\lambda_R \approx \lambda_S$, for which the ergodicity assumption holds (at least in comparison to the load process), an inner integration, such as for $\mathbf{Q}$ in the formulation above (eq. 6.2), is appropriate. Indeed, Figure 6-1 shows by example that the EUR error decreases as the correlation length of the barrier is reduced, and that it goes to zero as $\lambda_R \to \lambda_S$. Hence, in this limiting situation the EUR solution provides a close estimate of the first passage failure probability. The EUR solution, as stated elsewhere, is similar to, but not exactly, the "inner" integration scheme above. The situation of a slow-varying random barrier, with ($\lambda_S < \lambda_R < T$), falls in-between.

Use of the EUR approximation for slow-varying random process barriers has been suggested in Rackwitz (1993) and Schall et al. (1991), although no formal justification is given. In this chapter, an interpolation solution for the slow-varying barrier problem is proposed. This solution is an interpolation between the "outer" integration solution for RV barriers and the EUR approximation or "inner" integration solution for fast-varying barriers. It will be shown that it converges to these two limiting solutions, and provides sufficiently accurate results for the "intermediate" situation.

The formal solution to the slow-varying random barrier problem involves a discretization of the slow varying random process in a vector of (correlated) random variables (Vanmarcke, 1983). The outer integration is then performed, for example, by means of a Fast Probability FORM integration. One issue with this solution is the choice of the size of the discretization grid. If the grid is too fine, the discretized random variables are excessively correlated, and this represents a problem for the required FORM transformations. If the grid is too coarse, the random barrier is not properly discretized.

It should be pointed out that although some of the following developments are similar to solutions presented in Schall et al. (1991), the objective of the two studies are very different.

6.2 Interpolation solution

The main idea of this solution is to divide the time integration interval $(0, T)$ in blocks, replacing the time integration by a sum over a finite number of blocks n. For a deterministic barrier level r, with t_i the median of the i^{th} integration interval and $\Delta t = \frac{T}{n}$ the length of the integration intervals, one obtains:

$$\begin{aligned} P_S(r,T) &= P_{S_0}(r)\exp[-\int_0^T \upsilon^+(r,t)dt] \\ &= P_{S_0}(r)\exp[-\sum_{i=1}^{n}\int_{ti-\Delta t/2}^{ti+\Delta t/2}\upsilon^+(r,t)dt] \\ &= P_{S_0}(r).\prod_{i=1}^{n}\exp[-\int_{ti-\Delta t/2}^{ti+\Delta t/2}\upsilon^+(r,t)dt] \\ &= P_{S_0}(r).\prod_{i=1}^{n}P_{S_i}(r,\Delta t) \\ &= P_{S_0}(r)\cap P_{S_i}(r,\Delta t) \end{aligned} \tag{6.4}$$

The last equality in the formulation implies that the probability of survival for every interval Δt is independent. For the deterministic barrier, this assumption is appropriate as long as up-crossings can be considered independent as well. It is now assumed, as an approximation, that for the random barrier case the individual probabilities of survival $P_{S_i}(\Delta t)$ are independent as well:

$$P_S(T) = P_{S_0}\prod_{i=1}^{n}P_{S_i}(\Delta t) \tag{6.5}$$

Now one applies the random variable solution for each interval Δt, with $R_0 = R(t_i - \Delta t/2)$ for each interval, obtaining:

$$\begin{aligned} P_{S_0} &= \int_R P_{S_0}(r)f_R(r,0)dr \\ P_{S_i}(\Delta t) &= \int_R \exp[-\int_{ti-\Delta t/2}^{ti+\Delta t/2}\upsilon^+(r,t)dt]f_R(r,t_i-\Delta t/2)dr \end{aligned} \tag{6.6}$$

Integration over the resistance is known to affect the hypothesis of independency. However, if the $P_{S_i}(\Delta t)$ are not independent, such that $\cap P_{S_i}(\Delta t) > \prod_{i=1}^{n}P_{S_i}(\Delta t)$, equation (6.5) still provides a lower bound for the probability of survival:

$$P_S(T) \geq P_{S_0}.\prod_{i=1}^{n}\left(\int_R \exp[-\int_{ti-\Delta t/2}^{ti+\Delta t/2}\upsilon^+(r,t)dt]f_R(r,t_i-\Delta t/2)dr\right) \tag{6.7}$$

Expression (6.7) yields the random variable solution when $n = 1$ and converges to the EUR solution when $n \to \infty$. For the slow-varying barrier problem, it provides an interpolated solution by choosing the value of n. For $n = 1$, indeed, equation (6.7) yields:

$$P_S(T) = P_{S_0} \int_R \exp[-\int_0^T \upsilon^+(r,t)dt] f_R(r,0)dr \tag{6.8}$$

For $n \neq 1$, using Jensen's inequality (Schall et al., 1991):

$$E[g(x)] \geq g(E[x]) \tag{6.9}$$

for $g(x)$ a convex function from below and $E[.]$ the expected value, equation (6.7) becomes:

$$\begin{aligned} P_S(T) &\geq P_{S_0} . \prod_{i=1}^{n} \exp[-\int_R \int_{ti-\Delta t/2}^{ti+\Delta t/2} \upsilon^+(r,t)dt \; f_R(r, t_i - \Delta t/2)dr] \\ &= P_{S_0} \exp[-\sum_{i=1}^{n} \int_R \int_{ti-\Delta t/2}^{ti+\Delta t/2} \upsilon^+(r,t)dt \; f_R(r, t_i - \Delta t/2)dr] \end{aligned} \tag{6.10}$$

For $n = 1$, equation (6.10) now yields the "inner integration" lower bound for the failure probability (Schall et al., 1991). For $n \to \infty$, or $\Delta t \to 0$, the order of integration with respect to R and time can be interchanged, and the EUR approximation is obtained, since:

$$\int_{ti-\Delta t/2}^{ti+\Delta t/2} \upsilon^+(r,t)dt \to \upsilon^+(r,t_i)\Delta t$$

and:

$$\begin{aligned} P_S(T) &\gg P_{S_0} \exp[-\sum_{i=1}^{\infty} \int_R \upsilon^+(r,t_i) \; \Delta t \; f_R(r,t_i)dr] \\ &\simeq P_{S_0} \exp[-\int_0^T \int_R \upsilon^+(r,t) \; f_R(r,t)dr \; dt] \\ &\simeq P_{S_0} \exp[-\int_0^T \upsilon_E^+(t) \; dt] \end{aligned} \tag{6.11}$$

where $\upsilon_E^+(t)$ is the ensemble up-crossing rate and equation (6.11) is the ensemble up-crossing rate approximation to the P_f. For $n \to \infty$ the bound in equation (6.11) is expected to be close to the equality, since this result can actually be derived without resort to Jensen's inequality.

Indeed, directly from equation (6.7) with $n \to \infty$ and $\Delta t \to 0$, one obtains:

$$\begin{aligned} \int_{ti-\Delta t/2}^{ti+\Delta t/2} \upsilon^+(r,t)dt &\rightarrow \upsilon^+(r,t_i)\Delta t \ll 1 \\ \exp[-\upsilon^+(r,t_i)\Delta t] &\simeq 1-\upsilon^+(r,t_i)\Delta t \end{aligned} \tag{6.12}$$

and hence:

$$P_S(T) \geq P_{S_0} \prod_{i=1}^{\infty} \int_R (1-\upsilon^+(r,t_i)\Delta t)\ dr \tag{6.13}$$

Now since:

$$\begin{aligned} \int_R \upsilon^+(r,t_i) f_R(r,t_i)\ dr\ \Delta t &\ll 1 \\ 1-\int_R \upsilon^+(r,t_i) f_R(r,t_i)\ dr\ \Delta t &\simeq \exp[-\int_R \upsilon^+(r,t_i) f_R(r,t_i)\ dr\ \Delta t] \end{aligned} \tag{6.14}$$

equation (6.7) becomes:

$$\begin{aligned} P_S(T) &\geq P_{S_0} \prod_{i=1}^{\infty} \exp[-\int_R \upsilon^+(r,t_i) f_R(r,t_i)\ dr\ \Delta t] \\ &\simeq P_{S_0} \exp[-\sum_{i=1}^{\infty} \int_R \upsilon^+(r,t_i) f_R(r,t_i)\ dr\ \Delta t] \\ &\simeq P_{S_0}.\exp[-\int_0^T \int_R \upsilon^+(r,t) f_R(r,t)\ dr\ dt] \end{aligned} \tag{6.15}$$

This latter result is a consequence of the fact that, if $\int_0^T \upsilon_E^+(t)dt \ll 1$, then any sub-interval of this integral $\int_{ti-\Delta t/2}^{ti+\Delta t/2} \upsilon_E^+(t)dt$ is also much smaller than one. The same is not true if the integration over the resistance is divided in a finite number of intervals, and a similar solution is attempted.

The general solution in equation (6.7) requires a suitable choice of the number of time divisions n, which will be a function of the correlation length of the slow-varying random process barrier. The choice of n actually provides a balance between conservative and unconservative approximations implied in equation (6.7), and which depend on the correlation length of the barrier. The conservative approximation is implied in equation (6.5) and it is of course a function of the time interval Δt. This approximation tends to be eliminated as the correlation of the barrier between successive intervals goes to zero ($R_{RR}(t_i, t_i+\Delta t) \to 0$). The unconservative approximation is implied in equation (6.6), due to integration over R, and it tends to be reduced as the correlation of the barrier between the lower and upper time integration limits tends to one ($R_{RR}(t_i-\Delta t/2, t_i+\Delta t/2) \to 1$). Some numerical results presented below illustrate this behavior. The appropriate value of n for time-invariant barriers

is found to be such that $R_{RR}(t_i - \Delta t/2, t_i + \Delta t/2) = R_{RR}(\Delta t) \approx 0.5$.

6.3 Computational aspects

Integration over the resistance in the random variable or "outer integration" solution is based on a parametric description of the resistance:

$$r(t) = \deg(t)\ r_0 \tag{6.16}$$

where $\deg(t)$ is a deterministic degradation function and r_0 is one outcome of the initial resistance random variable R_0. For a slow-varying random process barrier this description is generally not available, but the variation in time of the resistance probability density function is known. An approximate "deterministic" description of the resistance variation inside each integration interval (equation 6.6) can, however, be obtained by projecting the percentiles of the initial resistance distribution for each interval:

$$r_i(r_0, t) = \frac{(r_0\ \sigma_R(t_{0i}) + \mu_R(t_{0i}) - \sigma_R(t)}{\mu_R(t)} \tag{6.17}$$

where $t_{0i} = t_i - \Delta t/2$ is the lower integration limit for the i^{th} interval and r_0 is one outcome of $f_R(r, t)$ at $t = t_{0i}$. Although an approximation, equation (6.17) is only used in a narrow time interval where the resistance is highly correlated ($R_{RR}(\Delta t) \approx 0.5$). Anyway, equations (6.17) and (6.7) are likely to provide better results than a projection of percentiles from $t = 0$ to $t = T$, which would be required if a simple random variable solution were to be used for a random process barrier problem.

Another issue to be considered is when the correlation of the barrier is such that the appropriate number of time divisions n is smaller than the desirable number of time evaluation points n_e. In this case, the time-integration interval $\Delta t = T/n$ is divided in n_s sub-intervals, such that $n_e = n \cdot n_s$. Hence, for each sub-interval t_{ei} , $(i = 1, n_e)$ the time integration is performed over the last n_s intervals (such that $R_{RR}(\Delta t) \approx 0.5$), the multiplication of the probabilities of survival (eq. 6.5) is performed over groups of n_s intervals, and the solution is repeated for every evaluation time t_{ei}. When $n > n_e$ the solution is simply evaluated at n time points. Such solution may look very costly, but it is not expected to be encountered in practice as it represents a fast-varying random process barrier. In this way, a single algorithm is obtained to handle all situations from $n = 1$ to $n > n_e$.

6.4 Numerical results

The interpolation solution is tested for the range of time-invariant and time-variant random barriers considered in chapter 3. A broad band First Order Markov load process is considered, with distribution $N(0,1)$, correlation function $R_{SS}(t_2 - t_1) = \exp[-\frac{t_2-t_1}{\lambda_S}]$ and correlation length $\lambda_S = 1$ cycle. The correlation function of the random (process) barriers is also exponential, with correlation length given by multiples of λ_S: $\lambda_R = m_f\ \lambda_S$ and $m_f = \{1, 10, 100, 200, \infty\}$.

Figure 6-2 compares interpolation results with EUR and FPI results for different correlation lengths of the barrier. It can be seen in the figure that the interpolation solution converges to the "outer" integration solution (FPI solution) with $\lambda_R = \infty$ and $n = 1$ and to the "inner" integration solution (EUR solution) when $\lambda_R = 1$ and $n = 300$. The rule $R_{RR}(\Delta t) \approx 0.5$, provides the values of $n = \{900, 90, 9, 4.5, 1\}$ for the correlation lengths considered, respectively. For $\lambda_R = 1$, however, it turns out that $n = 300$ comes close enough to the EUR solution. For the intermediate situations, with $\lambda_R = \{10, 100, 200\}$, the interpolation solution follows Monte Carlo simulation results very closely, with the choice $n = \{100, 10, 5\}$, respectively, making these results slightly conservative. The seesaw behavior observed for $\lambda_R = 200$ is due to the small number of time divisions ($n = 5$) required for this barrier. It is interesting to note that $n = 5$ was chosen to be conservative, but with $n = 4$, for some of the tested barriers, the interpolation solution clearly zigzags above and below simulation results, illustrating the conservative and unconservative character, respectively, of the opposing approximations implied in the interpolation solution.

Similar results for time-variant barriers are shown in figure 6-3. The barriers used in these examples are the same considered in chapter 3, with barrier parameters being indicated in the figures. Results obtained are similar to the time-invariant case. For the faster varying barriers ($\lambda_R = 1$ and 10), however, the interpolation solution becomes significantly more conservative, as compared to the time-invariant case. One way to obtain a closer bound is to reduce the number of time divisions, as done for the results presented in the figures. These results were obtained using $n = 150$ and $n = 50$, for $\lambda_R = 1$ and $\lambda_R = 10$, respectively, as opposed to the values $n = 900$ and $n = 90$ obtained by the $R_{RR}(\Delta t) \approx 0.5$ rule.

6.5 Discussion

In view of the results presented in the last section and of the insight gained elsewhere in this work, an important issue becomes to define when such an interpolation solution is necessary

and when can it be avoided. As stated earlier, a fast varying barrier is not expected to be encountered in practice. For barriers with small correlation lengths ($\lambda_R < 10\ \lambda_S$) an averaging of the up-crossing rate over the barrier (EUR solution) could be close enough (see results in the figures). The important case are the barriers with long correlation lengths (say, $100\ \lambda_S \leq \lambda_R$ or $T/6 \leq \lambda_R \leq T/2$), but certainly with $\lambda_R < T$. For such barriers, an ensemble up-crossing rate solution can be too conservative and, as $\lambda_R \to \infty$, one can expect the "order of magnitude" EUR error to be of the same size of the error found for the random variable barriers (chapter 3). An outer integration, on the other hand, is unconservative for such barriers. Hence, these are the barriers for which an interpolation solution is quite adequate. For these barriers, the number of time divisions is small, and the increase in computation time, as comparing to an overly conservative EUR approximation or to an unconservative FPI solution, is clearly outweighed by the quality of the interpolation solution. One important application where such "long" correlation lengths might be present are problems involving barriers obtained from or derived as Markov diffusive processes.

In fact, regardless of the number of divisions n, it should be noted that the computational cost of an interpolation solution is not more than the cost of an "outer" integration solution for multiple time evaluation points, as long as the number of time divisions (and/or subdivisions) is less or equal to the number of time evaluation points.

The interpolation solution developed herein is equivalent to a formal solution involving discretization of the slow-varying random barrier. The interpolation solution represents a discretization with a grid size Δt chosen such that: $R_{RR}(\Delta t) = 0.5$, and with the additional approximation that "discretized" random variables are considered fully correlated for $\Delta t = \Delta t | R_{RR}(\Delta t) > 0.5$ and uncorrelated when $\Delta t = \Delta t | R_{RR}(\Delta t) < 0.5$.

6.6 Figures

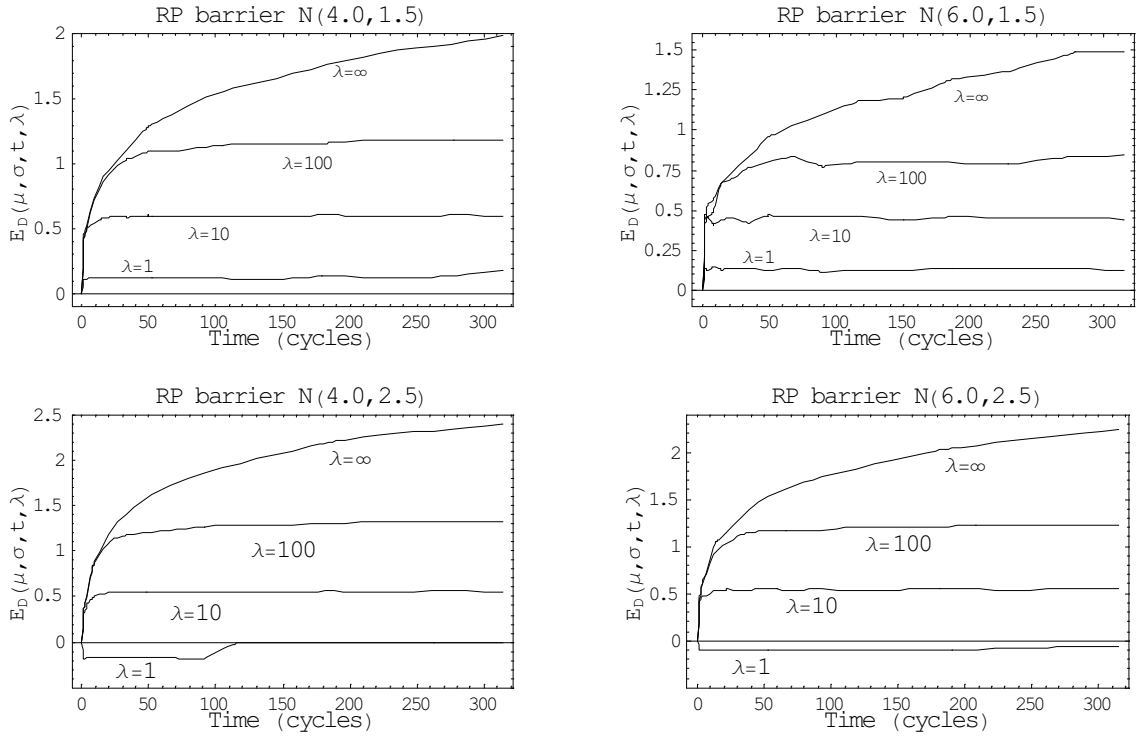

Figure 6-1: Error $E_D(\mu, \sigma, T)$ for four Gaussian $N(\mu, \sigma)$ random process barriers as a function of correlation length $\lambda = \lambda_R$ ($\lambda_S = 1$).

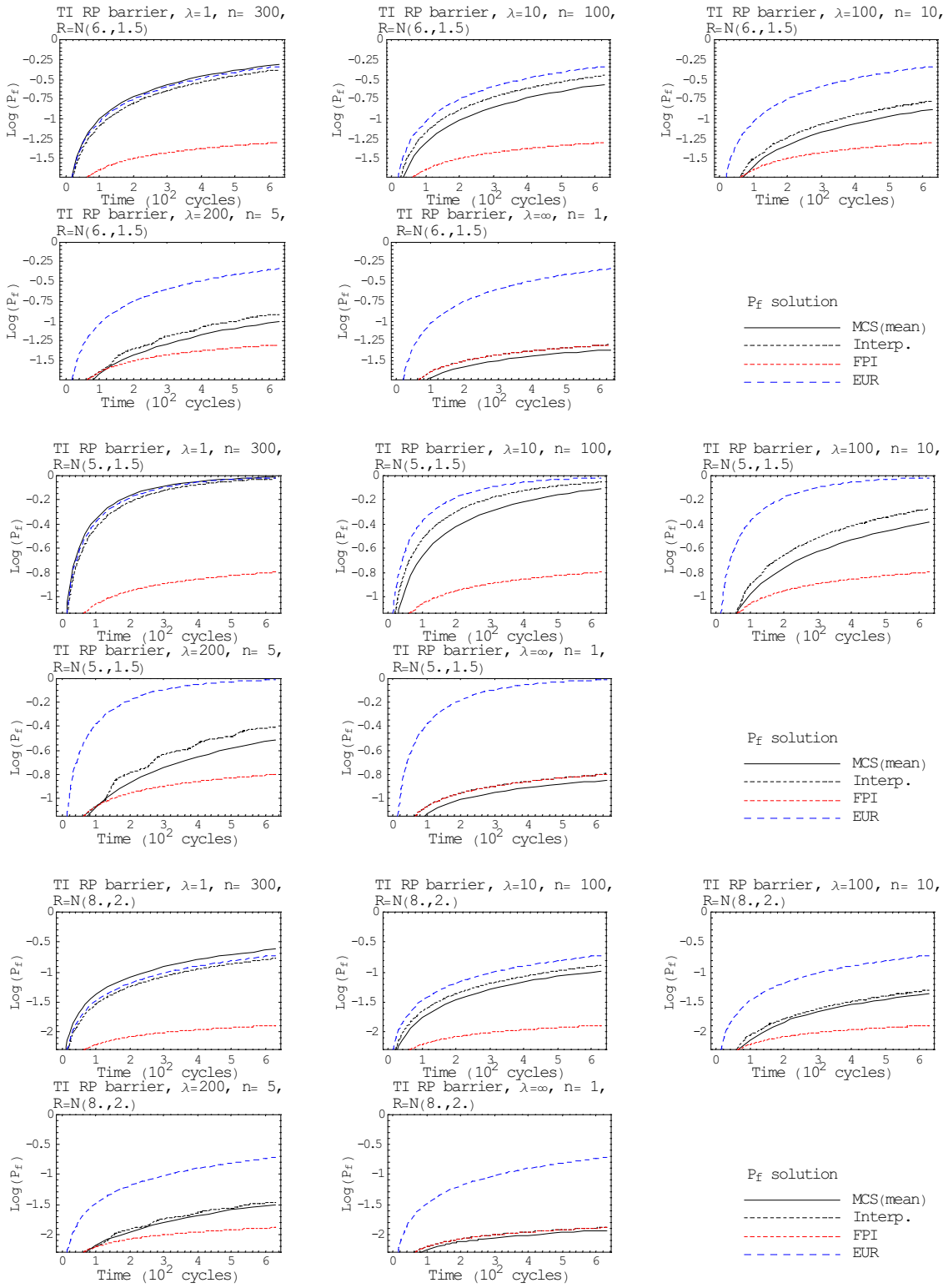

Figure 6-2: Interpolation results for 3 time-invariant barriers and 5 values of the correlation lenght λ_R, BB load process.

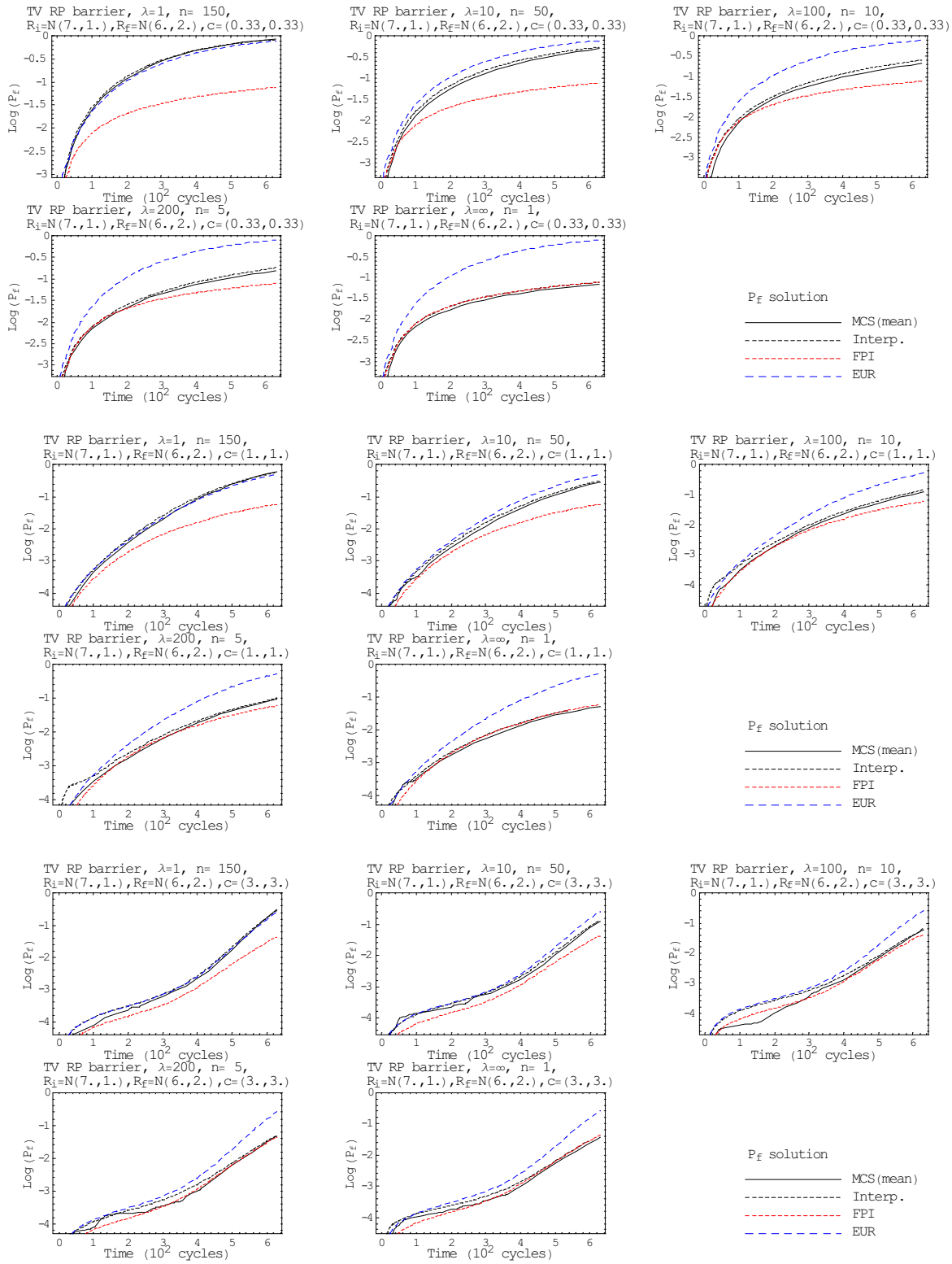

Figure 6-3: Interpolation results for 3 time-variant barriers and 5 values of the correlation lenght λ_R, BB load process.

Part II

FATIGUE AND FRACTURE RELIABILITY ANALYSIS UNDER RANDOM LOADING

Chapter 7

LITERATURE REVIEW PART II

7.1 Linear elastic fracture mechanics

In a generic cracked body, cracks represent discontinuities and stress concentrators. Due to the small radius of curvature of the crack tip, theories of continuum mechanics predict the stresses ahead and near the crack tip to be infinite. In practice, localized yielding occurs anywhere the yielding stress of the material is exceeded (figure 7-1). Therefore, special theory is necessary to describe the state of stresses and strains around the crack tip.

Linear Elastic Fracture Mechanics (LEFM) is one of such theories, perhaps the most widely known and used. In LEFM, the state of stresses and strains around the crack tip is characterized by stress intensity factors (SIF), according to the loading mode of the crack. Three stress intensity factors, namely K_I, K_{II} and K_{III}, are used for, respectively, the opening, sliding and tearing loading modes (figure 7-2). The stress intensity factors depend on crack and body geometry, and on the applied far field stress. In the opening load mode, one has $K_I = S\sqrt{\pi a}Y(a)$, where S is the applied far field stress, a is half the crack length and $Y(a)$ is a geometry function, which accounts for the shape of the body and geometry of the crack. For a through the thickness crack in an infinitely wide plate, for example, $Y(a) = 1$.

Stress intensity factors characterize both stable (crack growth) and unstable (fracture) crack propagation. In LEFM the overall behavior of the body is assumed to remain elastic, and the theory is therefore limited to small scale yielding around the crack tip. The scale of yielding can be measured as the ratio between the radius of plasticity and a characteristic length such as crack size or the remaining cross section. The radius of plasticity is approximated as:

$$r_p = \frac{1}{\upsilon\pi}\left(\frac{K_I}{2\sigma_y}\right)^2 \tag{7.1}$$

where $\upsilon = 2$ for plane stress and $\upsilon = 6$ for plane strain.

Other fracture parameters derived from elasto-plastic fracture mechanics are sometimes used in the context of LEFM. The energy release rate C, the path independent J integral and the crack tip opening displacement (CTOD) are all equivalent to the SIF under the condition of small scale yielding. Following Kanninen and Popelar (1985), the choice between these parameters under small scale yielding is merely a question of convenience. The J integral and CTOD, however, remain valid under large plasticity, i.e., in elasto-plastic fracture mechanics. Unfortunately, although the J integral and CTOD yield correct predictions of failure loads and collapse of cracked structures, these parameters are not very accurate at predicting crack propagation (Wang et al., 1997).

For the problem addressed in this thesis, namely fatigue and fracture reliability analysis under random loading, LEFM has some appealing characteristics. One is its simplicity, another is the wide availability of results, including results revealing and dealing with the stochastic nature of crack propagation. Another positive characteristic of LEFM is the fact that, under the limitation of small scale yielding, the state of damage and the residual strength of the structure can be related to the same physical variable, namely the size of a leading crack.

7.1.1 Crack propagation under constant amplitude loading

Paris crack propagation law

The most widely accepted crack growth law was proposed by Paris and Erdogan (1969). It was derived from constant amplitude loading experiments and identifies the stress intensity factor range ($\Delta K = K(S_{\max}) - K(S_{\min})$) as the major force driving crack propagation. It describes the crack propagation rate as a linear function of ΔK in a log-log scale (figure 7-3):

$$\frac{da}{dn} = c \cdot (\Delta K)^m \tag{7.2}$$

where c and m are material parameters and $\frac{da}{dn}$ is the crack propagation rate (mm/cycle).

The Paris law is valid for intermediate values of ΔK (figure 7-3). Other expressions have been proposed and adapted to include crack propagation near the fatigue threshold ΔK_{th} and/or near the fracture toughness K_{IC}. Other equations were derived to include secondary effects such as mean stress, maximum stress, etc. Good references in fracture mechanics offer a complete description of such equations (Kanninen and Popelar, 1985; Ellyin, 1997). An important observation is that for specific applications of fracture mechanics, there are specific crack propagation equations, which have been calibrated to work on very specific (and limited)

circumstances. Hence, general reliability solutions for crack propagation should be derived considering and should be valid for generic and not specific crack growth equations.

Crack closure model

A significant improvement over the Paris equation is the crack closure model of Elber (1970). This model recognizes that during significant part of the loading cycle, including initial tension, the crack surfaces are closed due to tensile residual stresses at the crack tip, oxidation, debris, etc. Elber concluded that the crack only grows when its surfaces are completely open, i.e., that the crack driving force is only part of the stress intensity factor range. The author proposes the use of an effective stress range, calculated as the maximum stress less the stress required for the crack to open:

$$\Delta K_{eff} = K_{\max} - K_{op} \tag{7.3}$$

Elber and following researchers further found that the opening stress intensity factor K_{op} is independent of crack size and $K_{\max}$, but is a function of the stress ratios. Several equations were proposed for constant amplitude loading. Under random loading, K_{op} is generally considered to be constant and its value is obtained experientially.

The crack closure concept and the use of an effective stress intensity factor range addresses important aspects of fatigue crack propagation, like the influence of stress ratios (Wirsching, 1998; Wang, 1999; Dolinski and Colombi, 1999). According to Wang (1999), it actually reduces the scatter in crack propagation data and accounts for small crack behavior under constant amplitude and spectrum loading. This author observed that the crack growth rate c is a linear function of the effective stress intensity range near the crack growth threshold ΔK_{th}.

7.1.2 Crack propagation under variable amplitude loading

The Paris-Erdogan crack propagation law and most of its variations were derived from constant amplitude loading experiments. Some 99% of all available experimental crack propagation data is for constant amplitude loading (Sobzyck and Spencer, 1992). Service loads, however, are generally of variable amplitude (spectrum or random loading). One important issue that arises when Paris-type equations are applied to variable amplitude loading is the identification of stress intensity factor ranges (ΔK).

Cycle counting techniques

Cycle counting techniques are used to identify stress cycles in a random loading process. One frequently adopted technique is rainflow-counting (Dowling, 1985), which identifies stress ranges corresponding to closed hysteresis loops of the material's stress-strain response (figure 7-4). The technique identifies the number and amplitude of stress ranges contained in a sample of the random load process. Such stress ranges are then used, on a step-by-step basis, to predict crack growth in service using a constant amplitude crack growth equation:

$$a(n) = a_0 + \sum_{i=1}^{n} c \cdot (\Delta K_i)^m \tag{7.4}$$

The rainflow cycle counting technique randomizes the sequence of cycles in the stress process and therefore loading sequence effects are completely ignored.

Equivalent constant amplitude stress range

The use of a single equivalent (constant amplitude) stress range that yields the same crack propagation life as the variable amplitude loading has been proposed by some authors. Sobczyk (1986), for example, proposes the equivalent stress range to be the random mean square (RMS) value of the stress process ($\Delta S_{eq} = S_{RMS}$). Wirsching (1998) proposes the expected value of stress ranges ($\Delta S_{eq} = (E[\Delta S^m])^{\frac{1}{m}}$) to be used as equivalent constant amplitude stress range. There is little experience about the validity of such equivalent stress ranges, and one can assume that they work well for specific problems.

Sequence effects

Experiments under cyclic loading including deterministic overloads reveal retardation of the crack propagation rate after large tensile overloads. Wheeler (1972) assumed that retardation occurs as long as the monotonic plastic zone is smaller than the overload-affected plastic zone, and that the retarded crack growth rate is a function of the ratio between the two plastic zones.

Veers (1987) developed a solutions based on Wheelers model and on a reset stress, a history dependent parameter that indicates the state of residual compression at the crack tip. Veers extended the crack closure concept of Elber for constant amplitude loading ($S_{op} = c_f S_{\max}$) to the case of variable amplitude loading ($S_{op} = c_f S_R$), where S_R is the reset stress which is a function of the stress ratio. The reset stress is defined as the stress necessary to reset the maximum extent of the overload-affected zone at the crack tip. In this way, the magnitude

of the retarded crack growth is related to the magnitude of the overload and the overload-affected plastic zone.

This solution is based on deterministic time-histories and depends on a cycle counting method that preserves the sequencing of stress cycles. Range counting is such a method, but although it preserves the stress range sequences, it is said to ignore some of the largest stress ranges, in comparison with rainflow counting (Sobzyck and Spencer, 1992). When loading is random, sequence effects are random too, and accounting for sequence effects in a deterministic basis only provides conditional crack growth time-histories. Under high cycle fatigue, sequence effects can generally be neglected, provided that experimental crack propagation parameters are obtained using the same type of loading (spectrum) as expected in service (Wang, 1999; Yang et al., 1987).

7.1.3 Fracture criteria

In fracture mechanics, the words fracture and crack propagation are sometimes used to describe the same thing. A distinction is made between "stable" and "unstable" crack propagation. Crack propagation is said to be stable if it is halted by holding the load, and it relates to (generally slow) crack growth. Unstable crack propagation is characterized when the crack keeps on growing even when the load is held still, and it relates to fracture of the component or structure. In this thesis, the terms "crack propagation" and "fracture" are used to refer to "stable" and "unstable" crack propagation. In this section, fracture criteria are reviewed. Linear elastic and a completely plastic fracture criteria are seen first, followed by an elasto-plastic criterion.

Elastic and plastic fracture

The fracture (or unstable crack propagation) of a cracked body is governed by the state of stresses at the crack tip, which is dependent on body dimensions, the size of the plastic zone, crack size and fracture load.

In a center cracked panel, for example, lateral surfaces are on a state of plane stress, whereas the mid-section is in a plane strain state. This balance, however, is affected by the size of the plastic zone ahead of the crack tip.

When the plastic zone is small in comparison to the plate's thickness, a tri-axial state of stresses prevails (with exception of a thin layer in the traction-free lateral surfaces); fracture is characteristically fragile; the fracture surface is flat and fracture is governed by the fracture toughness, a material property. Brittle or elastic fracture is therefore characterized when the

material's critical stress intensity factor or fracture toughness, K_{IC}, is reached.

On the other extreme, when the plastic zone is of the magnitude of the plate width, plane stress prevails, significant yielding occurs before fracture and the fracture surface is slant (with shear lips). There is an increase in the fracture load, which can be much greater than K_{IC}. In this case, a resistance curve based on the plastic flow stress is used instead of the fracture toughness. In addition, fracture parameters depend on specimen thickness and fracture resistance increases with increasing crack length.

In the intermediate situation, a mixed mode of fracture is encountered, with plain strain fracture in the mid section and plane stress fracture near the lateral surfaces.

Elasto-plastic fracture

High toughness low strength materials, such as most damage tolerant aeronautical aluminium alloys, fail under significant yielding, including yielding of the whole remaining cross section. Such large scale yielding is beyond the limits of application of linear elastic fracture mechanics and, in principle, an elasto-plastic analysis is required. Based on the equivalence between elastic and elasto-plastic fracture parameters, however, it is possible to derive an elasto-plastic correction for elastic fracture predictions, in a procedure that leads to a simple fracture criterion that accommodates brittle, ductile and mixed mode fracture.

One such fracture criteria is based on Dugdale's elasto-plastic crack propagation model (Kanninen and Popelar, 1985). Dugdale considered the effect of yielding ahead of the crack tip to be equivalent to a crack extended by the size of the plastic zone. The material's yielding restrains opening of the crack within the yielded strip. By adding the solution for an uncracked sheet loaded by far field stress σ to the solution for a cracked sheet with no remote loading, but with a crack surface pressure σ and a yield strip pressure $\sigma - \sigma_y$, Dugdale derived an expression for the crack tip opening displacement (δ_t), i.e., the displacement at the original crack tip position, due to yielding ahead of the crack tip:

$$\delta_t = \frac{8}{\pi}\frac{\sigma_y}{E}a \cdot \log\left[\sec\left(\frac{\pi}{2}\frac{\sigma}{\sigma_y}\right)\right] \tag{7.5}$$

Similar expressions have been derived for fracture in modes II and III. The crack tip opening displacement δ_t can be interpreted as a measure of deformation in the plastic zone. Ductile fracture is characterized by δ_t reaching a critical value or, by equivalence, by LEFM parameters J or K_I reaching critical values:

$$J_C = \sigma_y \delta_{tC} = \frac{K_{IC}^2}{E} \tag{7.6}$$

where sub-index $_C$ stands for critical. Manipulation of the two expressions leads to:

$$\left(\frac{K_I}{K_{IC}}\right)_f = \frac{\sigma_f}{\sigma_y}\sqrt{\frac{8}{\pi^2}\log\left[\sec\left(\frac{\pi}{2}\frac{\sigma_f}{\sigma_y}\right)\right]} \tag{7.7}$$

where σ_f is the far field stress at fracture. When the fracture stress σ_f is measured, in an experiment, this relation is used to obtain an equivalent K_{IC} for intermediate scale yielding. It is then used to predict the fracture stress σ in applications for which K_{IC} was determined.

Equation (7.7) includes the two extreme fracture situations: when $\frac{\sigma}{\sigma_y} << 1$ it describes brittle fracture under small scale yielding, when $\frac{\sigma}{\sigma_y} \to 1$ it describes fracture under large scale yielding. Furthermore, the yielding stress can be replaced by a plastic collapse stress σ_c, in order to accommodate different cracked configurations and strain hardening (Kanninen and Popelar, 1985).

A failure assessment diagram or "R6 curve" is constructed by plotting equation (7.7) as a function of K_r and S_r, where $K_r = \frac{K_I}{K_{IC}}$ and $S_r = \frac{S_f}{S_y}$ (figure 7-5). Each point (K_r, S_r) in the diagram corresponds to one crack size and loading condition, with K_I being proportional to crack size and both K_I and σ being proportional to loading. The failure assessment diagram divides the failure and safe domains for mixed-mode fracture. Crack growth moves points towards the failure domain, i.e., away from the origin, in what is called a failure path. Load application moves points as rays emanating from the origin. Vertical moves towards the top characterize brittle fracture, whereas horizontal moves to the right characterize ductile fracture (ligament yielding). Diagonal moves correspond to mixed mode fracture.

7.2 Random aspects of fatigue

7.2.1 Fatigue is a random process

The theory reviewed so far is within the limits of what could be called deterministic or mean-value fracture mechanics. In this section, the sources of uncertainty and randomness of fatigue and crack growth are identified. It is also seen how these statistical or probabilistic aspects of fatigue are incorporated into LEFM, and how probabilistic models are constructed based on deterministic LEFM results. The term fatigue is used here in the broader sense, as the process through which damage accumulates in a metal structure or component, due to a cyclical tensile load action. It is not used in reference to any specific damage rule such as Palmgreen-Miner's.

Early fatigue researches have already realized that fatigue is a random phenomena. These researchers employed a range of probability distributions (exponential, normal, log-normal,

Gamma, Gumbel) in attempts to fit experimental fatigue lives (Provan, 1987). In fact, some of the probability distribution functions widely used in engineering today, such as the Weibull distribution, have been developed by researchers who were trying to describe the statistical dispersion observed in fatigue life data.

Uncertainties in fatigue have several sources: initial flaws; metallurgical inhomogenities; component stress variations due to production tolerances; residual stresses due to welding, cold working, heat treatment; structural assemble stress variations; surface quality and variations in external loading (Wang, 1999). Other, more general sources of uncertainty are material properties such as yielding and ultimate stresses, fracture toughness and the effect of non-destructive inspections.

Following Wang (1999), it is unlikely that any probabilistic analysis or model will be able to deal with all sources of uncertainty, especially with those arriving from component assembly and usage. The only way to address this variety of uncertainty sources is by reproducing operational conditions in laboratory tests. This necessity has already been widely recognized by fatigue researchers.

However, scatter observed in experimental results can be related to random material properties and dealt with using suitable probabilistic models. Gradually, and eventually, other sources of uncertainty can be identified, quantified and included in the models. In this section, the most important sources of uncertainty in fatigue crack propagation are identified. In the following section, stochastic crack propagation models which incorporate these uncertainties are reviewed.

7.2.2 Material in-homogeneity and the crack propagation rate

Closely controlled large replicate constant amplitude fatigue experiments such as those by Virkler et al. (1979) and Ghonen and Dore (1987) reveal significant dispersion of crack growth time histories, as illustrated in figure 7-6. Experimental crack propagation rates obtained from such diverse crack growth time-histories show significant scatter too (figure 7-7). An interpretation of these results is that material inhomogenities such as grains, grain boundaries, inclusions, voids, etc., continuously affect the crack propagation rate as the crack tip moves through new material. Hence, it becomes natural to model the crack propagation rate as a random process.

Some general results were obtained by Yang et al. (1987), studying crack propagation in fastener holes of aircraft structures and in a centre cracked panel, both subject to spectrum loading. The authors modeled the crack propagation rate as a lognormal random process of

time:

$$\frac{dA}{dn} = C(t)(\Delta K)^m \tag{7.8}$$

The use of upper-case A and C for crack size and crack propagation rates, respectively, is to stress that these are now considered as random processes. In the study by Yang et al. (1987), two extreme possibilities for the correlation length of random process $C(t)$ were considered: for zero correlation length it becomes a white noise process; for an infinite correlation length it becomes a random variable. The white noise process introduced little scatter in crack propagation time histories, whereas the random variable option resulted in high scatter (figure 7-8). Experimental results, illustrated in figure 7-6, were found to be in-between, and hence the correlation parameter of the process was calibrated to reproduce the scatter observed in experimental results. This simple lognormal random process model, with a calibrated correlation length, is able to reproduce acceleration and retardation of individual crack growth histories observed in experiments. The small statistical dispersion resulting from the white noise model can be seen as a consequence of the summation of a large number of small random increments in the crack propagation evaluation, which tends to average the crack growth rate over a couple of cycles.

Although excellent agreement with experimental results was obtained with this model, time is not necessarily the best parameter to describe the random process $C(t)$. Since variations in the crack propagation rate are attributed to material inhomogenities, it would be more appropriate to model C as a random process of crack length, $C(a)$, i.e., assuming that the crack propagation rate changes randomly as the crack tip moves through new material. When time is used as a parameter, results become dependent on the level of loading, since the crack propagates over more or less material in the same time depending on loading level. However, modeling the crack propagation rate as a function of time greatly facilitates derivation of crack transition probability densities, as will be seen later.

Models that consider C as a function of crack size also have been proposed. Ortiz (1984), for example, distinguished randomness in the crack propagation rate as a fluctuation between mean behavior of different specimens and a deviation of mean crack growth within a specimen:

$$\frac{dA}{dn} = \frac{C_1}{C_2(a)}(\Delta K)^m \tag{7.9}$$

where C_1 is a random variable describing fluctuation between mean behavior of different specimens and $C_2(a)$ is a lognormal random process of crack size describing deviation of

mean crack growth within a specimen. Based on comparison to experimental data, Ortiz verified that, for this model, the correlation length was close to zero and $C_2(a)$ could be approximated as a white noise process.

Itagaki et al. (1992) reached similar conclusions by considering a random variable crack exponent M and a random process crack propagation rate $C(a)$:

$$\frac{dA}{dn} = C(a) \left(\frac{\Delta K}{K_0} \right)^M \tag{7.10}$$

The authors assumed M to follow a normal distribution and the crack propagation rate was found to follow a 3 parameter Weibull distribution. The correlation length of the process was also obtained from experimental data.

Stochastic crack propagation models, including random crack propagation rates and other random parameters, are reviewed in detail later. First, other sources of uncertainty are considered.

7.2.3 Random load processes

Rainflow counting of stress ranges

Random loading introduces additional uncertainty in crack propagation. A modelling error or uncertainty is originated when constant amplitude Paris-type crack propagation equations are used with random process stress ranges. This type of modelling error is hard to evaluate, and one way around it is the identification of proper cycle counting techniques. Additional uncertainty comes from the random process itself, i.e., from the fact that stress ranges of a random stress process are a random process themselves.

Experimental verification of random loading effects is virtually impossible, because these effects cannot be separated from the effect of other parameters such as material inhomogeneity. Generally speaking, modelling of random loading uncertainty is an analytical exercise that provides some insight into how random loading affects crack propagation uncertainty.

Rainflow counting of distinct sampled trajectories (time-histories) of the same load process results in slightly different stress ranges and therefore in different crack propagation time-histories. Wirsching and Shehata (1977) studied this effect by direct simulation: a large number of stress trajectories was simulated, stress ranges were identified and crack growth was computed for every sampled trajectory.

To overcome this rather cumbersome procedure, it was proposed to fit a probability distribution function to the stress ranges computed from particular stress processes. Crack

growth can then be computed by sampling stress ranges from the stress range PDF. Because rainflow-counting randomizes the sequences, stress ranges are sampled as if they were an uncorrelated process (Zheng and Ellingwood, 1998).

Probability distributions of rainflow-counted stress ranges

The probability distribution of rainflow-counted stress ranges can often be adjusted to a two parameter Weibull distribution (Madsen et al., 1986; Nigam and Narayanan, 1994):

$$F_{\Delta S}(s) = 1 - \exp\left[-\left(\frac{s}{A}\right)^B\right] \tag{7.11}$$

where A and B are scale and shape parameters. This distribution is quite flexible, but not necessarily the best for all applications. It is often used in probabilistic fracture mechanics because the load parameter $(\Delta S)^m$ can be evaluated in closed form.

Narrow-band process The stress ranges of ideally narrow-band Gaussian processes follow Rayleigh distributions (figure 7-9):

$$f_{\Delta S}(s) = \frac{s}{\sigma_s^2} \exp\left[-\frac{1}{2}\left(\frac{s}{\sigma_s}\right)^2\right] \tag{7.12}$$

where parameter σ_s is the standard deviation of the load process. Some (minor) corrections to this distribution for nearly narrow-band processes ($1.0 \leq \alpha \leq 0.9$) are quoted in Bouyssy et al. (1993).

Broad-band process Derivation of distribution functions for rainflow-counted stress ranges of broad-band Gaussian stress processes is more complicated, due to large variability in possible spectrum ranges and irregularity factors. A comparative study of distributions proposed for uni-modal load processes is presented in Bouyssy et al. (1993). Using extensive Monte Carlo simulation, the authors conclude that:

> " Dirlik's (1985) model appears to be the best over the full range of spectra, exponents m and irregularity factors α."

The distribution proposed by Dirlik (1985) is shown in figure 7-10 for an uni-modal process with $\alpha = 0.4$. This distribution is a combination of an exponential and two Rayleigh distributions, with parameters $\frac{1}{2q}$, $\frac{1}{2r}$ and $\frac{1}{2}$, as follows:

$$f_{\Delta S}(s) = \frac{1}{2}\left[\frac{d_1}{q}\exp(-\frac{s}{2q}) + \frac{s \cdot d_2}{2r^2}\exp(-\frac{1}{2}(\frac{s}{2r})^2) + \frac{s \cdot d_3}{2}\exp(-\frac{1}{2}(\frac{s}{2})^2)\right] \tag{7.13}$$

where:

$x_m = \frac{\lambda_1}{\lambda_0}\sqrt{\frac{\lambda_2}{\lambda_4}}$; $\quad d_1 = \frac{2(x_m - \alpha^2)}{1-\alpha^2}$;

$r = \frac{\alpha - x_m - d_1^2}{1 - \alpha d_1 + d_1^2}$; $\quad d_2 = \frac{1 - \alpha - d_1 + d_1^2}{1-r}$;

$q = \frac{\alpha - d_3 - r d_2}{4 d_1}$; $\quad d_3 = 1 - d_1 - d_2$.

For multi-modal loads, Nagode and Fajdiga (1998) proposed a general multimode 3 parameter Weibull distribution that can be fitted to rainflow computed stress ranges of general stationary processes, regardless of bandwidth and distribution function. A methodology for parameter estimation is also proposed.

Random sequencing effects

Cycle-by-cycle computation of sequence effects under random loading is a cumbersome practice, because it is conditional to particular outcomes of the load process. As for the problem of rainflow counting, direct simulation can be employed. This costly and cumbersome procedure is only justifiable under low cycle fatigue, where sequencing effects have some importance. Under high cycle fatigue sequencing effects are negligible (Wang, 1999). Stochastic models of crack propagation that take sequencing effects into account are still an important matter of current research (Sobczyk and Spencer, 1992).

7.2.4 Random initial crack size

In many LEFM applications, cracks originating from the manufacturing or construction process are assumed to exist in structural components and structural details. Several random crack propagation studies identify the initial crack size as one of the most important factors affecting crack growth uncertainty. Due to limitations of non-destructive inspection methods, the measurement of initial crack sizes, and especially their statistics, is not a straightforward task. Direct measuring requires very accurate inspections methods and large sample sizes. Destructive or tear-down inspections provide a more reliable way of measuring small flaws in fabricated structures, but these are very costly alternatives.

Although some results exist for specific structural elements and manufacturing procedures, statistical information on size and frequency of occurrence of flaws is not available for general applications. Some results are available for welded steel structures, where slag inclusions are rather common. Flaw size in welded structures is often found to follow an exponential

distribution (Moan et al., 1994; Ayala-Uraga and Moan, 2002).

One approach to overcome the difficulty of deriving crack size statistics for very small crack sizes, commonly adopted in the durability analysis of aerospace structures, is the Equivalent Initial Flaw Size (EIFS) distribution (Yang et al., 1987). The idea is to derive crack size statistics from the distribution of larger crack sizes occurring later on during service life. Cracks may be detected during in-service inspections or through laboratory coupon testing. They are then grown backwards yielding an equivalent distribution at time zero. The EIFS distribution is not the actual distribution of cracks in the structure, but it is used as an indication of the fatigue-quality of specific combinations of type of structural detail, material and manufacturing process. Hence, different EIFS distributions have to be derived for different design variables (material, sheet thickness, geometry, loading spectra, etc.) Another difficulty with the EIFS approach is that it assumes LEFM, and specific crack growth equations, to remain valid for very short crack lengths, which is not strictly correct.

Another equivalent approach is the Time-To-Crack-Initiation (TTCI) distribution. This distribution is obtained by measuring the time taken for an in-service crack to grow from an (unknown) initial size to a specific (and measurable) crack size. A proper PDF (generally lognormal or Weibull) is then fitted to the time-to-grow statistics. Under the same design and loading conditions, the EIFS and TTCI distributions are equivalent (Yang et al., 1987), and percentiles of both distributions can be related. Distributions for specific design parameters are often obtained by pooling together fractographic results from different data sets.

7.2.5 Non-destructive periodic inspections

Assuring the operational safety of structures subject to fatigue often involves the realization of periodic inspections and repairs. Non-destructive inspections introduce additional uncertainty, in a life-time assessment, due to limitations and inaccuracy of inspection techniques. These limitations concern the imperfect measurement of a detected crack, and the possibility of missing an existing crack. A (small) crack can only be detected with a given probability, and the resolution or quality of a particular inspection method can be characterized by a Probability of Detection (POD) distribution $P_D(a)$. Following the POD distribution, larger cracks are detected with a probability that converges asymptotically to one (figure 7-11). POD curves for the most common non-destructive inspections methods are currently available (e.g., Moan et al., 1997), but these curves are highly susceptible to the type of structure being inspected, material, operator, and acquaintance with the inspection method.

For an arbitrary inspection at a time T_i, two results are possible: 1) no cracks are found

- implying that any existing cracks are smaller than the minimal detectable crack size A_{d_i} and 2) a crack of length A_{m_i} is detected and measured. Both A_{d_i} and A_{m_i} are generally random. The incorporation of non-destructive inspection uncertainty in life-time reliability assessments is studied later, in connection with specific random variable - random process stochastic crack propagation models.

7.2.6 Other random parameters

Other material properties, related to the resistance of the cracked member rather than to crack propagation itself, are also typically random. This includes yielding, fracture and ultimate stresses as well as critical stress intensity factors of the material. These random variables have to be included in a fracture reliability analysis but will not be important in a random crack propagation analysis.

Additional variables are often introduced in crack propagation models to account for modelling errors (e.g., Ayala-Uraga and Moan, 2002). It is agreed that crack propagation models do not exactly portray the actual crack propagation process being modelled. Modeling variables are generally introduced empirically, and although that could suggest that they be treated as random variables as well, determination of parameters of such empirical random variables is always subjective.

Geometric variables generally represent insignificant uncertainty in crack propagation problems, but an exception is the geometry function $Y(a)$, used to relate stress intensity factors of particular geometries with the theoretical infinite plate case ($\Delta K = S(t)Y(a)\sqrt{\pi a}$). The geometry function is often treated as a random variable. This can be done by including a modelling random variable D such that $\Delta K = D\,S(t)\,Y(a)\sqrt{\pi a}$, or by randomizing parameters of empirical geometry functions for particular geometries.

Sometimes, the parameters of particular crack growth parameters are also considered as random variables. For example, the parameters A and B of the Weibull stress range distribution (equation 7.11) can be modelled as random variables (Ayala-Uraga and Moan, 2002). Parameters of the random load processes could also be found to be random, in particular applications.

7.3 Stochastic models of crack propagation

7.3.1 Overview

In the last two decades a significant number of stochastic models of fatigue crack propagation have been developed by a variety of researchers. Generally speaking, the resulting crack propagation process becomes a non-stationary random process of time, whose mean and standard deviation increase with time. The major goal of most models is to describe how the crack size PDF, or at least its statistics, vary in time. Alternatively, stochastic crack propagation models are used to describe the statistics of the time to reach a given crack size.

Loosely speaking, stochastic models of crack propagation can be divided in three types: the very simple ones, obtained by considering parameters of empirical crack growth equations to be random variables; some more complex ones, carefully derived and calibrated to reproduce scatter observed in fatigue experiments; and the very refined ones, aiming at describing peculiar aspects of crack propagation.

In terms of practical applications, the simplest models are useful mainly for studying the relative importance of the uncertainty of the different parameters of the model. On the other hand, too refined models often have parameters that can hardly be related or obtained from experimental data, and their solution is generally very expensive.

The above classification should become clearer as particular models are analyzed. Alternatively, stochastic models of crack propagation can be divided according to their mathematical formulation. Following Sobczyk and Spencer (1992), they are: differential equation, evolutionary and cumulative jump models. Differential equation models include random variable and random process models; evolutionary models are Markov chain and diffusive Markov models. These models will be reviewed next.

7.3.2 Random variable models

Random variable models of crack propagation are obtained by modelling parameters of deterministic, empirical crack growth equations as random variables. For a generic crack propagation function Q one obtains:

$$\frac{dA}{dn} = Q(A, C, \Delta K, M, \Delta S, ...) \tag{7.14}$$

where upper-case A represents the now random variable crack size.

This approach has been extensively applied to Paris's crack propagation equation and its variants. When crack growth parameters are randomized at will (i.e., without a reasonable

criterion) two problems arise: 1) random variable statistics and distribution functions cannot be derived experimentally, because different parameters (e.g. c and m) cannot always be isolated; 2) resulting crack propagation models do not reproduce experimental or actual crack growth behavior. Random variables can model specimen-to-specimen crack propagation rate variations, but cannot model deviation from mean crack growth within a specimen (Ortiz, 1984). These models cannot reproduce the intermingling effect observed in large replicate tests (Yang et al., 1987).

Random variable crack propagation models are, however, useful for studying the relative importance of the uncertainty or randomness of crack growth parameters. Several studies along these lines, for a variety of applications and considering typical values of random crack growth parameters, are available (Provan, 1987; Sobzyck and Spencer, 1992). Many of these studies identify the crack propagation rate C, the initial crack size A_0 and, to a lesser extent, the stress ranges ΔS as the most important random factors affecting crack growth uncertainty.

Random variable models are very simple to use, since crack propagation is deterministic for each realization of the model's random variables. This solution can be used in Monte Carlo simulation, in FORM reliability analysis or just to project percentiles of initial crack size distributions. The evolution in time of crack size probability distributions, although not usually needed, can be derived by projecting percentiles of the initial crack size distribution.

7.3.3 Random process models

When one or more parameters of deterministic crack propagation equations are modelled as random processes, random process crack propagation models are obtained:

$$\frac{dA}{dn} = X(t) \cdot Q(c, A, \Delta K, \Delta S, M, ...) \tag{7.15}$$

The models briefly described in section 7.2.2 are of this type. Derivation of crack size transition probability densities for some of these models is studied in chapter 9. Solution of the resulting stochastic differential equation (7-8) strongly depends on the nature of the random process $X(t)$. It should be clear that random process $X(t)$ in equation (7-8) represents the non-dimensional unit-mean random crack propagation rate.

A special class of evolutionary models, namely diffusive Markov models, are obtained when the process $X(t)$ is modelled as a white noise process of time. Diffusive Markov models are reviewed in a later section.

7.3.4 Markov chain models

Evolutionary stochastic models of crack propagation may be constructed by assuming (or approximating) the crack propagation process as a Markov chain or, alternatively, as a diffusive Markov process. The major assumption is to consider the crack propagation process to be a memory-less process: the future state of the process depends only on its current state. Such Markovian assumption is not very restrictive, as will be seen in the sequel, and it leads to the use of some results from the theory of Markov Stochastic Processes.

Markov chain models of crack propagation were introduced by Bogdanoff and Kozin (1978) and further developed, in a variety of papers by these and other authors (references in Sobzyck and Spencer, 1992). For this reason, Markov chain models are known also as BK-models. In brief, the damage process (crack size) is considered to be a discrete state and discrete time Markov chain. The initial state of the process is described by the vector $\mathbf{P}_0 = [\pi_1, \pi_2, \pi_3, ..., \pi_n]$, where n is the number of possible initial states and π_i are their individual probabilities, with $\sum_{i=1}^{n} \pi_i = 1$.

The damage evolution is based on duty cycles, which are characteristic periods of operation of the structure. For every duty cycle i, p_i is the probability that the damage remains at the same level, and q_i is the probability that the damage increases to the next level, with $p_i + q_i = 1$. The transition probability matrix is:

$$\mathbf{P}_i = \begin{bmatrix} p_0 & q_0 & 0 & 0 \\ 0 & p_1 & q_1 & 0 \\ 0 & ... & ... & 0 \\ 0 & 0 & p_n & q_n \end{bmatrix} \tag{7.16}$$

Time evolution of the damage is then given by a simple multiplication of matrices. If all duty cycles are of same severity, one has:

$$\mathbf{P}_t = \mathbf{P}_0 \cdot \mathbf{P}_i^t \tag{7.17}$$

Use of the BK model is therefore very easy, once the transition probability matrices are constructed. The difficulty, however, lies exactly in the experimental determination of the component transition probabilities, which requires a prohibitive large database of crack sizes as function of time. The assumption of independence between crack increments is also not always adequate. Attempts to relate BK-models and their parameters to empirical crack growth equations or to other physical aspects of the problem (Gansted et al., 1991 and Bea et al., 1999) have achieved little success. Diffusive Markov processes are more capable, in

this sense, as will be seen in the sequel.

7.3.5 Diffusive Markov models

Overview

Stochastic crack propagation models based on diffusive Markov processes have been extensively developed over the last few years: Lin and Yang (1985), Sobczyk (1986), Tsurui and Ishikawa (1986), Tsurui et al. (1989), Zhu et al. (1992), Farhangdoost and Provan (1996), Zheng and Ellingwood (1998) are just a few examples. The well-established mathematical foundations of Markov Stochastic Processes make them appealing for such application.

Diffusive Markovian processes are governed by the Ito stochastic differential equation:

$$dA = m(A,t)dt + \sigma(A,t)dB(t) \tag{7.18}$$

where $B(t)$ is an unit Brownian motion or Wiener process (whose derivative is a white noise process). The drift coefficient $m(A,t)$ accounts for mean crack growth whereas the diffusion coefficient $\sigma(A,t)$ accounts for variations around the mean. The drift and diffusion coefficients can be derived from (specific) crack growth equations, hence solutions based on fracture mechanics can be derived. Transition probability densities of the crack process, $f_A(a,t)$, are obtained as solution to the Fokker-Planck-Kolmogorov (FPK) equation:

$$\frac{\partial}{\partial t}f_A(a,t) + \frac{\partial}{\partial a}(m(A,t)f_A(a,t)) - \frac{\partial^2}{\partial a^2}(\sigma(A,t)f_A(a,t)) = 0 \tag{7.19}$$

subject to the initial condition:

$$f_A(a,t_0) = \delta(a - a_0) \tag{7.20}$$

which represents a deterministic initial crack size. When the initial crack size is random the theorem of total probability is used to calculate the unconditional crack size distribution:

$$f(a,t) = \int_{-\infty}^{\infty} f(a,t|x,t_0)f_{a_0}(x)dx \tag{7.21}$$

The diffusive Markov process in equation (7.18) is an approximation of the crack propagation process in equation (7-8). Due to its uncorrelated nature, the white noise process $dB(t)$ in (7.18) implies that the transition probability depends only on the current state of the process and not on the past, an assumption not always valid for the crack propagation process. It also implies a small probability of negative crack growth, due to its unrestricted

distribution tail. Both restrictions, however, can be softened, as will be seen in the sequel.

Diffusive models for the crack propagation rate

Lin and Yang (1985) modelled $X(t)$ in equation (7-8) as a random pulse train representing the combined effect of unknown contributions towards changing the crack propagation rate in time. The authors introduced the zero-mean auxiliary process $Y(t)$ such that $X(t) = [\mu_X + Y(t)]$, which minimizes the probability of negative crack growth, given that the deviation of $Y(t)$ is small comparing to μ_X. The generic crack growth function becomes:

$$\frac{dA}{dt} = [\mu_X + Y(t)]Q(A) \tag{7.22}$$

The correlation function of process $Y(t)$ is triangular:

$$\begin{aligned} R_{YY}(\tau) &= 2\beta\left(1 - \frac{|\tau|}{\Delta}\right) \quad \text{if} \quad |\tau| < \Delta \\ &= 0 \qquad\qquad\qquad\quad \text{otherwise} \end{aligned} \tag{7.23}$$

The authors assumed the Markov assumption to remain valid given that "the correlation length of the process (Δ) is short in comparison to the characteristic size of A". A stochastic averaging method is used to calculate the drift and diffusion coefficients. For a generic crack propagation function $Q(A)$, the authors derive:

$$\begin{aligned} m(A,t) &= \mu_X Q(.) + \int_{-\infty}^{0} Q(.)\frac{\partial Q}{\partial A}E[Y(t)Y(t+\tau)]d\tau = Q\left(\mu_X + \frac{\partial Q(.)}{\partial A}\beta\Delta\right) \\ \sigma(A,t) &= 2\int_{-\infty}^{0} Q^2(.)E[Y(t)Y(t+\tau)]d\tau = 2Q^2(.)\beta\Delta \end{aligned} \tag{7.24}$$

Hence, the drift and diffusion coefficients can be evaluated for specific crack propagation equations $Q(A)$ and for a specified correlation lengths of process $Y(t)$. However, introducing the process:

$$Z(t) = \int_{a_0}^{a(t)} \frac{dx}{Q(x)} \tag{7.25}$$

the drift and diffusion coefficients can be made independent of the crack growth function. The crack propagation function (equation 7.22) becomes:

$$dZ(t) = [\mu_X + Y(t)]Q(A)dt \tag{7.26}$$

Applying the stochastic averaging procedure to this equation leads to:

$$\begin{aligned} m(A,t) &= \mu_X \\ \sigma(A,t) &= \sqrt{2\beta\Delta} \end{aligned} \tag{7.27}$$

The FPK equation, in terms of random process Z, becomes:

$$\frac{\partial}{\partial t} f_Z(z,t) + \mu_X \frac{\partial}{\partial z} f_Z(z,t) - \beta\Delta \frac{\partial^2}{\partial z^2} f_Z(z,t) = 0$$

A solution of this equation which satisfies the initial condition $f_Z(z,t_0) = \delta(z-0)$ is:

$$f_Z(z,t|0,t_0) = \frac{1}{\sqrt{2\pi}\sqrt{2\beta\Delta(t-t_0)}} \exp\left[\frac{-\left[z-\mu_X(t-t_0)\right]^2}{4\beta\Delta(t-t_0)}\right] \tag{7.28}$$

Replacing A for Z yields the solution of the original problem, i.e., equation (7.19) with coefficients (7.24):

$$\begin{aligned} f_A(a,t|a_0,t_0) &= \frac{f_Z(Q(a),t|0,t_0)}{Q(a)} \\ &= \frac{1}{\sqrt{2\pi}\sqrt{2\beta\Delta(t-t_0)}Q(a)} \exp\left[\frac{-\left[\int_{a_0}^{a(t)} \frac{dx}{Q(x)} - \mu_X(t-t_0)\right]^2}{4\beta\Delta(t-t_0)}\right] \end{aligned} \tag{7.29}$$

The Markovian process $A(t)$ in this solution is an approximation to the physical crack growth process. The solution allows the crack to grow backwards, i.e., it allows values of A smaller than a_0. This inconsistency error is small as long as the tendency to drift (mean crack growth) dominates the tendency for diffusion (variance of crack growth). For long intervals $(t-t_0)$ this error is negligible, for shorter intervals it can be compensated.

This Markov model was applied (Yang et al., 1987) to cracks originating in fastener holes of aircraft structures and to centre cracked specimens under spectrum loading. Excellent agreement with experimental results is reported by the authors. The correlation parameter Δ was used to calibrate the model to experimental results.

Lin and Yang's (1985) original model has been built upon by a variety of authors. Sobczyk (1986) considered the rigorous case in which $X(t)$ is an uncorrelated white noise process. Despite the limited usefulness of this model, the author discovered additional inconsistencies of the Markov diffusive approximation: for some values of the crack exponent m, the crack can grow to infinity in a finite number of cycles. The problem was attributed to unstable crack propagation at what was called the "explosion time". Tsurui and Ishikawa (1986) introduced

the notion of a death point to deal with the explosion time problem, in the interpretation and solution of the FPK equation. Analytical solutions for the crack size distribution could still be obtained.

Sobczyk and coauthors, as cited in Sobczyk and Spencer (1992), updated the white noise model by introducing an auxiliary random process, a linear filter of the original white noise excitation. By doing this, they eliminated the possibility of negative crack growth and introduced some memory in the crack growth process. The PDF of the resulting two state vector diffusion process was solved through a non-trivial finite difference - finite element scheme, a solution that starts at the known zero boundary condition ($a = a_0$) at t_0, marches back in crack size and forward in time, and is very involved. The authors, however, were able to demonstrate excellent agreement with Virkler's (1979) and Ghonen and Dore's (1987) experimental data.

Zheng and Ellingwood (1998) generalized previous diffusion models by incorporating a time-dependent noise term described by arbitrary marginal distributions and auto-correlation functions. Their model resulted in a four state vector diffusion process, solved through a finite difference scheme. Despite the better modelling capacity, the advantage of a closed form solution is lost in this model as well.

Diffusive models for random loading

Diffusive Markov models that include both random process crack propagation rate and random loading are also available. The generic crack growth equation, in this case, can be written as:

$$\frac{dA}{dt} = X(t)\Delta S(t)^m Q(A) \tag{7.30}$$

The difficulty in the solution of this model lies in evaluation of the drift and diffusion coefficients, as they become functions of the covariance of the crack propagation rate and stress range random processes. A complete second order description of these processes is required, which can be particularly difficult for the stress range process.

Ishikawa et al. (1993a) developed a solution considering $X(t)$ and $\Delta S(t)$ to be uncorrelated, and both with exponential correlation functions. Their model includes the "death point" of Tsurui and Ishikawa (1986) and a correction to account for the fact that $X(t)$ should be a process of crack length rather than time. However, a closed form solution for the crack size distribution is only derived for the case of infinite plate width (unitary geometry function).

A similar model was constructed by Ishikawa et al. (1993b) to study the effect of stress ratios in crack propagation under random loading. This models does not include a random crack propagation rate, but it considers random stress ranges and random stress ratios. A closed form solution is derived for the infinite plate case. The authors conclude the paper attributing a small influence of random stress ratios in random crack propagation.

Zhu et al. (1992) obtained a closed form solution of the crack size distribution for the case of narrow-band load processes, for which stress ranges can be approximated by the envelope of the load process.

Random load effects can also be taken into account indirectly through simulation. Zheng and Ellingwood (1998) used stress range simulation in conjunction with their diffusive crack propagation model to conclude that, for high cycle fatigue, the influence of random loading on random crack propagation is negligible in comparison with the influence of random crack propagation rate.

Diffusive models with load sequence effects

Due to the Markov assumption that crack increments depend only on the actual state of the process, consideration of load sequence effects requires additional state variables to be incorporated in the model. Such state variables incorporate, in the present state of the process, the effects or the memory of past loading history. Such an approach has been developed by Veers (1987) to model crack growth retardation after large tensile overloads. The author introduced the reset stress, a variable that describes the state of residual compression at the crack tip and defines the retarded crack growth rate. This variable and the actual stress were introduced in Sobczyk's (1986) two state Markov model, resulting in a four state vector diffusion process. The model was solved by Monte Carlo simulation, and it was confirmed that load sequence effects are only important in low cycle fatigue.

7.4 Fatigue and fracture reliability models

A review of fatigue and fracture reliability models encountered in the literature reveals that the overwhelming majority of them consider either the problem of crack growth to a critical size or the problem of fracture of a cracked structure under a single (quasi-static) load application (Provan, 1987; Harris, 1987; Sobczyk and Spencer, 1992). Two fundamental failure modes can be used to differentiate these models: critical crack growth and overload failure modes. In the former, fatigue failure is characterized as a leading crack propagating to a critical size. In the later, failure is characterized as the ultimate capacity of a cracked structure

being exceeded, due to a single load application. In both cases, the underlying reliability problem is time-invariant, and can be solved though a range of well-researched techniques such as FORM, SORM and Monte Carlo simulation.

This separation between failure modes is not always possible, e.g. in crack propagation under random loading. Cracks grow due to stress reversals, reducing the capacity of the structure. An overload failure can happen at any time due to a peak of the load process exceeding the instantaneous resistance. If an overload does not happen, a major crack can still grow to a critical size. The coupling between crack propagation and fracture requires a time variant reliability analysis. However, when loading is of constant amplitude, the problems of crack propagation and fracture can be combined and still be solved by means of time-invariant reliability methods.

In the next two sections, time-invariant reliability models addressing critical crack growth and overload failure modes are reviewed. In the following section, existing solutions for crack propagation and fracture under random loading are reviewed.

7.4.1 Critical crack growth failure mode

Evaluation of the probability of failure due to critical crack growth includes basically two approaches. For random variable crack propagation models, the problem can be stated in terms of the time to failure, explicitly in terms of crack sizes or in terms of (any) damage function of crack size. For random process crack propagation models, the solution is based on an integration of the crack distributions over crack size and time.

In the random variable case, an explicit solution can be given in terms of crack size, based on the limit state function:

$$\begin{aligned} g(\mathbf{Z},N) &= A_c - A(N) \\ &= A_c - (\sum_{i=0}^{N} C\,(\Delta K(A_i))^m - A_0) \end{aligned} \tag{7.31}$$

where $\mathbf{Z}$ is the vector formed by all random variables of the crack propagation model, $\mathbf{Z} = \{C, m, A_o, A, A_c, \Delta S, ...\}$, and N is the number of cycles. Because only random variables are involved, the problem can be solved through time-invariant reliability methods such as FORM or SORM.

In terms of the time to failure, still for the random variable case, the limit state function

for an expected design life T is (Madsen et al., 1986; Besterfield et al., 1991; Bea et al., 1999):

$$g(\mathbf{Z},T) = T_f(\mathbf{Z}) - T \tag{7.32}$$

where the time to failure is:

$$T_f(\mathbf{Z}) = \int_{A_o}^{A_c} \frac{da}{C\,(\Delta K)^m} \tag{7.33}$$

A similar solution, still for the random variable case, can be stated in terms of a damage function and a load effect. For a generic crack growth function $da/dn = C(Y(a)\sqrt{\pi a}\Delta S)^m$, a separation of variables leads to:

$$\frac{da}{(Y(a)\sqrt{\pi a})^m} = C\,(\Delta S)^m dn \tag{7.34}$$

A damage function is introduced as (Madsen et al., 1986; Nigam and Narayanan, 1994):

$$\Psi(A) = \int_{A_o}^{A} \frac{da}{(Y(a)\sqrt{\pi a})^m} \tag{7.35}$$

The corresponding load effect, for N cycles, is: $\Psi(A_N) = C\sum_{i=1}^{N}(\Delta S_i)^m$. When the number of cycles N is large, the uncertainty in the sum can be neglected and replaced by its expected value: $\Psi(A_N) = C\,E[(\Delta S)^m]$. For Weibull distributed stress ranges, the load effect becomes:

$$\Psi(A_N) = C\,N\,A^m\,\Gamma\left(1+\frac{m}{B}\right) \tag{7.36}$$

where A and B are the parameters of the Weibull stress range distribution (equation 7.11) and $\Gamma()$ is the Gamma function. The limit state function, in terms of the damage function and the load effect for a critical crack size A_c, becomes (Madsen et al., 1986; Nigam and Narayanan, 1994):

$$\begin{aligned} g(\mathbf{Z}) &= \Psi(A_c) - \Psi(A_N) \\ &= \int_{A_o}^{A_c} \frac{da}{(Y(a)\sqrt{\pi a})^m} - C\,N\,A^m\,\Gamma\left(1+\frac{m}{B}\right) \end{aligned} \tag{7.37}$$

Again, only random variables are involved, and the problem can be solved by FORM, SORM or Monte Carlo simulation.

The choice of a critical crack size is not always straightforward. For some problems, the critical crack size can be related to a serviceability limit state of the structure, such as a through-the-thickness crack in a pressurized container. In other situations, critical crack is chosen as a limiting value, after which crack propagation becomes unstable. In this situation,

unless a very conservative value is chosen, convergence problems may arise in the random variable based solutions due to the high non-linearity of the problem in the critical crack region.

For evolutionary or random process crack propagation models, where the crack size transition probability density function $f_A(a,t)$ is usually known, the critical crack growth probability of failure, at a particular point in time, is obtained by integrating $f_A(a,t)$ over the crack size (Sobczyck and Spencer, 1992):

$$P_{fcr}(t^*) = \int_{a_c}^{\infty} f_A(a,t^*)\ da \tag{7.38}$$

In this expression, $P_{fcr}(t^*)$ is the probability that the crack reaches the critical crack size at time $t = t^*$. Evaluation of the cumulative probability of failure, up to a given time, becomes a first passage problem. A simple integration of (7.38) over time cannot be done because $P_{fcr}(t)$ for different times t is correlated.

In some situations, the first passage problem can be included in the formulation and a solution for the cumulative probability of failure $P_{fcr}(T)$ is obtained directly (Sobczyk and Spencer, 1992). When overload failure is important, such as under highly stochastic loading, it is more appropriate to solve the first passage problem in terms of the loading and the ultimate capacity of the structure. Such solution is more explicit and accommodates both critical crack growth and overload failure modes, as will be seen in the sequel.

7.4.2 Overload fracture failure mode

Fracture under static loading

The probability of fracture of a cracked structure due to a single (quasi-static) but uncertain load application is addressed in some models (Rahman and Kim, 1988; Lee and Ang, 1994). The extreme load and crack size, in this case, are modelled as random variables and there is no crack propagation. The limit state function can be written in terms of the fracture toughness, for brittle fracture, or flow stress for ductile fracture, both of which can be random variables as well:

$$\begin{aligned} g(\mathbf{Z}) &= K_{IC} - K_I(A, S_{\max}, ...) = 0 \\ g(\mathbf{Z}) &= \sigma_y - \sigma(A, S_{\max}, ...) = 0 \end{aligned} \tag{7.39}$$

The problem can also be formulated in terms of elasto-plastic fracture mechanics para-

meters. Again, the problem is completely described by random variables and can be solved by time invariant reliability methods such as FORM or SORM.

Fracture under constant amplitude loading

Under constant amplitude loading, a leading crack grows in time, decreasing the ultimate capacity of the structure. The fracture load is known (it will be a peak of the constant amplitude loading), hence the crack propagation and ultimate capacity problems are independent and the resulting reliability solution is still time-invariant.

Basically, the two failure modes are combined in one limit state function. The probability of fracture in equation (7.39) increases with time as the crack increases. For a given time T, crack size A is calculated from (7.33) (with A_{cr} replaced by A) and substituted into (7.39). Alternatively, the critical crack size can be obtained from (7.39) (with A replaced by A_{cr}) and used in (7.32) to evaluate the failure probability for a given design life T.

The solution is numerical for all but the simplest problems, since the critical crack size cannot be isolated from (7.39), and crack size cannot be isolated from (7.33). However, the problem can, in principle, be solved by FORM or SORM. Not many application examples are available. Harris (1997) derives analytical results for some very simple problems. Madsen et al. (1986) present FORM and SORM solutions for a plate with a centre crack.

7.5 Fatigue and fracture reliability models for random loading

7.5.1 Crack growth and fracture under random loading

Under random loading, cracks grow due to stress reversals, reducing the resistance of the structure. At any instant, a peak of the random load process can exceed the instantaneous capacity of the structure, characterizing an overload type of failure. If an overload does not happen, the crack can still grow to a critical size. Under random loading, the artificial separation between the crack propagation and the ultimate capacity problems is not always possible (Marley and Moan, 1994). The problems of crack propagation and fracture (ultimate resistance) are interconnected (the "synergistic effect" referred to by Wirsching, 1998). This situation has had little attention in the literature, in part because fracture under non-stochastic or mildly stochastic fatigue loading has a low probability of occurrence. However, when fatigue loading is highly stochastic, as can be expected in some applications, the overload probability of failure may not be negligible.

When critical crack size is defined by a serviceability limit state function, the failure

modes (critical crack growth and ultimate fracture) have to be considered individually. When critical crack size is related to the ultimate capacity of the structure, either by being a value that is critical under a typical load action, by limiting unstable crack propagation, or by corresponding to the fracture of a member or component, the two failure modes can be combined. Unstable crack propagation, in this case, corresponds to a certain overload, because the capacity of the structure is reduced almost instantaneously. If the reliability solution for the overload failure probability remains valid under unstable crack propagation, then only the overload limit state function has to be considered.

In the next two sections, existing time variant reliability models for fatigue and fracture under random loading are reviewed. It is shown that existing approaches to the problem are limited to random variable crack propagation models, and limitations of these solutions are observed. In the next chapter, a novel solution based on random process crack propagation models is introduced.

7.5.2 A time-integrated solution for random variable crack propagation models

As seen in the first part of the literature review, the time-integrated approach is a simplification of time-variant reliability problems. It is exact for a single stationary load process, and for a time-invariant barrier. For resistance degradation problems, such as crack propagation, it can only be considered as an approximation, i.e., a constant resistance level has to be assumed. A conservative approximation is to consider the constant resistance level to be equal to the resistance at the end of the life period T (Marley and Moan, 1994). In this case, the limit state function becomes:

$$g(\mathbf{z}) = R(T, \mathbf{z}) - S_T(\mathbf{z}) = 0 \tag{7.40}$$

where $\mathbf{Z}$ is the vector of resistance random variables and $S_T(\mathbf{z})$ is the extreme value of the load process $S(t)$ in the interval $(0, T)$. Equation (7.40) can be solved through any time-invariant reliability technique such as FORM or SORM.

Clearly, the (conservative) approximation made by the authors is that the lifetime maximum load coincides with the lifetime minimum resistance. There are, however, justifications for using T as the resistance linearization point. Following the authors:

" The resistance linearization is selected at $\tau = T$ for convenience and conservatism. There is a time $(0 \leq \tau^* \leq T)$ for which the time integrated approximation $R = R(\tau^*)$ would give

identical results as the up-crossing rate formulation. The linearization at T provides enough accuracy because of three characteristic features of most practical random crack propagation problems:

i) the upcrossing rate is exponentially dependent on level r;

ii) the threshold level $R(t)$ is sensitive to $\mathbf{Z}$;

iii) the uncertainties in $\mathbf{Z}$ are rather large.

For most random processes i) holds. Because fatigue is extremely sensitive to loading, geometry and environment, ii) is generally valid. Finally, the C.O.V. of stress ranges, crack growth parameters and initial crack size are typically large, thus condition iii) is met.

Because of i) the "correct" linearization point is near T. Due to ii) a small change in the design point $\mathbf{z}^*$ leads to a relative large change in $R(t)$, i.e., a change in threshold from $R(T) \rightarrow R(\tau^*)$ is similar to a minor perturbation in $\mathbf{z}^*$ and due to iii) this corresponds to a minor change in $\mathbf{u}^*$ and hence in the reliability index."

Results presented in the study show increased agreement between the time-variant and time-invariant solutions for increasing uncertainties in $\mathbf{Z}$, i.e., for increasing failure probabilities. For the range of failure probabilities expected in engineering problems, errors of up to 30% were obtained.

One refinement of the time-integrated solution is the discretized approach, where the extreme value load distribution is calculated over the duration of a known or random number of discrete events, instead of over the entire lifetime. This approach is quite popular in the aircraft industry. Examples are the codes NERF (Graham and Mallison, 1999) and PROF (Berens, 1996), which are used to calculate single flight probabilities of fracture, given the distributions of crack size, maximum stress per flight, and fracture toughness. The (instantaneous) crack size distribution is obtained by projecting the percentiles of an equivalent initial crack size distribution using a deterministic crack grown equation.

It is clear that the time-integrated solution, as well as the discretized approach, are limited to random variable crack propagation models and scalar load processes.

7.5.3 Fast Probability Integration solution for RV crack propagation models

A less restrictive and more accurate solution for the problem of crack propagation under random loading, which is however also limited to random variable crack propagation models, is Fast Probability Integration.

The random variable crack propagation model implies that a distinct, deterministic crack

propagation time-history is obtained for every outcome of the models random variables. Each crack growth time-history leads to a resistance degradation curve, and conditional failure probabilities are evaluated as:

$$P_f(t|\mathbf{r}) = P_{f_0}(0|\mathbf{r}) + (1 - P_{f_0}(0|\mathbf{r})) \cdot (1 - \exp(-\int_0^t \upsilon^+(\mathbf{r}, s)ds)) \tag{7.41}$$

where $\mathbf{R} = \{C, m, A_o, A_c, \Delta S, ...\}$ is the vector of random crack growth and other resistance parameters. Unconditional failure probabilities are obtained by averaging $P_f(t|\mathbf{r})$ over $\mathbf{R}$:

$$P_f(t) = \int_{\mathbf{R}} P_f(t|\mathbf{r}) f_{\mathbf{R}}(\mathbf{r}) d\mathbf{r} \tag{7.42}$$

The multi-dimensional integration can be approximated by FORM or SORM, using Wen and Chen's (1987) Fast Probability Integration technique. This solution was applied to random crack propagation problems by Kuo (1998) and is also described in Wirsching (1998). Advantages of the solution are:

1. a large number of random variables can be considered, with little additional effort required for each additional random variable;

2. crack growth computations, for each realization of $\mathbf{R}$, are deterministic and can be performed using existing crack growth software;

3. the solution of (7.42) by FORM or SORM can be performed by most existing reliability programs.

However, some drawbacks have to be pointed out:

1. the solution is clearly restricted to random variable crack propagation models;

2. there can be convergence problems due to small conditional failure probabilities in equation 7.41 (Marley and Moan, 1994) and;

3. the solution of (7.42), even by fast computational methods such as FORM, may require an excessive number of deterministic (and possibly numerical) crack growth computations, especially when inspections are considered, as illustrated in the sequel.

Solution of equation (7.42) through FORM, for a single evaluation time, requires $(n_{rv} + 1) \cdot n_{conv}$ crack growth evaluations, where n_{rv} is the number of resistance random variables and n_{conv} is the number of iterations required for convergence of the FORM algorithm. In a

life-time assessment, the solution has to be repeated for every evaluation time t_i. Consideration of non-destructive inspections requires evaluation of intersections of limit state functions (Madsen et al., 1987) and $(1+n_{ins})\cdot(n_{rv}+1)\cdot n_{conv}$ crack growth computations are required for n_{ins} inspections before evaluation time t_i, and results start becoming inaccurate (to be detailed in section 7.6). Improvement of accuracy through SORM or through specific algorithms for intersections of limit states (Melchers and Ahammed, 2001) again increases the required number of crack growth computations. When, as a last resort, Monte Carlo simulation is required (Wirsching, 1998), the number of crack growth computations may again become excessive.

In practical engineering problems, crack growth analysis is sometimes numerical and computationaly intensive. Stress intensity factors are evaluated from numerical (finite element) models, and the progression of the crack requires expensive re-meshing schemes. Hence, solution methods that avoid repetitive "brute force" crack growth computations are of utmost importance.

The excessive number of crack growth computations of both the FPI and the TI solutions is consequence of a random variable approach to the crack propagation problem. In is believed by the author that the random variable approach is an attempt to simplify the problem, which can in some circumstances result in unnecessary repetitive brute-force computations. It will be shown in the chapters that follow that, in some cases, the fatigue and fracture reliability problem can be solved with a single mean crack growth computation, by adopting a random process approach to the solution

The discussion between random variable - random process crack propagation models and the resulting reliability solutions has important implications in the life-time assessment of structures under periodic inspections, as will be seen next.

7.6 Life-time assessment under periodic inspections

In section 7.2.5 it was seen that, following a non-destructive inspection at a time T_1, two results are possible:

$$A(T_1) < A_{d_1} \tag{7.43}$$

$$A(T_1) = A_{m_1} \tag{7.44}$$

In the first case, no cracks are detected, implying that any existing crack is smaller than

the minimal detectable crack size A_{d_1}. In the second case, a crack of length A_{m_1} is detected and measured. Due to the imperfection of non-destructive inspections methods, both A_{d_1} and A_{m_1} are generally random. The way in which these results are taken into account depends directly on the type of random crack propagation model considered.

7.6.1 Life-time assessment for random variable models

For random variable models, the safety or probability of survival can be stated in terms of a safety margin (Madsen et al., 1986):

$$M(\mathbf{Z}) = \int_{A_o}^{A_c} \frac{da}{C\,(\Delta K)^m} - T = 0 \tag{7.45}$$

where the structure fails if the crack grows to a critical size A_c in a time smaller than the design life or expected life T ($M(\mathbf{z}) \leq 0$). The failure probability then is:

$$P_f(T) = P\left[M(\mathbf{Z}) \leq 0\right] \tag{7.46}$$

This probability of failure can be up-dated following the result of a non-destructive inspection. If no crack is found (eq. 7.43), an event margin is written as:

$$M_1^{ND}(\mathbf{Z}) = \int_{A_o}^{A_{d_1}} \frac{da}{C\,(\Delta K)^m} - T_1 > 0 \tag{7.47}$$

This margin is positive due to equation (7.43). The up-dated probability of failure becomes:

$$\begin{aligned} P_f^{UPD}(T) &= P\left[M \leq 0 | M_1^{ND} > 0\right] \\ &= \frac{P\left[M \leq 0 \cap M_1^{ND} > 0\right]}{P\left[M_1^{ND} > 0\right]} \end{aligned} \tag{7.48}$$

Computation of (7.48) now requires the analysis of two systems, one in the numerator and one in the denominator. For a crack detected and measured at the inspection, the event margin becomes:

$$M_1^{DT}(\mathbf{Z}) = \int_{A_o}^{A_{m_i}} \frac{da}{C\,(\Delta K)^m} - T_1 = 0 \tag{7.49}$$

The up-dated probability of failure becomes:

$$
\begin{aligned}
P_f^{UPD}(T) &= P\left[M \leq 0 | M_1^{DT} = 0\right] \\
&= \frac{P\left[M \leq 0 \cap M_1^{DT} = 0\right]}{P\left[M_1^{DT} = 0\right]}
\end{aligned}
\tag{7.50}
$$

Strictly, the probability in the denominator of (7.50) is not defined. The probability in the first line of the equation, however, exists. Again, two systems have to be analyzed. Each system corresponds to one reliability analysis, with the system in the numerators corresponding to two limit state functions.

The consideration of additional inspections at later times requires additional event margins to be defined. For a second inspection resulting in no cracks found, following a first inspection with no cracks found, the event margin is:

$$
M_2^{ND}(\mathbf{Z}) = \int_{A_o}^{A_{d_2}} \frac{da}{C\left(\Delta K\right)^m} - T_2 \geq 0 \tag{7.51}
$$

The failure probability becomes:

$$
\begin{aligned}
P_f^{UPD}(T) &= P\left[M \leq 0 | M_1^{ND} > 0 \cap M_2^{ND} > 0\right] \\
&= \frac{P\left[M \leq 0 \cap M_1^{ND} > 0 \cap M_2^{ND} > 0\right]}{P\left[M_1^{ND} > 0 \cap M_2^{ND} > 0\right]}
\end{aligned}
\tag{7.52}
$$

It can be seen that even the case with two inspections only becomes quite involved. The accuracy of approximate solution methods such as FORM and SORM in evaluating the probabilities in the numerators becomes very low. Specific algorithms for intersections of non-linear limit states can be used to increase the accuracy (Melchers and Ahammed, 2001), but the required number of crack growth computations grows dramatically. More often, Monte Carlo simulation has to be employed (Wirsching, 1998; Engelund et al., 2000). The number of required crack growth computations, in this case, is simply boosted.

When the life-time assessment is done "a priori", each inspection introduces a new branch in the possible event tree. For the case of two inspections, for example, not only one, but four equations like (7.52) have to be solved. A common simplification, suitable for high reliability structures where the development of a major crack is highly unlikely, is to consider the "a priori" outcome of all inspections to be of no-crack-found (Engelund et al., 2000). Still, it can be seen that life-time assessment for random variable models becomes quite complicated, and the number of crack growth computations becomes prohibitive.

7.6.2 Life-time assessment for random process models

Random process crack propagation solutions are based on the time evolution of crack size distributions, which makes consideration of non-destructive inspection considerably easier. The crack size distribution at a given time can be updated directly, based on results of an inspection. For the case of no-crack-found at an inspection at time T_1, for example, one has (Sobczyk and Spencer, 1992):

$$\begin{aligned} f_A^{ND}(a,t)da &= P\left[a \le A(t) \le a + da | A(T_1) < A_{d_1}\right] \\ &= \frac{P\left[a \le A(t) \le a + da \cap A(T_1) < A_{d_1}\right]}{P\left[A(T_1) < A_{d_1}\right]} \end{aligned} \tag{7.53}$$

The probability in the denominator is nothing more than the probability of not detecting a crack in this first inspection, and it is given as:

$$\begin{aligned} P^{ND}(T_1) &= P\left[A(T_1) < A_{d_1}\right] \\ &= \int_0^\infty \left\{1 - F_{A_{d_1}}(x)\right\} f_A(x,T_1)dx \end{aligned} \tag{7.54}$$

where $F_{A_{d_1}}(x)$ is the POD curve for the considered inspection method and $f_A(x,T_1)$ is the original (prior to inspection) expected crack size distribution at time T_1. The numerator of equation (7.53), considering A_{d_1} to be independent of $A(T_1)$, can be shown to be (Sobczyk and Spencer, 1992):

$$f_A^{ND}(a,t) = \frac{1}{P^{ND}(T_1)} \int_0^\infty f_A(a,t|x,T_1) \left\{1 - F_{A_{d_1}}(x)\right\} f_A(x,T_1)dx, \quad t > T_1 \tag{7.55}$$

where $f_A(a,t|x,T_1)$ is the crack size distribution conditional to a particular size x at the time of inspection. Similarly, for the case of a crack detected and measured during an inspection, one obtains:

$$f_A^{DT}(a,t) = \frac{1}{P^{DT}(T_1)} \int_0^\infty f_A(a,t|x,T_1) f_{A_{m_1}}(x) f_A(x,T_1)dx, \quad t > T_1 \tag{7.56}$$

where

$$\begin{aligned} P^{DT}(T_1) &= P\left[A(T_1) = A_{m_1}\right] \\ &= \int_0^\infty f_{A_{m_1}}(x) f_A(x,T_1)dx \end{aligned} \tag{7.57}$$

is the probability of detecting a crack of size A_{m_1}. For multiple inspections, the above formulas become recursive, and it suffices to replace index $_1$ by $_2$. The distribution $f_A(x,T_2)$,

in the case of a second inspection, is simply given by the result of the previous inspection (equations 7.55 or 7.56).

Hence, the systems solutions of the random variable case are replaced by unidimensional numerical integrations in the random process case. The analysis of systems with multiple limit state functions is completely avoided. Moreover, the random process solution provides the expected probabilities of detecting - not detecting a crack at a given time. This information is very important in an "a priori" determination of the inspection times and in the "a priori" simplification of the event tree.

7.6.3 Complex structural systems

In order to understand the full dimension of results in the two previous sections, it is convenient to draw a picture of what life-time assessment of a complex structural system is, or what it can be. In a more basic level, life-time assessment can be just the evaluation of the safety of a structure, subject to fatigue, at several points in time. At a greater level of complexity, life-time assessment involves the optimization of inspection strategies and intervals, for a fleet of structures, such as to minimize total expected costs (Moan et al., 1994; Faber et al., 1996; Engelund et al., 2000 and Ayala-Uraga and Moan, 2002). Non-destructive periodic inspections and repairs of complex structures like aircraft, bridges and off-shore platforms often involves considerable amount of resources. Total expected costs can involve an initial cost (production of the structure), an operational cost (governed by the cost of inspections and repairs) and an expected cost of failure (proportional to the failure probability). Also, more often than not, the comprehensive analysis of a complex structure includes multiple critical locations and multiple failure paths. As long as the overall response of the structure is not affected by crack growth (problem of stiffness degradation), crack growth in a structural detail is a local problem. It only depends on local stress ranges, initial crack size, crack propagation rate and geometry of the particular structural detail. This localized characteristic of crack growth can be very important in simplifying or scaling the solution of complex systems. In view of this broader problem, it can be seen that RV solutions do not take advantage of the local aspect of crack propagation, with "local" random crack growth parameters being present throughout the systems analysis and the inspection optimization. In Engelund et al. (2000), for example, inspection intervals are optimized with respect to local crack growth parameters, like C, A_0 and ΔS. In random process crack propagation solutions, inspection intervals can, in principle and for scaling purposes, be optimized with respect to (random) crack size in critical locations. Local random crack growth parameters are replaced by the

crack size distribution for each structural detail, and the systems analysis is carried out based on those crack size random variables.

To illustrate the argument, consider a complex structure formed by multiple welded members. A dynamic analysis of the whole structure, considering the random environmental loads, provides the local stress time-histories in the critical locations. The growth of a crack in the weld-foot of a particular joint is a local problem, affected only by the initial crack size, the crack propagation rate, the geometry of the particular joint and the local stress ranges. The local random process crack propagation problem can be solved, providing a description of the crack size TPD for that critical location. This crack size distribution, together with the crack size distributions at the other critical locations, can then be used to evaluate the probability of failure (fracture) of that member, as well as the probability of collapse of the whole structure (multiple member failure). If significant load redistribution occurs when one member fails, the global dynamic and the local crack growth analysis may have to be repeated, but crack propagation in a particular detail is still a local problem.

7.7 Discussion

It was seen in this literature review that the majority of existing fatigue and fracture reliability models address either critical crack growth or overload failure, and that under random loading this separation is not possible. The available solutions to combine both failure modes in a way suitable for reliability analysis under random loading are restricted to random variable crack propagation models. On the other hand, it was seen that failure probability analysis of random process crack propagation models requires solution of a first passage problem, even when only critical crack growth is considered. It was suggested that, when loading is highly stochastic and the overload failure mode becomes important, it is more interesting to solve the first passage failure problem explicitly in terms of loads and the strength of the structure. In this way, the failure probability analysis for random process crack propagation models incorporates both overload and critical crack growth failure modes. To the authors knowledge, no such solution exists. In the next chapter, a random process (and EUR approximation) based solution for the fatigue and fracture reliability problem is proposed.

Random variable crack propagation models may require an excessive number of deterministic crack growth computations, especially when life-time assessment under periodic inspections and repairs is considered. When the geometry of the problem is simple such that analytical expressions for geometry functions and crack growth equations can be derived, a "brute force" solution through Monte Carlo simulation can still be considered. When the

underlying crack propagation model is numerical, however, the random variable approach becomes prohibitive. A random process solution becomes advantageous in this case as, it will be seen in the chapters that follow, it can be derived from a single mean crack growth computation.

Of course, the actual physical crack growth process should define whether the crack propagation rate should be modelled as a random variable or random process. It seems likely, however, that in many cases other than the one presented earlier (Yang et al., 1987; section 7.2.2), the crack propagation rate is modelled as a random variable in a conservative attempt to simplify the resulting crack propagation model. This simplification, it is suggested, results in a perhaps unnecessarily large number of crack growth computations, and may be trading off the possibility of a very efficient random process solution. Even when crack propagation is modeled in terms of random variables, a random process approach to the problem is still possible, since the crack size distribution at any time can be calculated by projecting percentiles of the initial crack size distribution.

7.8 Figures

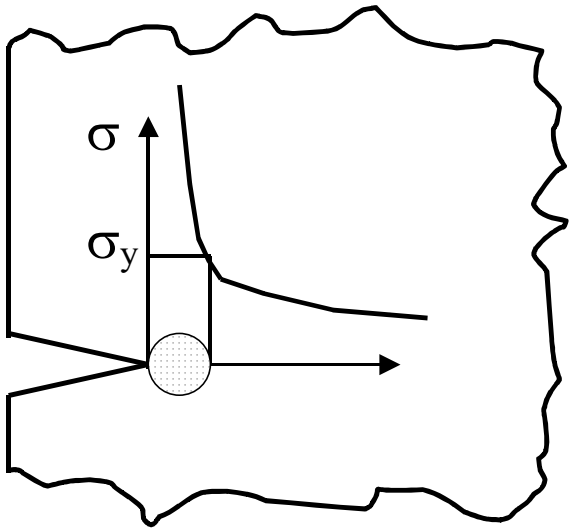

Figure 7-1: Plasticity ahead of the crack tip.

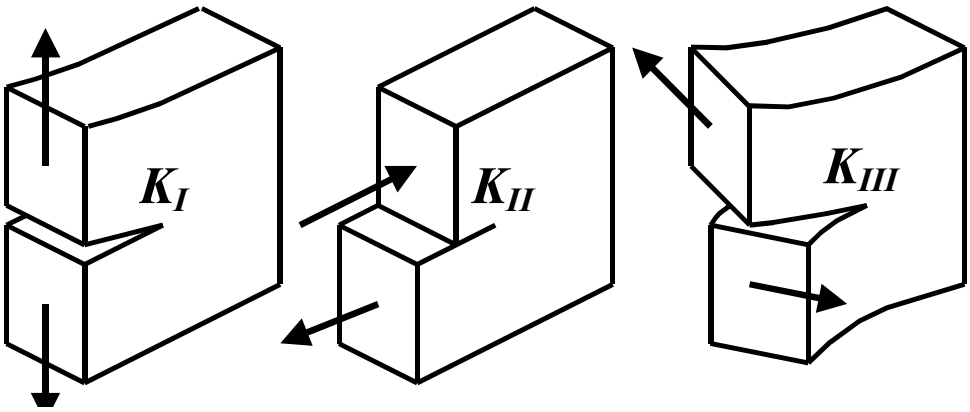

Figure 7-2: Crack loading modes

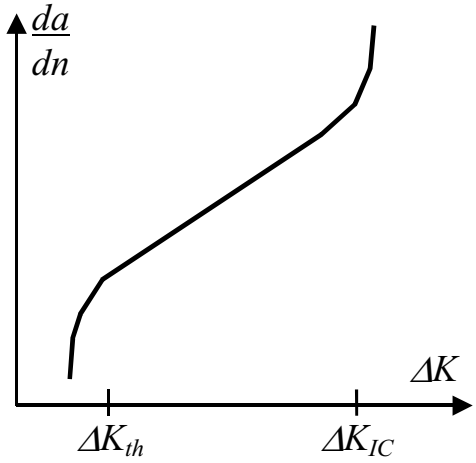

Figure 7-3: Crack propagation rate.

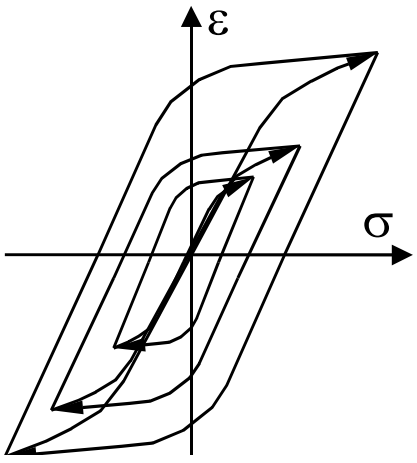

Figure 7-4: Hysteresis loops corresponding to stress cycles.

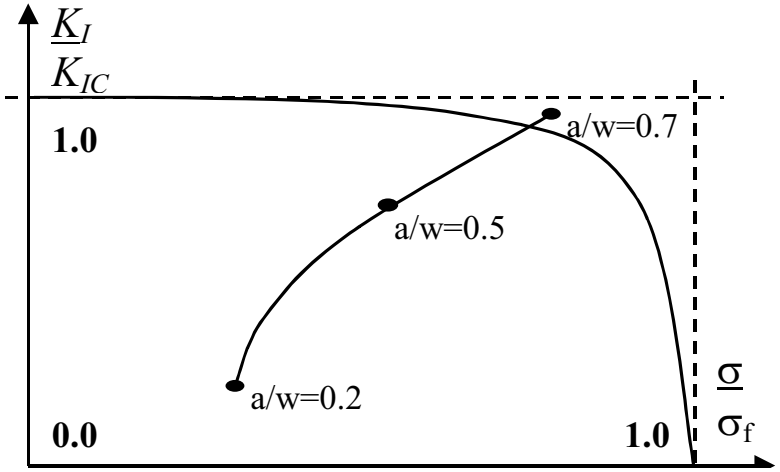

Figure 7-5: R6 failure assessment diagram.

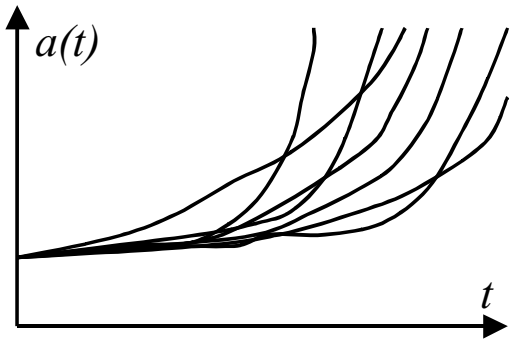

Figure 7-6: Scatter in large replicate constant amplitude crack growth experiments.

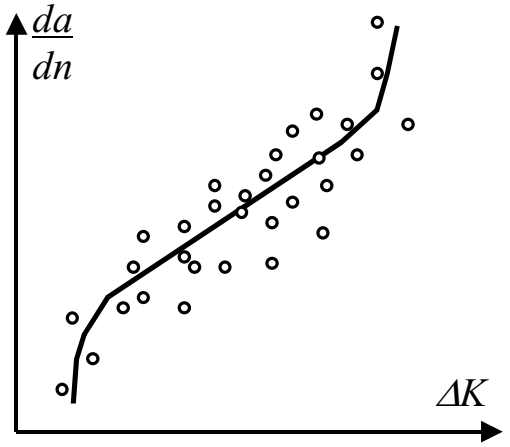

Figure 7-7: Scatter in the crack propagation rate.

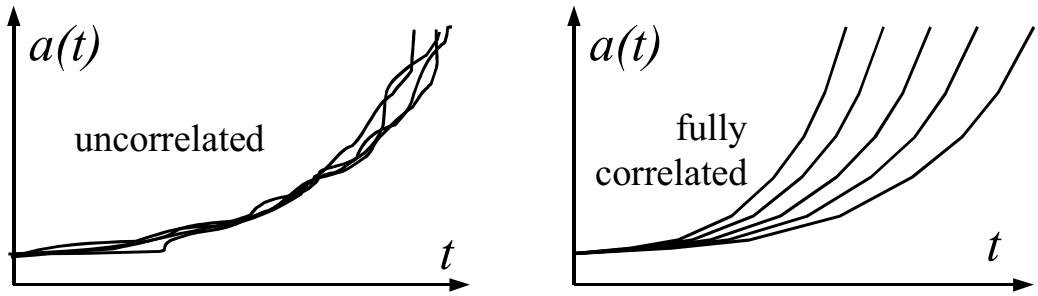

Figure 7-8: Time-histories for uncorrelated and fully correlated crack propagation rate.

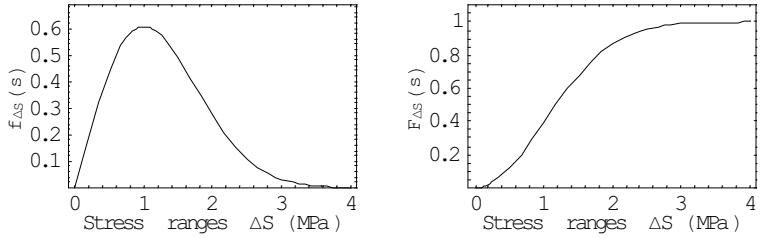

Figure 7-9: Distributions of stress ranges of narrow-banded process $N(0,1)$.

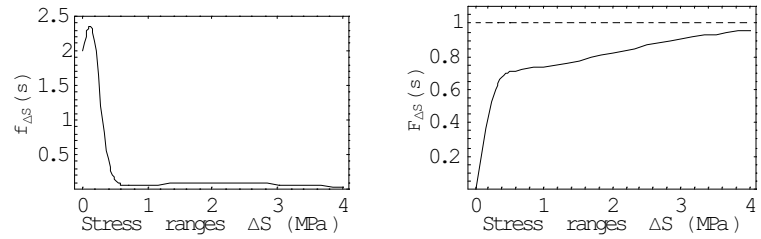

Figure 7-10: Distributions of stress ranges of broad-banded process, $N(0,1)$ and $\alpha = 0.4$.

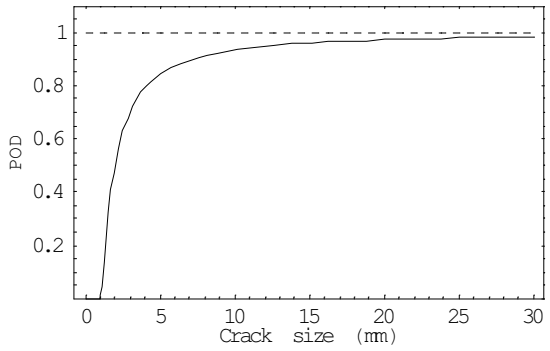

Figure 7-11: Probability of detection of an inspection method.

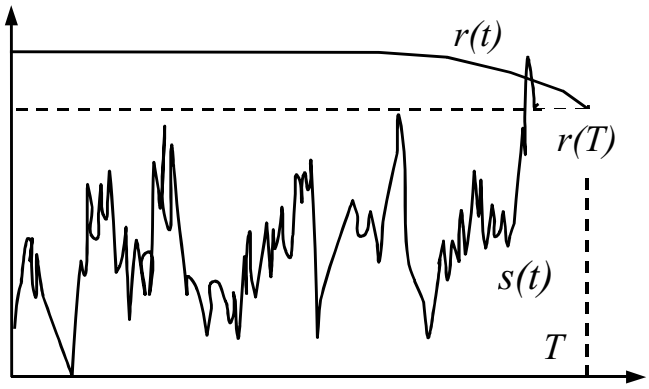

Figure 7-12: Time Integrated approximation.

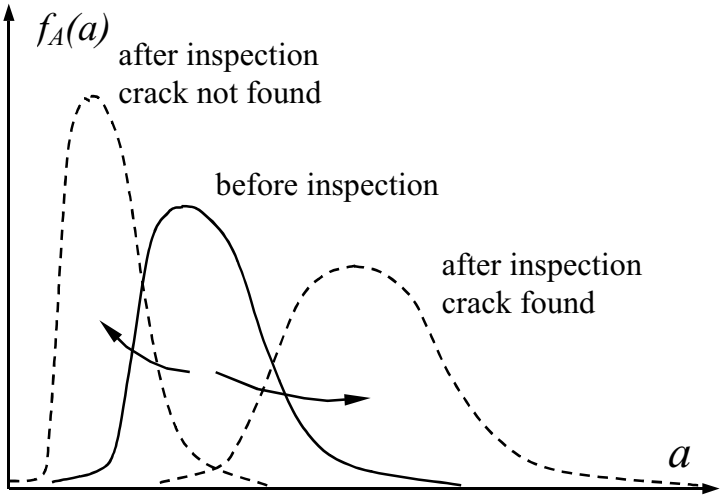

Figure 7-13: Effect of non-destructive inspection in crack size distribution.

Chapter 8

A RANDOM PROCESS BASED SOLUTION FOR THE FATIGUE AND FRACTURE RELIABILITY PROBLEM

In this chapter, a random process based solution for the fatigue and fracture reliability problem under random loading is introduced. This solution is constructed by combining a random process model of crack propagation with the first passage failure model. It addresses both critical crack growth and overload failure modes, and simplifies significantly life-time assessment in the presence of non-destructive inspections.

Crack size transition probability densities (TPD), or the time evolution of crack size distributions, are obtained as the solution to a stochastic crack propagation problem, as will be explored in detail in chapter 9. It will be seen that, for some problems, the crack size distributions can be obtained from a single mean crack growth computation, making this solution very efficient to compute.

The evolution in time of resistance distributions, in terms of an appropriate failure criterion (elasto, plastic or elasto-plastic failure) is derived from the distributions of crack size and other random resistance variables, as will be addressed in chapter 10. This requires a sequence of static (possibly stochastic finite element) analysis for the resistance at various times.

Once crack size and resistance distributions are obtained, solution for failure probabilities is straightforward. The rate at which the load process up-crosses a given resistance level r is

integrated over the resistance distribution, yielding an ensemble up-crossing rate:

$$\upsilon^{+}_{ED}(R,t) = \int_{R(t)} \upsilon^{+}(r,t) f_R(r,t) dr \tag{8.1}$$

The ensemble up-crossing rate is then used to evaluate failure probabilities at any point in time:

$$P_f(t) = P_{f_0}(R) + (1 - P_{f_0}(R)) \cdot (1 - \exp(-\int_0^t \upsilon^{+}_{ED}(R,s) ds)) \tag{8.2}$$

Advantages of the random process - EUR solution, in comparison to a random variable - FPI (or TI) solution, are:

1. life-time assessment, for distinct times, is readily available;
2. no convergence problems;
3. better representation of the crack propagation process, through the use of random process crack propagation models;
4. solution for crack size distributions can be obtained with as little as one mean crack growth computation;
5. solution for resistance distributions can be obtained from a sequence of static (stochastic finite element) analysis;
6. avoids excessive "brute-force" crack growth computations;
7. it can easily accommodate non-destructive inspections, since crack size probability distributions can be up-dated after each inspection (Sobczyk and Spencer, 1992; section 7.6) and;
8. it permits a proper scaling of the solution of complex structural systems.

Some of these statements are illustrated in the following chapters. Disadvantages of the random process - EUR solution are:

1. it is approximated, with the error depending on the relative magnitude between variance of the load process and variance of the resistance;
2. it can only handle a limited number of crack growth random variables, as will be seen in chapter 9 and;

3. solution is more elaborate to derive, requiring evaluation of time evolution of crack size distributions.

The solution clearly suits random process crack propagation models, for which crack size distributions are normally derived, but it is certainly not limited to them. As long as the evolution of crack size distribution can be derived, the random process - EUR solution applies equally well to random variable crack propagation models. One interesting point to consider is what the correlation length of the resulting crack propagation process can be expected to be. It was seen in chapter 6 that the EUR approximation can be fairly crude when the correlation length of the barrier is long (random variable case) and that the error is much smaller when the correlation length of the barrier becomes shorter and approaches the correlation length of the load process.

The correlation length of the resulting crack process, λ_A, clearly depends on the correlation length of the underlying crack propagation rate process, λ_X. Because crack growth is a cumulative process, λ_A can be expected to be significantly larger than λ_X. Random stress ranges can be expected to reduce λ_A, when, in the solution, stress ranges are simulated as uncorrelated processes . In a random variable solution, random stress ranges will increase λ_A. Random initial crack size leads to a fully correlated crack growth process, hence λ_A is increased. When all variables are put together, the correlation length of the resulting crack process will most likely be between the fully correlated and the uncorrelated cases. This issue is addressed in chapter 11, in connection with the analysis of typical random crack propagation problems.

The random process - EUR solution described above must not necessarily be based on an explicit integration of up-crossing rates over the random resistance distribution. As noted in the first part of the literature review, ensemble up-crossing rates can be obtained directly from a numerical up- or out-crossing rate solution with a random failure domain boundary. This is actually a very interesting alternative, as it avoids the necessity of deriving resistance distributions and allows a significant reduction in computation time. Ensemble up-crossing rates can be calculated directly, for example, by means of the parallel system sensitivity solution described in the first part of the literature review.

In the chapters that follow, evaluation of crack size distributions, resistance distributions and failure probabilities are addressed. Throughout these chapters, a typical random crack propagation problem is solved, for illustration purposes. In the next section, data for this problem is described.

8.1 Description of a NB reference problem

The problem analyzed throughout the following chapters consists of a centre cracked panel subject to random loading. The initial crack size, crack propagation rate, stress ranges, yielding stress and critical stress intensity factor are considered as random variables in the problem. In order to obtain consistency between the various problem parameters, data for the problem is based largely on the large replicate tests of Virklers (1979), which consisted of 64 centre cracked specimens of 2024-T3 aluminum subject to a constant amplitude cyclic loading. Deterministic parameters and material properties are presented in table 8.1.

The constant amplitude loading of Virkler's experiments had a stress amplitude of 50 MPa and stress ratio R = 0.2. In the present problem, this constant amplitude loading is replaced by a Gaussian random load process with parameters $S(t) = N(\mu_S, \sigma_S) = N(80, 18)$ MPa. The load process is typically narrow-banded (NB), with an uniform Power Spectrum Density between $(2\pi - 1, 2\pi + 1)$ radians. The design life for the reference problem is $T = 10^6$ cycles. This design life and load process certainly do not resemble Virklers experiment, but they are used in order to obtain a high cycle fatigue problem.

Typical values for the random variable parameters are considered, as indicated in table 8.2. Stress ranges of the narrow-band load process follow a Rayleigh distribution with parameter σ_S. Stress ranges are not considered explicitly as random variables, rather their distribution function is used to simulate stress range outcomes for the crack growth computations. Probability distribution functions for the random variables of the reference problem are illustrated in figure 8-1.

Random variables of the problem are grouped in a vector $\mathbf{Z} = \{S_T, A_o, X, S_y, K_{IC}\}$. A mean vector $\mu_{\mathbf{z}}$ and a standard deviation vector $\sigma_{\mathbf{z}}$ are formed by grouping these parameters accordingly. A lower case $\mathbf{z}$ indicates a particular outcome of $\mathbf{Z}$ and $f_{\mathbf{Z}}(\mathbf{z})$ is the joint probability distribution function of $\mathbf{Z}$. In some instances, a 3-sigma rule is used to obtain an (low-probability) outcome of the problems random variables: $\mathbf{z} = \mu_{\mathbf{z}} + 3\sigma_{\mathbf{z}}$. Although the rule is indicated with a positive sign, the outcome of random resistance variables is negative with the rule (eg. $s_y = \mu_{S_y} - 3\sigma_{S_y}$).

Although most of the solutions in the following chapters are derived for generic crack growth functions, at some stage these solutions are particularized. The Paris crack growth equation is considered in this case:

$$\frac{dA}{dn} = X\ c\ (\Delta K(A))^m \tag{8.3}$$

Table 8.1: Deterministic parameters of the problem.

Parameter	Symbol	Value	Unit
Thickness	b	2.54	mm
Width	w	152.40	mm
Critical crack size	a_c	65.00	mm
Crack exponent	m	3.00	-
Crack grown rate	c	10^{-12}	mm/cycle
Stress intensity factor	$\Delta K(a)$	$\Delta S\sqrt{\pi a}Y(a)$	MPa$\sqrt{\text{mm}}$
Geometry function	$Y(a)$	$\sqrt{\sec(\frac{\pi a}{w})}$	-

Parameters of the equation are as indicated in Table 8.1. This equation is equivalent to the hyperbolic sine function in the mid-ΔK range:

$$\frac{dA}{dn} = X\ 25.4\ 10^{(C1\sinh[C2(\log_{10}[\frac{\Delta K}{35.0}]+C3)]+C4);} \tag{8.4}$$

which was fitted to Virklers data by Yang et al.. (1987) using the parameters $C_1 = 0.5$; $C_2 = 3.4477$; $C_3 = -1.3902$ and $C_4 = -4.5348$ (adapted to SI units). This particular crack growth equations do not include stress ratio effects, but it shouldn't be difficult to generalize solutions in order to include stress range effects (Dover and Hibbert, 1977).

Design life for the reference problem is $T = 10^6$ cycles (which could be hours, minutes or seconds). In order to perform the crack growth evaluations, the total number of cycles is divided in 10 load blocks. Time-variant quantities of interest (such as crack size distributions and failure probabilities) are evaluated at the end of each load block. With a total of 10^6 cycles, each load block should, in principle, be formed by 10^5 stress cycles. It turns out that the cycle-by-cycle crack growth computations (in equation 8.3) can be avoided, and the computation time significantly reduced, by considering 100 stress cycles per load block. The crack propagation rate is adjusted accordingly, and becomes: $c' = c\,10^3$ mm per thousand cycles. Hence, each load block consists of a different set of 100 simulated stress range values.

The data presented in this section forms what is called herein the NB reference problem, which leads a NB reference solution. Whenever deemed necessary or appropriate, in order to study specific aspects of the problem or of the solutions, individual parameters of the problem are changed. When this happens, parameters that are changed are indicated, other parameters remaining as for the reference problem.

Table 8.2: Description of the problems random variables.

Random Variable	Symbol	Distribution	Mean	C.O.V.	Unit
Initial crack size	A_o	log-normal	9.0	0.20	mm
Crack propagation rate	X	log-normal	1.0	0.20	-
Stress ranges	ΔS	Rayleigh	22*	0.52*	MPa
Extreme value of $S(t)$	S_T	extreme	176**	0.024**	MPa
Yielding Stress	S_y	log-normal	240	0.05	MPa
Critical SIF	K_{IC}	log-normal	2000	0.05	MPa$\sqrt{\text{mm}}$

*following load process. **for 10^6 load cycles.

8.2 Concluding remarks

The random process - ensemble up-crossing rate solution for fatigue and fracture reliability analysis under random loading, introduced in this and further developed in the following chapters, is a contribution of this thesis. It jointly accounts for critical crack growth and overload failure modes. It accounts for the random effects of crack propagation and random loading and leads to a computationally efficient solution, which can be applied to analytical as well as numerical problems, as will be seen in the sequel.

8.3 Figures

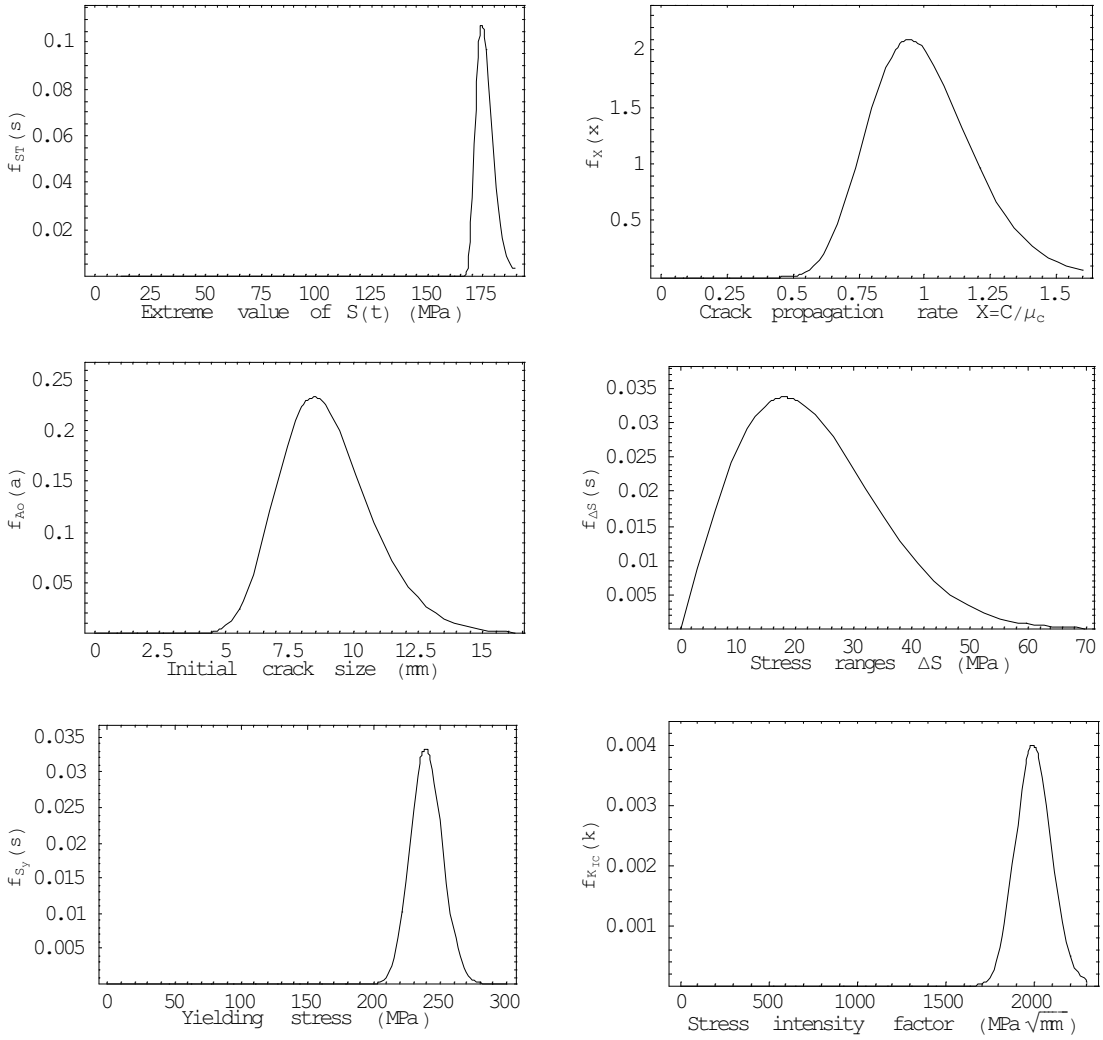

Figure 8-1: Probability density functions of random variables of the NB reference problem.

Chapter 9

EVALUATION OF CRACK SIZE TRANSITION PROBABILITY DENSITIES

When crack growth parameters are modelled as random variables or random processes, crack size becomes a random process of time. The crack size probability density function changes in time, as cracks are loaded and grow. The mean of the crack size distribution increases, due to mean crack growth. The standard deviation generally increases as well, due to random factors affecting crack growth, and causes a widening of the distributions tails.

Evaluation of crack size transition probability densities (TPDs) depends, to some extent, on the underlying stochastic crack propagation model. Analytical expressions can be obtained for random process models including random crack propagation rate and random stress ranges. Numerical integration can then be used to include random initial crack sizes. More complex random process models, especially multi-state vector models, require completely numerical solutions for crack size TPDs, generally a combination of finite element and finite difference solutions.

In this chapter, distinct solution methods for evaluation of crack size TPDs are compared. In section 9.1, random variable based solutions are studied. In section 9.2, solutions for three distinct random process models are addressed. Section 9.3 addresses Monte Carlo simulation, which can be used for both RV and RP models. A numerical comparison of distinct solution methods is presented in section 9.5, in an application to a typical problem.

Solutions studied in this chapter are not novel, but important aspects of their derivation are pointed out. Also, such a comparative study between distinct solution methods has not been found elsewhere.

9.1 Random variable based solutions

9.1.1 Convolution Integration

When the random crack propagation model includes only a few random variables, a convolution integral can be used to evaluate the crack size TPD after a load block. When initial crack size A_0 and crack propagation rate C are random variables, for example, the crack increment for one load block is a random variable too:

$$\Delta A_1 = C \cdot \sum_{i=1}^{n_{sr}} (\Delta S_i \sqrt{\pi A_0} Y(A_0))^m \tag{9.1}$$

where n_{sr} is the number of stress ranges in the load block. To facilitate the analysis, instead of modelling the crack propagation rate C directly as a random variable, a random variable X is considered, such that $C = cX$. In practical terms, X stands as a non-dimensional unit mean crack propagation rate. A mean crack increment function is introduced:

$$A_{inc}(a, \Delta t) = \sum_{i=1}^{n_{sr}} c(\Delta S_i \sqrt{\pi a} Y(a))^m \tag{9.2}$$

where Δt is the duration of one load block. Function $A_{inc}(a, \Delta t)$ gives the mean crack increment in one load block for an initial crack size a. The crack increment after the first load block becomes:

$$\Delta A_1 = X \cdot A_{inc}(a, \Delta t) \tag{9.3}$$

The PDF of crack increment ΔA_1 can be related to that of X for one particular outcome of A_0 :

$$f_{\Delta A_1}(\Delta a \mid a_0) = \frac{f_X\left(\frac{\Delta a}{A_{inc}(a_0, \Delta t)}\right)}{A_{inc}(a_0, \Delta t)} \tag{9.4}$$

Assuming A_0 and ΔA_1 to be independent, their joint PDF becomes:

$$f_{\Delta A_1, A_0}(\Delta a, a_0) = f_{\Delta A_1}(\Delta a \mid a_0) \cdot f_{A_0}(a_0) \tag{9.5}$$

Since A_1 is the sum of A_0 and ΔA_1, its PDF can be obtained from a convolution integral

(Sobczyk and Trebicki, 2000):

$$\begin{aligned} f_{A_1}(a) &= \int_{-\infty}^{+\infty} f_{\Delta A_1, A_0}(a-z, z)dz \\ &= \int_{-\infty}^{+\infty} f_{\Delta A_1}(a-z \mid z) \cdot f_{A_0}(z)dz \\ &= \int_{-\infty}^{+\infty} \frac{f_X\left(\frac{a-z|z}{A_{inc}(z,\Delta t)}\right)}{A_{inc}(z,\Delta t)} \cdot f_{A_0}(z)dz \end{aligned} \tag{9.6}$$

By changing A_1 for A_2 and A_0 for A_1 in the formulation above, and so on, crack size TPD for successive load blocks is obtained. However, since the whole solution is based on integrations over the previous crack size distribution (variable z in equation 9.6), it is necessary to fit an appropriate analytical PDF to a few points calculated from equation (9.6). The function $A_{inc}(z, \Delta t)$, which gives the mean crack increment for one load block, can be derived from one single crack growth computation, which starts at the smallest possible crack size (say, $a_1 = \max[\mu_{a_o} - 4\,\sigma_{a_o}, a_{th}]$), and goes on, cycle by cycle, until the critical crack size is reached:

$$a_{i+1} = a_i + c(\Delta s_i \sqrt{\pi a_i} Y(a_i))^m \tag{9.7}$$

This computation yields a sequence of points of n (cycle number) versus crack size or time versus crack size. A mean crack size function $A_\mu(t)$ is interpolated to these points, so that intermediate values can also be obtained. The inverse of $A_\mu(t)$, the mean time to grow function $T_\mu(a)$, is simply obtained by interpolating the crack size versus time data. For every value assumed by z in the integration of equation (9.6), the mean crack increment for one load block is simply calculated as:

$$A_{inc}(z, \Delta t) = A_\mu(T_\mu(z) + \Delta t) \tag{9.8}$$

where Δt is the duration of the load block. Although the mean crack growth computation is interrupted at the critical crack size, the tail of the crack size distribution (equation 9.6) can still spread behind the critical crack size after some crack growth.

The division in load blocks obviously speeds computations, as less numerical integrations are required. Every load block is formed by a sequence of load cycles. For constant amplitude loading the solution is straightforward, as the computation of (9.7) is based on a single stress range value. When the loading is random, two possibilities exist: 1) include the PDF of stress ranges in the solution through an additional (nested) numerical integration; 2) form load blocks by simulating stress range samples and use simulated load blocks to evaluate

equation (9.7). Simulation of stress ranges is a shortcut, which avoids the nested numerical integration and accounts for the mean effect of random stress ranges, but neglects the influence of random stress ranges in the variance of the crack growth process. Before analyzing the implications of simulating stress ranges, the formal random variable solution is presented.

When initial crack size A_0, crack propagation rate X and stress ranges ΔS are random variables, the PDF of the crack increment after one load block, conditional to one particular outcome of A_0 and ΔS, becomes:

$$f_{\Delta A_1}(da \mid a_0, \Delta s) = \frac{f_X\left(\frac{\Delta a}{A_{inc}(a_0, \Delta s, \Delta t)}\right)}{A_{inc}(a_0, \Delta s, \Delta t)} \tag{9.9}$$

Assuming $A_0, \Delta S$ and ΔA_1 to be independent, their joint PDF becomes:

$$f_{\Delta A_1, A_0, \Delta S}(\Delta a, a_0, \Delta s) = f_{\Delta A_1}(\Delta a \mid a_0, \Delta s) \cdot f_{A_0}(a_0) \cdot f_{\Delta S}(\Delta s) \tag{9.10}$$

An additional numerical integration is hence necessary to account for random stress ranges:

$$f_{\Delta A_1, A_0}(\Delta a, a_0) = \int_{-\infty}^{+\infty} \left[f_{\Delta A_1}(\Delta a \mid a_0, y) \cdot f_{A_0}(a_0) \cdot f_{\Delta S}(y)\right] dy \tag{9.11}$$

The final convolution integral results:

$$f_{A_1}(a) = \int_{-\infty}^{+\infty} \int_{-\infty}^{+\infty} \frac{f_X\left(\frac{a-z|z}{A_{inc}(z,y,\Delta t)}\right)}{A_{inc}(z, y, \Delta t)} \cdot f_{A_0}(z) \cdot f_{\Delta S}(y) dy dz \tag{9.12}$$

Because the two numerical integrations in equation (9.12) are nested, the computation time increases drastically. To avoid the nested integration and still include random stress ranges in the analysis, simulation of stress ranges in the load block is proposed. This procedure is supposed to be equivalent to one commonly adopted in analytical solutions where the random stress ranges are replaced by their expected value (Madsen et al., 1986; Nigam and Narayanan, 1994):

$$\sum_{i=1}^{n_{sr}} (\Delta S_i)^m \simeq E[(\Delta S_i)^m] \tag{9.13}$$

It takes into consideration the mean effect of random stress ranges but neglects the influence of random stress ranges in the variance of the crack size distribution. For high cycle fatigue the approximation is assumed to be appropriate (Ishikawa et al., 1993; Zheng and Ellingwood, 1998; Wang, 1999).

The principal approximation involved in the convolution solution is the assumption that

crack increments ΔA_i be independent of crack size A_{i-1}. The implications of this approximation are studied in section 9.5 in connection with an example problem.

9.1.2 Series expansion and second order - second moment approximation

For a crack propagation model with random initial crack size A_0, random crack propagation rate C and random stress ranges ΔS, random crack size A_n can be written as (ASCE, 1982):

$$\begin{aligned} A_n(\mathbf{X}) &= A_0 + \sum_{i=1}^{n} C \cdot (\Delta K_i)^m \\ &= A_0 + \sum_{i=1}^{n} C \cdot (\Delta S_i \sqrt{\pi A_{i-1}} Y(A_{i-1}))^m \\ &= A_0 + \sum_{i=1}^{n} X_2 \cdot (X_3 \sqrt{\pi X_1} Y(X_1))^m \end{aligned} \tag{9.14}$$

where $\mathbf{X} = \{X_1, X_2, X_3\} = \{A_{n-1}, C, \Delta S\}$ is the vector of random variables.

A second moment approximation to the crack TPD is obtained by perturbing equation (9.14), expanding it in a series and truncating the expansion (Bea et al., 1999):

$$\begin{aligned} A_n(\mathbf{x}) \simeq\ & A_n(\overline{\mathbf{x}}) + \sum_{i=1}^{n} \sum_{j=1}^{3} \frac{\partial A_i}{\partial X_j} (X_j - \overline{X}_j) \\ & + \frac{1}{2!} \sum_{i=1}^{n} \sum_{j=1}^{3} \sum_{k=1}^{3} \frac{\partial^2 A_i}{\partial X_j \partial X_k} (X_j - \overline{X}_j)(X_k - \overline{X}_k) + ... \end{aligned} \tag{9.15}$$

where a bar represents the mean value. Taking the expectation of the truncated expansion, the second term vanishes and one obtains:

$$E[A_n] \simeq A_n(\overline{\mathbf{x}}) + \frac{1}{2!} \sum_{i=1}^{n} \sum_{j=1}^{3} \sum_{k=1}^{3} \frac{\partial^2 A_i}{\partial X_j \partial X_k} E[(X_j - \overline{X}_j)(X_k - \overline{X}_k)] \tag{9.16}$$

and because the three random variables are independent this reduces to:

$$E[A_n] \simeq A_n(\overline{\mathbf{x}}) + \frac{1}{2!} \sum_{i=1}^{n} \sum_{j=1}^{3} \frac{\partial^2 A_i}{\partial X_j^2} var[X_j] \tag{9.17}$$

or:

$$\begin{aligned} E[A_n] \simeq\ & \overline{A}_n = \overline{A}_0 + \sum_{i=1}^{n} \overline{C} \cdot (\overline{\Delta S} \sqrt{\pi \overline{A}_{n-1}} Y(\overline{A}_{n-1}))^m \\ & + \frac{1}{2!} \sum_{i=1}^{n} \left(\frac{\partial^2 A_i}{\partial A_{n-1}^2} var[A_{n-1}] + \frac{\partial^2 A_i}{\partial C^2} var[C] + \frac{\partial^2 A_i}{\partial \Delta S^2} var[\Delta S] \right) \end{aligned} \tag{9.18}$$

Taking the variance of equation (9.15) one obtains:

$$\begin{aligned} var[A_n] &= E[(A_n - \overline{A}_n)^2] \\ &= E\left[\left(\begin{array}{c} A_n(\overline{\mathbf{x}}) + \sum_{i=1}^{n}\sum_{j=1}^{3}\frac{\partial A_i}{\partial X_j}(X_j - \overline{X}_j) \\ +\frac{1}{2!}\sum_{i=1}^{n}\sum_{j=1}^{3}\sum_{k=1}^{3}\frac{\partial^2 A_i}{\partial X_j \partial X_k}(X_j - \overline{X}_j)(X_k - \overline{X}_k) \\ -A_n(\overline{\mathbf{x}}) - \frac{1}{2!}\sum_{i=1}^{n}\sum_{j=1}^{3}\frac{\partial^2 A_i}{\partial X_j^2}var[X_j] \end{array}\right)^2\right] \end{aligned} \tag{9.19}$$

The term in the second line of equation (9.19) vanishes due to independence between the random variables. The last term is neglected, resulting in:

$$var[A_n] \simeq E\left[\left(\sum_{i=1}^{n}\sum_{j=1}^{3}\frac{\partial A_i}{\partial X_j}(X_j - \overline{X}_j)\right)^2\right] \tag{9.20}$$

For $n = 2$ this results:

$$\begin{aligned} var[A_2] &\simeq E\left[\left(\sum_{j=1}^{3}\frac{\partial A_2}{\partial X_j}(X_j - \overline{X}_j) + \sum_{j=1}^{3}\frac{\partial A_1}{\partial X_j}(X_j - \overline{X}_j)\right)^2\right] \\ &= E\left[\begin{array}{c} \left(\sum_{j=1}^{3}\frac{\partial A_2}{\partial X_j}(X_j - \overline{X}_j)\right)^2 + \left(\sum_{j=1}^{3}\frac{\partial A_1}{\partial X_j}(X_j - \overline{X}_j)\right)^2 \\ +2\left(\sum_{j=1}^{3}\frac{\partial A_2}{\partial X_j}(X_j - \overline{X}_j)\right)\left(\sum_{j=1}^{3}\frac{\partial A_1}{\partial X_j}(X_j - \overline{X}_j)\right) \end{array}\right] \\ &= \sum_{j=1}^{3}\left(\frac{\partial A_2}{\partial X_j}\right)^2 var(X_j) + \sum_{j=1}^{3}\left(\frac{\partial A_1}{\partial X_j}\right)^2 var(X_j) \\ &\quad +2\sum_{j=1}^{3}\sum_{k=1}^{3}\frac{\partial A_2}{\partial X_j}\frac{\partial A_1}{\partial X_k}cov(X_j, X_k) \qquad (9.21) \\ &= \sum_{i=1}^{2}\sum_{j=1}^{3}\left(\frac{\partial A_i}{\partial X_j}\right)^2 var(X_j) + \sum_{i=1}^{2}\sum_{j=1, j\neq i}^{2}\sum_{k=1}^{3}\frac{\partial A_i}{\partial X_k}\frac{\partial A_j}{\partial X_k}var(X_k) \\ &= \sum_{i=1}^{2}\sum_{j=1}^{2}\sum_{k=1}^{3}\frac{\partial A_i}{\partial X_k}\frac{\partial A_j}{\partial X_k}var(X_k) \qquad (9.22) \end{aligned}$$

since the term in line (9.21) vanishes for all $j \neq k$. The covariance between successive crack sizes ($cov(A_1, A_0)$) appearing in (9.21) is also neglected. Generalizing the result for any n one obtains:

$$var[A_n] = \sum_{i=1}^{n}\sum_{j=1}^{n}\sum_{k=1}^{3}\frac{\partial A_i}{\partial X_k}\frac{\partial A_j}{\partial X_k}var(X_k) \tag{9.23}$$

Approximations involved in this solution are the neglection of the covariance between successive crack sizes ($cov(A_n, A_{n-1})$), disconsideration of the last term of equation (9.19) and the truncation of the expansion in equation (9.15). Truncation of the series expansion

neglects third order and higher terms. Elimination of the last term of equation (9.19) neglects second order influences of the variance of each random variable in the variance of A_n, including the term $\frac{\partial^2 A_n}{\partial A_{n-1}^2} var[A_{n-1}]$.

The series expansion approximation can lead to serious errors, especially when the variances of crack growth parameters is not small. Therefore, this solution is not pursued any further in this thesis.

9.2 Random process solutions

In most random process stochastic crack propagation models reviewed in chapter 7, the crack propagation rate is modelled as a random process of time. This includes Yang et al.'s (1987) lognormal crack propagation model and the diffusive Markov models of Lin and Yang (1985), Sobczyk (1986), Tsurui and Ishikawa (1992) and others. It would perhaps be more natural to model the unit-mean crack propagation rate $X(t)$ as a random process of crack length, since the variations in $X(t)$ are being attributed to material inhomogenities. Modelling $X(t)$ as a function of time makes the parameters of this process dependant on the level of loading, as more severe loading makes the crack advance over more material in the same time. Modelling $X(t)$ as a function of time, however, greatly facilitates derivation of crack size TPDs, because the variables crack size and time can be separated. For a generic crack propagation function $Q(A)$ and a non-dimensional crack propagation rate $X(t)$, one can write:

$$\frac{dA}{dt} = X(t)Q(c, \Delta K, A, \Delta S, m, ...) \quad \text{or} \quad \frac{dA}{Q(A)} = X(t)dt \tag{9.24}$$

A random process $W(t)$ is introduced such that:

$$W(t^*) = \int_{a_0}^{a(t^*)} \frac{dz}{Q(z)} \tag{9.25}$$

It then follows that:

$$dW = X(t)dt \quad \text{or} \quad W(t^*) = \int_0^{t^*} X(\tau)d\tau \tag{9.26}$$

Equations (9.25) and (9.26) show that $W(t)$ is, at the same time, a function of the time t^* required for a crack to grow from a_0 to $a(t^*)$ and an integral over the random process $X(t)$ in the same time period. In other words, because $X(t)$ is modelled as a random process of time, the variance in crack size at a time t^* becomes a function of the time required to reach

that crack size. It is convenient to introduce a total time to grow function, $TTTG(a)$:

$$TTTG(a) = \int_{a_0}^{a} \frac{dz}{Q(z)} \tag{9.27}$$

This function gives the time required to grow from an initial crack size a_0 to a given crack size a, for a mean crack growth rate c. As will be seen in the sequel, this function is used to derive crack size TPDs for both lognormal and diffusive Markov random process models.

9.2.1 Lognormal crack propagation rate model

Yang et al. (1987) modelled the crack propagation rate $X(t)$ in equation (9.24) as a stationary lognormal random process of time, with an exponential correlation function:

$$\text{cov}[X(t_1), X(t_2)] = \sigma_X^2 \cdot \exp[-\frac{(t_2 - t_1)}{\lambda_X}] \tag{9.28}$$

It follows from equations (9.25) and (9.26) that the distribution of $A(t)$ can be derived from the distribution of $W(t)$, since:

$$F_A(a,t) = F_W(TTTG(a), t) \tag{9.29}$$

The distribution of $W(t)$ cannot be derived in closed form, but a second order approximation (Yang and Manning, 1996) can be used to fit a proper probability distribution function to the mean and standard deviation of $W(t)$. From equation (9.26) one obtains:

$$\begin{aligned} \mu_W(t) &= E[W(t)] = \int_0^t E[X(\tau)]d\tau = \mu_X \cdot t \\ \sigma_W^2(t) &= \int_0^t \int_0^t \text{cov}[X(\tau_1), X(\tau_2)]d\tau_1 d\tau_2 \\ &= 2\sigma_X^2 \lambda_X^2 \left[\exp(-\frac{t}{\lambda_X}) + \frac{t}{\lambda_X} - 1\right] \end{aligned} \tag{9.30}$$

Now one has to assume a specific probability distribution function for process $W(t)$. Assuming a lognormal distribution, the crack size process also becomes lognormally distributed. The PDF can then be given in terms of the parameters of the process $Y(t) = \log[W(t)]$, which has a normal distribution:

$$F_A(a,t) = \Phi\left(\frac{\log(TTTG(a)) - \mu_Y(t)}{\sigma_Y(t)}\right) \tag{9.31}$$

From the relations between normal and lognormal distributions, one obtains:

$$\begin{aligned} \mu_Y(t) &= \log\left[\sqrt{\frac{\mu_W(t)}{1+V_W^2(t)}}\right] \\ \sigma_Y(t) &= \sqrt{\log(1+V_W^2(t))} \end{aligned} \tag{9.32}$$

where $V_W(t) = \frac{\sigma_W(t)}{\mu_W(t)}$ is the coefficient of variation. Often in experiments it is the distribution of $Z(t) = \log[X(t)]$ that is obtained, rather than the distribution of $X(t)$ itself. Since $X(t)$ has lognormal distribution and unit mean, process $Z(t)$ has a normal distribution with zero mean. The parameters of the lognormal crack size distribution (eq. 9.31) can be given directly in terms of parameters of the process $Z(t)$. Inserting the parameters in equation (9.30) into equations (9.32), one obtains:

$$\begin{aligned} \mu_Y(t) &= \log(t) - \frac{\sigma_Z^2}{2}\log\left[\sqrt{1+\xi^2(t)\exp(\sigma_Z^2)-\xi^2(t)}\right] \\ \sigma_Y(t) &= \sqrt{\log\left[\sqrt{1+\xi^2(t)\exp(\sigma_Z^2)-\xi^2(t)}\right]} \end{aligned} \tag{9.33}$$

where:

$$\xi^2(t) = \frac{2\lambda_X^2}{t^2}\left[\exp(-\frac{t}{\lambda_X}) + \frac{t}{\lambda_X} - 1\right] \tag{9.34}$$

Similar solutions are also given in (Yang et al., 1987) for Weibull and Gamma approximations of process $W(t)$ and of the crack size distribution.

The Yang et al. (1987) model was implemented by McAllister and Ellingwood (2002) and was shown to agree well with Monte Carlo simulation.

9.2.2 Diffusive Markov models

In section 7.3.5 of the literature review it was seen that the drift and diffusion coefficients of the FPK equation can be derived assuming specific correlation functions for the crack propagation rate process and for generic crack growth equations. For the simpler of these models, such as single state models considering only a random crack propagation rate, solutions for the crack size TPD are analytical. The derivation of crack size TPDs is not reproduced here. Rather, final results are presented, and some practical aspects of the calculations are pointed out.

Assuming a triangular correlation function for the crack propagation rate process, for example:

$$\begin{aligned} R_{XX}(\tau) &= \sigma_X^2 \left(1 - \frac{|\tau|}{\Delta}\right) \quad \text{if} \quad |\tau| < \Delta \\ &= 0 \qquad\qquad\qquad \text{otherwise} \end{aligned} \tag{9.35}$$

one obtains the following expressions for the crack TPD (Lin and Yang, 1985):

$$F_A(a,t) = \Phi\left[\frac{\int_{a_0}^{a(t)} \frac{dx}{Q(x)} - \mu_X(t-t_0)}{\sqrt{2\sigma_X^2 \Delta(t-t_0)}}\right] \tag{9.36}$$

For an exponential correlation function:

$$R_{XX}(\tau) = \sigma_X^2 \exp[-\frac{\tau}{\lambda_X}]$$

a very similar solution is obtained (Ishikawa et al., 1993):

$$F_A(a,t) = \Phi\left[\frac{\int_{a_0}^{a(t)} \frac{dx}{Q(x)} - \mu_X(t-t_0)}{\sqrt{\sigma_X^2 \lambda_X(t-t_0)}}\right] \tag{9.37}$$

Limitations of these solutions, following section 7.3.5, is that the characteristic length of the crack size process be larger than the correlation length of the crack propagation rate random process. Hence, solutions are limited to small λ_X.

The term $\int_{a_0}^{a(t)} \frac{dx}{Q(x)}$ in the expressions above is nothing less than the total time to grow function $TTTG(a)$ introduced earlier. Hence it is seen that this function is used in the solution of both lognormal random process models and diffusive Markov models. The role of this function arises from the fact that the crack propagation rate is being modelled as a random process of time, which allows the variables time and crack size to be isolated.

When a lognormal distribution is assumed for the crack propagation rate $X(t)$, it is often the parameters of the (normal) distribution $Z = \log(X)$ that are derived in experiments. The parameters of process $X(t)$, in this case, can be derived by means of the normal - lognormal relationships:

$$\begin{aligned} \mu_X &= \exp\left[\frac{\sigma_Z^2 \log(10)^2}{2}\right] \\ \sigma_X^2 &= \mu_X^2 \left[\exp(\sigma_Z^2 \log(10)^2) - 1\right] \end{aligned} \tag{9.38}$$

9.2.3 Random initial crack size

The lognormal and diffusive Markov random process solutions just presented are based on a deterministic initial crack size a_0. A random initial crack size is included in these solutions by considering the distribution $F_A(a,t)$ in equations (9.31, 9.36 and 9.37) to be conditional to a_0 at time t_0. The unconditional crack size TPD is then obtained by numerical integration:

$$F_A(a,t) = \int_{-\infty}^{\infty} F_A(a,t|z,t_0) \cdot f_{A_0}(z)dz \tag{9.39}$$

In practical terms, the total time to grow function (equation 9.27) becomes an explicit function of a_0:

$$TTTG(a_0,a) = \int_{a_0}^{a} \frac{dz}{Q(z)} \tag{9.40}$$

One point that hasn't been stressed elsewhere in the literature, and which is seen as a major advantage of random process based solutions, is that function $TTTG(a_0,a)$, and subsequently the crack size TPD, is obtained from a single mean crack growth integration. This integration starts at the smallest practical crack size (say, $a_1 = \max[a_{th}, \mu_{ao} - 3\sigma_{ao}]$), and goes on, cycle by cycle, until the critical crack size is reached. It yields a sequence of points of n (cycle number) versus crack size or time versus crack size:

$$a_{i+1} = a_i + \mu_X \cdot Q(a_i) \tag{9.41}$$

A mean time to grow function $T_\mu(a)$ is interpolated to the crack size versus time data, so that intermediate values can also be obtained. The total time to grow from any initial crack size a_0 to any final crack size a is then simply given as:

$$TTTG(a_0,a) = T_\mu(a) - T_\mu(a_0) \tag{9.42}$$

The mean time to grow function, $T_\mu(a)$, is the same used in the convolution integration.

Random stress ranges can be included in the analysis using the same simulation shortcut adopted in the convolution solution.

9.3 Monte Carlo simulation and probability density fit

Evaluation of the crack size TPD thought Monte Carlo simulation is straightforward but very time consuming. Basically, a (large) number of crack growth time-histories is computed, for sampled values of the random crack growth parameters. Some classical results from the

theory of model selection in statistics can then be used to obtain crack size distributions from sampled crack values.

There are two different methods by which probability distributions can be generated from a set of simulated crack values. Both of them require the selection of a (hypothetical) probability distribution model, e.g., that the crack size distribution at a given time t follows a normal distribution with parameters $\mu_A(t)$ and $\sigma_A(t)$ or $(A(t) = N(\mu_A(t), \sigma_A(t))$. The task then becomes to estimate the parameters of the hypothesized distribution model and to verify the appropriateness of the chosen distribution model.

In the so-called "method of moments" (Benjamin and Cornell, 1970), distribution moments are approximated by the sample moments. For n crack size samples at time t, one has:

$$\begin{aligned} \mu_A(t) &\simeq \frac{1}{n}\sum_{i=1}^{n} a_i(t) \\ \sigma_A^2(t) &\simeq \frac{1}{n-1}\sum_{i=1}^{n}(a_i(t) - \mu_A(t))^2 \end{aligned} \tag{9.43}$$

where the explicit dependency on t is a remainder that, $A(t)$ being a random process of time, distribution fit and model parameter estimation have to be repeated over time. The goodness-of-fit of the resulting distribution can then be "checked" as shall be seen in the sequel.

In the "method of maximum likelihood" (Benjamin and Cornell, 1970), the distribution model and parameters that would more likely produce (or re-produce, for this matter) the observed samples is sought. This can be done by comparing a hypothesized distribution model with either a probability distribution histogram or a cumulative histogram of the observed samples. In terms of a probability distribution histogram with n_b bins, the χ^2-statistic of the sample is:

$$\varkappa^2(t) = \sum_{i=1}^{n_b} \frac{(N_i(t) - n\ f_i(t))^2}{n\ f_i(t)} \tag{9.44}$$

where $N_i(t)$ is the number of observed samples in the i^{th} bin, at time t, and $n\ f_i(t)$ is the number of expected samples, in n realizations, according to the hypothesized distribution model:

$$f_i(t) = \int_{a_1}^{a_2} f_A(x,t)dx \tag{9.45}$$

where a_1 and a_2 are the lower and upper limits of the i^{th} bin and $f_A(a,t)$ is the PDF of the hypothesized model.

The $\varkappa^2$ statistic is then used for a goodness-of-fit check of the hypothesized distribution. As long as no n $f_i(t)$ term is too small, the χ^2 variable follows a χ^2-distribution with $\upsilon = n_b - n_p - 1$ degrees of freedom, where n_p is the number of model parameters estimated from the same data set. It is then possible to estimate the probability $P_\chi(\upsilon/2, \varkappa^2/2)$ that the sum of squares of the n_b standard Gaussian variables be greater than $\varkappa^2$, which comes to be confidence or likelihood that the observed samples were drawn from the hypothesized distribution (Zwillingner, 1996):

$$P_\chi(p,x) = \frac{\Gamma(p,x)}{\Gamma(p)} = \frac{1}{\Gamma(p)} \int_x^\infty e^{-t} t^{p-1} dt \tag{9.46}$$

where $\Gamma(p,x)$ and $\Gamma(p)$ are the incomplete and complete Gamma functions. The distribution model and parameters can then be optimized such as to maximize the likelihood measure $P_\chi(\upsilon/2, \varkappa^2/2)$, or as to minimize the quantity:

$$\chi^2_{\min} = |E[\chi^2] - \varkappa^2(t)| \tag{9.47}$$

$$= |\upsilon - \varkappa^2(t)| \tag{9.48}$$

Another useful goodness-of-fit test, based on a comparison between cumulative distributions, is the Kolmogorov-Smirnov or KS test (Benjamin and Cornell, 1970). The sample statistics used in this test is the maximum distance between the CDF of the hypothesized distribution model and the sample cumulative histogram $\mathbf{F} = \{F_i\} = \{i/n\},\ i = 1, ..., n$, giving the fraction of data points to the left of the (ordered) a_i crack size observations. The KS-statistic is:

$$ks(t) = \max_{i=1}^{n} [|F_i - F_A(a_i, t)|] \tag{9.49}$$

where $F_A(a,t)$ is the CDF of the hypothesized distribution model. The distribution of the variable $KS(t)$, as per equation (9.49), is independent of the hypothesized model $F_A(a,t)$ and its only parameter is the number of samples n. From its distribution, the likelihood that the observed samples were generated from the hypothesized model is then given by (Zwillingner, 1996):

$$P_{KS}(t) = P[KS > ks(t)] = 2 \sum_{i=1}^{\infty} (-1)^{i-1} e^{-2i^2 n\, ks(t)^2} \tag{9.50}$$

Both goodness-of-fit tests just presented can also be used to check the hypothesized model and parameters obtained via the simpler method of moments. Derivation of crack size TPDs through MC simulation is not necessarily part of a random crack propagation reliability analysis. It would be simpler to compute failure probabilities directly, were simulation really

required. However, simulation-based distribution functions are used in the sequel as a means of verifying the accuracy of other numerical solutions.

9.4 Distribution fit for numerical crack size TPD solutions

The Convolution Integration, lognormal random process and Diffusive Markov process crack size TPD solutions presented earlier in this chapter are all numerical, due to the (numerical) integration over initial crack size distributions. These solutions can be evaluated strictly numerically, resulting in lists of crack values $\mathbf{a}_{t_j} = \{a_i\}$, $i = 1, ..., n$; $j = 1, ..., n_{lb},$, and corresponding probability distribution values $\mathbf{f}_{t_j} = \{f_i\}$ (convolution solution - equation 9.6) or cumulative distribution values $\mathbf{F}_{t_j} = \{F_i\}$ (random process solutions - equations 9.31 and 9.37). In a strictly numerical solution, a large number of points n has to be considered and results are interpolated between these points. It is very convenient, however, although not strictly necessary, to obtain an analytical expression for the crack size distribution at a given time. This can be done by means of curve fitting and by a suitable choice of crack size distribution model. The procedure has some similarities, but is not the same, as estimating distribution models from sampled histograms. Whereas a sampled histogram is only one set amongst many possible outcomes of the underlying random variable, the lists of points $\mathbf{f}_{t_j}$ and $\mathbf{F}_{t_j}$ represent the actual probability distributions of the random variable. Hence, although the closest fit to a sampled histogram, in a classic curve fitting sense, does not necessarily represent the best distribution model for the random variable, classical curve fitting procedures can be used for $\mathbf{f}_{t_j}$ and $\mathbf{F}_{t_j}$. Hence, a specific probability distribution function can be fitted to the numerically evaluated list of points, for example, by minimizing the mean-square error:

$$\begin{aligned} ms_f(t) &= \sum_{i=1}^{n} (f_i - f_A(a_i, t))^2 \\ ms_F(t) &= \sum_{i=1}^{n} (F_i - F_A(a_i, t))^2 \end{aligned} \tag{9.51}$$

where $f_A(a, t)$ and $F_A(a, t)$ are the fitted (and not hypothesized, in this case) probability distribution and cumulative distribution functions of the crack size random variable.

In an analogy to maximum likelihood parameter estimation and goodness-of-fit model

checks, the "best" fit PDF and CDF curves can also be obtained by minimizing the function:

$$\begin{aligned}\chi^2_{\min} &= E[\chi^2] - \varkappa^2 \\ &= \upsilon - \sum_{i=2}^{n} \frac{\left[m\frac{(f_i+f_{i-1})}{2}(a_i - a_{i-1}) - m\int_{a_{i-1}}^{a_i} f_A(x,t)dx\right]^2}{m\int_{a_{i-1}}^{a_i} f_A(x,t)dx}\end{aligned} \tag{9.52}$$

- in terms of PDF values, or the function:

$$\chi^2_{\min} = \upsilon - \sum_{i=2}^{n} \frac{[m(F_i - F_{i-1}) - m(F_A(a_i,t) - F_A(a_{i-1},t))]^2}{m(F_A(a_i,t) - F_A(a_{i-1},t))} \tag{9.53}$$

- in terms of CDF values, where m is a normalization factor to make the n $f_i(t)$ terms large enough.

In a strict probabilistic sense, expressions (9.52) and (9.53) are formally more appropriate than expressions (9.51). In practice, however, experience with some problems to be presented in the sequel reveals little difference between the two alternatives.

9.5 Comparison of solution methods

In this section, distinct solution methods are compared in an application to the random crack propagation problem introduced in section 8.1. The unit-mean crack propagation rate $X(t)$ is modelled as a lognormal random process of time, with distribution parameters: $X(t) = LN(\mu_X, \sigma_X) = LN(1, 0.2)$ and with an exponential correlation function: $R_{XX}(\tau) = \sigma_X \exp[-\tau/\lambda_X]$. The correlation length λ_X is used to vary between a random process and a random variable solution in the results that follow.

The following notation is used for the crack size TPD solutions:

Notation	$f_A(a,t)$ Solution Method
CONV	Convolution Integration
LOGN	lognormal model
MKV	Diffusive Markov model
MCS	Monte Carlo simulation - χ^2 fit

9.5.1 Simulation-based crack size TPD

Figure 9-1 shows crack size distributions obtained via simulation, for the reference problem, at $t = T$ (after 10 load blocks) and with $\lambda_X = 10^4$ cycles. The figure shows an histogram corresponding to 10^4 crack samples at time T, a lognormal distribution obtained by χ^2 maximum likelihood fit to the sampled histogram, and a lognormal distribution obtained from

the sampled moments. The figure shows that, for a lognormal initial crack size distribution and for the problem parameters considered, the crack size distribution after 10^6 cycles can still be approximated by a lognormal distribution. It is also seen that the histogram fit and the sample-moment approximation provide slightly different distributions.

The χ^2 goodness-of-fit test gives confidence percentages fluctuating between 20 and 80% for the distinct time steps, which indicate a high confidence in the lognormal distribution fit. The KS goodness-of-fit test gives a confidence dropping from 96 to around 60%, from the first to the last time step, which again shows a high level of confidence. Confidence in the sample moments distribution fit is similar, although slightly less than for the χ^2 distribution fit.

That the crack size distribution can still be approximated by a lognormal distribution after a large number of load cycles can be attributed to the fact that the lognormal distribution can follow the natural trend of crack growth, with its upper tail spreading towards larger and larger crack sizes. Crack size distribution fits are considered again in chapter 11, in connection with some variations from the reference problem. Histogram χ^2-fitted crack size distributions are used as a basis of comparison with numerical solutions in the sequel. Clearly, other distribution models such as Weibull could also have been used to fit the crack growth data. However, due to the simplicity of the log-normal distribution and due to the good results obtained using it, the fit using other distribution models was not attempted.

9.5.2 Effect of λ_X on convolution integration, lognormal model and diffusive Markov model solutions

Figure 9-2 shows the distributions obtained using convolution integration, the lognormal crack propagation rate of Yang et al. (1987), the diffusive Markov model of Ishikawa et al. (1993) and Monte Carlo simulation. It can be seen in the figure that an excellent agreement between all solutions is obtained, for a correlation length of $\lambda_X = 10^4$ cycles. Following results presented earlier, for the lognormal model a lognormal distribution was assumed for process $W(t)$. Both lognormal and diffusive Markov solutions assume explicitly a lognormal distributed crack propagation rate with an exponential correlation function. The convolution integration, which completely neglects crack propagation rate and crack size correlations, is accurate enough for $\lambda_X = T/100 = 10^4$ cycles.

For a correlation length of $\lambda_X = T = 10^6$ cycles, significant differences start to appear between the distinct solutions (figure 9-3). However, even for such long correlation length, the error is moderate and the approximate solutions can still be deemed useful. This result

shows that the restriction of the diffusive Markov solution, regarding the smallness of the crack propagation rate correlation length in comparison to the characteristic crack length, is not that restrictive at all. After all, the correlation coefficient between initial and final crack propagation rates for $\lambda_X = 10^6$ cycles is $R_{XX}(T)/\sigma_X = \exp[-1] \approx 0.4$, which is not far to the random variable case ($R_{XX}(T)/\sigma_X \approx 1.0$). When the correlation length is extended to $\lambda_X = 10T$ (figure 9-4), which is virtually the random variable case ($R_{XX}(T)/\sigma_X \approx 0.9$), then the Markov solution becomes useless. In this case, negative crack growth is also significant, as can be seen in figure 9-4. The Markov solution depends explicitly on the correlation length λ_X, as can be seen in the figure, whereas the convolution and lognormal solutions are still reasonable, and are hence not directly affected by λ_X.

A comparison of figures 9-4 and 9-2 shows that the convolution integration, which is commonly applied in conjunction with random variable crack propagation models (Besterfield et al., 1991; Sobczyk and Trebicki, 2000), is actually more accurate for random process problems. Such a result is explained by the fact that the assumption of independence between crack increment and crack size ($\text{cov}(A_i, \Delta A_i)$, equation 9.5) is more appropriate when the crack propagation rate is a random process of time.

Results presented in this section, regarding the correlation length λ_X, are, to some extent, dependent on the standard deviation σ_X of the crack propagation rate random process. Figure 9-5 shows crack TPD results for $\lambda_X = T = 10^6$ cycles and $\sigma_X = 0.5$, instead of the original value of $\sigma_X = 0.2$. A comparison of this result with figure 9-3 reveals that the numerical solutions "degenerate" faster (in terms of an increasing λ_X) for larger σ_X. The numerical solutions are still very good, however, for $\lambda_X = 10^4$ cycles and $\sigma_X = 0.5$ (figure 9-6).

It is important to interpret these results in view of λ_X and σ_X values that can be expected to be encountered in practice. As a reference, parameters obtained by Yang et al. (1987) based on a statistical analysis of Virklers (1979) large replicate tests, were $\lambda_X = 15380$ cycles and $\sigma_X = 0.08$, which are well within the range considered in this section. Hence, it can be said that the convolution integration, the lognormal and the Markov solutions are equivalent and sufficiently accurate for the proper practical applications.

The three approximate solutions are based on a single mean crack growth computation and are very fast to compute. For this example, crack growth computation was analytical ($\Delta K(A)$ and $Y(A)$ given in closed form) and hence the total computation time was not very large even for the Monte Carlo simulation (≈720 seconds). 720 seconds for 10^4 crack growth computations gives little under 0.1 seconds per crack growth computation. Approximate solutions were obtained in roughly 60 seconds, with 0.4 seconds spent in the mean crack

growth computation (because it starts at a very small crack size and goes on until the critical crack size is reached, the mean crack growth computation took four times as many load cycles as an "average" 10^6 cycle crack growth computation). Hence, most of the 60 seconds spent in the approximate solutions were actually spent in numerical integrations and distribution fittings. This time, however, does not increase when crack growth computation is numerical. Hence, when a single numerical (FE) crack growth computations takes considerably more that one minute, the actual speed-up of the solution would be close to $10^4/4 = 1000$-fold (for 10^4 simulation samples). This is not surprising, as simulation is always time-consuming. However, it will be seen that a significant speed-up is also obtained when random variable failure probability solutions, such as TI and FPI FORM, are considered.

9.5.3 Effect of λ_X and σ_X on crack size TPDs

Clearly, parameters λ_X and σ_X also have an effect on the resulting crack size distributions. Figure 9-7 compares crack size distributions at time T for varying λ_X, with $\sigma_X = 0.2$ (left) and $\sigma_X = 0.5$ (right). It is seen that the variation of λ_X from 10^3 to 10^7 cycles causes a significant increase in the crack size variance, especially for $\sigma_X = 0.5$. Figure 9-8 shows the same results, but now for varying σ_X and fixed λ_X ($\lambda_X = 10^3$ cycles on left and $\lambda_X = 10^7$ cycles on right). It is seen that final crack size distribution is more affected by λ_X than by σ_X. Indeed, for the case with $\lambda_X = 10^3$ cycles, a change from $\sigma_X = 0.2$ to $\sigma_X = 0.5$ does not affect the crack size distribution at all. This result is a consequence of the fact that crack increments with a highly variable crack propagation rate tend to be averaged over a couple of cycles. Moreover, in both cases $\mu_X = 1.0$ and increasing σ_X from 0.2 to 0.5 increases the occurrence of both smaller and larger crack propagation rates.

9.5.4 Simulation of stress ranges

All crack size TPD results shown so far in this section have been derived using a single set of simulated stress ranges, with ten load blocks and one hundred stress range samples per load block. As stated in the literature review, simulation of stress ranges is a shortcut that avoids a formal inclusion of random stress ranges in the crack size TPD solutions, and which accounts for the effects of random stress ranges in the mean but not in the standard deviation of the crack size distributions. In this sub-section, the effects of this stress range simulation shortcut are studied.

In order to do that, crack size TPDs obtained from 5000 MC simulation samples, using a single (fixed) set of simulated stress ranges, (single ΔS TH in the figures) are compared

with crack size distributions obtained from another 5000 sample MC simulation, where a new stress range set is simulated for each crack growth time-history. Results are compared in figure 9-9, which also includes a solution using only the mean of the stress range distribution (equivalent to constant amplitude loading). The figure shows that using one hundred stress ranges per load block, which actually accounts for one crack increment computation for every thousand load cycles ($\frac{10^6 \text{ load cycles}}{10 \text{ load blocks} \quad 100 \text{ stress ranges per load block}} = 10^3$ load cycles per sampled stress range) provides sufficiently accurate results. Naturally, the number of required stress ranges will also depend on the degree of non-linearity of the problem (e.g., crack exponent m), the variance σ_S^2 of the load process and the actual number of load cycles.

Under low-cycle fatigue, the influence of random stress ranges in crack size variance is known to be greater (Zheng and Ellingwood, 1998). It is interesting to check whether the stress range simulation shortcut remains valid for low cycle fatigue. Figure 9-10 shows stress range simulation results obtained for a low-cycle fatigue problem described in section 11.3, with $T = 10^3$ cycles. It is seen that also for this low-cycle fatigue problem the stress range simulation shortcut is accurate enough. Results in figure 9-10 were also obtained with 10 load blocks and 100 stress ranges per load block, making it one sampled stress range per actual load cycle.

Were the problem non-linearity any greater, there is always the possibility of computing a set of total time to grow functions $TTTG(a_0, a)$, each with one set of simulated stress ranges, and average the growth time obtained from these functions. In this case, the random process based crack size TPD's would not be obtained from a single mean crack growth computation, but from a couple of them. Still, the solution would be much faster than straight MC simulation.

9.6 Concluding remarks

Crack size TPD solutions presented in this chapter are not novel, but comparative results like the ones presented here have not been found elsewhere. It was seen that when the problem is not excessively non-linear and when the correlation length λ_X is moderate, the Convolution, the lognormal RP model and the Diffusive Markov model solutions are all very much equivalent. When the crack propagation rate is modelled as a random process of time, when random stress ranges are simulated and when random parameters of the problem are limited to A_0, C and ΔS, crack size TPDs can be efficiently and accurately evaluated from a single mean crack growth computation.

9.7 Figures

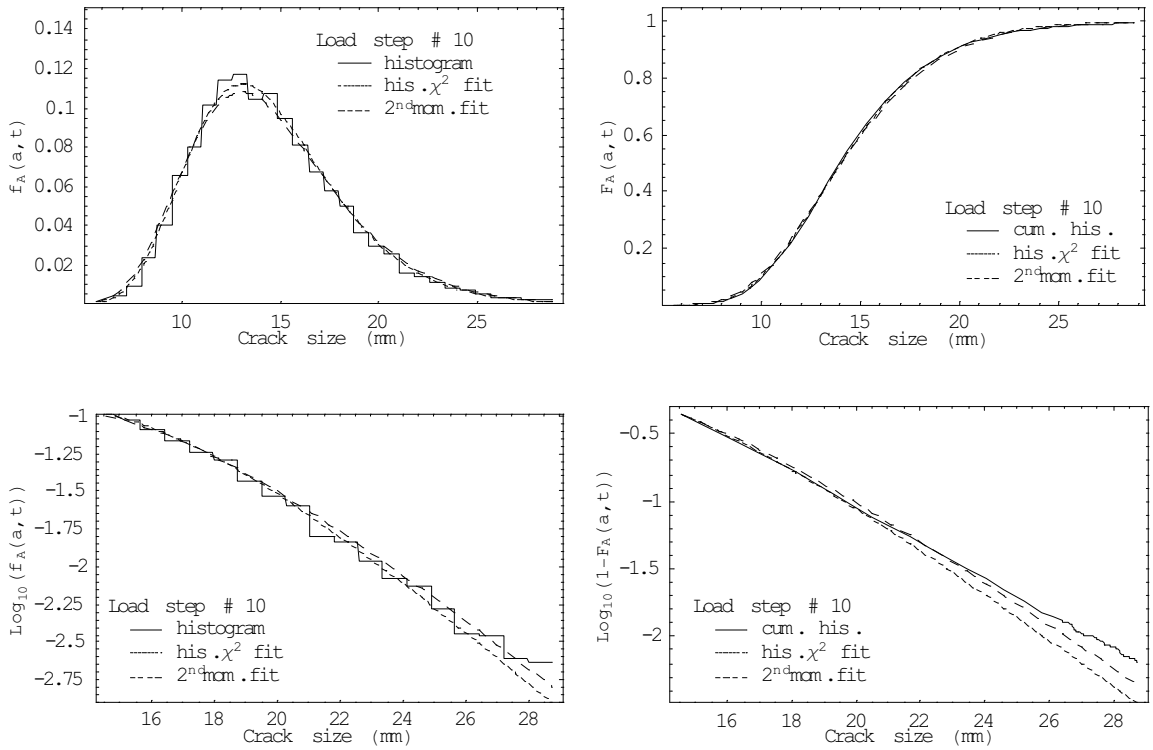

Figure 9-1: Histogram fit of crack size TPD at $t = T$ and for $\lambda_X = 10^4$ cycles.

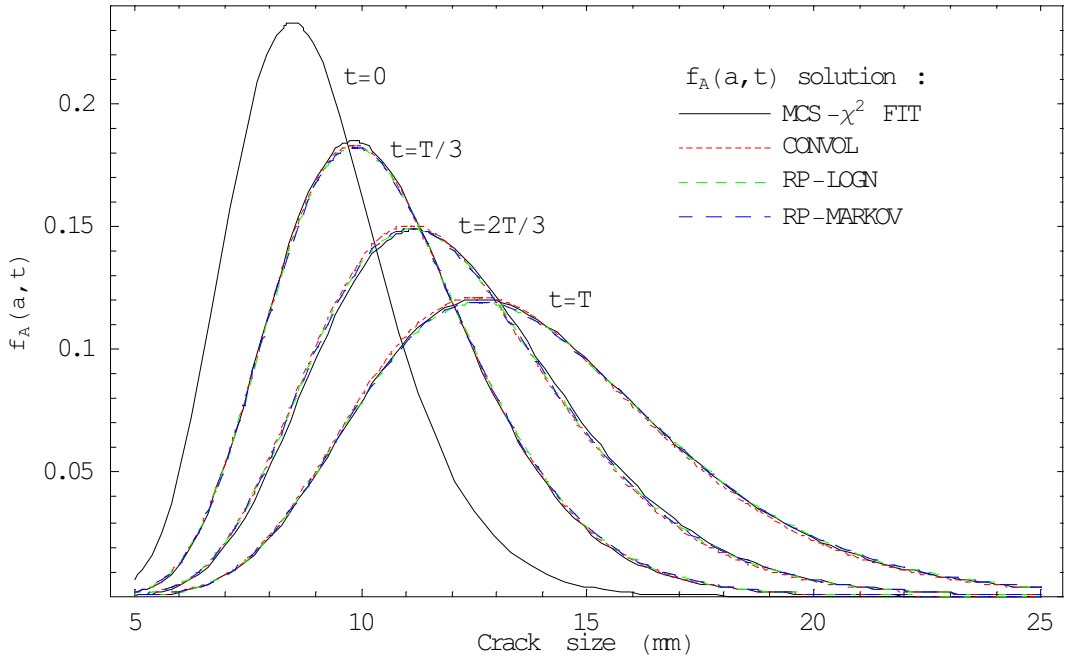

Figure 9-2: Crack size TPD for $\lambda_X = 10^4$ cycles.

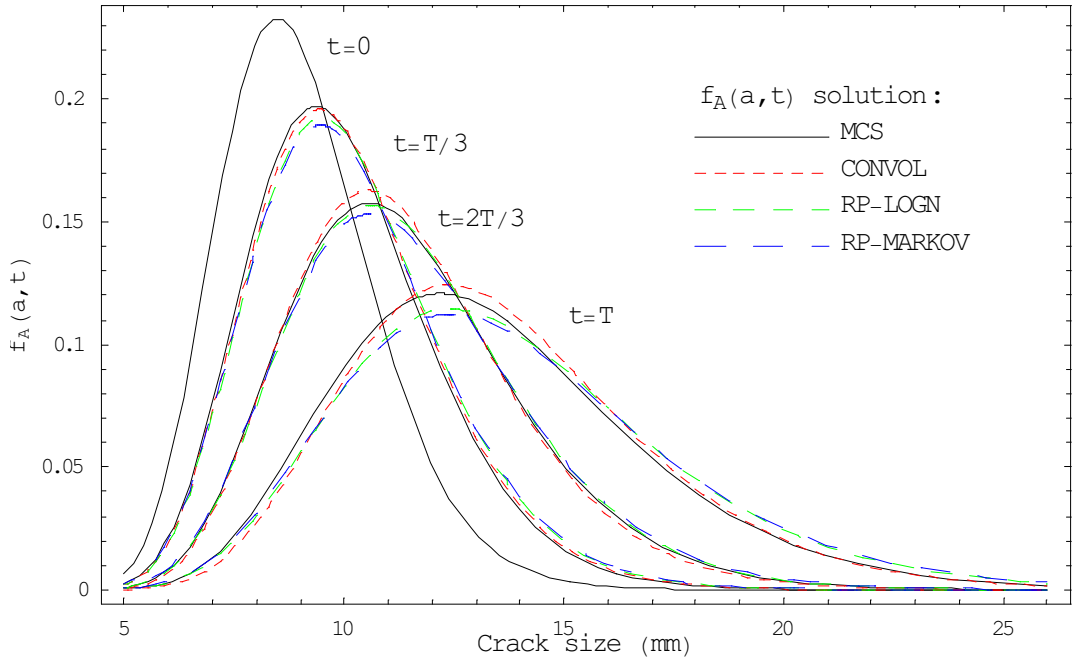

Figure 9-3: Crack size TPD for $\lambda_X = T = 10^6$ cycles.

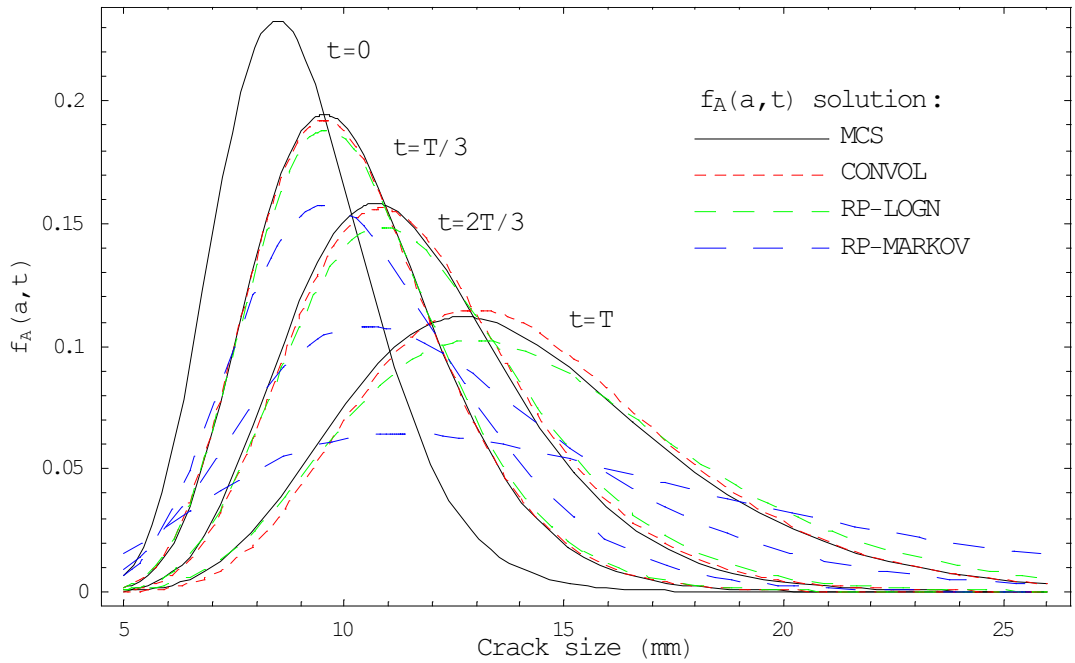

Figure 9-4: Crack size TPD for $\lambda_X = 10\ T$ cycles.

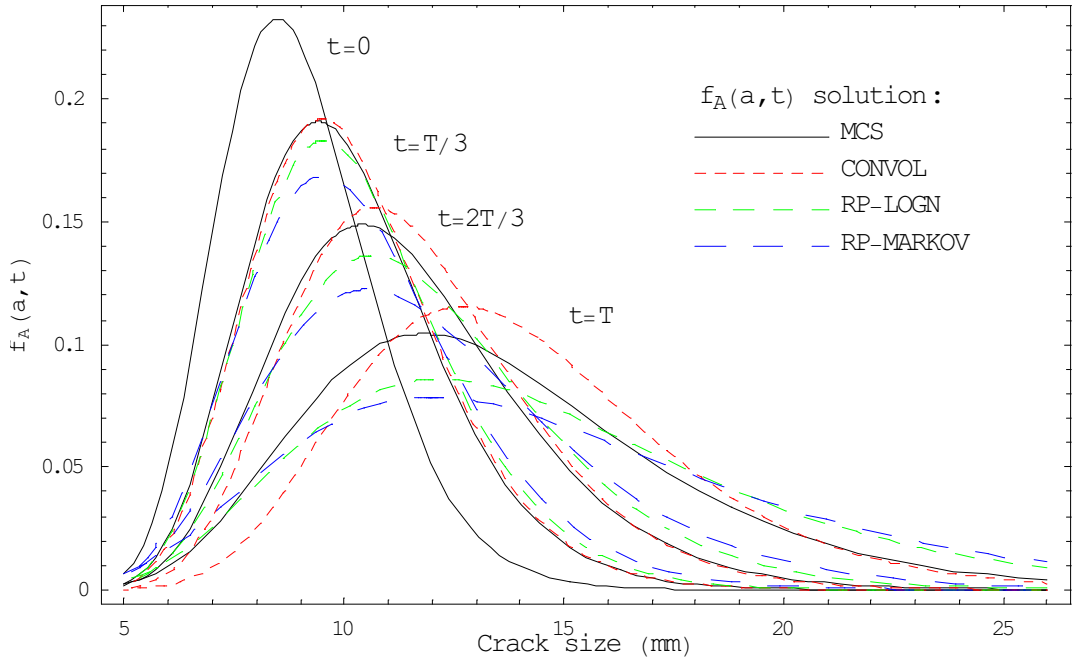

Figure 9-5: Crack size TPD for $\lambda_X = T$ cycles, $\sigma_X = 0.5$.

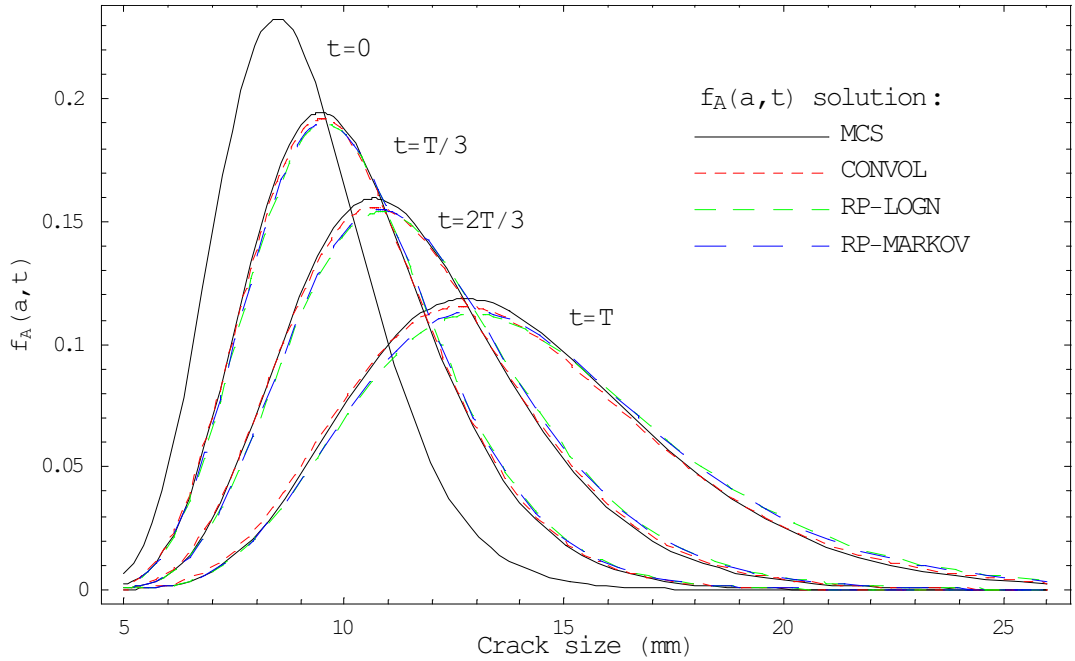

Figure 9-6: Crack size TPD for $\lambda_X = 10^4$ cycles, $\sigma_X = 0.5$.

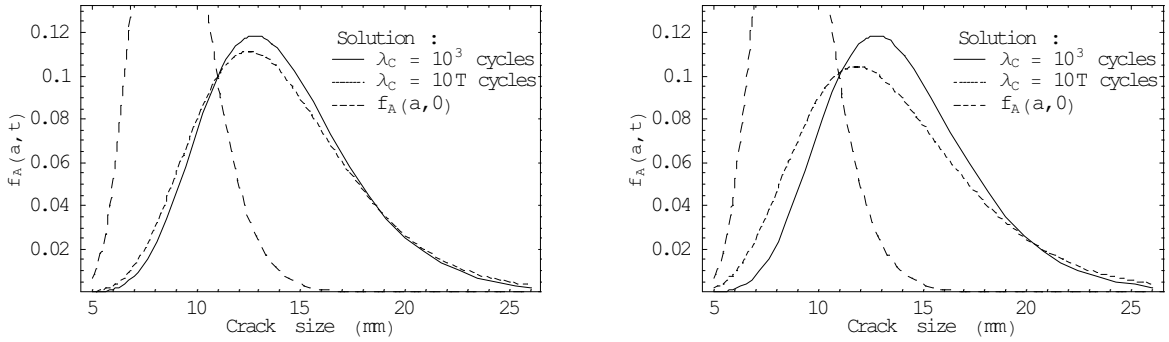

Figure 9-7: Influence of λ_X ($=\lambda_C$) on crack size distribution, $\sigma_X = 0.2$ (left), $\sigma_X = 0.5$ (right).

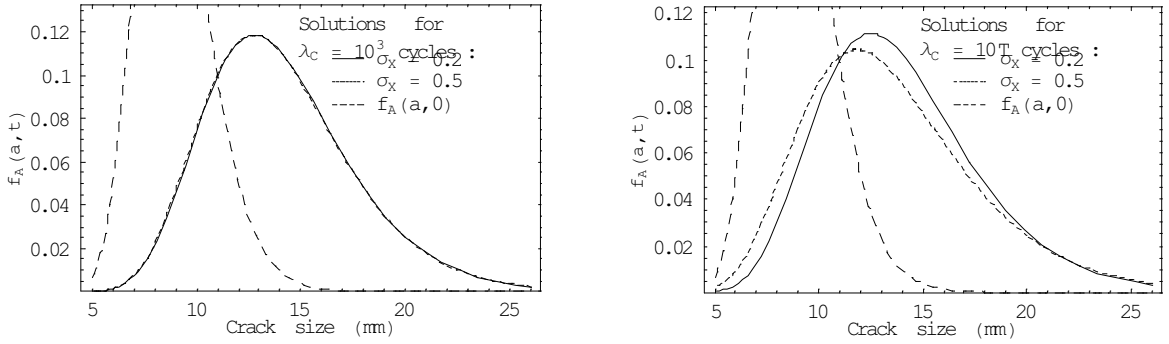

Figure 9-8: Influence of σ_X on crack size distribution, $\lambda_X = 10^3$ cycles (left), $\lambda_X = 10T$ cycles (right).

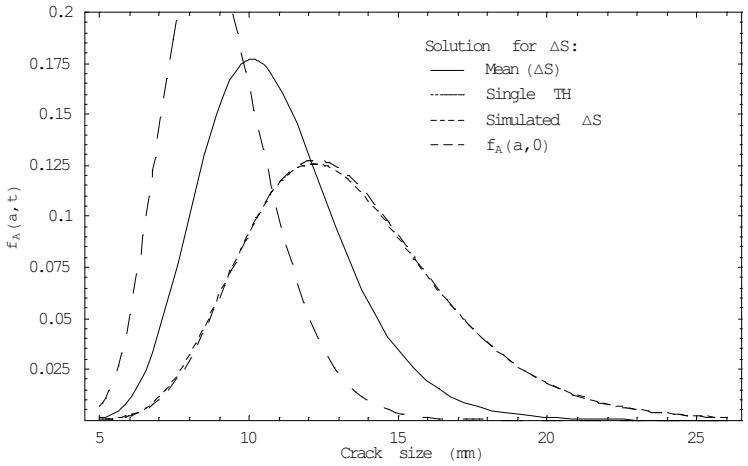

Figure 9-9: Simulation of stress ranges in crack size TPD evaluation, 10^2 stress ranges per load block.

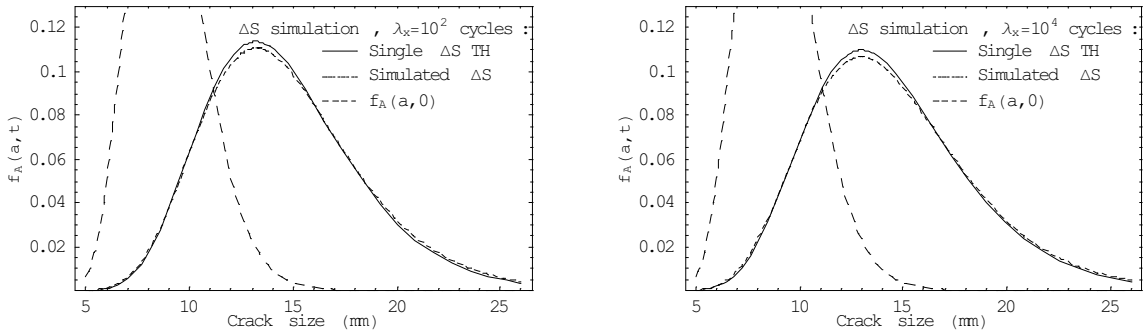

Figure 9-10: Simulation of stress ranges in crack size TPD evaluation, low cycle fatigue problem ($T = 10^3$ cycles).

Chapter 10

EVALUATION OF RESISTANCE TRANSITION PROBABILITY DENSITIES

10.1 Introduction

Evaluation of the time evolution of resistance distributions depends on the specific fracture or failure criterion considered, the number of cracks in a specific structural detail, the number of (additional) resistance random variables and whether the limit state function is given as an analytical or numerical function of crack size.

Two different methods of deriving resistance distributions are presented in this chapter. The first involves a second order approximation of resistance moments and an (arbitrary) choice of resistance distribution model. The second is a numerical solution where the probability content under the resistance cumulative distribution curve is obtained from a sequence of FORM or SORM analysis. Both solutions are illustrated through the NB reference problem described in section 8.1 and already studied in section 9.5. Solutions are developed based on a specific failure criterion, but are easily generalized to other failure criteria. Solutions derived in this chapter are also applicable to problems where resistance is not given in closed form, but as the solution to a numerical (FE) model.

10.2 Failure criterion and resistance degradation

The R6 failure assessment diagram (Kanninen and Popelar, 1985) is used as the overload failure criterion. According to this criterion, failure is characterized by points (K_r, S_r) falling

outside the curve:

$$K_r = \frac{S_r}{\sqrt{\frac{8.0}{\pi^2} * \log[\sec[\frac{\pi}{2} S_r]]}} \tag{10.1}$$

where K_r and S_r are functions of loading stress S and crack size A. For the center cracked panel problem, one has:

$$\begin{aligned} S_r(S_{pl}, A) &= \frac{S_{pl}}{S_{pc}} \frac{w}{(w - A)} \\ K_r(S_{el}, A) &= \frac{K_I(S_{el}, A)}{K_{IC}} = \frac{S_{el}\sqrt{\pi A}\sqrt{\sec(\frac{\pi A}{w})}}{K_{IC}} \end{aligned} \tag{10.2}$$

where S_{pl} and S_{el} are the effective plastic and elastic fracture stresses for the panel. One common simplification is to approximate the materials plastic collapse stress S_{pc} by the yielding stress, S_y. In this case, the effective plastic fracture criterion actually corresponds to yielding of the remaining cross section, and strain hardening is disconsidered. This (conservative) approximation is commonly made for very ductile materials.

Inserting equations (10.2) into (10.1) one obtains failure assessment curves that vary with crack size and which are functions of the effective elastic fracture stress S_{el} (vertical axes) and of the plastic fracture stress S_{pl} (horizontal axes). The failure stress for a given crack size (and time) is then given by the point where the identity line $S = S_{el} = S_{pl}$ crosses the failure assessment diagram for that crack size. Figure 10-1 shows what these curves look like for the NB reference problem described in section 8.1. Shown in the figure are failure curves for $t = 0$, $t = T/2$ and $t = T$, considering the mean value of the problems random variables ($\mu_{\mathbf{z}}$ - left in figure) and using the three-sigma rule ($\mu_{\mathbf{z}} + 3\sigma_{\mathbf{z}}$ - right in figure). It can be seen that, with these parameters, fracture of the panel is well within the elasto-plastic zone, hence justifying the use of the R6 failure assessment diagram in the failure probability assessment. It can also be seen in the figure that, for the large crack size at $t = T$ and with the three-sigma rule, fracture of the panel shifts slightly towards a more elastic fracture, due to the stress intensity factor growing faster than the plastic fracture stress.

Solving equation (10.1) with parameters (10.2) and with $S = S_{el} = S_{pl}$ one obtains an expression for the R6 failure load, as a function of crack size, yielding stress and critical stress intensity factor. This expression provides an R6 resistance degradation curve, or limit state function, which is given in terms of stresses and can hence be used directly in an overload failure probability evaluation:

$$R6(A, S_y, K_{IC}, t) = 6.710^{-6}(95000 - 625\ A(t))\ S_y \arcsec\left[\exp\left(\frac{0.4K_{IC}^2 \cos[0.021\ A(t)]}{(1 - 0.0066\ A(t))^2\ A(t)\ S_y^2}\right)\right] \tag{10.3}$$

Figure 10-2 shows resistance degradation in time corresponding to the failure assessment curves in figure 10-1. This figure provides an idea of the degree of non-linearity of the problem, in consideration of the variance of the random crack growth parameters.

10.3 Second-order second-moment approximation

In this section, two simple analytical solutions are presented for a plastic fracture criterion with (1) deterministic and (2) random yielding stress. An approximate solution is then derived for an elasto-plastic fracture criterion (using R6 failure assessment diagrams) with random yielding stress and random critical stress intensity factor.

As for the crack size TPDs, resistance distributions are evaluated at the end of each load block. A distribution model for the resistance is hypothesized and verified via Monte Carlo simulation.

10.3.1 Plastic fracture with deterministic yielding stress

The limit state function for the plastic fracture criterion and the centre cracked panel problem is:

$$R(A, t) = \frac{(w - A(t))}{w} s_y \tag{10.4}$$

with s_y being the deterministic yielding stress. Moments of the resistance are obtained, for a given crack size $A(t)$ at time t, as:

$$\begin{aligned} \mu_R(t) &= \frac{(w - \mu_A(t))}{w} s_y \\ \sigma_R^2(t) &= \left(\frac{s_y}{w}\right)^2 \sigma_A^2(t) \end{aligned} \tag{10.5}$$

Although this problem is very simplistic, it presents an interesting result. The smallest crack size corresponds to the largest resistance. If $A(t)$ has a log-normal distribution, limited by $a \geqslant 0$, then the resistance distribution becomes limited to $r \leqslant R(0, t) = s_y$. Hence, if the distribution of $A(t)$ is log-normal at all times, as was seen to be the case for the reference problem (section 9.5), the plastic fracture resistance follows a log-normal distribution on the variable $(s_y - r)$, with moments given by equations (10.5).

10.3.2 Plastic fracture with random yielding stress

For a random yielding stress S_y and the plastic fracture criterion (equation 10.4), resistance moments become:

$$\begin{aligned} \mu_R(t) &= \frac{(w-\mu_A(t))}{w}\mu_{S_y} \\ \sigma_R^2(t) &= \left(\frac{w-\mu_A(t)}{w}\right)^2 \sigma_{S_y}^2 + \mu_{S_y}^2 \left(\frac{1}{w}\right)^2 \sigma_A^2(t) + \left(\frac{1}{w}\right)^2 \sigma_A^2(t)\sigma_{S_y}^2 \end{aligned} \tag{10.6}$$

When a log-normal distribution is assumed for the yielding stress, the resistance becomes unbounded from above. The resistance, in this case, is the product of an inverted $(w-A(t))$ by a straight log-normal distribution. Hence, in this case, it is not straightforward to hypothesize on the form of the resistance distribution. As will often be the case, the form of the resistance distribution will depend on the relative values of crack size and other resistance parameters.

10.3.3 Elasto-plastic fracture with random S_y and K_{IC}

In section 10.2, an elasto-plastic (R6) failure assessment equation, providing failure stresses in terms of crack size, yielding stress and critical stress intensity factor, was derived (equation 10.3). In this section, this expression is used to derive an elasto-plastic resistance distribution from the distributions of crack size, yielding stress and critical stress intensity factor. Resistance moments are obtained by a second order approximation. Expanding expression (10.3) in a Taylor series, one obtains:

$$\begin{aligned} R6(\mathbf{x},t) &\approx R6(\overline{\mathbf{x}},t) + \sum_{i=1}^{n} \frac{\partial R6}{\partial x_i}(x_i - \overline{x_i}) + \frac{1}{2}\sum_{i=1}^{n}\sum_{j=1}^{n} \frac{\partial^2 R6}{\partial x_i \partial x_j}(x_i - \overline{x_i})(x_j - \overline{x_j}) + ... \\ &\approx R6(\overline{\mathbf{x}},t) + \boldsymbol{\nabla}_{R6}(\mathbf{x})|_{\overline{\mathbf{x}}} \cdot \{\mathbf{x}-\overline{\mathbf{x}}\} + \{\mathbf{x}-\overline{\mathbf{x}}\}^{\mathrm{T}} \cdot \mathbf{H}_{R6}(\mathbf{x})|_{\overline{\mathbf{x}}} \cdot \{\mathbf{x}-\overline{\mathbf{x}}\} + ... \end{aligned} \tag{10.7}$$

where:

$\mathbf{x}(t) = \{A(t), S_y, K_{IC}\}^{\mathrm{T}}$ is the vector of resistance random variables;

$\overline{\mathbf{x}}(t) = \{\mu_A(t), \mu_{S_y}, \mu_{K_{IC}}\}^{\mathrm{T}}$ is the mean-value vector;

$\boldsymbol{\nabla}_{R6}(\mathbf{x}) = \{\frac{\partial R6}{\partial A}, \frac{\partial R6}{\partial S_y}, \frac{\partial R6}{\partial K_{IC}}\}$ is the gradient vector;

$\mathbf{H}_{R6}(\mathbf{x}) = \{\frac{\partial \boldsymbol{\nabla}}{\partial A}, \frac{\partial \boldsymbol{\nabla}}{\partial S_y}, \frac{\partial \boldsymbol{\nabla}}{\partial K_{IC}}\}^{\mathrm{T}}$ is the Hessian matrix.

Taking the expectation over (10.7), one obtains:

$$\mu_{R6}(\mathbf{x},t) \approx E[R6(\overline{\mathbf{x}},t)] + E[\boldsymbol{\nabla}_{R6}(\mathbf{x})|_{\overline{\mathbf{x}}} \cdot \{\mathbf{x}-\overline{\mathbf{x}}\}] + E[\{\mathbf{x}-\overline{\mathbf{x}}\}^{\mathrm{T}} \cdot \mathbf{H}_{R6}(\mathbf{x})|_{\overline{\mathbf{x}}} \cdot \{\mathbf{x}-\overline{\mathbf{x}}\}] \tag{10.8}$$

where the second term vanishes. The expectation over the third term leads to the covariance matrix:

$$\mathbf{cov}(\mathbf{x}) = \begin{bmatrix} \sigma_A^2(t) & \mathrm{cov}(A, S_y) & \mathrm{cov}(A, K_{IC}) \\ & \sigma_{S_y}^2 & \mathrm{cov}(S_y, K_{IC}) \\ \text{sym.} & & \sigma_{K_{IC}}^2 \end{bmatrix} \tag{10.9}$$

where $\mathrm{cov}(A, S_y) = \mathrm{cov}(A, K_{IC}) = 0$ and the covariance between the two material properties is assumed to be zero ($\mathrm{cov}(S_y, K_{IC}) = 0$) although it is not necessarily so. In this case, equation (10.8) is reduced to:

$$\begin{aligned} \mu_{R6}(\mathbf{x}, t) &\approx R6(\overline{\mathbf{x}}, t) + \frac{1}{2}\mathbf{D}_{\mathbf{H}_{R6}}(\mathbf{x})|_{\overline{\mathbf{x}}} \cdot \boldsymbol{\sigma}_{\mathbf{X}}^{\mathbf{2}}(\mathbf{x})] \\ &\approx R6(\overline{\mathbf{x}}, t) + \frac{1}{2}\sum_{i=1}^{n} \frac{\partial^2 R6}{\partial x_i^2}\sigma_{X_i}^2 \end{aligned} \tag{10.10}$$

where $\mathbf{D}_{\mathbf{H}_{R6}}(\mathbf{x})$ is the vector formed by elements in the principal diagonal of the Hessian and $\boldsymbol{\sigma}_{\mathbf{X}}^{\mathbf{2}}(\mathbf{x})$ is the variance vector, formed by the elements in the principal diagonal of the covariance matrix $\mathbf{cov}(\mathbf{x})$.

The variance of the elasto-plastic resistance is obtained as:

$$\begin{aligned} \sigma_{R6}^2(\mathbf{x}, t) &\approx E[(R6(\mathbf{x}, t) - \mu_{R6}(\mathbf{x}, t))^2] \\ &\approx E\left[\begin{pmatrix} R6(\overline{\mathbf{x}}, t) + \boldsymbol{\nabla}_{R6}(\mathbf{x})|_{\overline{\mathbf{x}}} \cdot \{\mathbf{x}-\overline{\mathbf{x}}\} \\ +\{\mathbf{x}-\overline{\mathbf{x}}\}^{\mathrm{T}} \cdot \mathbf{H}_{R6}(\mathbf{x})|_{\overline{\mathbf{x}}} \cdot \{\mathbf{x}-\overline{\mathbf{x}}\} \\ -R6(\overline{\mathbf{x}}, t) \\ -E[\{\mathbf{x}-\overline{\mathbf{x}}\}^{\mathrm{T}} \cdot \mathbf{H}_{R6}(\mathbf{x})|_{\overline{\mathbf{x}}} \cdot \{\mathbf{x}-\overline{\mathbf{x}}\}] \end{pmatrix}^2\right] \\ &\approx E[\boldsymbol{\nabla}_{R6}^2(\mathbf{x})|_{\overline{\mathbf{x}}} \cdot \{\mathbf{x}-\overline{\mathbf{x}}\}^2] \\ &\approx \boldsymbol{\nabla}_{R6}^2(\mathbf{x})|_{\overline{\mathbf{x}}} \cdot E[\{\mathbf{x}-\overline{\mathbf{x}}\}^2] \\ &\approx \boldsymbol{\nabla}_{R6}^2(\mathbf{x})|_{\overline{\mathbf{x}}} \cdot \boldsymbol{\sigma}_{\mathbf{X}}^{\mathbf{2}}(\mathbf{x}) \\ &\approx \sum_{i=1}^{n}\left(\frac{\partial R6}{\partial x_i}\right)^2 \sigma_{X_i}^2 \end{aligned} \tag{10.11}$$

since the first and the fourth terms, as well as the third and the fifth terms in the inner sum in the second line of equation (10.11) cancel themselves out.

It is seen that the R6 resistance moments are not difficult to derive, once one takes the first and second order derivatives of the R6 resistance curve. As a conclusion to this sub-section, it is seen that resistance distribution moments, using the R6 failure assessment diagram as elasto-plastic failure criterion, considering random S_y and K_{IC}, with crack size distributions given as the solution of a random process crack propagation model, which by its turn includes

random ΔS, random A_0 and random crack propagation rate X, can be efficiently computed. In brief, the whole evaluation includes a single mean crack growth computation, with simulated stress ranges, a numerical integration for A_0, crack size distribution fits, evaluation of a couple of closed form derivatives and resistance moments, and finally a distribution fit to the resistance. The trick in this solution is to find the appropriate distribution model for the resistance, as will be seen in the sequel (section 10.6).

10.4 Evaluation of the resistance CDF by FORM

An alternative solution for the resistance distribution, which avoids the arbitrary choice of a distribution model, and which provides an accurate description of the resistance distributions tails, can be obtained by evaluating the probability content of the cumulative resistance distribution at successive resistance levels. Resistance can be an arbitrary function of crack size, yielding stress, K_{IC} and other variables, given in analytical or in numerical form. Using the R6 failure Assessment diagram, for example, the probability that the resistance be less than a fixed value r_i is: $P[R6(t) < r_i] = F_R(r_i, t)$. Hence, the probability content of the resistance cumulative distribution at point r_i can be evaluated as:

$$\begin{aligned} F_R(r_i,t) &= P[R6(A(t), S_y, K_{IC}) < r_i] \\ &= P[R6(A(t), S_y, K_{IC}) - r_i < 0] \\ &= \int_{g(\mathbf{z},r_i,t)<0} f_{\mathbf{Z}}(y)dy \end{aligned} \tag{10.12}$$

where $f_{\mathbf{Z}}(z)$ is the joint probability distribution of the resistance random variables and the limit state function is:

$$g(\mathbf{z},r_i,t) = R6(A(t), S_y, K_{IC}) - r_i = 0 \tag{10.13}$$

Equation (10.12) with (10.13) can be solved by FORM or SORM. By varying the parameter r_i and repeating the FORM analysis, the probability content of the whole resistance CDF is evaluated. By repeating the evaluation for distinct times, the whole resistance TPD is obtained, resulting in the lists $\mathbf{F}_{t_j} = \{F_i\}$, $i = 1, ..., n$; $j = 1, ..., n_{lb}$. The probability density function is evaluated numerically as: $f_R(r,t) = \frac{d}{dr} F_R(r,t)$.

In contrast with the second-order second-moment approximation, which approximates resistance moments by a series expansion around the mean, and extrapolated the probability content in the distribution's tails by an (arbitrary) distribution model, the numerical FORM

solution provides the actual probability content in the tails, apart from (second order) errors due to linearization of the limit state function. The FORM approximation is actually asymptotically exact, providing better results at the tails than around the means.

Clearly, a complete solution for $F_R(r,t)$ requires F_i to be evaluated at a significant number of points, which requires a huge number of FORM analysis and limit state function calls. The total number of limit state function calls can be reduced by a smart choice of starting point for the FORM algorithm. One possibility is to use the design point arrived at with parameter r_i as the starting point of the solution for r_{i+1}. Because r_i and r_{i+1} are only a small distance apart, convergence for r_{i+1} is much faster than for the first point r_i. Numerical results show that indeed the number of limit state function calls is significantly reduced.

A completely numerical solution requires a large number of r_i evaluation points, in an effort that could perhaps be comparable to Monte Carlo simulation. One alternative, which may permit the number of evaluation points to be reduced, is to fit a specific distribution function to a reduced number of r_i points. This solution also involves an arbitrary choice of resistance distribution model, but is supposedly better than the second moment approximation, because the density fit is done at the distributions (lower) tail and not at the means. These alternative solutions are compared in the sequel in an application to the reference problem introduced earlier.

10.5 Evaluation of the probability of failure due to critical crack growth using function $TTTG(a_0, a)$

In chapter 11, overload failure probabilities (using the R6 Failure Assessment diagram) are compared with critical crack growth probabilities of failure, for the reference problem and for some variations of it. A critical crack size value $a_{cr} = 65.0$ mm is chosen such as to limit explosive growth of the stress intensity factor.

The total time to grow function $TTTG(a_0, a)$ introduced in chapter 9 and used to evaluate the crack size TPDs can also be used to compute critical crack growth failure probabilities by FORM or SORM. The critical crack growth probability of failure is calculated as:

$$P_{f_{A_{crit}}}(t) = \int_{g(\mathbf{z},t)<0} f_{\mathbf{Z}}(y)dy$$

where the limit state function is:

$$
\begin{aligned}
g(\mathbf{z},t) &= g(a_0, a_{crit}, x, t) \\
&= x\ TTTG(a_0, a_{crit}) - t = 0
\end{aligned}
$$

The unitary crack propagation rate X enters the equation as a multiplication factor because time to grow is a linear function of the crack propagation rate. One is also reminded that the function $TTTG(a_0, a)$ is derived using a mean crack propagation rate $\mu_X = 1$.

The solution is very fast to compute because each limit state evaluation represents only an ordinary function evaluation. The efficiency of this solution arises from the fact that repetitive (possibly numerical) cycle-by-cycle crack growth computations are replaced by repetitive evaluations of the interpolated function $TTTG(a_0, a)$, which by its turn is obtained from a single (mean) crack growth computation. The solution, although very efficient, is limited to problems involving random A_0, random crack propagation rate X, random A_{crit} and, via simulation, random ΔS. Some results are shown in chapter 11.

10.6 Comparison of solution methods

In this section, resistance TPD's for the reference problem described in section 8.1 and already studied in chapter 9 are derived. The following notation is used for resistance TPD solutions:

Notation	$f_R(r,t)$ Solution Method
MCS - χ^2 fit	Sampled histogram min. χ^2 fit
SM AP.	Second order - second moment approximation
FORM - ANAL	FORM with analytical distribution model
FORM - NUMER	fully numerical FORM solution

10.6.1 MC simulation and histogram distribution fit

As was done for the crack size TPDs, MC simulation is used to estimate the resistance distribution model. The R6 resistance, as derived above, is a non-linear function of crack size, S_y and K_{IC}. Hence, it becomes difficult to know beforehand what the distribution of the resistance will be. However, the deterministic R6 limit state function (equation 10.3) is used to simulate 10^4 resistance samples, from 10^4 sampled crack size, S_y and K_{IC} values. Results are presented in figures 10-3 and 10-4, which show an histogram of the sampled resistance values, a χ^2 distribution fit to the sampled histogram and a distribution fit to the second-order approximated resistance moments, in both linear and logarithmic scales.

The distribution fit shown in figures 10-3 and 10-4 is obtained by assuming a log-normal distribution of the resistance at the first load block, a normal distribution between the 2^{nd} and 5^{th} load blocks, and inverted log-normal distributions from the 6^{th} load block onwards, with limiting values varying from $r_{\max} = 550$ to $r_{\max} = 400$. The PDF of the inverted log-normal distribution is:

$$f_R(r,t) = \frac{1}{\sqrt{2\pi}(r_{\max} - r)\ \sigma^2_{\ln(r_{\max}-r)}} \exp\left[-\frac{1}{2}\left(\frac{\ln(r_{\max} - r) - \mu_{\ln(r_{\max}-r)}}{\sigma^2_{\ln(r_{\max}-r)}}\right)^2\right], \qquad r < r_{\max} \tag{10.14}$$

where $\mu_{\ln(r_{\max}-r)}$ and $\sigma^2_{\ln(r_{\max}-r)}$ are the mean and variance of the normal variable $Y = \ln(r_{\max} - R)$.

The χ^2 goodness-of-fit test gives confidence varying from around 10% at the first load blocks to 0% at the last load blocks, but the KS goodness-of-fit test results in confidence varying from 80% to 10%, which is not a bad confidence level. Apart from the goodness-of-fit tests, the visual evidence in figures 10-3 and 10-4 is to a shift of the resistance distribution's tail from right to left, i.e., from larger to smaller values of the resistance. Hence, it is seen that the resistance distribution shifts from (something like) a log-normal, to (something like) a normal and to (something like) an inverted log-normal distribution as the crack grows. The explanation of this behavior is not difficult to grasp: it can be said, for instance, that at earlier times the distributions of S_y and K_{IC} dominate the resistance distribution and that, as the crack grows, the crack size distribution plays an increasingly dominant role in the resulting resistance distribution. It was seen earlier, for example, that for a plastic failure criterion with deterministic yielding stress and a log-normally distributed crack size, the resistance follows an inverted log-normal distribution (section 10.3.1).

Figures 10-3 and 10-4 also show that, given the appropriate choice of distribution function, the second order - second moment approximation to the resistance is quite accurate, with the resulting second order and histogram-fitted distributions being nearly indistinguishable. The critical part of the solution is hence to identify the appropriate distribution model. In terms of the EUR approximation, the appropriate distribution model is the one that results in the correct ensemble up-crossing rate, as will be seen in the sequel. The log-normal to normal to inverted log-normal distribution model, referred in short as LN-N-iLN distribution model, is used in the sections that follow.

10.6.2 Derivation of resistance distribution by FORM

A completely numerical resistance TPD, which does not require an arbitrary distribution model for the resistance, is obtained from a series of FORM analysis, using the R6 resistance curve as limit state function. The resistance distribution is evaluated between $r_{\min} = \mu_R - 9\sigma_R$ and $r_{\max} = \mu_R + 3\sigma_R$, with the second-order resistance moments being used to define the evaluation interval. The Markov-approximated crack size distributions are used. Two hundred r_i evaluation points are considered, for each of the 10 time steps, resulting in a total of 2000 FORM analysis. The resulting resistance distribution is shown in figure 10-5. Also shown in the figure are resistance distributions obtained by fitting the LN-N-iLN distribution model 1) to a reduced number of r_i evaluation points (30 points for each load block, in this case) and 2) to the second-order resistance moments. It can be seen that the FORM-based solutions are virtually indistinguishable, whereas the second-order resistance moment solution is slightly offset.

The total number of limit state function calls, for the fully numerical solution and using a smart starting point for the FORM algorithm, was around 10^4 limit state function calls. This is a huge number when one considers a numerical limit state function. However, it still represents an improvement over MC simulation, because these limit state functions are time-independent, whereas the straight MC simulation solution required 10^4 time-dependent crack growth computations. The approximated (analytical, distribution model based) FORM solution required 2900 limit state function calls. The computation time for the distinct solutions was 770 seconds for the MC simulation, 70 seconds for the second order approximation, 80 seconds for the distribution-based FORM resistance (30 r_i evaluation points) and 90 seconds for the fully numerical FORM resistance (200 r_i evaluation points). These evaluation times and number of limit state function calls depend on the particular convergence criteria adopted in the FORM solutions. The convergence criterion used was a variation in the reliability index: $\Delta\beta < 10^{-1}$. This convergence criterion is not very strict, but it is nevertheless enough as will be seen in the sequence.

Although there seems to be little difference between the three resistance distributions shown in figure 10-5, one has to consider what ensemble up-crossing rates result from these distributions. This is done in figure 10-7. In the first column (left), the lower tail of the three distribution is shown, in logarithmic scale, together with the barrier crossing rate expression $\upsilon^+(r,t)$ for the load process considered in the problem. In the second column (right), the product $\upsilon^+(r,t) f_R(r,t)$ is shown, in a linear scale. It can be seen that ensemble crossing rates obtained from the three distributions (the area under the curves) differ by a factor of

2 or 3. Although these results are not too bad, the analysis reveals that slight disturbances of the resistance's lower tail result in major changes both in the region where the product $\upsilon^+(r,t)f_R(r,t)$ attains its maximum as well as in the size of this maximum. It will be seen in the sequel that the quality of an EUR solution using an arbitrary resistance distribution model depends on the distance between the maximum of product $\upsilon^+(r,t)f_R(r,t)$ (the kernel of equation 8.1) and the maximum of the resistance distribution $f_R(r,t)$, as shown in figure 10-6.

10.7 Concluding remarks

It was seen in the previous section that the EUR solution can be highly dependent on the resistance distribution model, making solutions based on an arbitrary distribution model highly unreliable. Such a result should not come as a great surprise. It is widely known that small failure probabilities are largely affected by the tails of the underlying distributions. While (small) failure probabilities evaluated by FORM depend on the tail of the joint PDF at a single point (the design point), the EUR solution depends on the resistance distribution's tail in a small (unknown) area around which the product $\upsilon^+(r,t)f_R(r,t)$ attains its maximum.

This result can also be related to a broader discussion comparing second-moment and reliability analysis (Sudret and Kiureghian, 2002). There are a handful of methods which aim at characterizing second order statistical moments (i.e., means and variances) of response quantities. These include the Perturbation method, the Weighted Integral method and in a general sense, stochastic finite element methods. Although these methods can be quite accurate in evaluating resistance moments, their use in reliability analysis is questionable. Using second-moment results in reliability analysis is equivalent to extrapolating "around the mean" results to the tails of the distribution, by means of an implicit or explicit distribution model. Reliability methods, on the other hand, including FE reliability methods (Sudret and Kiureghian, 2002), aim at calculation the failure probability associated with a limit state function. This calculations (and all approximations involved) are performed in the tail of the distribution, in one point rather than over the whole resistance domain, and provide the actual (less approximation errors) probability content *beyond* the limit state function.

The discussion is pertinent to the problem in hands. The EUR approximation aims at evaluating failure probabilities. When this evaluation is based on the resistance distribution, which by its turn is based on a second order approximation and on an arbitrary choice of resistance distribution model, failure probabilities become dependant on the distribution model.

The alternative developed here, which involves a number of FORM analysis for the resistance distribution, and requires a large number of limit state function calls, is certainly not the most efficient. However, it is a numerical solution which is not based on arbitrary distribution models. A similar numerical solution, certainly more efficient, can perhaps be obtained from a numerical up- or out-crossing rate evaluation with a random failure domain boundary. One example is the parallel system sensitivity solution with random resistance parameters described in the first part of the literature review. Although there is a sense of having missed on the most important aspect of the solution, due to time restrictions this possibility was not investigated. The possibility, however, should be kept in mind, as a numerical solution which allows a drastic reduction in computation time. It is definitely suggested for a continuation of this research. In comparison to a numerical FORM solution for the resistance distribution, which requires to the order of 200 FORM analysis for the resistance distribution at one specific time, and a subsequent numerical integration for the ensemble up-crossing rate, the parallel system sensitivity solution (could) yield the ensemble crossing rate directly, with as little as one parallel system FORM analysis.

10.8 Figures

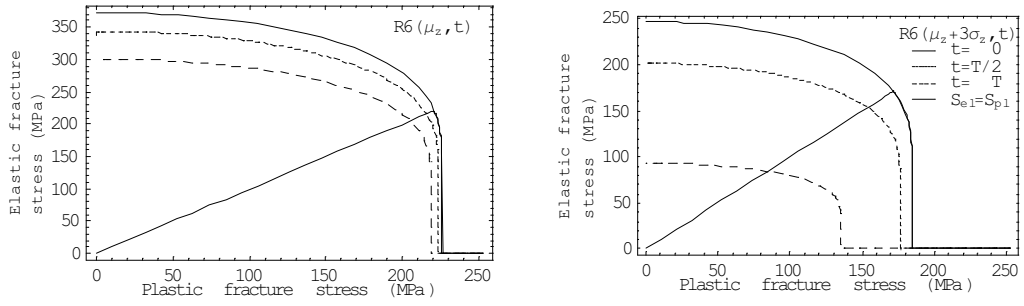

Figure 10-1: R6 failure assessment diagrams for mean $\mu_{\mathbf{z}}$ and for $\mu_{\mathbf{z}} + 3\sigma_{\mathbf{z}}$.

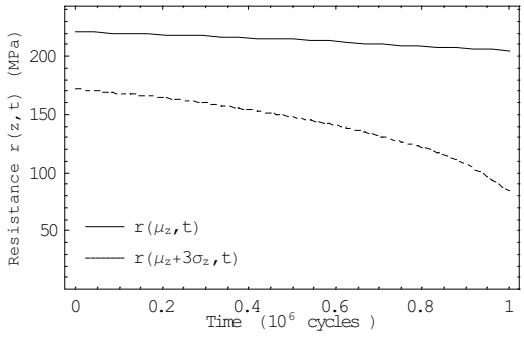

Figure 10-2: Resistance degradation for mean $\mu_{\mathbf{z}} + 3\sigma_{\mathbf{z}}$.

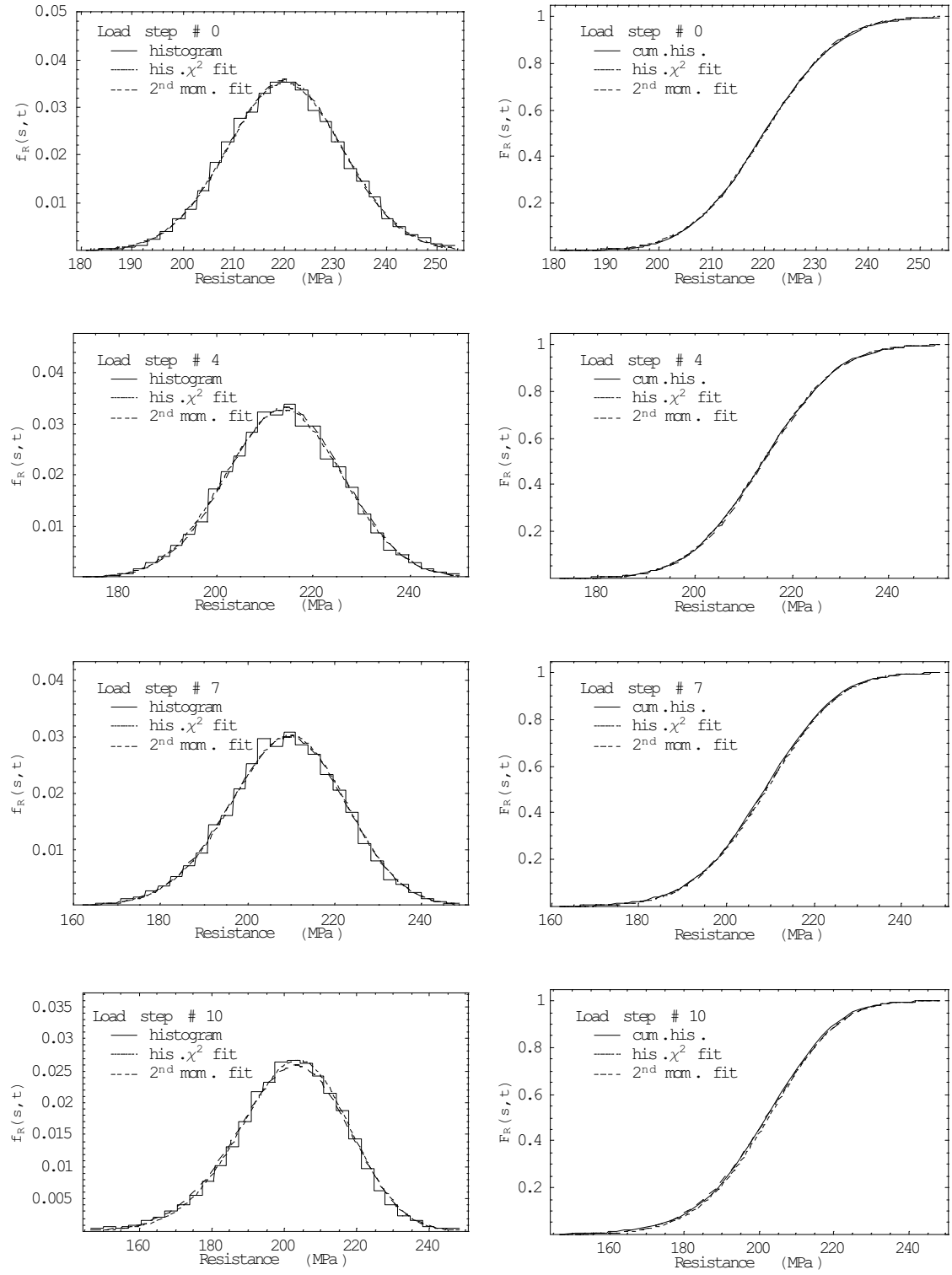

Figure 10-3: Histogram and second moment distribution fit, NB reference problem.

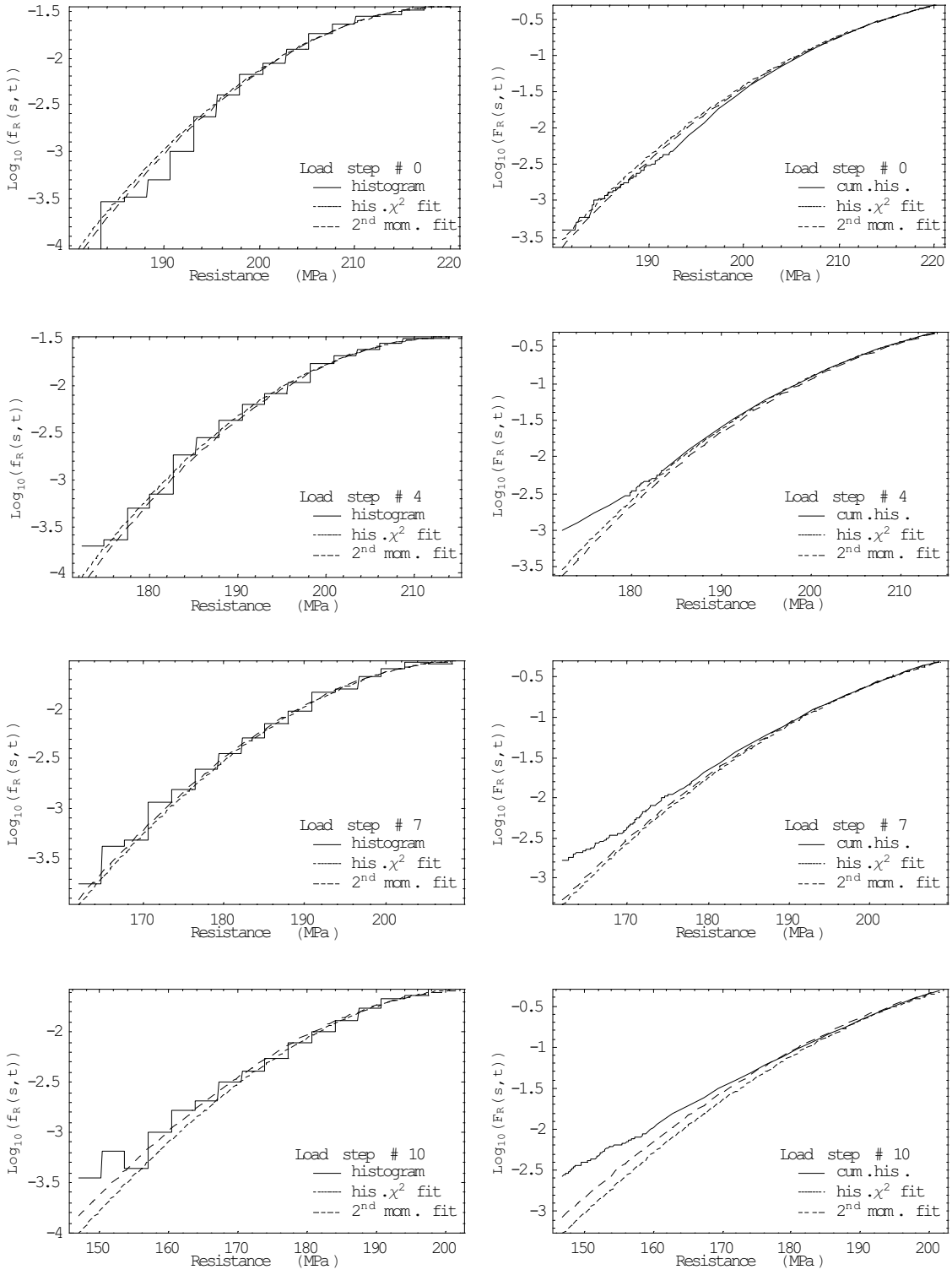

Figure 10-4: Histogram and second moment distribution fit, NB reference problem (log-scale).

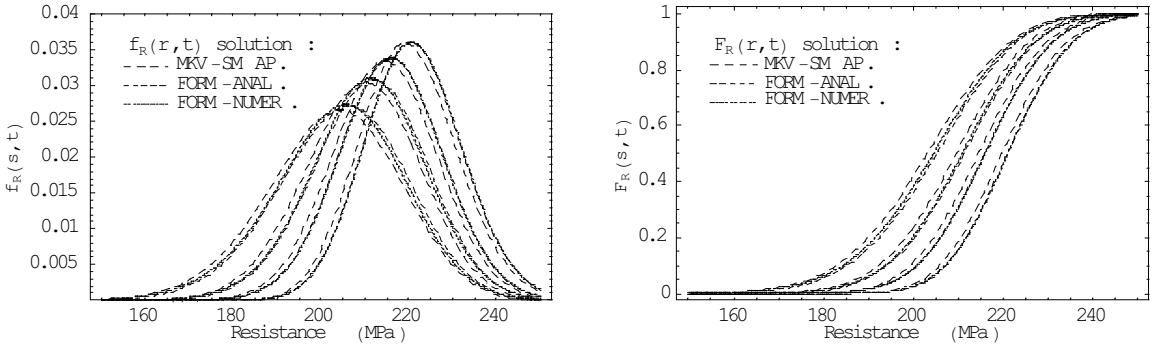

Figure 10-5: Resistance distribution by FORM, NB reference problem.

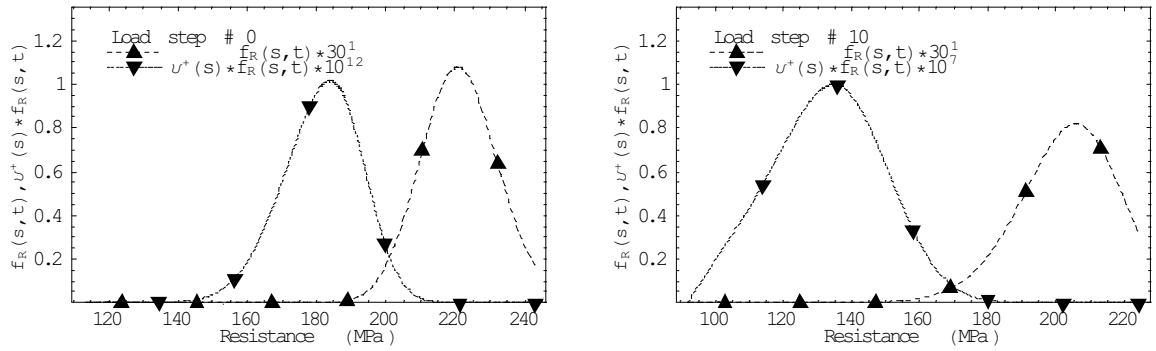

Figure 10-6: Distance between $\upsilon^+(r,t)f_R(r,t)$ and resistance mean, NB reference problem.

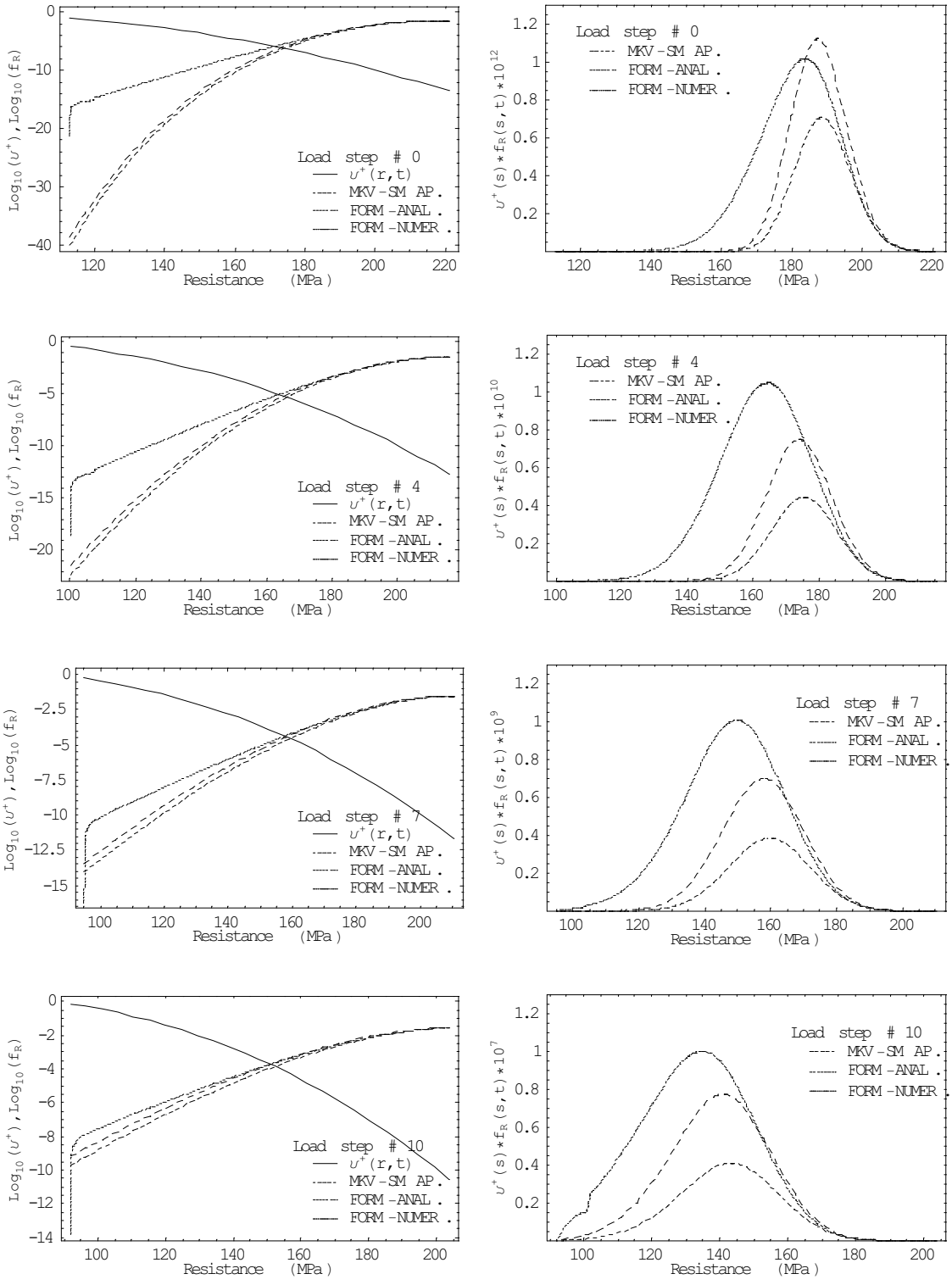

Figure 10-7: Resistance distribution and product $\upsilon^+(r,t)f_R(r,t)$, NB reference problem.

Chapter 11

FAILURE PROBABILITY RESULTS AND VARIATIONS OF THE REFERENCE PROBLEM

11.1 Failure probability results for NB reference problem

In chapters 9 and 10, crack size and resistance TPDs for the NB reference problem described in section 8.1 were evaluated. Crack size TPDs where obtained as the solution to a random process crack propagation problem. Resistance TPD's where derived from crack size TPDs by adopting a specific failure criterion. As a summary of previous computations for the reference problem, figure 11-1 shows a comparison between the time evolution of crack size (left) and resistance (right) distributions, using the elasto-plastic fracture criterion. It can be seen in the figure that, due to the additional resistance random variables (S_y and K_{IC}), the time-variation of the resistance distribution, especially its variance, is not as pronounced as the time-variation of the crack size distribution.

In this section, failure probability results for the NB reference problem are presented. EUR failure probability results obtained through three resistance distributions are compared. EUR failure probability results are also compared with Monte Carlo simulation and with (RV-based) FORM solutions. Overload failure probabilities are compared with critical crack growth failure probabilities. The following notation is used to refer to failure probability results throughout this and further sections:

Notation	$P_f(t)$ Solution Method
TI	Time Integrated (extreme value FORM)
FPI	Fast Probability Integration (time-variant rel. FORM)
EUR	Ensemble Up-crossing Rate approximation
MCS	Monte Carlo simulation (mean)
MCS-68% CI	Upper bound of MCS 68% confidence interval
Acrit	Critical crack growth

Unless otherwise stated, the Diffusive Markov solution is adopted for the crack size distributions. Resistance distributions considered are indicated using the abbreviations introduced in section 10.6.

11.1.1 Comparison of EUR solutions and appreciation of the EUR error

Figure 11-2 shows overload failure probability results for the NB reference problem, obtained by the EUR approximation and by Monte Carlo simulation. Monte Carlo simulation results are not based on a complete simulation of load process samples, but on the integration of expression (7.42) based on 10^4 resistance samples. Three EUR solutions are shown, using the three resistance distributions derived in section 10.6. One can see that the numerical FORM-based resistance distribution leads to the (exact) MC simulation result for most of the observed time interval. For larger times, the (conservative) error of the EUR approximation starts to appear. The FORM and the second-order approximated resistance solutions, based on the LN-N-iLN distribution model, lead to approximations of the correct failure probabilities. These approximations are not too bad, considering the EUR results shown in figure 11-1. However, as stated before, these results are highly sensitive to the resistance distribution model.

The EUR failure probability correction cannot be used in this problem because the EUR error function derived in chapter 5 is strictly valid for Gaussian barriers only. For this problem, for the large times where the error is significant, the resistance distribution is strongly squewed, as seen by the inverted Log-normal distribution fit. Nevertheless, where MC simulation results not available, a crude idea of the order of magnitude of the EUR error could be obtained from a Gaussian error estimate. Figure 11-3 shows a representation of the normalized random barrier (μ_R, $\mu_R + \sigma_R$ and $\mu_R - \sigma_R$ curves, left in figure), and the evolution of the (Gaussian) error parameter $\sqrt{(\sigma_R^2 + 1)/\mu_R}$ (center). The Gaussian-predicted EUR error is shown right in the figure. It can be seen that the predicted Gaussian error (figure 11-3) is smaller than the actual error seen in figure 11-2. Again, this difference is due to the

squeweness of the resistance distribution.

11.1.2 Comparison with other failure probability results

Figure 11-4 shows overload failure probability results obtained by TI FORM analysis and by Fast Probability Integration FORM, as well as critical crack growth failure probabilities obtained by FORM (limit state function 7.32). The time-variation of sensitivity coefficients of the TI and FPI FORM solutions is shown in figure 11-5. Sensitivity coefficients provide an estimate of the relative contribution of each random variable towards the failure probability. At time $t = T = 10^6$ cycles, these sensitivity coefficients are:

$$\begin{aligned} \boldsymbol{\alpha}^2_{TI} &= \{0.03, 0.70, 0.18, 0.04, 0.04\}; \\ \boldsymbol{\alpha}^2_{FPI} &= \{0.03, 0.72, 0.20, 0.03, 0.02\}; \end{aligned} \tag{11.1}$$

for the variables $\mathbf{Z} = \{Z_1, A_0, X, S_y, K_{IC}\}$, where $Z_1 = S_T(s)$ in the extreme-value analysis and $Z_1 = \Phi^{-1}\left[P_f(T \mid \mathbf{z})\right]$ in the FPI solution. It can be seen that, at time T, the initial crack size A_0 dominates the failure probability, followed by the crack propagation rate X.

It is also interesting to note how the sensitivity coefficient of the initial crack size random variable A_0 increases in time. Such result could be seen as counter-intuitive in a first view. However, it is important to remember that this is a fairly non-linear problem on crack size $A(t)$. Hence, the larger A_0, the faster $A(t)$ grows. So, the importance of random variable $A(t)$ in the problem, which increases as $A(t)$ increases, is reflected directly in variable A_0. This is an issue regarding the initial condition in a highly non-linear problem.

The (RV-based) FPI solution, shown in figure 11-4, agrees fairly well with the random process-based MC simulation and EUR solutions. This is a consequence of the fact that the resulting crack size random process turns out to be highly correlated. This can be seen in figure 11-6, which shows correlation coefficients $\rho(A_0, A(t))$ and $\rho(A(t), A(T))$ estimated from the crack growth samples used in section 9.5.1. The fact that the resulting crack size random process is highly correlated does not affect the EUR approximation, as long as the correlation length of the crack propagation rate random process ($\lambda_X = 10^4$ cycles) is not too large, and the crack size distribution can still be properly evaluated.

The computation time for the MC simulation failure probability solution was 935 seconds. This includes sampling of crack growth random variables, crack growth computations, sampling of resistance random variables and evaluation of resistance degradation. At 10^4 samples, this computation time corresponds to around 0.1 seconds per sample. As stated

earlier, single crack growth computations are very fast because the stress intensity factor and geometry function are analytical for this problem, but this is not necessarily the case. Total computation time for the TI and FPI FORM solutions was 150 and 85 seconds, with 414 and 550[1] limit state function calls, respectively, for 15 time evaluation points. This corresponds to 414 and 550 crack growth computations. For comparison, the numerical FORM EUR solution was obtained in 220 seconds, with around 0.4 seconds being spent in the mean crack growth computation, 75 seconds spent in the crack TPD computation and another 150 seconds spent in the resistance distribution computation. Evaluation of the resistance distribution required 10^4 static limit state function evaluations.

Computation time for the critical crack growth FORM analysis (equation 7.32) was 25 seconds, with 216 limit state function calls. This computation is very fast, comparing to the TI and FPI FORM analysis, because it is based on the $TTTG(a_0, a)$ function (equation 9.42) used in the crack size TPD evaluation. Hence, 0.4 seconds are spent in the mean crack growth computation, and the remaining time is spent in the FORM algorithm and in repetitive calls to equations (7.32) and (9.42).

11.1.3 Barrier failure dominance in the fatigue and fracture reliability problem

The fact that the EUR error is non-zero at large times, and the sensitivity coefficients shown in figure 11-5, in a rough comparison with results of chapter 5, suggest *barrier failure dominance*. These results suggest that, at large times, failure is dominated by variance of the barrier. Barrier random variables, in this problem, are A_o, X, S_y and K_{IC}, which jointly account for 97% of the failure probability in the two FORM analysis.

It is interesting to note that the so-called barrier failure dominance increases in time, as seen by the sensitivity factors in figure 11-5 and by the relation between overload and critical crack growth failure probabilities (figure 11-4). Sensitivity coefficients of the load (variables S_T and $\Phi^{-1}[P_f(T \mid \mathbf{z})]$) decreases from around 0.4 to nearly zero. As barrier failure dominance increases, so does the error of the EUR approximation.

Barrier failure dominance also helps understand the time-integrated (extreme-value FORM) results shown in figure 11-4. The TI solution is conservative, as expected, although not excessively so. This can again be attributed to barrier failure dominance or, more specifically, to the fact that barrier variance is much larger than load process variance. Two indications

[1] These numbers, of course, deppend on the efficiency of the optimization algorithm and on the convergence criterion used in the FORM analysis. They where obtained using the HLRF algorithm, with the convergence criterion: $\Delta\beta < 10^{-3}$.

of the small (relative) variance of the load process are the small sensitivity coefficient of the extreme value random variable and the extreme value distribution itself, which at 10^6 load cycles shows very little scatter (figure 8-1, top left).

Interestingly, although the problem can be said to be barrier failure dominated, the overload failure probability is still a few times larger than the critical crack growth failure probability. It is perhaps adequate to introduce a new concept here. Critical crack growth, for this instance, is a barrier defined - not dominated - failure. When critical crack growth occurs, an overload is certain, and whether it happens one cycle earlier or later makes no difference. An overload only occurs when the barrier "collapses". Barrier failure dominance, in terms of the overload failure problem, means that an overload is more likely to occur due to a (small) outcome of the barrier rather than due to a (large) peak of the load process. In terms of the present problem, for example, barrier failure dominance means that an overload is more likely to occur due to a large random outcome of the initial crack size, rather than due to an exceptionally large peak of the load process. An overload failure, it should be remembered, can be dominated by the load process, by the barrier or by none.

11.1.4 Using barrier failure dominance to choose the appropriate solution method for a problem

In chapter 5 it was argued that increasing barrier failure dominance would benefit those solution methods that simplify the problem in the load side, like the time-integrated approach. On the other hand, vanishing barrier failure dominance or load process dominance would benefit those solutions that simplify the problem in the barrier side, like the EUR approximation. In this context, it is appropriate to make a distinction between the barrier variables A_o, X, S_y, K_{IC} (and ΔS). A_o, X and ΔS are crack growth random variables, whereas S_y and K_{IC} are resistance random variables. An increase in the variance of any of these variables will contribute to barrier failure dominance, and will be reflected in an increase of the respective sensitivity factor. It can be argued that an increase in the variance of resistance variables will lead to a more linear barrier dominated problem, where the overload failure probability is significant and the EUR approximation is inaccurate. On the other hand, an increase in the variance of crack growth random variables will lead to increasingly non-linear problems, and to a shift from barrier-dominated to barrier-defined failure (i.e., critical crack growth). For problems of barrier-defined failure, the overload failure problem can be by-passed altogether, as the overload failure probability becomes equal to the critical crack growth failure probability.

In summary, sensitivity coefficients of a preliminary time-integrated analysis can be used to choose the appropriate solution method for a given problem. It is difficult to establish strict limits for generic problems. However, it can be said that when barrier sensitivity coefficients are large, the problem is barrier failure dominated. When sensitivity coefficients of resistance variables are large, the overload failure probability is likely to be significant, but the preliminary time-integrated solution should be accurate enough. When crack growth variables sensitivity coefficients are large, the problem is likely to be highly non-linear, and critical crack growth dominates failure probabilities. When load process (extreme value) sensitivity factors are large, barrier failure dominance is minimal, the overload failure probability is likely to be significant, and the EUR solution is not just appropriate but accurate.

Some support for the argumentation above is provided by making some variations to the NB reference problem. First, barrier failure dominance is increased by increasing the C.O.V. of resistance random variables. Then, barrier failure dominance is reduced by increasing the variance of the load process, and by reducing the number of load cycles (low-cycle fatigue problem). In the third problem, the effect of large non-linearity is studied by increasing the crack exponent m. Finally, another low-cycle fatigue problem is obtained by considering a BB load process.

11.2 Increased barrier failure dominance

In the NB reference problem just studied it was suggested that the failure probability was dominated by the barrier. In this problem, barrier failure dominance is increased by increasing the variance of resistance random variables (S_y and K_{IC}) from 5 to 10%. Due to (increased) barrier failure dominance, the TI solution is expected to be increasingly accurate, whereas the EUR solution is expected to show significant error.

The crack size TPD for this problem in identical as for the reference problem. What changes significantly is the resistance distribution. Figure 11-7 compares evolution of crack size and of resistance distributions. It can be seen that, due to the increased variance of the resistance, crack growth does not affect the variance of the resistance distribution, but mainly its mean. The problem becomes more linear. The distributions of S_y and K_{IC} tend to dominate the resistance distribution, which now seems to follow a Log-normal to Normal (LN-N) distribution model, the normal distribution being used at the last three load blocks. KS goodness-of-fit confidence levels for this distribution model vary from 80 to 20% .

Figure 11-8 shows resistance distributions lower tails and the product $\upsilon^+(r,t)f_R(r,t)$ for the FORM-evaluated and for the second-order second-moment approximated resistances, us-

ing the LN-N distribution model. The reason for the large differences in product $\upsilon^+(r,t)f_R(r,t)$ can be identified in figure 11-9. Due to the large variance of the resistance, the product $\upsilon^+(r,t)f_R(r,t)$ is shifted away from the resistance's mean (in comparison to figure 10-6), making the EUR solution largely dependent on the resistance distribution model. The FORM-based resistance TPD solutions require around $3 \cdot 10^3$ and 10^4 limit state function calls, for the distribution-model and for the fully numerical solutions, respectively.

EUR failure probabilities using the fully numerical resistance distribution are shown in figure 11-10. It can be seen that, as expected, the error of the original EUR approximation is considerable. The EUR error function is used to obtain a Gaussian estimate of the EUR error (figure 11-11). When used to correct original EUR failure probabilities, for this problem, the Gaussian error estimate leads to a slight overcorrection (figure 11-10), since the barrier mainly follows a log-normal distribution. The error is overpredicted and the correction becomes unconservative. Figure 11-12 shows EUR failure probability results obtained using the distribution-model based solutions. It confirms that the distribution-model based solutions are highly unreliable for this problem because results show strong dependency to the distribution model.

Figure 11-13 shows other failure probability results. As supposed, the conservative error of the TI approximation is quite small for this problem. The critical crack growth failure probability for this problem is the same as for the reference problem, and is out of the scale in figure 11-13. The FPI solution is slightly unconservative for this problem, perhaps due to the approximation involved in the linearization of the limit state function.

The increased barrier failure dominance can be seen in the sensitivity coefficients, shown in figure 11-14. It is seen that S_y plays a dominant role in the probability of failure, while the load process sensitivity coefficient is nearly zero at all times for this problem. The slight tendency to shift towards a more elastic fracture as the crack grows, observed in figure 10-1, can also be seen here, with $\alpha^2_{K_{IC}}$ increasing slightly as $\alpha^2_{S_y}$ decreases.

11.3 Reduced barrier failure dominance (NB low-cycle fatigue problem)

In this problem, barrier failure dominance is eliminated by increasing the variance of the load process and reducing the total number of cycles, effectively increasing the uncertainty associated with the load process. Parameters of the load process are $S(t) = N(\mu_S, \sigma_S) = N(20, 35)$ MPa, and the process is narrow-banded with an uniform PSD between $2\pi - 1$ and

$2\pi + 1$ radians. The design life is 10^3 cycles and the crack propagation rate is 1.5 10^{-10} mm/cycle. The correlation length of the crack propagation rate random process is reduced to 10 cycles, following the idea that this correlation length is dependent on the level of loading. Computations are divided in 10 load blocks of 100 simulated stress ranges each, hence resulting in one crack increment computation per actual load cycle. The resulting problem is one of low cycle fatigue.

Because of the small value of the load process mean and the large standard deviation, a significant part of the load cycles would be in the negative range, i.e., would represent compression of the crack tip. This detail is overlooked here, and the whole load cycle is considered in tension. Strictly speaking, the problem being solved is formally one translated "up", with a larger load process mean and larger yielding stress and stress intensity factors.

Monte Carlo simulation results are based on 10^3 crack growth time histories. Because of the increased role of stress range random variables in this problem, a distinct stress range set is simulated for each simulated time-history. Also because of the increased role of stress range random variables in the problem, the $TTTG(a_0, a)$ function is obtained as the average of 10 mean time to growth computations, each with a distinct set of simulated stress ranges.

The crack size distribution follows a log-normal distribution very closely, with KS goodness-of-fit confidence parameters varying from 99% to 40%. An excellent approximation of the resistance distribution is obtained with a distribution model varying from a log-normal to normal to inverted log-normal distribution (LN-N-iLN). The evolution of crack size and resistance distributions are compared in figure 11-15.

11.3.1 Comparison of EUR solutions

Figure 11-16 shows an excellent agreement between the EUR solution based on the more accurate numerically-evaluated resistance distribution and the solutions based on the resistance distribution model. This is not just a coincidence due to a good choice of distribution model, nor is it in contradiction with results obtained in chapter 10. The quality of the distribution model based solutions can be attributed to small variance of the barrier. Because barrier variance is small in comparison with variance of the load process, the product $\upsilon^+(r,t)f_R(r,t)$ attains its maximum closer to the mean of the barrier (figure 11-17), where the distribution model is more accurate. This can be seen in a comparison between figures 10-6, 11-9 and 11-17. It can also be seen in figure 11-18, where resistance distributions are shown along with the product $\upsilon^+(r,t)f_R(r,t)$. Because of the small variance of the barrier, the EUR integration is performed closer to the resistance mean, where the distribution model and the

second-order second-moment approximation are more accurate, and not at the tail of the resistance distribution. Hence, the extrapolation of the resistance distributions tail through a particular distribution model is avoided or at least minimized.

11.3.2 Comparison with other failure probability solutions

The error of the EUR approximation is essentially zero, a result that can be attributed to the elimination of barrier failure dominance. This is also shown by the "zero" Gaussian error estimate (figure 11-19) and by the FORM sensitivity coefficients (figure 11-20), which show dominance of the failure probability by the load process over most of the time interval. Other failure probability results are shown in figure 11-21. The error of the TI solution, as expected, is larger in this problem, due to the greater role played by the load process in the failure probability.

Since the load process plays such an important role in this problem, as a result of eliminating barrier failure dominance, it is pertinent to ask whether barrier variance could be neglected altogether. In order to investigate this possibility, failure probability results using a deterministic resistance (the mean) are also shown in figure 11-21. The resulting failure probabilities are around one order of magnitude smaller than the original result, showing that although barrier variance is small in comparison to load process variance, it still plays a significant role in the failure probability.

11.3.3 Final remarks

In summary, two major results, in terms of the EUR approximation, were obtained in the analysis of this problem. First, it was shown that the EUR approximation is accurate when it is mostly needed, i.e., when barrier failure dominance is absent and the load process plays a significant role in the overload failure probability. Secondly, it shows that in this same situation, because barrier variance is small compared to load process variance, the resistance distribution can effectively be calculated by a second-order second-moment approximation and by a proper choice of distribution model, at a huge saving of limit state function calls and computation time.

11.4 Increased problem non-linearity

The problems studied so far resulted in overload failure probabilities significantly higher than critical crack growth failure probabilities. In this problem, it is tested whether the overload failure probability solutions based on the first passage failure model still hold when the

problem becomes highly non-linear and failure is due to critical crack growth. Barrier failure dominance is increased to a point where failure becomes barrier-defined, i.e., failure is due to critical crack growth. This is done by increasing the crack propagation exponent from $m = 3$ to $m = 3.8$. This increases, indirectly, the importance of crack propagation random variables in the failure probability. The standard deviation of the load process is reduced from 18 to 12 MPa, and the crack propagation rate changed to 10^{-13} mm/cycle, all other parameters remaining as for the reference problem. Due to the high non-linearity of the problem, crack growth computations are divided in 20 load blocks, with 50 stress range values per load block. Figure 11-22 gives an idea of the degree of non-linearity of this problem.

Figure 11-23 shows an histogram of 10^4 simulated crack samples at $t = 10^6$ cycles. The large histogram bar at $a = 65$ mm corresponds, of course, to the critical cracks simulated. Because crack growth computations are interrupted at $a = a_{crit}$, the critical crack size works as an absorbing barrier, and all probability mass that reaches a_{crit} gets absorbed by this barrier. The crack size CDF shows a jump at $a = a_{crit}$, which corresponds to the critical crack growth probability of failure. The rest of the histogram (to the left of a_{crit}) still roughly follows a log-normal distribution. Hence, one can obtain a conditional distribution from a maximum likelihood χ^2 fit to the sampled histogram ($a < a_{crit}$) or from the conditional sample moments, as shown in figure 11-23. The resulting distributions are crack size distributions conditional to no critical crack growth.

In figure 11-24 the χ^2-fitted conditional distribution is compared with other numerically evaluated crack size distributions. Some differences can now be seen between the distinct solutions. The convolution solution seems to underpredict the spread of the crack size distributions upper tail past a_{crit}, and to be actually closer to the simulation-based conditional distributions. The random process-based solutions (Log-normal and Diffusive Markov) seem to project the crack size distribution better towards a_{crit}, hence they are believed to remain valid for this problem.

Conditional resistance distributions can also be obtained from an histogram fit or from conditional sample moments. However, these can now only provide a gross idea of the resistances distribution shape, since the distribution-model based solutions are actually based on the Markov crack size distribution. The distribution model obtained this way varies from a log-normal to a normal to an inverted log-normal distribution, in the first 5 load blocks. The maximum value of the inverted log-normal distributions changes from 500 to 340 MPa, in the 15 load blocks that follow, gradually increasing the squeweness of the resistance distribution.

Resistance distributions obtained using the described distribution model and the second-

order approximation, as well as the distribution model - FORM based resistance distribution, are compared in figure 11-25 with the fully numerical (FORM-based) solution.

Figure 11-26 shows the corresponding EUR-approximated failure probabilities, in a comparison with MC simulation results. It can be seen that, despite the high non-linearity of this problem, an EUR resistance distribution-based solution can still be obtained. The solution is not very accurate, though. The bumps observed in the figure are due to linear interpolation of results between load blocks, which are plotted in logarithmic scale.

Figure 11-27 shows corresponding critical crack growth probabilities of failure. It can be seen that indeed failure is defined by critical crack growth in this problem. The first passage (overload) failure model still provides results, as seen by the EUR and TI solutions, although failure is completely defined by the barrier. An overload (or up-crossing) is certain as the barrier collapses towards the load process! The critical crack growth dominance can also be seen in the sensitivity coefficients of the TI solution (figure 11-28), where it is seen that the probability of failure depends only on A_0 and C. Figure 11-28 also shows sensitivity coefficients of the FORM-based critical crack growth solution. FPI results could not be obtained for this problem, due to convergence problems.

11.5 Broad-band low-cycle fatigue problem

A broad-band low-cycle fatigue problem was constructed and solved in as much the same way as the narrow-band low-cycle problem. The load process is $S(t) = N(\mu_S, \sigma_S) = N(20, 30)$ MPa, with an exponential correlation function and parameter $\lambda_s = 1.0$ cycle. The crack propagation rate is 10^{-10} mm/cycle with a correlation length of 10 cycles. Design life is 10^3 cycles. The calculations were divided in 10 load blocks of 100 stress ranges each.

The stress range distribution of the broad-band load process is a combination of an exponential and two Rayleigh distributions, following Dirlik (1985). The broad-band problem, especially the low-cycle broad-band problem, is highly non-linear on the stress range distribution, due to the asymmetry of this distribution and the small probability of very large stress range outcomes (figure 11-29). Hence, even more so than for the NB low-cycle problem, the Monte Carlo simulation has to be performed by simulating new stress range values for each crack growth computation. The $TTTG(a_0, a)$ function is also computed as the average of 100 mean time to grow evaluations, each with a distinct simulated stress range set.

The crack size follows a log-normal distribution, and the resistance distribution model varies from log-normal to normal to inverted log-normal. The resistance distributions and resulting ensemble up–crossing rates are shown in figure 11-30. The evolution of crack size

and resistance distributions is compared in figure 11-31. EUR failure probability results are compared in figure 11-32, which shows, again, an excellent agreement between the solution based on the more accurate numerical resistance distribution and the solutions based on resistance distribution models. Again, this can be attributed to the fact that, due to the small variance of the barrier in comparison to the variance of the load process, the EUR integration occurs not far from the resistances mean, where the distribution model is more accurate. The EUR error estimate is zero for this problem as well as shown in figure 11-33.

TI and FPI failure probability results are shown in figure 11-34, with sensitivity coefficients shown in figure 11-35. Again, the significant role of the load process in the failure probability is evident. Critical crack growth failure probabilities evaluated by FORM using the $TTTG(a_0, a)$ function are also shown in figure 11-34. Interestingly, some disagreement is seen towards the end of the design life, where the critical crack growth and the FPI failure probabilities are larger than the MC simulation and the EUR overload failure probabilities.

This disagreement can be attributed to the fact that both FPI and critical crack growth FORM solutions are based on a RV crack propagation rate, when it is actually modelled as a random process (the correlation length is $\lambda_X = T/100 = 10$ cycles). The EUR and MC simulation solutions, on the other hand, are based on the proper RP representation of the crack propagation rate. Interestingly, both the FORM-based critical crack growth solution and the EUR solution are based on the same mean time to grow function $TTTG(a_0, a)$. However, the EUR solution is based on a random process solution for the crack propagation rate, whereas the FORM-based critical crack growth solution is obtained by multiplying function $TTTG(a_0, a)$ by a (RV) crack propagation rate X. Further evidence that the RV versus RP crack propagation rate is the issue here can be seen in the sensitivity coefficients of C, which grow considerably towards the end of the design life (figure 11-35). Interestingly, the correlation coefficient of the sampled crack sizes is nearly one for all times.

11.6 Periodic inspections

In order to illustrate that the proposed random process - EUR solution can be applied also to problems involving periodic non-destructive inspections, some brief results are presented here. The NB reference problem is considered again, with a design life of $T = 10^6$ cycles. Crack growth computations are divided in 20 load blocks. Two inspections are considered, at times $T/3$ and $2T/3$. For a particular type of non-destructive inspection method, the probability of detection curve can be given by (Moan et al., 1997):

$$P_D(a) = \frac{\exp[\alpha + \beta \log(a - A_d)]}{1 + \exp[\alpha + \beta \log(a - A_d)]} \tag{11.2}$$

For illustration purposes, the arbitrary parameter values of $\alpha = 0.01$, $\beta = 1.2$ and $A_d = 1$ mm are used in this section. The resulting POD curve is shown in figure 11-36.

In this brief analysis, the effect over failure probabilities of not finding any cracks in both inspections is considered. Clearly, this effect will be to reduce failure probabilities, as not finding any cracks means that any existing crack is smaller than the (uncertain) minimal detectable crack size.

The crack size distributions for this problem are obtained by means of the diffusive Markov model, as shown in chapter 9. Following discussion in section 7.6.2, the crack size distributions are up-dated following the result of an inspection. The hypothetical inspection method considered (or its POD curve) and the crack size distributions of the NB reference problem at the two inspections times, result in probabilities of not detecting a crack around 7%. Hence, not finding a crack is an unlikely outcome for these inspections. The hypothesis of not finding a crack, at this small probability of not detecting, makes the effect over $P_f(t)$ all the more significant as will be seen. The crack size distributions, for the case of no inspection, for the first inspection only and for two inspections, are shown in figure 11-37. Note that for the case of two inspections only the crack size distributions at times $2T/3$ and T are affected.

Resistance distributions are obtained by means of the second-order second-moment approximation, and by up-dating the original LN-N-iLN distribution model according to the effect of the inspections over the crack size distributions. A more general solution, less dependant on the effects that the POD curve has over the resulting crack size distributions, is a numerical (FORM-based) solution for resistance distributions or a direct numerical solution for ensemble up-crossing rates.

Overload failure probabilities for the cases of no inspections, for one inspection at time $T/3$ and for two inspections at times $T/3$ and $2T/3$ are shown in figure 11-38. The sharp fall of failure probabilities right after each inspection and the subsequent increase of failure probabilities in the load cycles that follow are a consequence of the fact that loading is stopped for the inspections (the structure is taken out of service). Hence, when the structure is put back in service, there is an initial failure probability, which then increases as the probability of an overload increases. Figure 11-38 also shows how non-destructive inspections can be used to maintain failure probabilities below a defined limit.

Clearly, the possibility of up-dating crack size distributions following inspections and of knowing apriori the probabilities involved in possible outcomes of the inspections goes

far beyond the limited analysis presented here. These possibilities were explored in section 7.6.2. The difficulties involved in obtaining similar results based on random variable crack propagation models have also been described in section 7.6.2.

11.7 Figures

11.7.1 NB reference problem

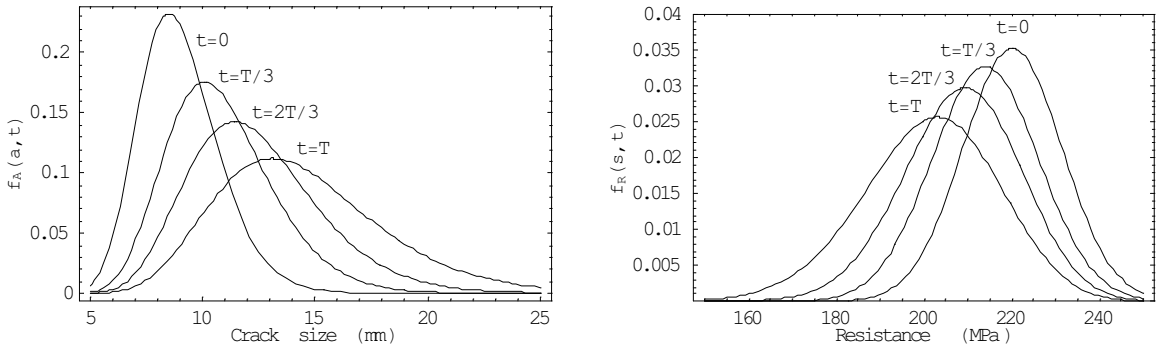

Figure 11-1: Comparison of crack size and resistance TPD evolution, NB reference problem.

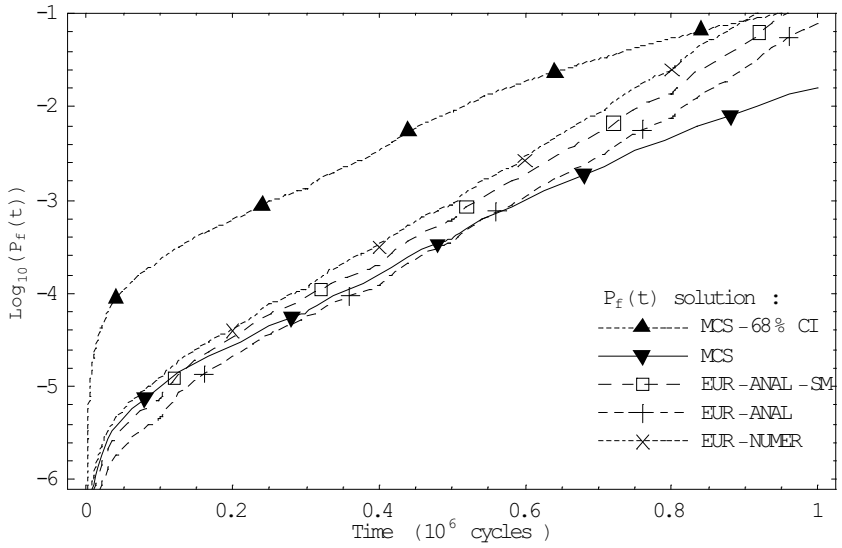

Figure 11-2: Ensemble up-crossing rate failure probabilities, NB reference problem.

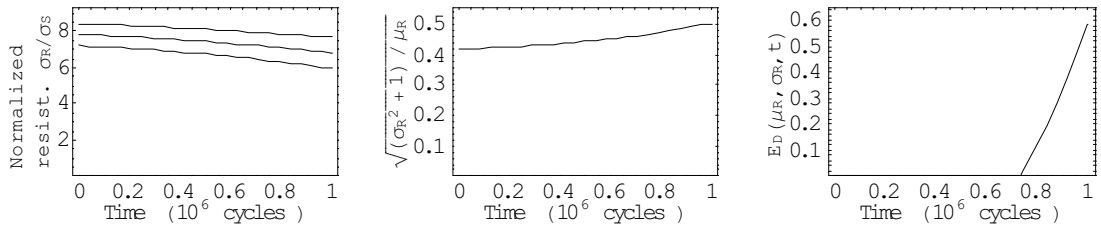

Figure 11-3: Normalyzed resistance, error parameter and estimated EUR error, NB reference problem.

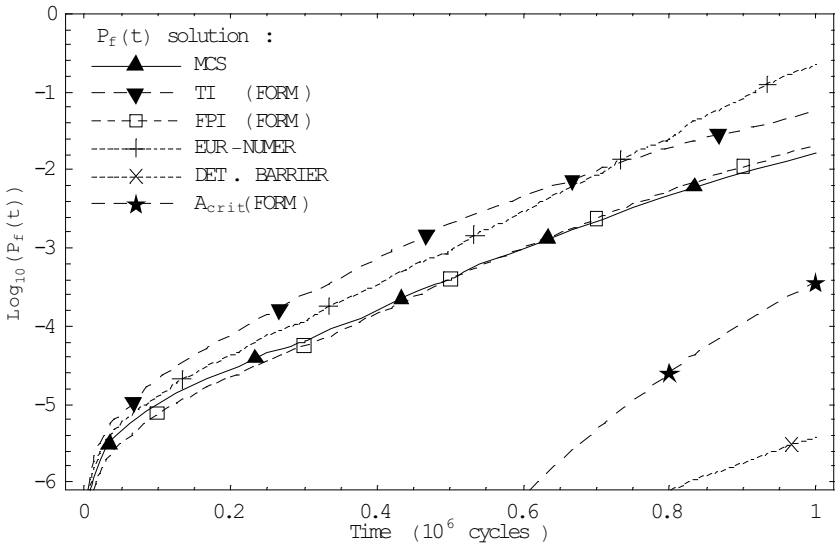

Figure 11-4: Other failure probabilities, NB reference problem.

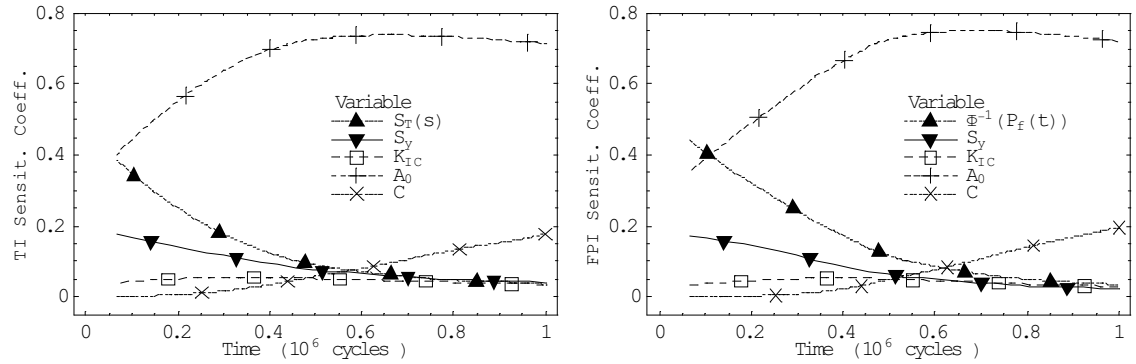

Figure 11-5: Sensitivity coefficients of TI and FPI FORM solutions, NB reference problem.

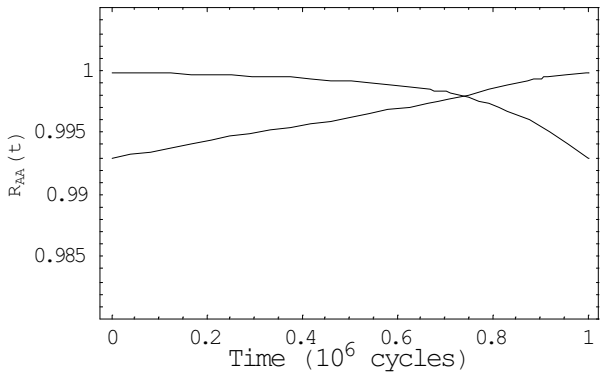

Figure 11-6: Estimated correlation coefficients $\rho(A_0, A(t))$ and $\rho(A(t), A(T))$.

11.7.2 Increased barrier failure dominance

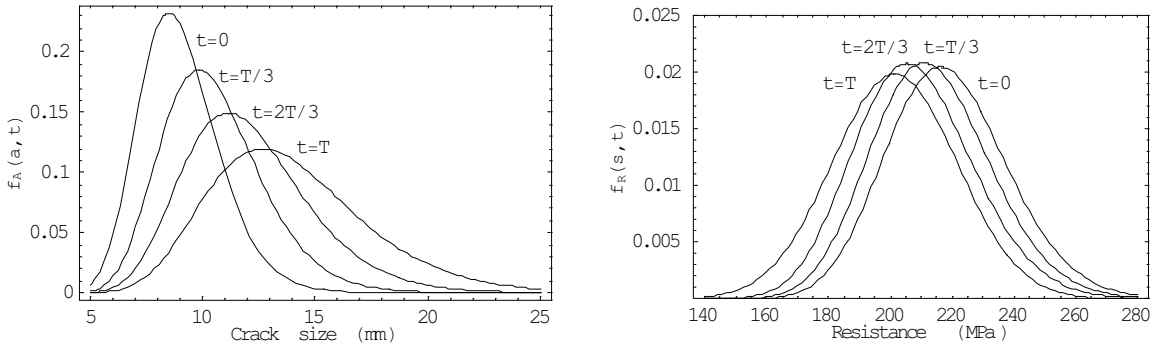

Figure 11-7: Comparison of crack size and resistance TPD evolution, increased BFD.

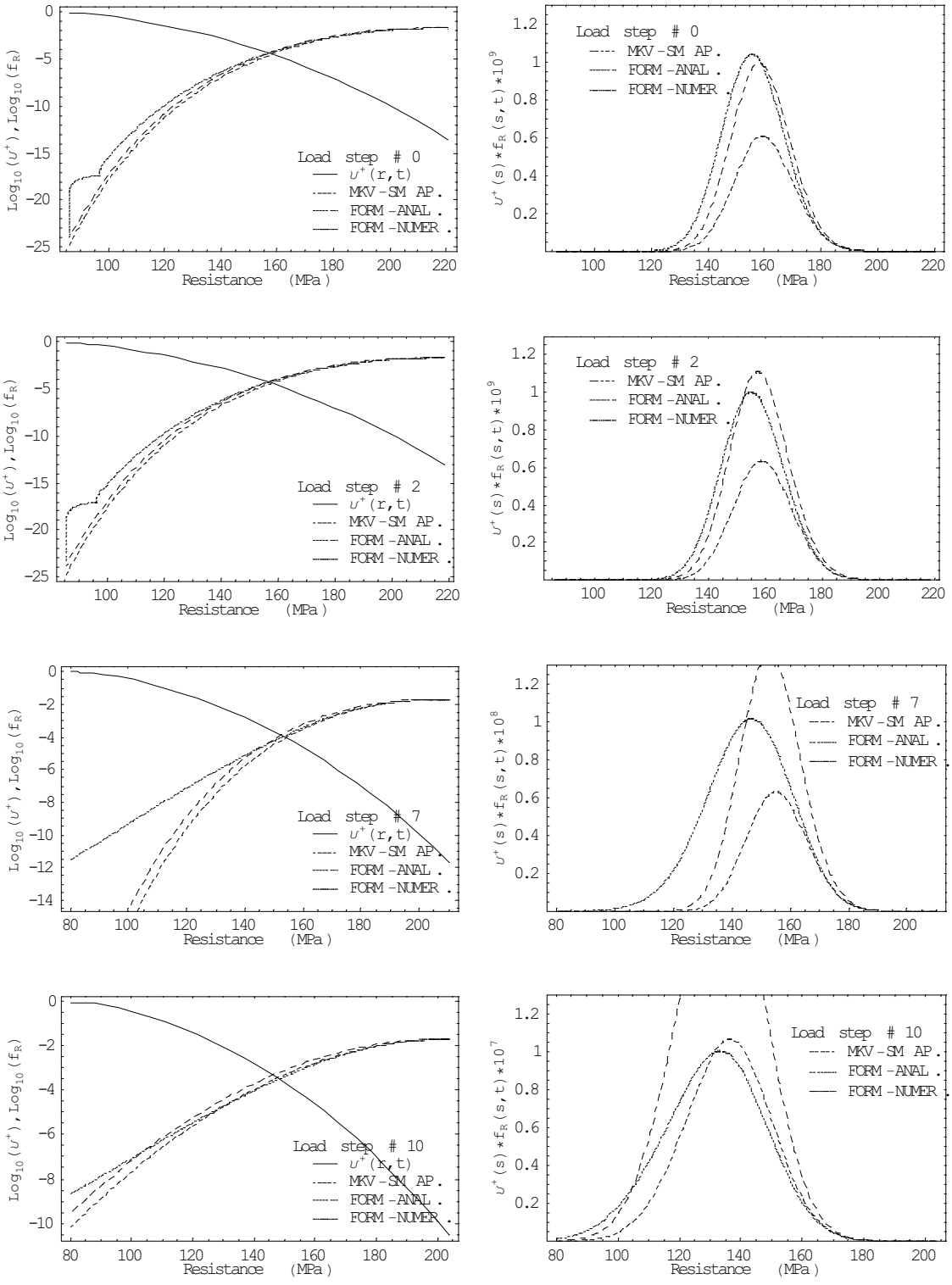

Figure 11-8: Resistance distribution and product $\upsilon^+(r,t)f_R(r,t)$, increased BFD.

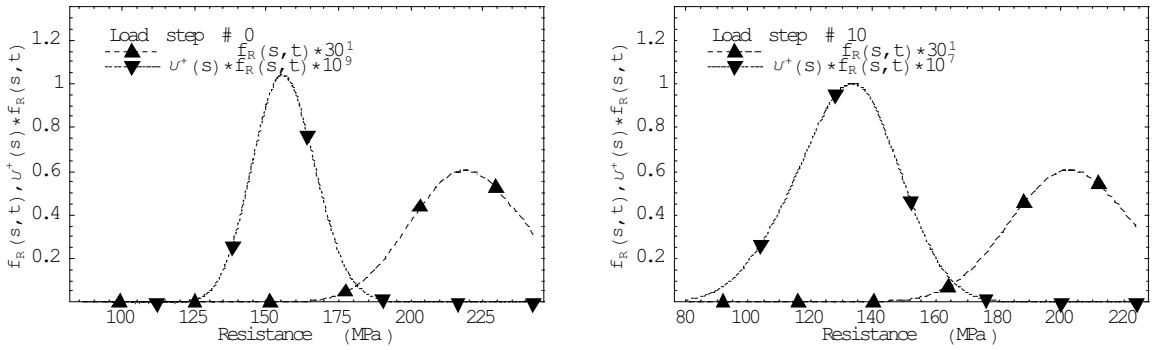

Figure 11-9: Distance between $v^+(r,t)f_R(r,t)$ and resistance mean, increased BFD.

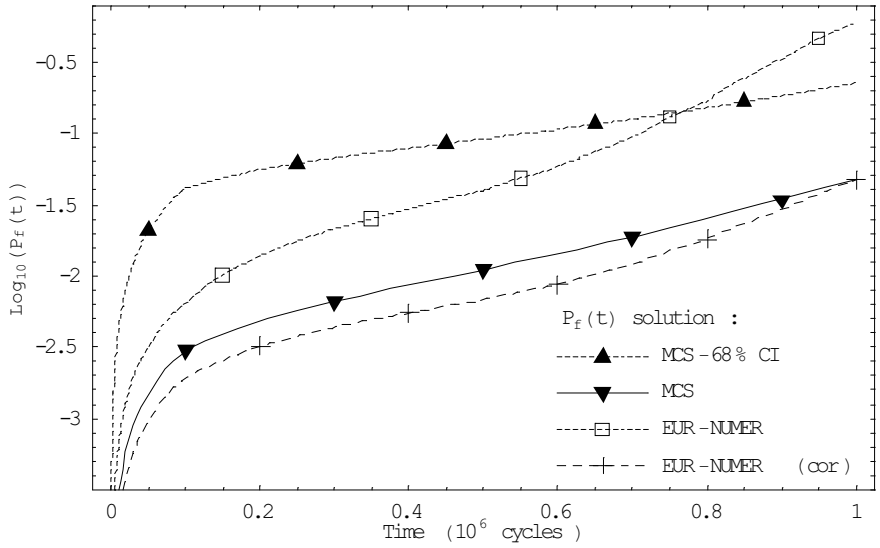

Figure 11-10: Ensemble up-crossing rate failure probabilities, increased BFD.

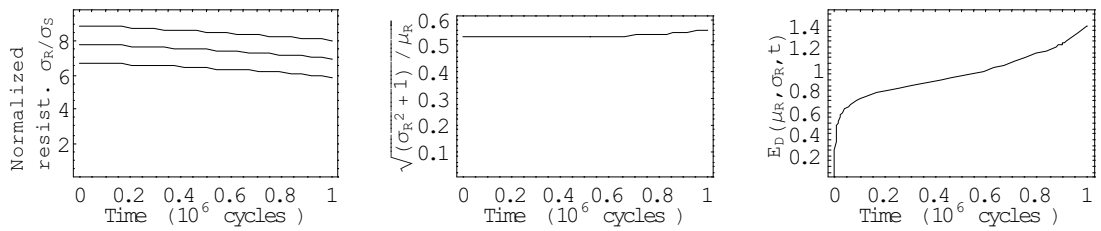

Figure 11-11: Normalyzed resist., error par. and estimated EUR error, increased BFD.

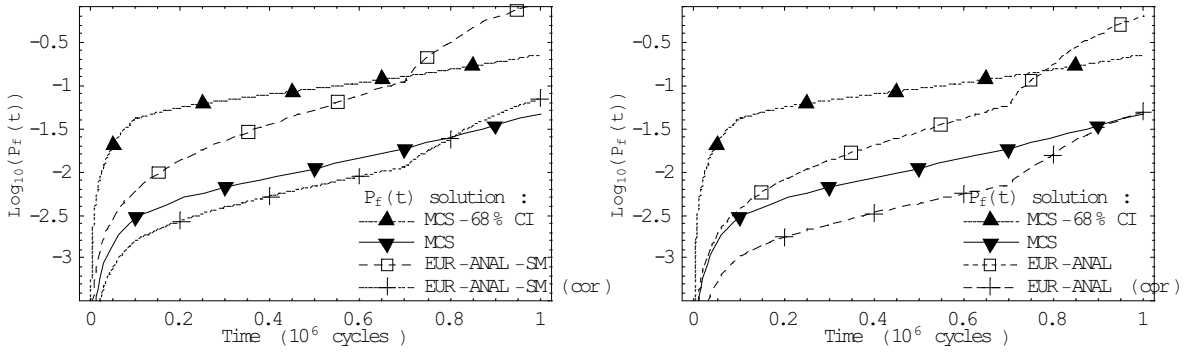

Figure 11-12: Other ensemble up-crossing rate failure probabilities, increased BFD.

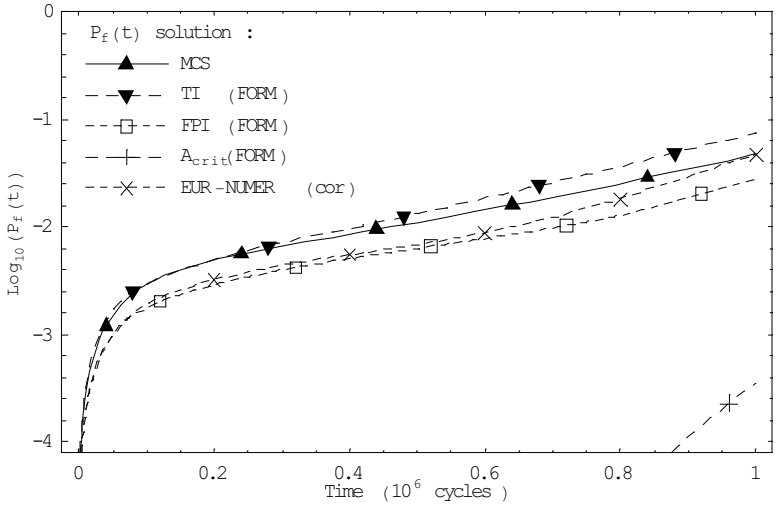

Figure 11-13: Other failure probabilities, increased BFD.

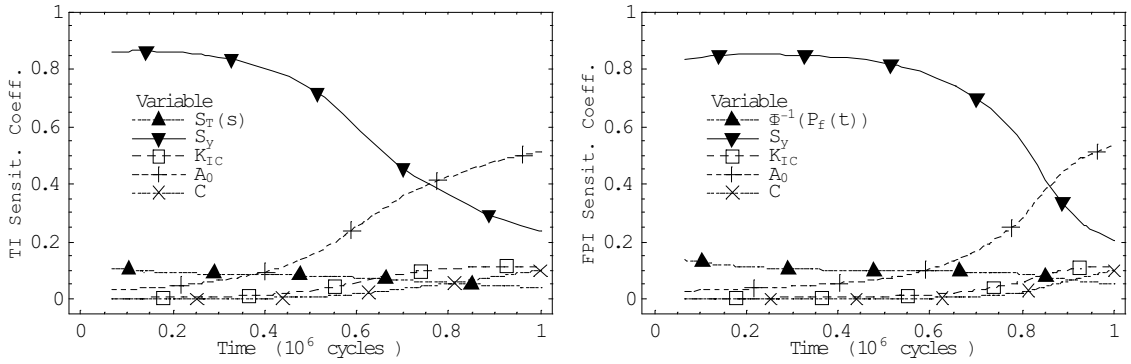

Figure 11-14: Sensitivity coef. of TI and FPI FORM solutions, increased BFD.

11.7.3 Reduced barrier failure dominance (NB low-cycle fatigue problem)

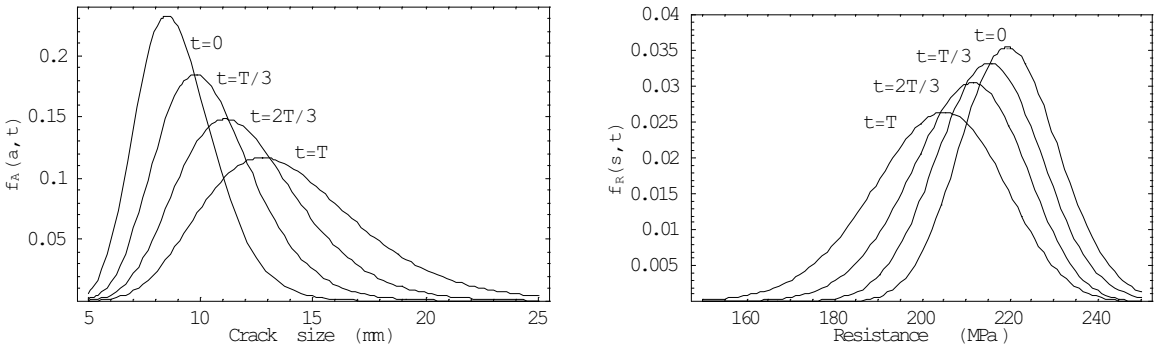

Figure 11-15: Comparison of crack size and resistance TPD evolution, reduced BFD.

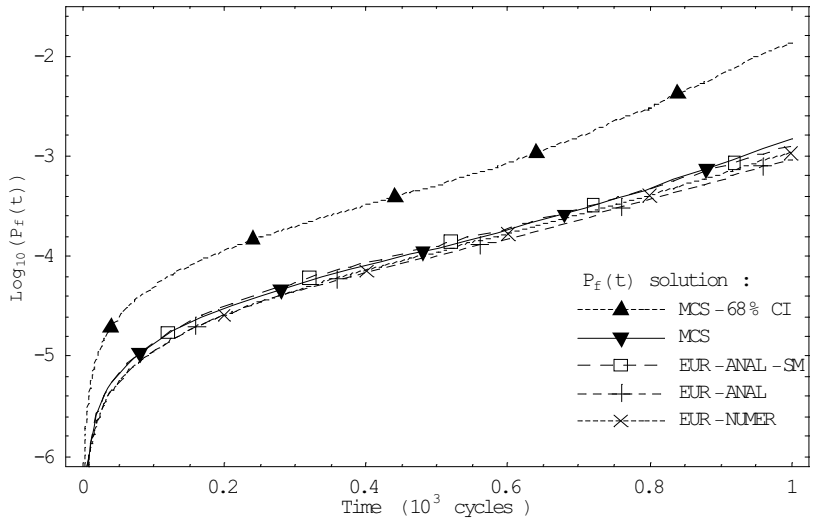

Figure 11-16: Ensemble up-crossing rate failure probabilities, reduced BFD.

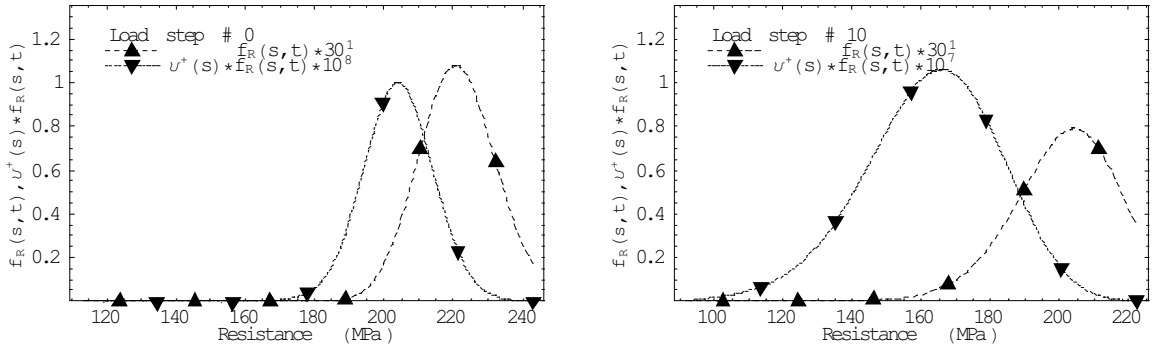

Figure 11-17: Distance between $v^+(r,t)f_R(r,t)$ and resistance mean, reduced BFD.

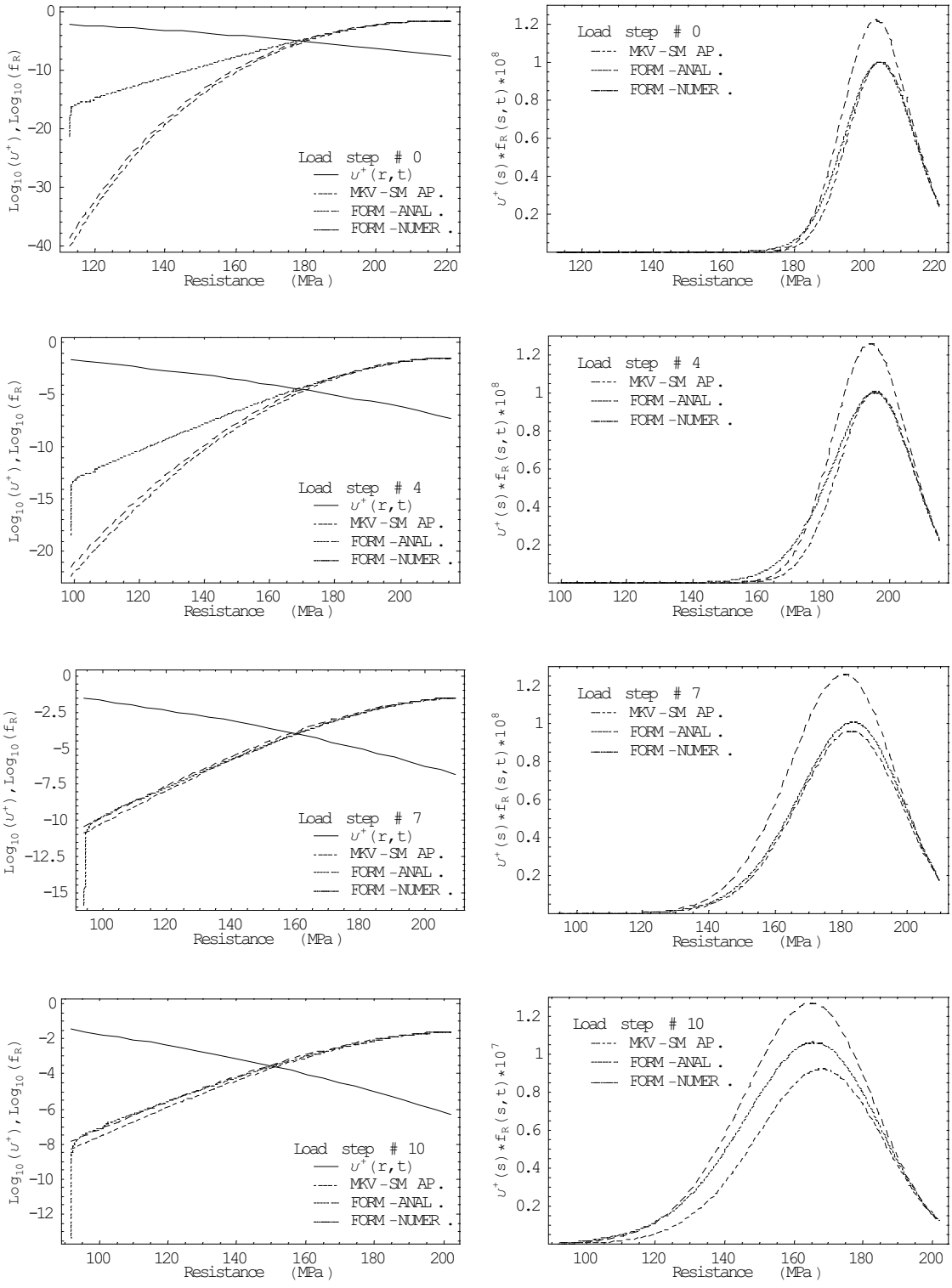

Figure 11-18: Resistance distribution and product $\upsilon^+(r,t)f_R(r,t)$, reduced BFD.

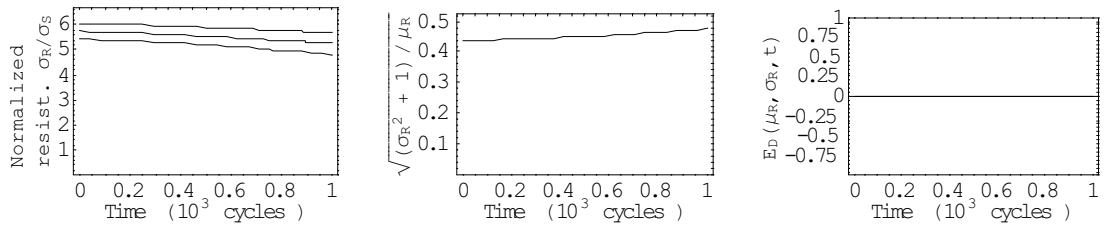

Figure 11-19: Normalyzed resist., error par. and estimated EUR error, reduced BFD.

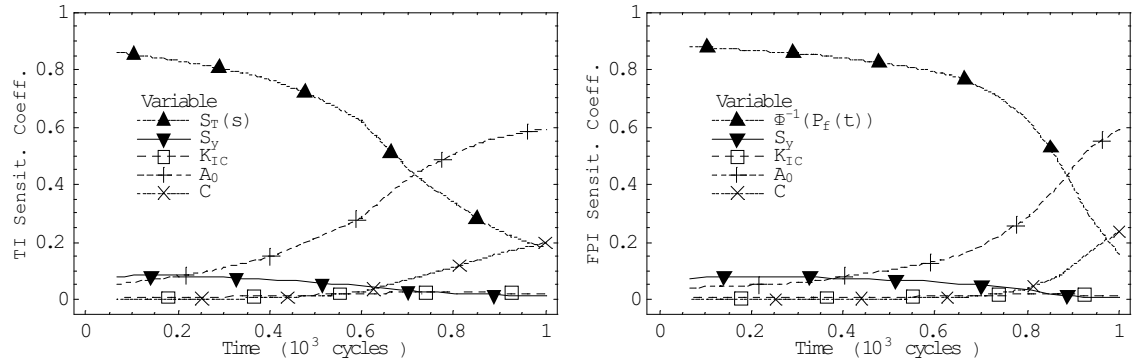

Figure 11-20: Sensitivity coef. of TI and FPI FORM solutions, reduced BFD.

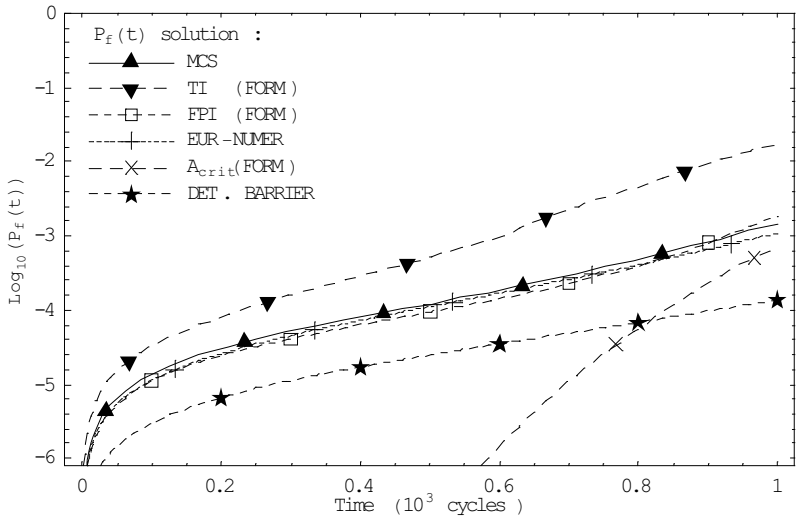

Figure 11-21: Other failure probabilities, reduced BFD.

11.7.4 Increased problem non-linearity

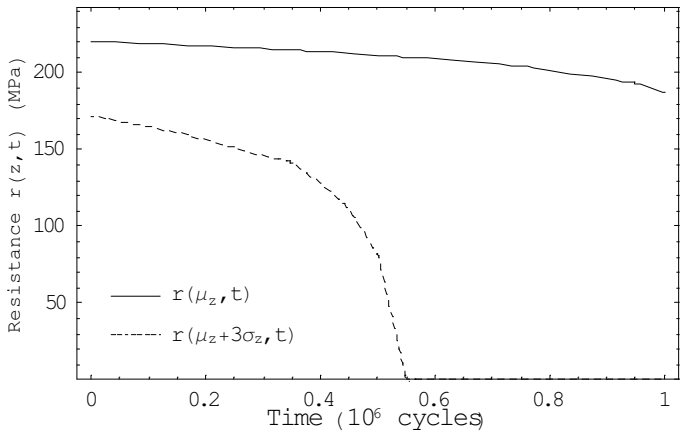

Figure 11-22: Resistance degradation for $\mu_{\mathbf{z}}$ and for 3-sigma rule, crack exponent $m = 3.8$.

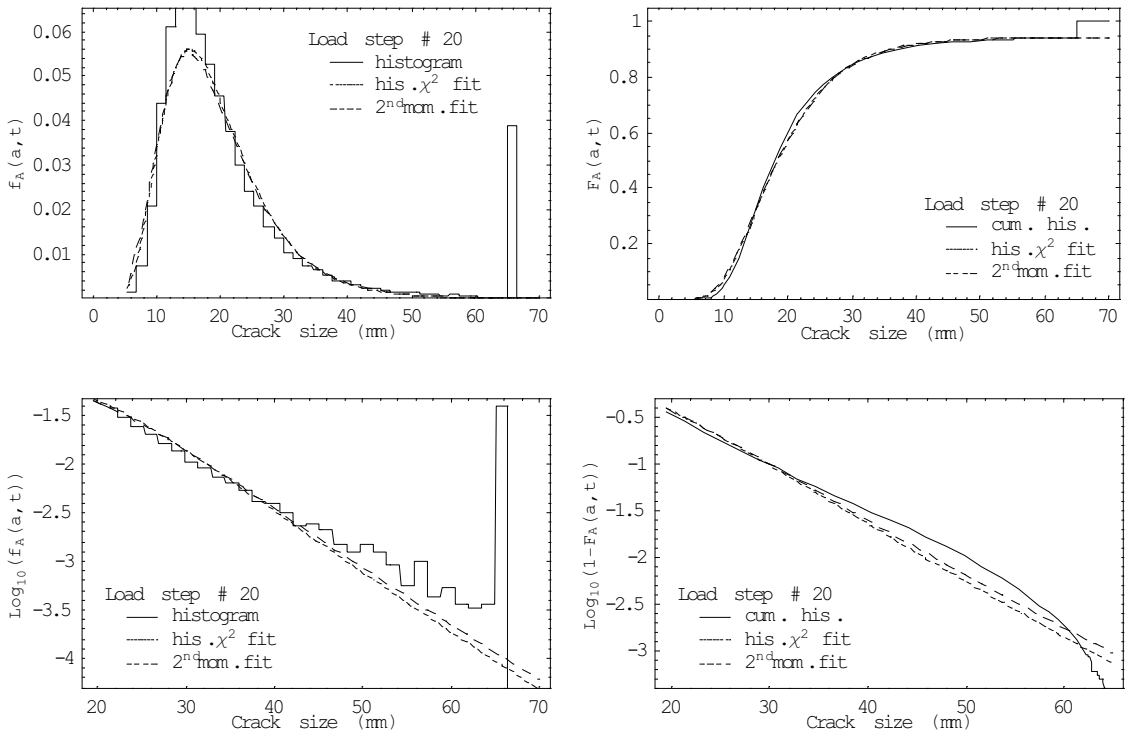

Figure 11-23: Crack size histogram and second moment dist. fit, crack exponent $m = 3.8$.

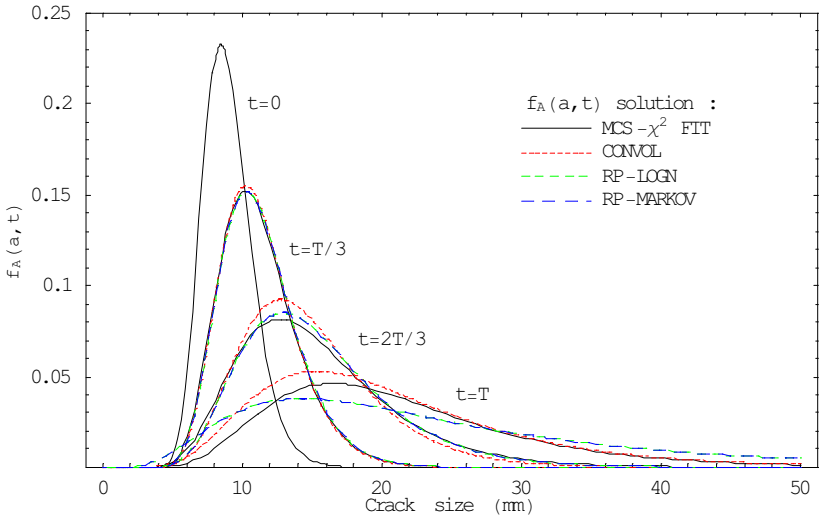

Figure 11-24: Crack size TPDs, crack exponent $m = 3.8$.

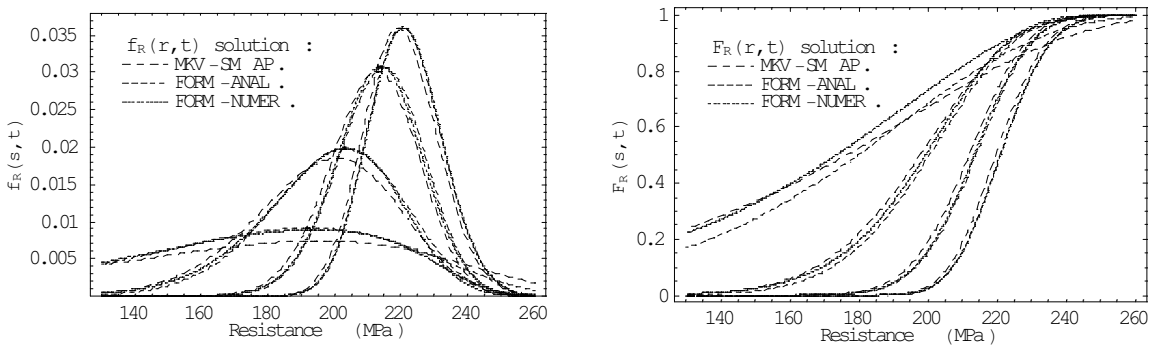

Figure 11-25: Resistance distribution, crack exponent $m = 3.8$.

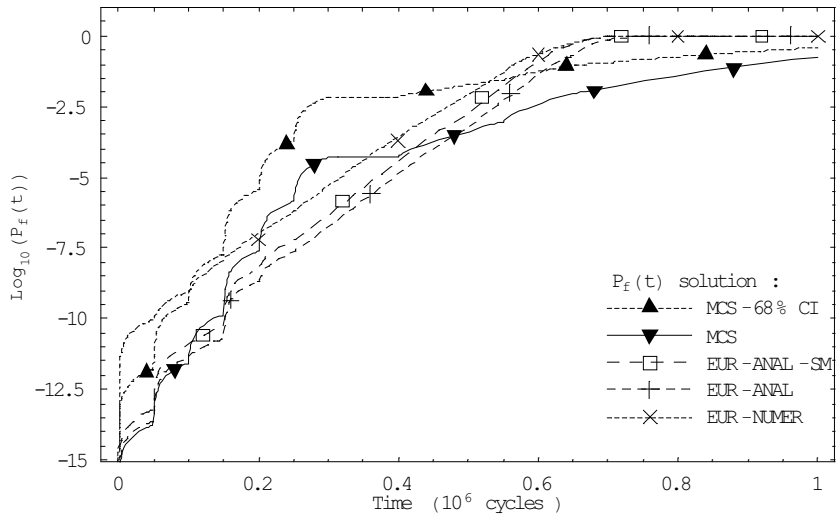

Figure 11-26: Ensemble up-crossing rate failure probabilities, crack exponent $m = 3.8$.

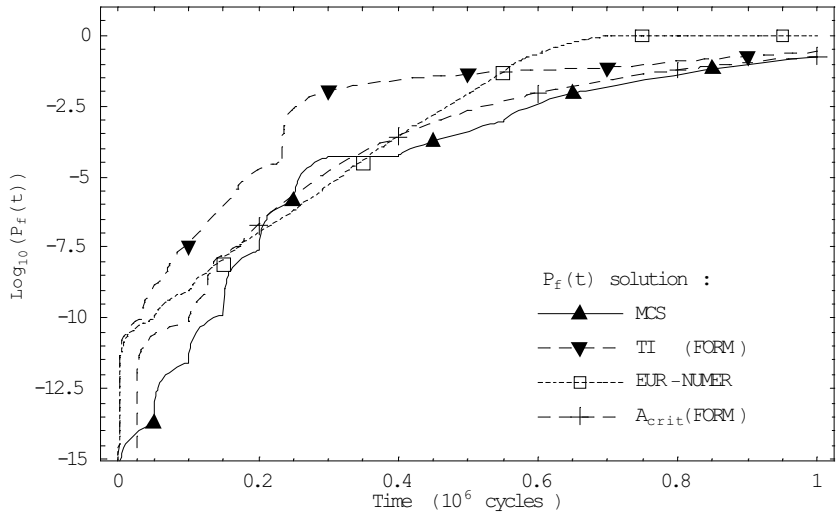

Figure 11-27: Other failure probabilities, crack exponent $m = 3.8$.

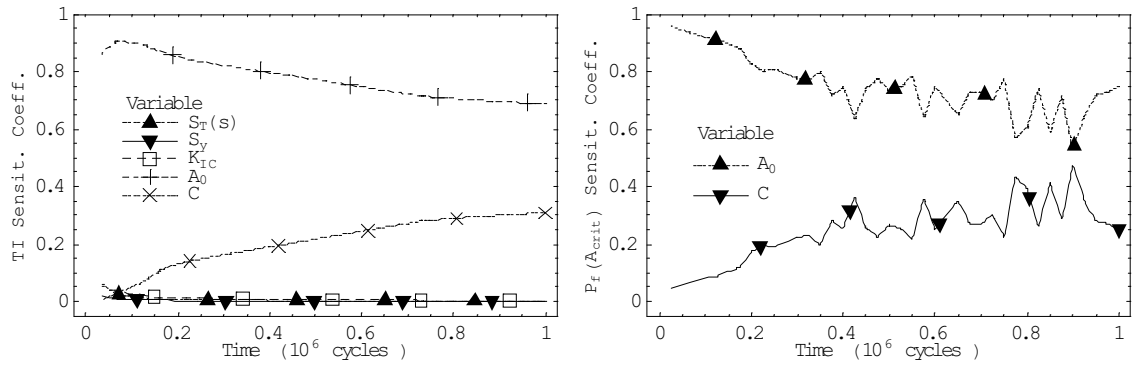

Figure 11-28: Sensitivity coefficients of TI and A_{crit} FORM solutions, crack exponent $m = 3.8$.

11.7.5 Broad-band low-cycle fatigue problem

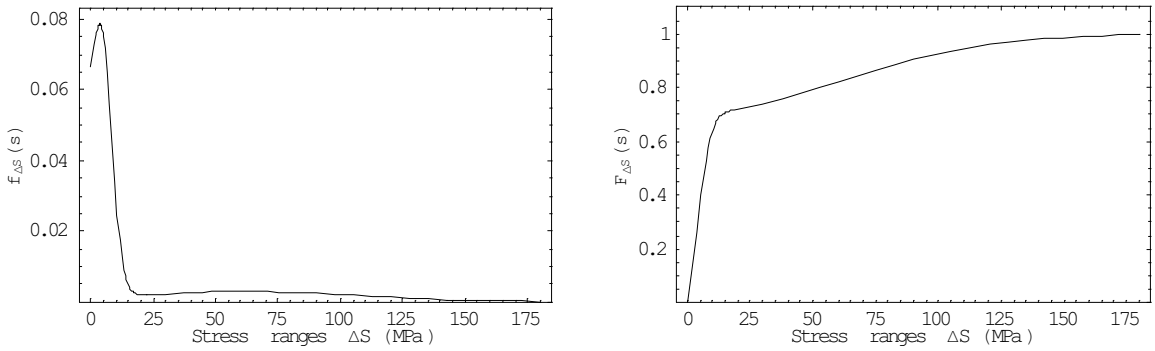

Figure 11-29: Stress range distribution for BB low-cycle problem.

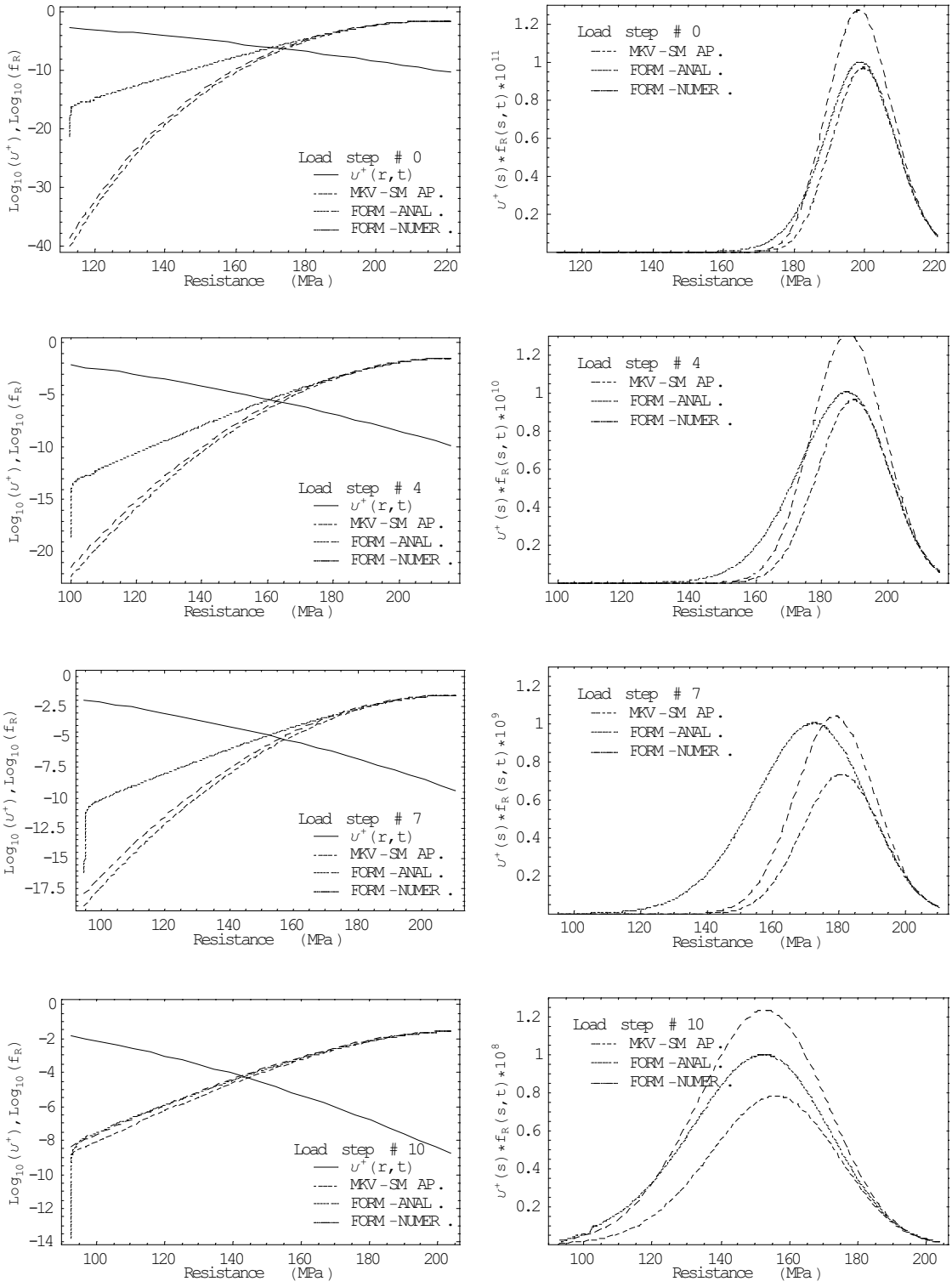

Figure 11-30: Resistance distribution and product $\upsilon^+(r,t)f_R(r,t)$, BB low-cycle problem.

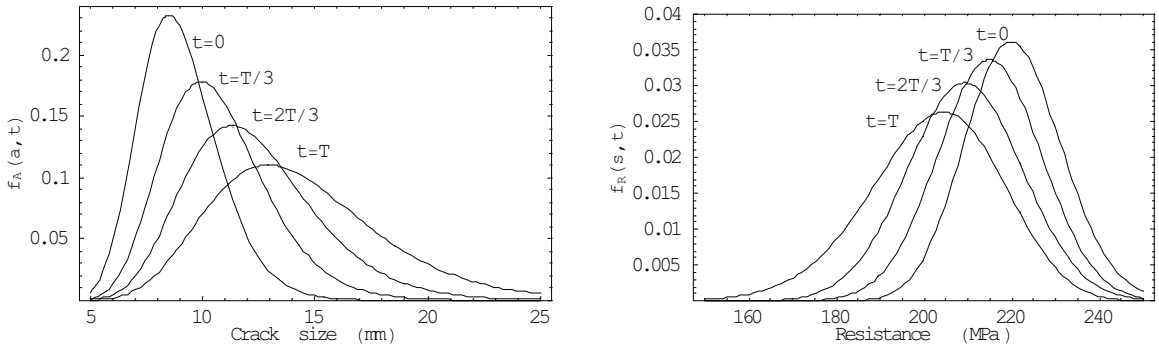

Figure 11-31: Comparison of crack size and resistance TPD evolution, BB low-cycle problem.

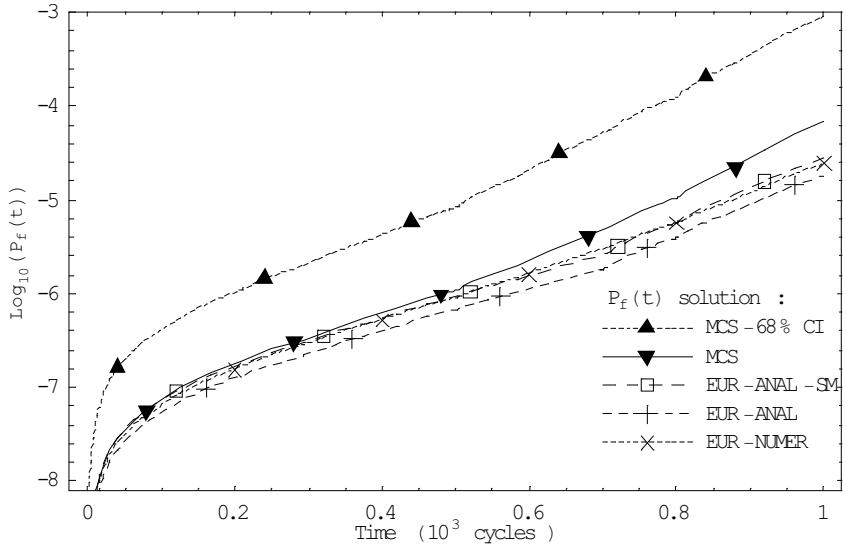

Figure 11-32: Ensemble up-crossing rate failure probabilities, BB low-cycle problem.

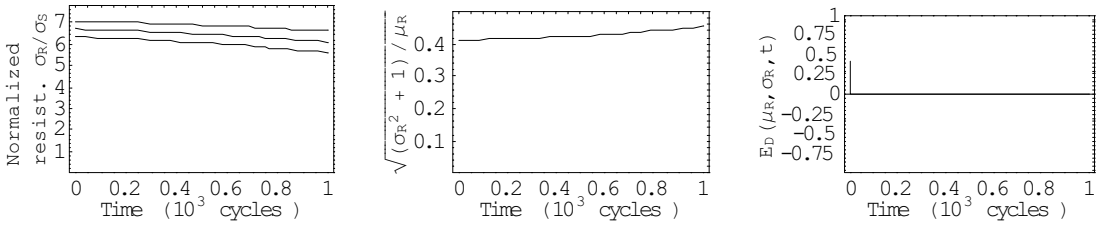

Figure 11-33: Normalyzed resist., error par. and estimated EUR error, BB low-cycle problem.

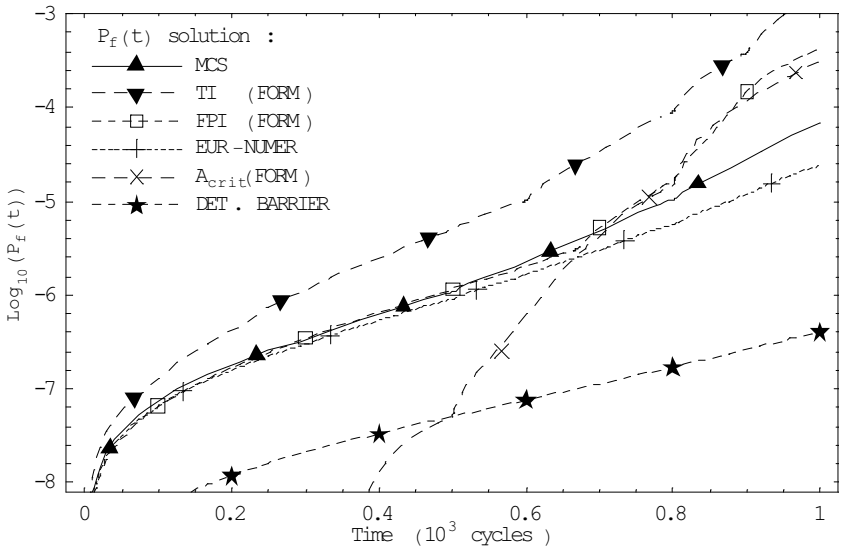

Figure 11-34: Other failure probabilities, BB low-cycle problem.

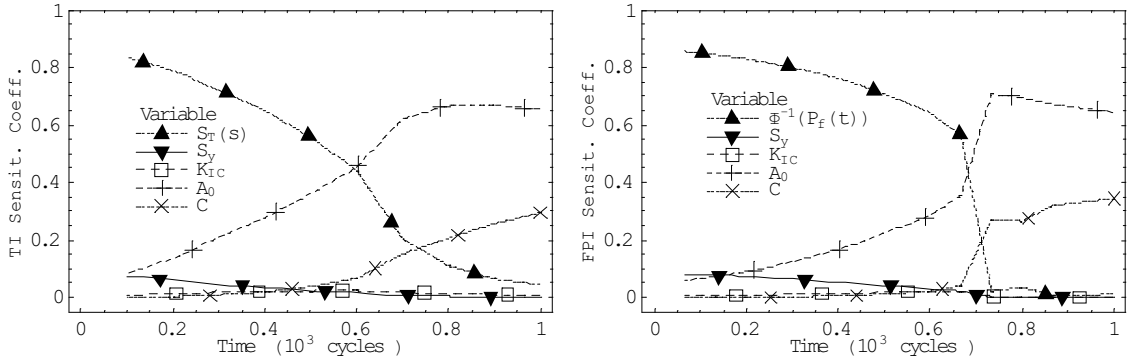

Figure 11-35: Sensitivity coefficients of TI and FPI FORM solutions, BB low-cycle problem.

11.7.6 Periodic inspections

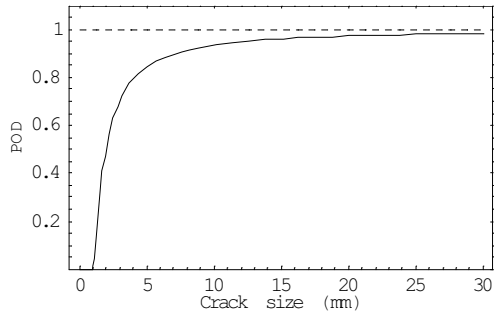

Figure 11-36: Probability of detection curve for non-destructive inspection method.

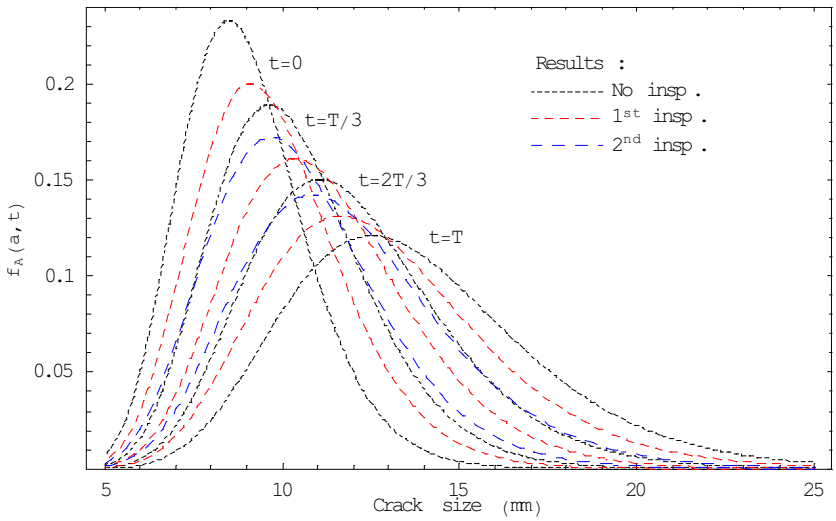

Figure 11-37: Crack size distributions for two inspections and no crack found.

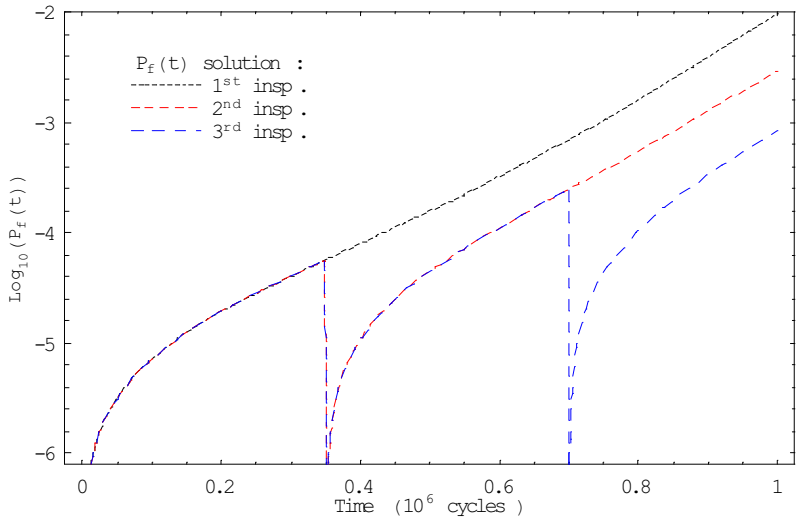

Figure 11-38: EUR failure probabilities for two inspections and no crack found.

Chapter 12

CONCLUSION

12.1 Conclusions

In this thesis, solution of time variant reliability problems through the ensemble up-crossing rate (EUR) approximation has been addressed. The potential of this approximation in simplifying the analysis of complex multi-dimensional problems under significant resistance degradation was emphasized. A simulation procedure to obtain Poissonian arrival rates of the first up-crossing over random barriers was introduced, and used to obtain a measure of the EUR approximation error. Error parameters were identified and error functions were constructed.

The EUR error parameter and functions derived are strictly valid only for Gaussian load processes and Gaussian barriers. Moreover, parameters of the derived error functions were found to be valid only for the random barrier domain considered in the simulation, which nevertheless represents the domain of practical applications. It was also found that assuming EUR errors to be proportional to failure probabilities can be misleading. Absolute errors can be small, but errors of two or three orders of magnitude are commonplace even for small failure probabilities. The realization that EUR errors are actually proportional to variance of the barrier, through error parameter $\sqrt{(\sigma^2+1)/\mu}$, is perhaps intuitive in retrospect, but has not been presented before in the literature in the present context.

An important outcome of the present study is the concept of *barrier failure dominance*. In time-variant reliability analysis of uncertain structures, barrier failure dominance characterizes those problems where an out-crossing (or overload) is more likely to be caused by a very small realization of the resistance than by an unfortunate combination of exceptionally large load peaks. The concept can be used to evaluate the appropriateness of common (and often required) simplifications of complex time variant reliability problems. Solutions that simplify the loading part of the problem are more likely to be adequate in the presence of

barrier failure dominance. Solutions that simplify the barrier part of the problem, like the EUR approximation, are better suited when barrier failure dominance is absent. Barrier failure dominance is not expected to be encountered in real structural engineering applications, where load process uncertainty is usually larger than resistance uncertainty. This is especially true for problems involving natural hazards like winds, earthquakes, floods, waves, etc. This clears the way for a range of potential applications of the EUR approximation.

One such applications, namely crack propagation and fracture under random loading, was addressed in some detail. The EUR approximation was applied in the solution of a problem formed by combining stochastic models of crack propagation with the First Passage failure model. The solution represents a fresh random process approach to the problem, where the evolution in time of crack size and resistance distributions are evaluated. It allows consideration of overload and critical crack growth failure modes, and rational optimization and planning of non-destructive periodic inspections.

Through some typical fatigue and fracture reliability problems, it was shown how barrier failure dominance increases in time as crack size variance increases, and how barrier failure dominance turns into a barrier-defined failure as critical crack growth dominates failure probabilities. It was shown how barrier failure dominance and its variation in time can be associated with the time-variation of FORM sensitivity coefficients, and how these coefficients can be used to choose the appropriate solution method for a specific problem. In particular, it was seen that for barrier failure dominance caused by resistance variables, the time-integrated solution is perhaps sufficiently accurate. Barrier failure dominance caused by random crack propagation variables most likely leads to highly non-linear problems where failure is barrier-defined. Finally, in the absence of barrier failure dominance, the EUR approximation is likely to be appropriate.

Strict quantitative characterization of barrier failure dominance for general problems has not been given. As a general guideline *only*, considering results derived in chapters 5 and 11, barrier failure dominance is unlikely when sensitivity coefficients of the load are larger than 0.1 ($\alpha_S^2 > 0.1$).

Some practical problems involved in evaluation of resistance distributions through a second order approximation and an arbitrary choice of resistance distribution model were illustrated in the study of fatigue and fracture reliability problems. It was shown that in the presence of considerable resistance variance, the ensemble up-crossing rate integration is dominated by the resistance distribution's tail, the largest contribution to the ensemble up-crossing rate occurs away from the resistance's mean and hence results become highly

dependant on the resistance distribution model. When variance of the barrier is modest, in comparison to variance of the load process, the largest contribution to the ensemble up-crossing rate occurs closer to the resistance mean, where the distribution model is more accurate. Hence, extrapolation of the resistance distribution model to the tails is avoided or at least minimized. The convenience of this result was pointed out, as it makes the second-order second moment (distribution model-based) approximation of the resistance distribution more appropriate precisely when the EUR solution is itself appropriate. Such a result, which has direct application to scalar problems, is also very useful in a directional simulation solution of multi-dimensional problems.

The complementary concept of *load process dominance* was also introduced, but was not characterized in any of the problems studied. Indeed, it was seen that even in the absence of barrier failure dominance, random barriers still contribute significantly to failure probabilities. This can perhaps be attributed to the fact that up-crossing rates decrease exponentially with the distance to the mean, being highly dependant on the resistance level. Hence, even very small barrier uncertainty affects failure probabilities. The numerical value of sensitivity coefficients also attest to barrier failure dominance. As suggested above, barrier failure dominance corresponds to resistance sensitivity coefficients adding to 0.9 or more, whereas load process sensitivity coefficients are hardly that large.

The large uncertainty typical of random crack propagation parameters could perhaps result in barrier failure dominance in practical problems, and could eventually make the EUR approximation inadequate. However, the fatigue and fracture reliability problems studied herein have shown that when the load process is highly stochastic, and when the overload failure probability is significant, barrier failure dominance is not likely. Because these problems involved scalar load processes, they were quite susceptible to barrier failure dominance, especially the high cycle fatigue problems (10^6 load cycles). Clearly, problems involving multiple load processes are less prone to barrier failure dominance and are likely more appropriate to solve by means of the EUR approximation.

12.2 Suggestions for continuing research

Perhaps the most important extension of results presented in this thesis that can be envisioned is the analysis of general multi-dimensional problems, in conjunction with a numerical (random failure domain boundary) ensemble out-crossing rate evaluation. Multi-dimensional extensions of EUR error estimates via simulation clearly requires some smart choice of combinations of load processes, which can perhaps be obtained for specific classes of problems.

For multi-dimensional problems, the barrier failure dominance concept and the EUR approximation are believed to be even more important.

A numerical (random failure domain boundary) ensemble out-crossing rate evaluation, such as the suggested parallel system sensitivity solution (section 1.6.3), has two major implications in the solution of general problems. The first implication, regarding scalar problems, is the avoidance of deriving a resistance distribution and, particularly, the avoidance of basing results on an arbitrary choice of resistance distribution model. The second implication of a numerical ensemble out-crossing rate evaluation is the obvious extension to multi-dimensional problems, where ensemble out-crossing rates are obtained directly, without the necessities of deriving scalar load process and resistance measures and of performing EUR integrations explicitly. It is also clear that the FORM-based solution for resistance distributions, used in this thesis for scalar problems, is difficult to generalize for multi-dimensional problems. The FORM-based resistance distribution solution, however, was presented as a numerical solution which avoids the arbitrary choice of resistance distribution model, and which in this context is very much equivalent to a numerical ensemble out-crossing rate evaluation for multi-dimensional problems.

A multi-dimensional extension of present results also has applications in problems of fatigue and fracture under combined loading, e.g., when a continuous load process causes crack growth and an impact loading (a pulse process) contributes to overload failure probabilities. Another application is crack propagation under multi-axial loading. Both problems involve a multi-dimensional extension of the EUR error estimate. The multi-axial problem, in addition to that, requires a proper fracture criterion based on the materials three-dimensional stress-strain response (tridimensional hysteresis loops).

Further potential applications of the random process - EUR solution and of the barrier failure dominance concept introduced in this thesis are problem involving general forms of resistance degradation (e.g., corrosion, fatigue) and problems of random vibration.

Bibliography

[1] ASCE, 1982: Fatigue Reliability - A State of the Art Report by the Committee on Fatigue and Fracture Reliability, Journal of the Structural Division, ASCE, No. 108(1), pp. 1 - 88.

[2] Ayala-Uraga, E. and Moan, T., 2002: System Reliability Issues of Offshore Structures Considering Fatigue Failure and Updating Based on Inspection, 1^{st} International ASRANet Colloquium, July 2002, Glasgow, Scotland.

[3] Barson, J. M. and Rolfe, S. T., 1987: Fracture and Fatigue Control in Structures: Applications of Fracture Mechanics, 2^{nd} edition, Englewood Cliffs, NJ, 1987.

[4] Bea, J. A., Doblare, M. and Gracia, L., 1999: Evaluation of the Probability Distribution of Crack Propagation Life in Metal Fatigue by means of Probabilistic Finite Element Method and B-models., Engineering Fracture Mechanics, vol. 63 (1999), pp. 675- 711.

[5] Beck, A.T., 1999: A Method of Reliability Analysis Using Finite Elements (in Portuguese), Masters thesis, Department of Mechanical Engineering, Federal University of Santa Catarina, SC, Brazil.

[6] Beck, A.T. and Melchers, R.E., 2002: Comparison of Some Methods for Fatigue and Fracture Reliability Analysis under Random Loading, in Advances in Mechanics of Structures and Materials, Loo, Chowdhury and Fragomeni (eds.), Swets & Zeitlinger, pp. 449 - 454.

[7] Beck, A.T. and Melchers, R.E., 2002(b): On the Ensemble Up-crossing Rate Approach to Time Variant Reliability Analysis of Uncertain Structures, Computational Stochastic Mechanics, Spanos and Deodatis (eds.), Milpress, Roterdam, pp. 43 - 52.

[8] Beck, A.T. and Melchers, R.E., 2003: On the Ensemble Up-crossing Rate Approach to Time Variant Reliability Analysis of Uncertain Structures, accepted for publication in Probabilistic Engineering Mechanics, September 2003.

[9] Beck, A.T. and Melchers, R.E., 2003(b): Fatigue and Fracture Reliability Analysis Under Random Loading, Computational Fluid and Solid Mechanics, K.J. Bathe (editor), Elsevier, pp. 2201 - 2203.

[10] Beck, A.T. and Melchers, R.E.: Barrier Failure Dominance in Time Variant Reliability Analysis, submitted for publication in Probabilistic Engineering Mechanics, December 2003.

[11] Beck, A.T. and Melchers, R.E.: Overload Failure of Structural Components under Random Crack Propagation and Loading - a Random Process Approach -, submitted for publication in Structural Safety, December 2003.

[12] Belyaev, Y.K., 1968: On the Number of Exits Across the Boundary of a Region by a Vector Stochastic Process, Theory Prob. Appl., Vol. 13, No. 2, pp. 320 - 324.

[13] Benjamin, J.R. and Cornell, C.A., 1970: Probability, Statistics and Decision for Civil Engineers, McGraw-Hill Book Company, New York.

[14] Berens, A.P., 1996: Applications of Risk Analysis to Ageing Military Aircraft, Sampe Journal, Vol. 32, No. 5, 1996.

[15] Besterfield, G. H., Liu, W. K., Lawrence, M. A. and Belytschko, T., 1991: Fatigue Crack Growth Reliability by Probabilistic Finite Elements, Computer Methods in Applied Mechanics and Engineering 86 (1991), pp. 297 - 320.

[16] Bogdanoff, J.L., 1978: A New Cumulative Damage Model, Part I, Journal of Applied Mechanics 45, pp. 245 - 250.

[17] Bouyssy, V., Naboishikov, S.M. and Rackwitz, R., 1993: Comparison of Analytical Counting Methods for Gaussian Processes, Structural Safety 12 (1993), pp. 35 - 57.

[18] Cherng, R.-H. and Wen, Y.K., 1994: Reliability of Uncertain Nonlinear Trusses Under Random Excitation I, Journal of Engineering Mechanics, ASCE, Vol. 120, No. 4, pp. 733 - 747.

[19] Cramer, H. and Leadbetter, M.R., 1967: Stationary and Related Stochastic Processes, John Wiley and Sons, NY.

[20] Ditlevsen, D., 1981: Principle of Normal Tail Approximation, Journal of the Engineering Mechanics Division, ASCE, vol. 107, nº EM6, pg. 1191 - 1208.

[21] Ditlevsen, O., 1986: Duration of Gaussian Process Visit to a Critical Set, Probabilistic Engineering Mechanics, vol. 1, pp. 82 - 93.

[22] Ditlevsen, O., 1986(b): Random Fatigue Crack Growth - A First Passage Problem, Engineering Fracture Mechanics, Vol. 23, No. 2, pp. 467 - 477.

[23] Ditlevsen, O. and Sobczyk, K., 1986: Random Fatigue Crack Growth with Retardation, Engineering Fracture Mechanics, Vol. 24, No. 6, pp. 861 - 878.

[24] Ditlevsen, O. and Madsen, H.O., 1996: Structural Reliability Methods, John Wiley and Sons, Chichester, England.

[25] Dirlik, T., 1985: Applications of Computers in Fatigue, Ph. D. Thesis, University of Warwick.

[26] Dolinski, K. and Colombi, P., 1999: Fatigue Lifetime under Stochastic Loading with Random Overloading Pulse Trains, Computer Methods in Applied Mechanics and Engineering, vol. 168 (1999), pp. 221 - 241.

[27] Dover, W.D. and Hibbert, R.D., 1977: The Influence of Mean Stress and Amplitude Distribution on Random Load Fatigue Crack Growth, Engineering Fracture Mechanics 9, 251 - 263.

[28] Dowling, N. E., 1985: Fatigue Failure Predictions for Complicated Stress-Strain Histories, Journal of Materials 7 (1), 71 - 87.

[29] Ghanen, R.G. and Spanos, P.D., 1991: Stochastic Finite Elements: A Spectral Approach, Springer-Verlag, NY.

[30] Ellyin, F., 1997: Fatigue Damage, Crack Growth and Life Prediction, Chapman & Hall.

[31] Engelund, S., Sorensen, J., Faber, M. and Bloch, A., 2002: Approximations in Inspection Planning, 8^{th} ASCE Specialty Conference on Probabilistic Mechanics and Structural Reliability.

[32] Faber, M.H., Kroon, I.B. and Sorensen, J.D., 1996: Sensitivities in Structural Maintenance Planning, Reliability Engineering and System Safety 51(1996), pp. 317 - 329.

[33] Farhangdoost and Provan , 1996: Stochastic System Approach to Fatigue Reliability - an Application to Ti-6Al-4V, Engineering Fracture Mechanics, vol. 53, no 5, pp. 687 - 706.

[34] Fuchs and Stephens, 1980: Metal Fatigue in Engineering, John Wiley and Sons, NY.

[35] Gansted, L., Brincker, R. and Hansen, L. P., 1991: Fracture Mechanical Markov Chain Crack Growth Model, Engineering Fracture Mechanics, vol. 38, no 6, pp. 475 - 489, 1991.

[36] Ghonen, H. and Dore S., 1987: Experimental Study of the Constant Probability Crack Growth Curves Under Constant Amplitude Loading, Engineering Fracture Mechanics, vol. 27, no 1, pp. 1 - 25, 1987.

[37] Grigoriu, M., 2000: A Spectral Representation Based Model for Monte Carlo Simulation, Probabilistic Engineering Mechanics, 15(2000), pp. 365 - 270.

[38] Hagen, O. and Tvedt, L., 1991: Vector Process Out-Crossing as a Parallel System Sensitivity Measure, Journal of Engineering Mechanics, Vol. 117, No. 10, pp. 2201 - 2220.

[39] Harris, D.O., 1997: Probabilistic Fracture Mechanics, in Probabilistic Structural Mechanics Handbook, C. R. Sundararajan (ed.), Chapman & Hall.

[40] Hasofer, A. M. and Lind, N. C.; 1974: Exact and Invariant Second Moment Code Format, Journal of Engineering Mechanics vol. 100(1), pp. 111 - 121.

[41] Igusa, T. and Kiureghian, A.D., 1988: Response of Uncertain Systems to Stochastic Excitation, Journal of Engineering Mechanics, vol. 114, No. 5, pp. 812 - 832.

[42] Ishikawa, H., Tsurui, A., Tanaka, H. and Ishikawa, H., 1993(a): Reliability Assessment of Structures Based Upon Probabilistic Fracture Mechanics, Probabilistic Engineering Mechanics 8 (1993), pp. 43 - 56.

[43] Ishikawa, H., Tsurui, A., Utsumi, A., Tanaka, H. and Ishikawa, H., 1993(b): Effect of Stress Ratio on Crack Propagation Life Distribution under Random Loading, Probabilistic Engineering Mechanics 8 (1993), pp. 35 - 41.

[44] Itagaki, H., Ishizuka, T. and Yan, H. P., 1993: Experimental Estimation of the Probability Distribution of Fatigue Crack Growth Lives, Probabilistic Engineering Mechanics, vol. 8 (1993), pp. 25 - 34.

[45] Kanninen, M.F. and Popelar, C.H., 1985: Advanced Fracture Mechanics, Oxford University Press, New York.

[46] Kuo, C.J., 1997: Reliability Assessment of Deteriorating Component due to Fatigue Crack Growth under Random Loading, Ph. D. thesis, University of Arizona, Tucson, Arizona.

[47] Larrabee, R.D. and Cornell, C.A., 1979: Up-crossing Rate Solution for Load Combinations, Journal of the Structural Division, ASCE, vol. 105, No. ST1, pp. 125 - 132.

[48] Lee, J. C. and Ang, A. H-S., 1994: Finite Element Fracture Reliability of Stochastic Structures, Structural Safety and Reliability, Schueller, Shinozuka and Yao (eds.), Balkema, Rotherdam.

[49] Li, C.Q. and Melchers, R.E., 1993: Gaussian Up-crossing Rate Solution for Structural Serviceability, Structural Safety 12 (1993), pp. 293 - 303.

[50] Lin, Y. K. and Yang, J.N., 1985: A Stochastic Theory of Fatigue Crack Propagation, AIAA Journal, vol. 23, no 1, January 1985, pp. 117 - 124.

[51] Lutes, L. and Sarkani, S., 1997: Stochastic Analysis of Structural and Mechanical Vibrations, Prentice Hall.

[52] Madsen, H.O., 1986: Fast Probability Integration for Time Variant Reliability, A.S. Veritas Report.

[53] Madsen, H.O. and Tvedt, L., 1990: Methods for Time-Dependent Reliability and Sensitivity Analysis, Journal of Engineering Mechanics, Vol. 116, No. 10, pp. 2118 - 2135.

[54] Madsen, H. O., Krenk, S. and Lind, N. C., 1986: Methods of Structural Safety, Prentice Hall Inc., Englewood Cliffs, NJ.

[55] Madsen, H.O., Skjong, R., Tallin, A.G. and Kirkemo, F., 1987: Probabilistic Fatigue Crack Growth Analysis of Offshore Structures with Reliability Updating Through Inspections, Proceedings of Marine Structural Reliability Symposium, Arlington, VA.

[56] Marley, M. J. and Moan, T., 1994: Approximate Time Variant Analysis for Fatigue, Structural Safety and Reliability, Schueller, Shinozuka and Yao (eds), 1994.

[57] McAllister, T.P. and Ellingwood, B.R., 2002: Evaluation of Crack Growth in Miter Gate Weldments Using Stochastic Fracture Mechanics, Structural Safety 23(4), pp. 445 - 465.

[58] Melchers, R.E., 1992: Load-Space Formulation for Time-Dependent Structural Reliability, Journal of Engineering Mechanics, vol. 118, no. 5, pp. 853 - 870.

[59] Melchers, R.E., 1999: Structural Reliability Analysis and Prediction, second edition, John Wiley and Sons, NY.

[60] Melchers, R.E., 2001: Assessment of Existing Structures - Approaches and Research Needs, Journal of Structural Engineering, ASCE, Vol. 127, No. 4, April 2001.

[61] Melchers, R.E. and Ahammed, M., 2001: Estimation of Failure Probabilities for Intersections of Non-linear Limit States, Structural Safety, Vol. 23(2001), 123 – 135.

[62] Moan, T., Hovde, G. and Jiao, G., 1994: Fatigue Reliability Analysis of Offshore Structures Considering the Effect of Inspection and Repair, Proceedings of Structural Safety and Reliability, 1994, Balkema, Rotterdam.

[63] Moan, T., Vardal, O.T., Hellevig, N.C. and Skjoldli, K., 1997: In-Service Observations of Cracks in Nord Sea Jackets. A Study of Initial Crack Depth and POD Values, Proc. of 16^{th} OMAE conference, Yokohama, Japan.

[64] Mori, Y. and Ellingwood, B., 1993: Time-dependent System Reliability Analysis by Adaptive Importance Sampling, Structural Safety 12(1), pp. 59 - 73.

[65] Nagode, M. and Fajdiga, M., 1998: A General Multi-modal Probability Distribution Function Suitable for the Rainflow Ranges of Stationary Random Processes, International Journal of Fatigue, vol. 20, no. 3, pp. 211 - 223.

[66] Nigam, N. C. and Narayanan, S.; 1994: Applications of Random Vibrations, Springer-Verlag, New York.

[67] Ortiz, K., 1984: Stochastic Modelling of Fatigue Crack Growth, Ph. D. thesis, Stanford University, Stanford, California.

[68] Ortiz, K. and Kiremidjian, A.S., 1988: Stochastic Modelling of Fatigue Crack Growth, Engineering Fracture Mechanics, Vol. 29, No. 3, pp. 317 - 334.

[69] Owen, D., 1980: A Table of Normal Integrals, Comm. Stat. Simul. Comp. B9(4), pp. 389-419.

[70] Paris, P. and Erdogan, F., 1963: A Critical Analysis of Crack Propagation Laws, Journal of Basic engineering, vol. 85, pp. 528 - 534.

[71] Pearce, H.T. and Wen, Y.K., 1984: Stochastic Combination of Load Effects, Journal of Structural Engineering, vol. 110, No. 7, pp. 1613 - 1629.

[72] Press, W.H., Flannery, B.P., Teukolsky, S.A. and Vetterling, W.T., 1989: Numerical Recipes - The Art of Scientific Computing, Cambridge University Press.

[73] Provan, J. (ed.), 1987: Probabilistic Fracture Mechanics and Reliability, Martinus Nijhoff Publishers, Dordrecht, The Netherlands, 1987.

[74] Rackwitz, R., 1993: On the Combination of Non-stationary Rectangular Wave Reneval Processes, Structural Safety 13 (1993), pp. 21 - 28.

[75] Rackwitz, R. and Fiessler, B.; 1978: Structural Reliability Under Combined Load Sequences, Computers and Structures vol. 9, pp. 489 - 494.

[76] Rahman, S. and Kim, J.S., 1998: Probabilistic Fracture Mechanics for Nonlinear Structures, Structural Safety and Reliability, Schueller, Shinozuka and Yao (eds.), Balkema, Rotherdam.

[77] Rice, S.O., 1944: Mathematical Analysis of Random Noise, Bell System Technical Journal, Vols. 23 and 24. Re-published in Selected Papers on Noise and Stochastic Processes, edited by N. Wax (1954), Dover Publications Inc, New York.

[78] Rocha, M. M. and Schueller, G. I., 1996: A Probabilistic Criterion for Evaluating the Goodness of Fatigue Crack Growth Models, Engineering Fracture Mechanics, vol. 53, no 5, pp. 707 -731, 1996.

[79] Sarveswaran, V. and Roberts, M.B., 1999: Reliability Analysis of Deteriorating Structures - The Experience and Needs of Practicing Engineers, Structural Safety 21 (1999), pp. 357 - 372.

[80] Schall, G., Faber, M.H. and Rackwitz, R., 1991: On the Ergocity Assumption for Sea States in the Reliability Estimation of Offshore Structures, Journal of Offshore Mechanics and Artic Engineering, ASME, Vol. 113, pp. 241 - 246.

[81] Shinozuka, M. and Jan, C.-M., 1972: Digital Simulation of Random Processes and its Applications, Journal of Sound and Vibration, vol. 25, No. 1, pp. 111 - 128.

[82] Sobczyk, K., 1986: Modelling of Random Fatigue Crack Growth, Engineering Fracture Mechanics, vol. 24, no 4, pp. 609 - 623, 1986.

[83] Sobczyk, K. and Spencer, B. F., 1992: Random Fatigue: from Data to Theory, Academic Press, 1992.

[84] Sobczyk, K. and Trebiki, J., 2000: Stochastic Dynamics with Fatigue Induced Stiffness Degradation, Probabilistic Engineering Mechanics, vol. 15 (2000), pp. 91-99.

[85] Solnes, J., 1997: Stochastic Processes and Random Vibrations - Theory and Practice, John Wiley and Sons Ltd., Chichester, England.

[86] Soong, T.T. and Grigoriu, M., 1993: Random Vibration of Mechanical and Structural Systems, Prentice Hall, Englewood Cliffs, NJ.

[87] Sudret, B. and Kiureghian, A.D., 2002: Comparison of Finite Element Reliability Methods, Probabilistic Engineering Mechanics 17 (2002), pp. 337 - 348.

[88] Sudret, B., Defaux, G., Lemaire, M. and Andrieu, C., 2002: Comparison of Methods for Computing the Probability of Failure in Time-Variant Reliability Using the Out-Crossing Approach, Fourth International Conference on Computational Stochastic Mechanics, Kerkyra (Corfu), Greece, June 2002.

[89] Tsurui, A. and Ishikawa, H., 1986: Application of the Fokker-Planck Equation to a Stochastic Fatigue Crack Growth Model, Structural Safety 4 (1986), pp. 15 - 29.

[90] Tsurui, A., Nienstedt, J., Schueller, G. I. and Tanaka, H., 1989: Time Variant Structural Reliability Analysis using Diffusive Crack Growth Models, Engineering Fracture Mechanics, vol. 34, no 1, pp. 153 - 167.

[91] Turkstra, C.J., 1970: Theory of Structural Design Decisions, Study No. 2, Solid Mechanics Division, University of Waterloo, Waterloo, Ontario.

[92] Turkstra, C.J. and Madsen, H.O., 1980: Load Combinations in Codified Structural Design, Journal of the Structural Division, ASCE, vol. 116, No. ST12, pp. 2527 - 2543.

[93] Vanmarcke, E.H., 1975: On the Distribution of the First Passage Time for Normal Stationary Processes, Journal of Applied Mechanics, ASME, vol. 42, pp. 215 - 220.

[94] Vanmarcke, E.H., 1983: Random Fields, Analysis and Synthesis, MIT Press, Cambridge, Massachusetts.

[95] Veers, P.J., 1987: Fatigue Crack Growth due to Random Loading, Ph. D. thesis, Department of Mechanical Engineering, Stanford University, Stanford, California.

[96] Virkler, D. A., Hillberry, B. M. and Goel, P. K., 1979: The Statistical Nature of Fatigue Crack Propagation, Journal of Engineering Materials and Technology, ASME, vol. 101 (1979), pp. 148 - 153.

[97] Wang, G. S.,1999: A Probabilistic Damage Accumulation Solution Based on Crack Closure Model, International Journal of Fatigue, Vol. 21 (1999), pp. 531 - 547.

[98] Wang, L., Brust, W. and Atluri, N., 1997: The Elasto-Plastic Finite Element Alternating Method (EPFEAM) and the Prediction of Fracture Under WFD Conditions in Aircraft Structures.

[99] Wen, Y.K. and Chen, H.C., 1987: On Fast Integration for Time-Variant Structural Reliability, Probabilistic Engineering Mechanics, vol. 2, no 3, pp 156 - 162.

[100] Wen, Y.K. and Chen, H.C., 1989: System Reliability Under Time-Varying Loads: I, Journal of Engineering Mechanics, vol. 115, no 4, pp 808 - 823.

[101] Wheeler, O. E., 1972: Spectrum Loading and Crack Growth, Journal of basic engineering, Vol. 94, pp. 181 - 186.

[102] Wirsching, P. H., 1998: Fatigue Reliability, Progress in Structural Engineering and Materials 1998, vol. 1(2), pp. 200 - 206.

[103] Wirsching, P. H. and Shehata, A. M., 1977: Fatigue Under Wideband Random Stresses Using the Rainflow Method, Journal of Engineering materials and Technology, ASME, vol. 99 (1977), pp. 205 - 211.

[104] Yang, J. N., Hsi, W. H., Manning, S. D. and Rudd, J.L., 1987: Stochastic Crack Growth Models for Application to Aircraft Structures, in Provan (ed.), Probabilistic Fracture Mechanics and Reliability, Martinus Nijhoff Publishers, Dordrecht, The Netherlands, 1987.

[105] Yang, J. N. and Manning, S. D., 1996: A Simple Second Order Approximation for Stochastic Crack Growth Analysis, Engineering Fracture Mechanics, vol. 53, no 5, pp. 677 - 686, 1996.

[106] Zheng, R. and Ellingwood, B. R., 1998: Stochastic Fatigue Crack Growth in Steel Structures Subject to Random Loading, Structural Safety 20 (1998), pp. 303 - 323.

[107] Zhu, W. Q., Lin, Y. K. and Lei, Y., 1992: On Fatigue Crack Growth under Random Loading, Engineering Fracture Mechanics, vol. 43, no 1, pp. 1 - 12, 1992.

[108] Zwillingner, D. (editor), 1996: Standard Mathematical Tables and Formulae, CRC Press, 30^{th} edition.